Pyare Püschel

Vom Fachbereich VI
Raum- und Umweltwissenschaften
der Universität Trier
zur Verleihung des akademischen Grades
Doktor der Naturwissenschaften
(Dr. rer. nat.)
genehmigte Dissertation

Assessing forest growth models using forest structural parameters derived from ground-based remote sensing

Betreuender:
Univ.-Prof. Dr. Joachim Hill

Berichterstattende:
Univ.-Prof. Dr. Joachim Hill
apl. Prof. Dr. Willy Werner

Datum der wissenschaftlichen Aussprache:
14. Juli 2014

Trier, 2014

Acknowledgements

First and foremost I would like to thank my family for their love, encouragement, and for always being there for me. I owe you so much. I am also deeply grateful to my partner Antje for her gentleness, dedication, and love.

I also would like to express my gratitude to everyone who contributed to the successful completion of this dissertation and to the following people in particular:

Prof. Dr. Joachim Hill, head of the Department of Environmental Remote Sensing and Geoinformatics and main supervisor of this thesis, for his invaluable advice and strong support. I am also very grateful for giving me the opportunity to conduct research abroad and for encouraging me to follow up on my research interests.

Prof. Dr. Willy Werner, second supervisor of this thesis, for his help and support, and above all for sharing his vast expertise on forest ecosystems.

Prof. Dr. Thomas Udelhoven for kindly providing the terrestrial laser scanner without which a lot of my research would not have been possible.

Drs Henning Buddenbaum, Antje Lewien, Achim Röder, Marion Stellmes for the valuable feedback on Chapters I, VI, and VII of this thesis. Dr. Johannes Stoffels for the beneficial discussions on forestry-related matters.

The senior researchers at the Department for always providing support and advice. Last but not least, all my colleagues for the good times - on and off duty!

Zusammenfassung

In unserer heutigen globalisierten Welt sind Waldökosysteme einem wachsenden Druck seitens ökonomischer Einflüsse und ökologischer Veränderungen, insbesondere als Folge des Klimawandels, ausgesetzt. Um die nachhaltige Entwicklung von Wäldern und ihre wichtigen Ökosystemdienstleistungen, beispielsweise den Schutz vor Bodenerosion, auch für zukünftige Generationen zu gewährleisten, ist es unverzichtbar, den Zustand und Zustandsveränderungen von Wäldern zu beobachten sowie ihre zukünftige Entwicklung zu prognostizieren. Für solche Prognosen werden zumeist ökophysiologische Waldwachstumsmodelle eingesetzt, die pflanzenphysiologische Wachstumsprozesse in Abhängigkeit externer Umwelteinflüsse abstrahieren bzw. simulieren. Der Grad der Modellabstraktion, d.h. die Komplexität der modellierten Wachstumsprozesse und -faktoren, entscheidet über die Praxistauglichkeit eines Modells. Da die moderne Forstwirtschaft einen ganzheitlichen Waldmanagement-Ansatz verfolgt, der die vielseitigen Ökosystemfunktionen berücksichtigt, verschwimmt zunehmend die Grenze zwischen den forschungsorientierten ökophysiologischen Modellen und den auf die Holzertragsschätzung ausgerichteten empirischen Modellen. Unabhängig vom Modelltyp ist jedoch eine Modellkalibrierung und -validierung anhand forstlicher Referenzdaten erforderlich.

Da die zentralen Parameter der forstlichen Wachstumsmodelle, die Biomassekompartimente, aufgrund der Anzahl und Dimension der Bäume in Wäldern nur sehr eingeschränkt direkt gemessen werden können, kommen in der Praxis sogenannte allometrische Beziehungen zum Einsatz. Diese verknüpfen die einzelnen Biomassekompartimente eines Baumes mit Messgrößen der Baumstruktur, die relativ einfach direkt erhoben werden können. Zu den wichtigsten dieser strukturellen Messgrößen zählen die Baumhöhe, der Stammdurchmesser, die Bestandsdichte (Bäume pro Fläche) sowie der Blattflächenindex. Die traditionell zur Bestimmung dieser Parameter eingesetzten Methoden sind vorwiegend manuelle Verfahren, die zeit- und kostenaufwendig sind. Die Datenerhebung ist somit zwangsläufig ineffizient und kann nur eingeschränkt die horizontale und vertikale Variabilität der strukturellen Größen und damit die Bestandsstruktur erfassen. Da die Bestandsstruktur das Wachstum der Bäume beeinflusst, ist die dreidimensionale Erfassung der Struktur jedoch erforderlich, um das Waldwachstum realistisch modellieren zu können. Bodengestützte Fernerkundung (FE) bietet die Möglichkeit, die Einschränkungen der traditionellen Messverfahren zu umgehen. Die

fernerkundlichen Verfahren haben den Vorteil, dass sie automatisierbar sind und folglich eine höhere Datenerhebungseffizienz und räumliche Abdeckung erlauben. Zudem ermöglichen bestimmte FE-Sensoren (terrestrische Laserscanner) eine dreidimensionale Erfassung der Bestandsstruktur. Die Ableitung der genannten strukturellen Forstparameter mittels bodengestützter Fernerkundung ist jedoch noch nicht hinreichend standardisiert. So besteht zum Beispiel noch erheblicher Forschungsbedarf, wie diese Methoden praktisch in Waldwachstumsmodelle eingebunden werden können und welche Faktoren die Ableitung der strukturellen Parameter beeinflussen.

Ziel der vorliegenden Arbeit war daher, für zwei bodengestützte fernerkundliche Methoden (Hemisphärische Photographie und Terrestrisches Laserscanning) Einflussfaktoren zu analysieren, die bis dato noch nicht oder nur wenig untersucht wurden. Zudem sollte ein ökophysiologisch-basiertes Modell mit den erhobenen Fernerkundungsdaten kalibriert werden, um exemplarisch die bodengestützte Fernerkundung in Waldwachstumsmodelle zu integrieren. Diese Ziele wurden umfassend erreicht. Somit konnte die Arbeit erheblich zu einer Standardisierung der bodengestützten fernerkundlichen Methoden für die Ableitung der strukturellen Parameter Blattflächenindex, Stammdichte und Stammdurchmesser beitragen. Hinsichtlich der Kalibrierung von Waldwachstumsmodellen konnte gezeigt werden, dass die Verwendung dieser Methoden nur unter gewissen Einschränkungen möglich ist. Diese Limitationen sind jedoch teilweise auf die Erhebungsmethodik zurückzuführen, so dass mit deren Optimierung künftig eine verbesserte Nutzbarkeit der bodengestützten fernerkundlichen Methoden für die Modellkalibrierung zu erwarten ist. Zudem wurden durch die vorliegende Arbeit Schwachstellen des verwendeten Waldwachstumsmodells aufgezeigt. Abschließend wurden hierfür mögliche Lösungsansätze präsentiert, die auf einer Kombination von boden- und luftgestützter Fernerkundung basieren. Diese Verknüpfung unterschiedlicher fern- erkundlicher Betrachtungsebenen wird erheblich zu einem zukunftsfähigen Waldmanagement beitragen, um eine nachhaltige Waldentwicklung – auch unter den wachsenden ökonomischen Zwängen und ökologischen Veränderungen – zu gewährleisten.

Contents

Chapter I: Introduction

1   Forest development, structure, and growth

In light of the increasing pressures from climatic, ecological, and economic forces, the monitoring and modelling of forest development is vital to provide information required for the alleviation of these pressures so that forests maintain their ecosystem services (Achard and Hansen, 2013). These services are diverse and include for example carbon storage, the prevention of soil erosion, or the provision of sustenance. This multi-purpose orientation of forest growth monitoring and modelling deviates distinctly from the management focus of traditional forestry, i.e. yield prediction, management planning, etc. (Burkhart and Tomé, 2012). Today's forestry orientation reflects not only the increase in knowledge about forest ecosystems and their highly complex functioning and interaction with other ecosystems but also the growing awareness that forests require protection to ensure a sustainable provision of their ecosystem services, i.e. to warrant a sustainable forest development. Forest development is closely linked to forest structure as it is changes in forest structure that are the most visible manifestation of forest development. So how is forest structure defined and how exactly does it relate to forest development and forest growth in particular?

Forest structure is defined as the three-dimensional distribution and arrangement of trees, and their parts and properties (Pretzsch, 2009; von Gadow, 2003). Therefore, forest structure and its description depend on the spatial scale at which forest structure is observed. Usually it is observed and described at the stand level, i.e. the basic forest management entity (Burkhart and Tomé, 2012). Forest and in particular forest canopy structure influence the exchange of material and energy with the lower atmosphere and the distribution of major environmental factors such as precipitation, radiation, and temperature within forest stands (Parker, 1995). As these factors affect tree growth, and tree growth in turn affects tree and stand structure, a feedback loop exists between forest structure and growth (Pretzsch, 2009).

Since individual tree growth and structural changes are steered by resource competition between neighbouring trees, it is important to also take these tree level interactions into consideration for analysing and modelling the stand level growth. Therefore, descriptors that explicitly account for the three-dimensionality of stand structure are crucial for modelling physiological processes related to growth, such as photosynthesis and transpiration (e.g. Pretzsch, 2009; Zheng and Moskal, 2009). The feedback loop between forest structure and growth stretches not only across spatial scales, though, but also over time since forests are

open and dynamic systems. In addition, as the lifetime of trees well exceeds that of a human being, modelling structural-functional growth relationships is crucial to predict forest development (Pretzsch, 2009), especially with regard to climate change effects (e.g. Cannell et al., 1995; Kirschbaum, 2000).

2   Forest growth modelling and remote sensing

In traditional forestry growth modelling or, more generally, the monitoring and prediction of stand development were mainly driven by economic considerations, i.e. to increase yield. This management orientation included the study of silvicultural practices (e.g. thinning) and their influence on stand growth and yield (Burkhart and Tomé, 2012). For this purpose, permanent monitoring sites were established as early as the 19th century (Pretzsch, 2009). These provided real time series of stand development which formed the basis for the so-called yield tables: empirical relationships between yield and stand height, respectively stand height and age. These tables can be considered as the first stand-based "growth models" (Pretzsch, 2009). Since then, growth research has boosted the knowledge of growth factors and processes in increasing detail and complexity. This was accompanied by the development of models accounting for this "growing" knowledge at different scales.

To date, forest growth models have become abundant, ranging from purely empirical to mechanistic matter balance models (e.g. Landsberg and Sands, 2011). The latter are also referred to as process-based or eco-physiological models because they are based on modelling the physiological processes of growth and the underlying mechanisms. As forests are open systems and their growth is therefore influenced by the environment, the explicit integration of cause-effect relationships between growth and environmental factors such as soil water and fertility has proven to be an important part of these models (e.g. Landsberg and Sands, 2011). Hybrid models that feature both empirical and mechanistic characteristics have also received increased attention (Mäkelä et al., 2000).

Forest growth models can also be classified according to the temporal and spatial resolution of the modelled processes, ranging from seconds to centuries, and from the individual tree to landscape level (Pretzsch, 2009). The scale has important implications for the requirement of the data input into these models as well as for the data output. In particular, individual tree-based and stand-based eco-physiological models, two of the most common types of growth models, require a huge amount of data for model initialisation, calibration, and evaluation. As this kind of data is not readily available, eco-physiological models, despite their theoretical advantages over the empirical models, have been mainly applied as research tools to date. Their practical use in forest management remains limited (e.g. Mäkelä et al., 2000; Tickle et al., 2001). Nevertheless, the eco-physiological models are of value for testing potential effects

of climate change or silvicultural practices on growth (Kirschbaum, 2000). Ultimately, the model choice depends on the objective of the modelling. Therefore, various researchers have pointed out that it is not a question of good and bad but rather of finding the model that best suits the purpose at hand (e.g. Burkhart and Tomé, 2012; Pretzsch, 2009).

Nevertheless, in practice, the choice of model is largely driven by data input requirements. The increasing detail and complexity of forest growth models has necessitated the availability of data matching this scale, both spatially and temporally. Long-term growth and yield monitoring has provided data invaluable for the calibration and validation of models and for revealing long-term effects of environmental factors (e.g. air pollution) and silvicultural practices (e.g. thinning) on growth. These monitoring sites are, however, limited in their coverage of data required by eco-physiological models and in their coverage of the spatial heterogeneity of forest productivity. Due to these limitations, alternative means to provide the required data have gained importance, including standard inventory data collected on a large scale for national forest inventories (e.g. Pretzsch, 2009; von Gadow, 2003). While the construction of artificial time series of forest development from this data was shown to be of value, traditional forest inventory is manual, labour intensive and time-consuming work and is therefore also limited in its spatial coverage and sampling efficiency.

The use of remote sensing (RS) has been suggested to overcome these problems (e.g. Kangas and Maltamo, 2009; Zheng and Moskal, 2009). Remote sensing is the science of collecting information about an object based on measurements made with a device that is not in direct contact with the object (Lillesand and Kiefer, 2000). This definition is usually associated with sensors utilizing electromagnetic energy for earth observation, but in a broader context this definition can include devices such as sonar sensors or even photography (Cracknell and Hayes, 1991). RS-systems are also often classified according to their platform, e.g. satellites or aircrafts[1].

With regard to the use of RS in forestry and its applications, RS has proven to be capable of providing valuable information on the type and coverage of forests, their state and dynamics (e.g. Achard and Hansen, 2013, Wulder and Franklin, 2003). This has been achieved by the successful retrieval of forest structural and bio-physical parameters from RS-observations at

---

[1] Since a detailed treatment of remote sensing sensors, platforms, and principles is beyond the scope of this dissertation, the reader is referred to the textbooks by Lillesand and Kiefer (2000) and Richards and Jia (2006).

multiple scales. These range from global scale studies on forest areas and their productivity (e.g. Nightingale et al., 2007; Turner et al., 2006) – crucial for the support of environmental programmes such as REDD[2] (Reducing Emissions from Deforestation and Forest Degradation) – to national and regional scale studies on forest type and tree species distribution (e.g. Stoffels et al., 2012; Wolter et al., 1995), relevant to upscaling and supporting traditional forest inventories. The mentioned applications are mainly based on multi-spectral sensors on satellite platforms with corresponding medium to low spatial resolutions and global coverage such as NASA's Landsat or TERRA MODIS.

By contrast, airborne sensors with high spatial and/or spectral resolutions such as HyMAP, Hyperion, or LiDAR (Light Detection and Ranging) technology facilitate regional or local scale studies on structural and physiological properties of canopies (e.g. Kokaly et al., 2009; Le Maire et al., 2008; Schlerf et al., 2005; Solberg, 2010; Zhao and Popescu, 2009). Information on these properties is important to assess the eco-physiological sensitivity of tree species to changing environmental conditions (Hill, 2010). Yet, an aspect common to all these different studies and RS-sensors is the necessity for ground reference data. These can be obtained by manual in situ measurements or by ground-based remote sensing sensors such as spectroradiometers (e.g. Lillesand and Kiefer, 2000).

With regard to the integration of remotely sensed data into forest growth models, two main potential links can be identified: The use of RS to (1) initialise the model, i.e. to provide information on factors that drive the model such as meteorological or site data, and (2) to calibrate the model, i.e. to assign values to model parameters. Ideally, parameters are derived by direct measurements but as these are often not feasible, parameterization or parameter estimation is usually applied (e.g. Landsberg and Sands, 2011; Sands, 2004). This process involves fitting the model outputs to observed data, where the set of parameters is obtained by minimizing the residuals of this fit. Figure 1 depicts these conceptual links using the example of a schematic eco-physiological model.
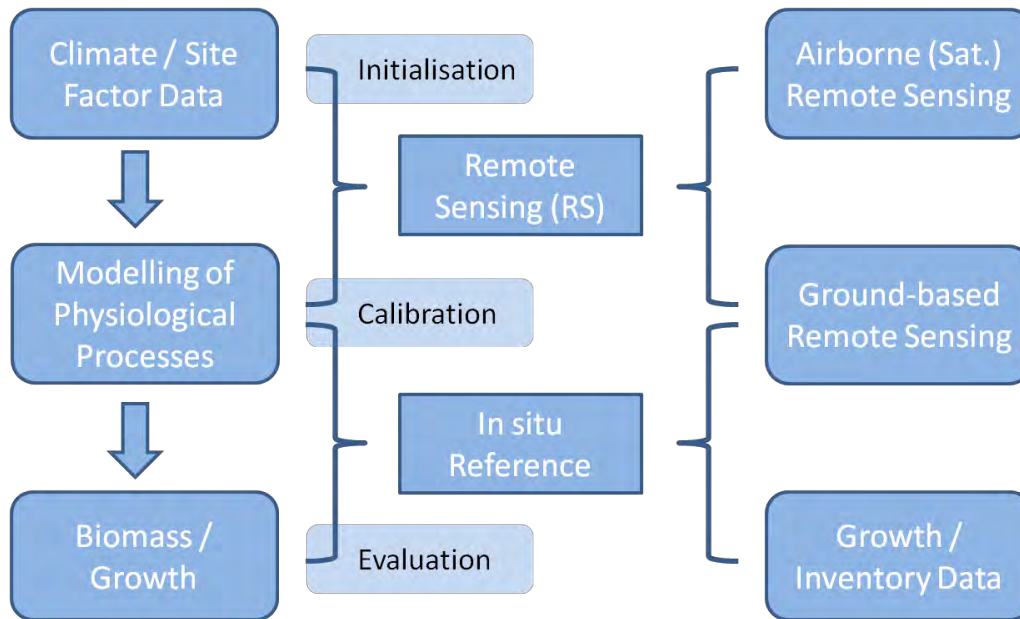
---

[2] http://www.un-redd.org/

Figure 1: Conceptual framework for the integration of remote sensing data into eco-physiological forest growth models. A schematic model structure is shown on the left, i.e. climate and site factor are the input data that drive the modelling of growth-related eco-physiological processes. The basic simulation output are measures of biomass production and growth. The potential sources of data required by these models are depicted in the middle and on the right side. The conceptual links of this data to main modelling tasks (calibration, etc.) are shown in light blue.

The exact links, however, mainly depend on the model type and structure and the properties of the RS-data. For example, the high temporal resolution of sensors (i.e. the frequency with which a fixed spot on earth is repetitively observed by a sensor), in particular the satellite-based sensors such as the upcoming German EnMAP[3], will facilitate a constant update of the model parameterization by adjusting model simulations to continuous RS-observations of forest structural and bio-physical parameters.

A third potential link is the evaluation of the model, respectively of model simulations with RS-observations. However, this implies that these observations yield some kind of ground truth which may be questioned as forest structural and bio-physical parameters derived from airborne and satellite RS are usually inferred from surrogate variables (e.g. vegetation indices). In addition, as airborne and satellite RS "senses" forests from above, the canopy structure influences the determination of these surrogate variables.

By contrast, as ground-based RS senses forests from below the canopy, these sensors might hold the potential to obtain much more accurate in situ data to calibrate and evaluate growth

---

[3] http://www.enmap.org/

models (e.g. Watt and Donoghue, 2005). While the integration of airborne and satellite RS data into forest growth models has been a main focus in previous research (e.g. Coops et al., 1998; Coops et al., 2009; Coops and Waring, 2001; Le Maire et al., 2005; Waring et al., 2010), the use of ground-based RS in growth modelling has not received much attention so far. This is surprising as ground-based RS, in particular terrestrial laser scanning, has been shown to successfully retrieve a wide range of forest parameters (see e.g. the review of Dassot et al., 2011). In the following sections, the reasons for this disparity will be illustrated, leading to the formulation of the general objectives of this PhD thesis.

3   Forest structural parameters

Due to the strong linkage of forest structure and growth through feedback loops (Pretzsch, 2009), structural parameters constitute key parameters in forest growth models regardless of model type. However, which exact forest structural parameters are used and how these are implemented in a model depends largely on the model type. For example, while for empirical yield table models stand-based measures such as mean stem diameter at breast height (DBH) or mean tree height suffice, more complex structural measures such as crown shape and cover are required for individual tree models. Yet, all these different models have in common that they yield a measure of biomass production and growth.

As the direct determination of forest biomass is destructive and practically not feasible due to the size and number of trees within forest stands, the principle of allometry is traditionally used to infer forest (i.e. tree and stand) biomass. This estimation is based on more accessible, non-destructive measurements of the structural parameters stocking (number of trees per defined area), stem diameter, and tree height for woody biomass on the one hand, and of leaf area[4] for foliage biomass on the other (e.g. Sands, 2004; Van Laar and Akça, 2007). The measurement of these parameters is therefore of particular importance to forest growth modelling; hence the above-mentioned can be considered as core structural parameters.

In the following, the methods that are traditionally applied in forestry to measure these core structural parameters are outlined and their main limitations are delineated. Possible solutions to overcome these limitations by way of ground-based RS are then presented in Section 4. The core parameters are grouped into standard forest inventory parameters (stocking, stem diameter, tree height) and into measures of canopy structure (leaf area).

3.1   Leaf area

Leaf biomass is traditionally inferred from an allometric relation with above-ground biomass or from measurements of litter fall (Pretzsch, 2009). As the construction of leaf biomass allometric equations is very time-consuming and laborious, it suffers from small sample sizes and a restricted transferability. Thus litter fall measurements are routinely used for monitoring of forest leaf dynamics and growth.

---

[4] In the context of this study the term leaf area is used to denote both leaf and needle area.

However, as these are also labour intensive and consequently mostly used to derive annual or seasonal plot-based averages of a limited spatial coverage (i.e. they are not able to depict temporal and spatial variability), indirect measures of leaf area to estimate leaf biomass have gained importance. It has to be noted that due to the key role of leaf area in photosynthesis and related physiological processes as well as in the interaction between bio- and atmosphere (e.g. rainfall interception, deposition of gases and particulates), determining leaf area is not only important for growth modelling but indeed crucial for a wide range of scientific disciplines and applications such as microclimate and light regime studies (e.g. Bittner et al., 2012; Parker, 1995) or for assessing the effects of air pollution on tree vitality (e.g. Fleck et al., 2012).

Leaf area is commonly defined in relation to ground area and expressed as the leaf area index (LAI). Various definitions of LAI exist, accounting for differences in the shape of leaves and needles, and in the shape of flat and non-flat leaves (see Gonsamo, 2009, for a detailed discussion of the different LAI definitions). One of the most common definitions was given by Chen and Black (1992) who define LAI as half the total leaf area per unit ground surface area. Leaf area is also sometimes defined in relation to volume as foliage density, called the foliage area volume density (Jupp et al., 2008). Methods for determining LAI can be grouped into direct and indirect methods. The direct methods comprise destructive sampling and litter fall measurements; the indirect methods are based on direct leaf contact such as the inclined point quadrat (Warren-Wilson, 1960) or on indirect optical measurements of light attenuation within the canopy (e.g. Jonckheere et al., 2004).

The main limitation of the direct LAI methods is their practical feasibility on a large scale. Therefore, the indirect optical ground-based remote sensing methods are used more routinely (e.g. Strahler et al., 2008). These can be further distinguished depending on their source of radiation, i.e. passive optical sensors utilizing the sun's radiation and active optical sensors providing their own source of radiation (e.g. Zheng and Moskal, 2009). Of the passive optical methods, hemispherical photography has become prevalent for a number of reasons, most notably for the ability to capture the canopy structure, i.e. providing an image of the spatial distribution of leaves, branches, stems, and gaps within the canopy (e.g. Frazer et al., 2001; Jonckheere et al., 2004). Other passive optical methods are not able to resolve the canopy structure (i.e. they average the incoming radiation to yield LAI), which constitutes one of their main limitations. The use of hemispherical photography to determine LAI and related

structural parameters is treated in more detail in Section 4.1. Active optical LAI sensors (i.e. terrestrial laser scanning) are discussed in Section 4.2.

3.2   Stocking, stem diameter, tree height

Standard forest inventory includes the measurement of the core structural parameters stocking (tree density), stem diameter, and tree height. These are usually carried out on a sub-sample of all trees within the inventory plot with the sample size depending on the sampling scheme applied. To standardize measurements for state and national inventories, special sampling designs such as concentric circular plots or point sampling based on the *Bitterlich* method were developed (e.g. Kangas and Maltamo, 2009; Van Laar and Akça, 2007).

To derive stocking, the number of trees within the inventory plot is recorded but usually without measuring exact tree locations. Stem diameter is measured at a standard stem height of 1.3 m (diameter at breast height or short DBH) using a tape or caliper; tree height is mainly determined using instruments based on trigonometry such as hypsometers (Van Laar and Akça, 2007). DBH and tree height are traditionally used to estimate tree volume and biomass based on species-specific allometric equations, standard volume tables or form factors (e.g. Pretzsch, 2009; Van Laar and Akça, 2007).

The standard inventory measurements of the core structural parameters are manual, which means that their accuracy is affected by an operator bias (e.g. Köhl et al., 2006; Van Laar and Akça, 2007). It is, however, difficult to quantify the proportion of this operator bias to the total measurement uncertainty, due to the difficulty to obtain unbiased control measurements and due to the general interference of different systematic and random error components (e.g. Berger et al., 2012; Köhl et al., 2006). In addition, site and stand properties such as slope, stand density or canopy layering impact the magnitude of measurement errors, most notably for tree height measurements (e.g. Van Laar and Akça, 2007).

As "true" forest reference measurements are hardly feasible (due to the size of trees), real accuracies are rarely specified for the standard inventory methods. Instead, the measurement uncertainty is usually expressed by the variability of repeated measurements, i.e. its precision (e.g. West, 2009). However, care should be exercised when comparing precision values from different studies because the calculation of precision is sensitive to small samples and outliers (Van Laar and Akça, 2007). Another drawback of the manual inventory measurements is that

they are time-consuming and therefore often limited in their temporal and spatial sampling. With regard to the use of the core structural parameters for forest growth modelling, Pretzsch (2009) points out that while "stand structure parameters are useful for analyzing and modeling forest stands dynamics", they are usually based on stand-level inventory measurements that are not spatially explicit and therefore unable to capture the three-dimensionality of stand structure, its most important trait.

4   Ground-based remote sensing

Ground-based remote sensing techniques have received increased attention in forestry and forest science due to the main limitations of the traditional measurements of forest structural parameters, namely the limited spatial and temporal coverage (resulting from the time-consuming data collection), the lack of an explicit spatial description of stand structure and the potential measurement error associated with an operator bias of the manual methods (e.g. Kangas and Maltamo, 2009). In this work, the focus lies on exploring both a technique well established in canopy structural analysis (hemispherical photography) and a state-of-the-art technique (terrestrial laser scanning) which has shown great promise for the retrieval of the standard inventory parameters and for canopy structural analysis.

4.1   Hemispherical photography

As already mentioned in Section 3.1, the ability to resolve canopy structure is the main advantage of hemispherical photography over the other passive optical instruments. Since hemispherical cameras are also comparatively cheap, easy to use, and do not rely on above-canopy measurements required for most other passive optical instruments, they have become widely used tools for canopy structural analysis.

Hemispherical photography (HP) or digital hemispherical photography (DHP) combines the use of commercial cameras and specialized hemispherical lenses to derive forest canopy structural parameters such as LAI, gap fraction, and canopy cover. As the name implies, the hemispherical lenses, also called fisheye lenses, produce a hemispherical image projection. Fisheye lenses can differ in their angle of view (e.g. capturing the full 180° hemisphere, called circular fisheye lenses, or capturing less than 180°, called full-frame fisheye lenses) and in their image distortion. For canopy structural analysis, the camera is usually mounted onto a tripod, pointed upwards, oriented, and levelled. Photos are then taken based on a number of specific camera settings (see Walter, 2009, for a detailed treatment of the hemispherical photo acquisition).

To derive canopy structural parameters, the most important step is the thematic classification of the hemispherical photo, i.e. the image pixels have to be separated into sky and canopy (foliage, wood) pixels. This separation, which is also referred to as thresholding, can be

carried out manually or automatically (using special image processing techniques) and can be based on either individual image channels or on the RGB colour image (e.g. Jonckheere et al., 2005; Walter, 2009). The proportion of sky pixels to total image pixels is taken as the gap fraction which, given certain theoretical assumptions about the canopy structure such as a random distribution of foliage, represents the gap frequency, i.e. the probability of non-interception of light passing through the forest canopy (e.g. Weiss et al., 2004). This gap probability or gap fraction is related to LAI according to the Monsi and Saeki (1953) formulation of the Lambert-Beer law, which is the common theoretical framework for the indirect optical LAI methods:

$$\text{Pgap}(\theta) = e^{-G(\theta)\text{LAI}/\cos(\theta)} \tag{1}$$

Where Pgap is gap probability, G is the foliage projection function toward a zenith angle θ, and the cosine of θ is used to account for different path lengths through the canopy as a function of zenith angle. Different solutions have been proposed to solve Equation (1) and the unknown G function (e.g. Lang, 1986; Miller, 1967). Particular modifications of Equation (1) have been proposed as in reality the distribution of canopy elements often deviates from the assumption of randomness (e.g. leaves are clumped around branches, tree crowns are clumped into tree clusters) and woody canopy elements contribute to the light interception. These modifications account for the deviations by including correction factors such as the clumping index and the wood area index (see Weiss et al., 2004, for a detailed review). Since these factors cannot be measured directly, they are usually inferred from hemispherical photos (e.g. Leblanc et al., 2005).

Despite its establishment as a standard method for retrieval of canopy structural parameters, DHP is also subject to measurement uncertainties. These stem from effects of camera settings such as image resolution and exposure (e.g. Frazer et al., 2001; Macfarlane et al., 2000), camera and lens type (e.g. Greve, 2010; Inoue et al., 2004) as well as threshold type and algorithms (e.g. Jonckheere et al., 2005; Leblanc et al., 2005; Nobis and Hunziker, 2005). This variety of influences is also the main reason why the acquisition and processing of hemispherical photos has not been successfully standardized to yield consistent estimates of LAI and gap fraction so far. One major drawback that DHP shares with other passive optical sensors is the sensitivity to variable sky illumination conditions, i.e. a diffuse sky illumination is required to warrant reliable and consistent measurements (e.g. Strahler et al., 2008). Direct sunlight in particular distorts the passive optical measurements and these distortions cannot be

corrected effectively. As ideal diffuse sky illumination conditions are sometimes hard to come by depending on weather conditions, the application of passive optical LAI sensors can be severely limited (e.g. Jupp et al., 2008). The use of active optical sensors such as terrestrial laser scanning is the only real solution to overcome this problem as these sensors have an own light source and are much less sensitive to ambient light conditions (e.g. Ramirez et al., 2013; Zhao et al., 2011). In addition, passive optical sensors are at best 2-D (Zheng and Moskal, 2009), hence they cannot resolve the three-dimensionality of canopy structure, an important characteristic of forest stand structure and key to individual tree growth conditions (Pretzsch, 2009). This limitation is also of relevance to the retrieval of the clumping index as clumping is a 3-D structural characteristic; the use of 2-D hemispherical photos to estimate such a 3-D parameter is therefore inherently limited.

4.2   Terrestrial laser scanning

Terrestrial laser scanning (TLS), also referred to as terrestrial LiDAR (Light Detection and Ranging), is an active optical ranging sensor based on the emission of a highly collimated laser pulse and the detection of potential pulse returns. These can be registered by the scanner if the emitted laser pulse is reflected diffusely by a target. If the pulse is reflected specularly (i.e. mirror-like), no return signal is registered. The distance between scanner and target can be measured based on different range measurement principles, the most common of which are the phase-shift and the time-of-flight principles (Newnham et al., 2012).

While the phase-shift is based on measuring the phase difference between the emitted and received continuous laser beam, the time-of-flight principle is based on measuring the time difference between the emission of a discrete laser pulse and the registering of a reflected return pulse (e.g. Van Genechten, 2008). Phase-shift scanners can only record a single range per emitted pulse; time-of-flight scanners can record multiple ranges per emitted pulse or even continuously record the pulse returns as a waveform (Newnham et al., 2012). The ranging principles also differ in a number of key scanner properties such as maximum range, range errors, and scan speed (e.g. Dassot et al., 2011).

However, both scanner systems yield explicit spatial information, i.e. a target's position relative to the scanner's beam emission point as well as the intensity of the return pulse, which allows the target identification assuming known target reflectance properties. Based on

the rotation of the scanner head and optics around the vertical and horizontal axes, a 3-D model of the scanner's surroundings can be obtained. This property constitutes one of the main advantages of TLS over the conventional inventory and canopy structural measurements (e.g. Zheng and Moskal, 2012, see also Sections 3.1 and 3.2) and potentially allows the direct determination of tree volume and biomass. In addition, TLS bears the potential to provide objective and consistent though not necessarily unbiased measurements as was shown by a number of studies (e.g. Lovell et al., 2011; Maas et al., 2008; Tansey et al., 2009). Another major advantage of TLS is that not only the scan data acquisition and processing but also the extraction of information from the scan data can be automated, therefore reducing the data workload and acquisition duration. This, in turn, enables the collection of larger samples, both spatially and temporally.

With regard to the core forest structural parameters, TLS was used to successfully estimate stocking (e.g. Litkey et al., 2008; Strahler et al., 2008), DBH (e.g. Brolly and Király, 2009; Lovell et al., 2011), tree height (e.g. Antonarakis, 2011; Kankare et al., 2013; Maas et al., 2008), and LAI (e.g. Jupp et al., 2008; Henning and Radtke, 2006; Moskal and Zheng, 2012). However, the measurement accuracies achieved in these studies vary strongly: RMSEs for DBH range from 1.48 cm (Maas et al., 2008) to 8 cm (Yao et al., 2011), RMSEs for the number of detected trees within the test plots range from 22 % (Thies and Spiecker, 2004) to 100 % (Tansey et al., 2009), RMSEs for tree height range from 1.54 m (Kankare et al., 2013) to 4.55 m (Maas et al., 2008), and R² for TLS-derived LAI with LAI derived from other indirect optical sensors range from 0.3 (Zhao et al., 2011) to 0.87 (Zheng et al., 2013).

Stem volume (e.g. Kankare et al., 2013) and biomass (e.g. Holopainen et al., 2011; Kankare et al., 2013; Yao et al., 2011) were also retrieved with TLS. Yao et al. (2011) estimated stand-level above-ground biomass from TLS-derived stem diameters and stocking and achieved a RMSE of 21.54 t/ha. Based on harvesting of 64 trees, Kankare et al. (2013) developed tree species-specific linear models relating components of above-ground biomass (total, stem, and branch biomass) to TLS-based features such as crown height and stem volume. They found average RMSEs of 12.4% for total above-ground biomass, 15.7% for stem biomass, and 30.2% for branch biomass.

The variability in estimation accuracy of structural parameters observed through these studies is to a large degree due to differences in methodology (e.g. scan mode, scan data processing

and algorithms, reference data), in stand characteristics (e.g. tree species, stand density and development phase, canopy layering), in laser scanner properties (e.g. ranging principle and errors, laser wavelengths, beam divergence) and laser scan properties (e.g. scan resolution, integration time). These fundamental differences make it difficult to compare the findings of previously published studies and impede a comprehensive analysis of the potential of TLS for estimating forest structural parameters. Above all, this necessitates a systematic assessment of the above-mentioned factors. To date, only few studies have contributed to such an approach and they also rather focus on single isolated factors. These include the influence of scan mode (Maas et al., 2008; Thies and Spiecker, 2004), of circle fitting for DBH estimation (Brolly and Király, 2009; Tansey et al., 2009), of scanner properties (Danson et al., 2008; Newnham et al., 2012), and of LAI model parameters (Béland et al., 2014).

In addition, most of the previously published studies were only experimental, i.e. they focused on investigating the general potential of TLS to estimate forest structural parameters instead of on the potential of its practical use in forest inventory and other applications. Nevertheless, the majority of these studies have contributed to the bigger picture by demonstrating the advantages, limitations, and challenges of TLS for the retrieval of forest structural parameters. Establishing such a framework is crucial for defining future research directions. Above all, assessing the limitations is an important part in the evaluation of a method as they usually define its practical application. For TLS, the effect of occlusion was shown to be the major limitation in its application for forest structural analysis (e.g. Béland et al., 2014; Watt and Donoghue, 2005; Yang et al., 2013).

Occlusion refers to the shadowing of background objects by foreground objects that both lie in the same path of a laser beam. The magnitude of this effect mainly depends on stand structure, laser scanner properties, and the number of scans and their positions relative to surrounding objects. Occlusion can be so severe as to impede the retrieval of certain structural parameters. As TLS scans from below the canopy, this particularly affects measurements of the upper canopy structure such as tree height. For example, retrieving tree height proved to be impossible due to the dense canopy of a Corsican pine stand (Tansey et al., 2009) or only possible with gross error margins of up to 10 m as reported by Antonarakis (2011). Occlusion also strongly impacts canopy structural analyses such as gap probability and LAI, especially those based on 3-D TLS point clouds (e.g. Hilker et al., 2010)

5   Research objectives and outline of the PhD thesis

Sections 1 and 2 illustrated the importance of the core forest structural parameters stocking, DBH, tree height, and LAI to forest growth modelling as these are routinely used to infer above-ground biomass components. The manual methods traditionally used to measure these parameters were addressed along with their main limitations in Section 3. In Section 4, two ground-based remote sensing techniques, one well established (DHP), the other state-of-the-art (TLS), were presented. Their potential to overcome the limitations of the manual methods, and issues that necessitate further research were described. Despite the distinct advantages of TLS over DHP for canopy structural analysis (see Section 4), DHP was deliberately included in the overall research concept. This is because, at present, TLS is far from being as cost-effective as DHP. Therefore, it is foreseen that DHP will remain the standard method of LAI retrieval for some time, which in turn necessitates the standardization of the hemispherical photo acquisition and processing.

The issues that demand further research are similar for digital hemispherical photography and terrestrial laser scanning insofar as they deal with factors influencing the retrieval of the core structural parameters from these methods. As a comprehensive and systematic assessment of the various influences and their interrelations is still lacking, the main general research objective of this PhD thesis was to investigate factors that were not or only scarcely the focus of previous research. This included optimizing the retrieval of the core structural parameters stocking, DBH, and LAI (i.e. standardizing the data processing and parameter extraction) in order to provide unbiased and consistent in situ measurements that could be used to calibrate and evaluate forest growth models. Due to the unreliability of TLS tree height measurements, which results from the effect of occlusion (see Section 4.2), the estimation of tree height was not attempted in this thesis. Instead the extraction of stem diameter height profiles to infer stem volume was tested.

In the context of forest growth modelling, the second main research objective of this thesis was to investigate whether estimates of the above-mentioned structural parameters including stem volume derived from ground-based passive and active optical remote sensing sensors can, in practice, be used to calibrate an eco-physiological forest growth model. Thereby, it is intended to exemplify the possible integration of RS-data into growth modelling (see Section

2). As part of these two general objectives, the following specific research objectives were formulated:

(1)   To assess the influence of external (exposure) and camera internal factors (radiometric image resolution, file format, and image band), and choice of threshold algorithm on the retrieval of gap fraction, LAI, and clumping index from hemispherical photography. Based on these evaluations, the focus then was to develop a standardized processing of hemispherical photos to warrant consistent and reproducible estimates of gap fraction and LAI (Chapter II).

(2)   To explore the potential of phase-shift terrestrial laser scanning to derive consistent estimates of gap fraction and LAI by assessing the effects of the main scan properties scan resolution (angular step size) and scan speed (pulses per second) as well as a scanner-specific noise compression and firmware based data filtering on the retrieval of these structural parameters. The comparison with the direct LAI method of litter fall measurement was also a primary aim of this investigation (Chapter III).

(3)   To explore the potential of phase-shift terrestrial laser scanning to retrieve stocking, stem diameter and volume by assessing the effects of circle fitting and TLS scan mode (Chapter IV) as well as the effects of scan resolution, scan speed, scanner-specific noise compression and firmware based data filtering (Chapter V) on the parameter retrieval.

(4)   To investigate the potential use of measurements of the core structural parameters stocking, DBH, and LAI derived from hemispherical photography and terrestrial laser scanning to calibrate an eco-physiological forest growth model. The comparison with model calibrations based on long-term growth data and conventional forest inventory data was also part of this study (Chapter VI).

Figure 2 depicts how these specific research objectives are embedded in the structure of the dissertation. The Chapters II–V each constitutes a peer-reviewed journal publication. Chapter VI ties the research objectives of these publications together in a final study on forest growth modelling. In Chapter VII a summary of the achieved specific objectives and how they relate to the general research objectives of the dissertation is presented. The implications of these findings for future research directions are also discussed.

Chapter I
Introduction:
Forest structure and growth modelling
Structural parameters
Ground-based remote sensing

Chapter II
An efficient approach to standardizing the processing of hemispherical images for the estimation of forest structural attributes

Gap Fraction and Leaf Area Index

Chapter III
Retrieval of gap fraction and effective plant area index from phase-shift terrestrial laser scans

Chapter IV
The influence of scanner parameters on the extraction of tree metrics from FARO Photon 120 terrestrial laser scans

Stocking, Stem Diameter and Volume

Chapter V
The influence of scan mode and circle fitting on tree stem detection, stem diameter and volume extraction from terrestrial laser scans

Chapter VI
Calibration of a forest growth model based on ground-based remote sensing measurements and long-term growth data

Chapter VII
Synthesis:
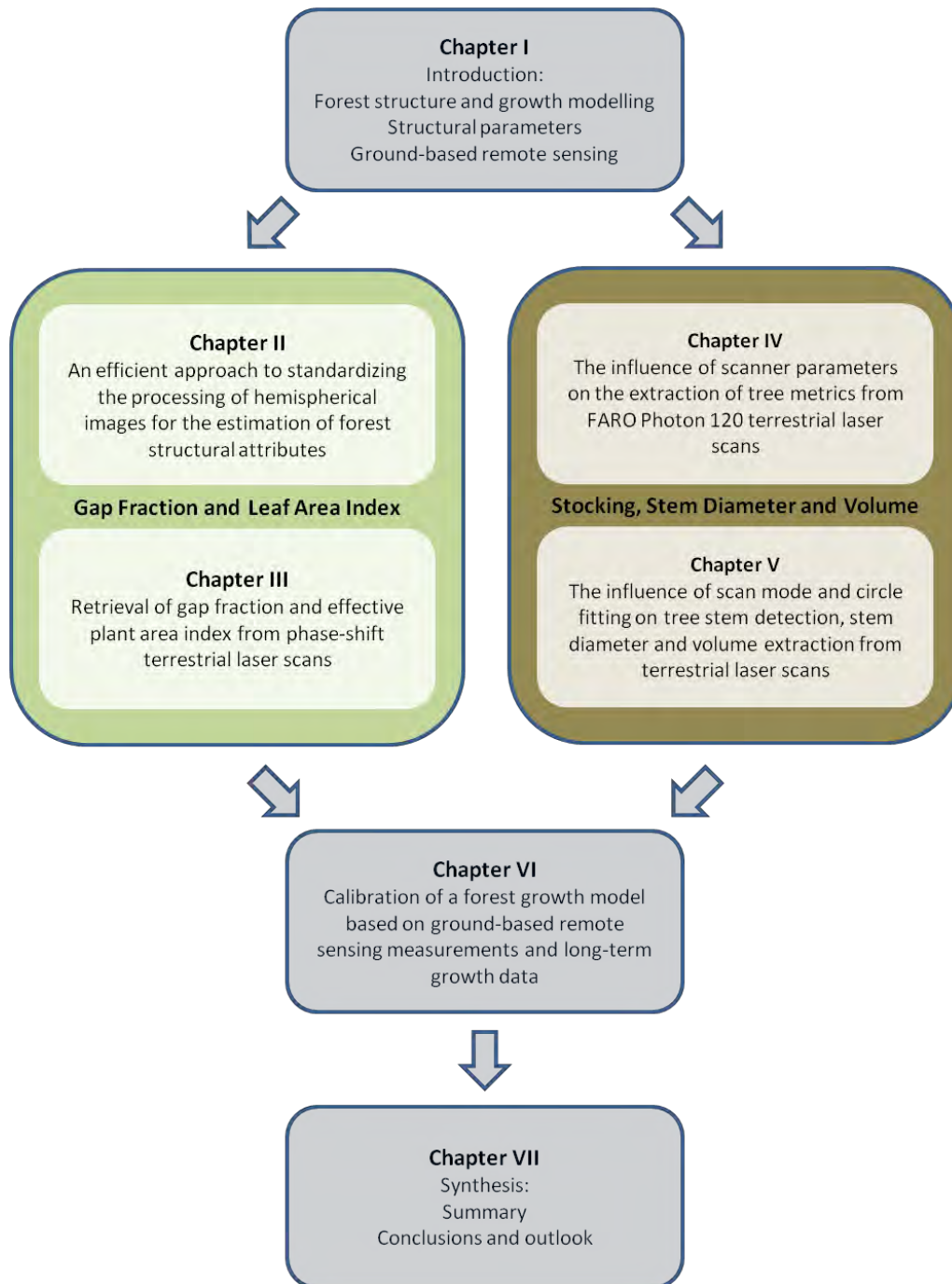Summary
Conclusions and outlook

Figure 2: Structure of the cumulative dissertation. Chapters I, VI, and VII constitute the framework for the main research part of the thesis made up of 4 peer-reviewed journal publications. Chapter II covers the research objective 1, Chapter III covers objective 2, and Chapters IV and V cover objective 3. Chapter VI ties these research objectives together in a final study on forest growth modelling (objective 4).
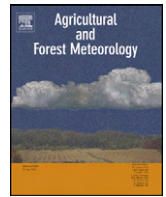
Chapter II: An efficient approach to standardizing the processing of hemispherical images for the estimation of forest structural attributes

Pyare Pueschel, Henning Buddenbaum, Joachim Hill

An efficient approach to standardizing the processing of hemispherical images for the estimation of forest structural attributes

Pyare Pueschel*, Henning Buddenbaum, Joachim Hill

Department of Environmental Remote Sensing and Geoinformatics, University of Trier, D-54286 Trier, Germany

ARTICLE INFO

ABSTRACT

Digital hemispherical photography (DHP) has become a widely used tool for the estimation of forest structural attributes, such as gap fraction, Leaf Area Index (LAI), effective Plant Area Index (PAI_e), and clumping. This development was boosted not only by a rapid technical advance in the field of digital photography but also by the inherent advantages of DHP for in situ measurements of forest structural attributes. However the major drawback of using DHP for the estimation of forest structural attributes is the lack of standardization which impedes a consistent compatibility with other indirect methods. This lack of standardization is mainly due to uncertainties introduced at the stage of image acquisition and processing. Of these, the determination of optimum exposure and thresholding in the image processing chain are two major influences. In this work influences on the estimation of forest structural attributes, namely the radiometric image resolution, the file format and the image band selection, were studied, in particular with regard to the inter-dependence with exposure and the threshold algorithm applied. For this purpose four different automatic threshold algorithms (Ridler, Otsu, Minimum, Isodata) were tested. Results show that the file format and the image band selection influence the estimation of gap fraction, PAI_e and clumping indices. The magnitude of this effect however varies with the threshold algorithm applied, i.e. with a strong effect for the Minimum and Isodata algorithms and little effect for the Ridler and Otsu algorithms. The radiometric image resolution was found to cause only a marginal effect. Based on a comparison with LAI-2000 measurements it could also be demonstrated that the file format and the image band selection affect the determination of the optimum exposure. To resolve these issues an efficient approach to standardizing the processing of hemispherical images is proposed. This approach constitutes the stacking of five differently exposed hemispherical images and passing them to an automated clustering algorithm (Isodata) with the subsequent generation of gap fraction images. The resulting PAI_e estimation performs better than or comparably to the estimation based on optimally exposed single images. In addition to being robust and objective, our approach provides consistent compatibility with the LAI-2000.

© 2012 Elsevier B.V. All rights reserved.

1. Introduction

1.1. Ground-based measurements of Leaf Area Index

Ground truth or ground lies? The importance of ground reference data for the validation of remotely sensed parameters is out of question. However, as remote and ground measurements both suffer from various degrees of measurement uncertainties the prime challenge is to minimize their magnitude. This is no trivial task especially when considering forest structural attributes which practically only allow for indirect measurements. One of these parameters is the Leaf Area Index (LAI), commonly defined as half the total leaf surface area per unit ground surface area

(Chen and Black, 1992). Since these parameters are routinely used to drive ecophysiological models, the accuracy of their estimation is of particular interest. While absolute accuracy may be difficult to achieve due to limitations of indirect measurement concepts, at least relative accuracy (i.e. comparability) between different indirect methods is a minimum requirement.

Ground-based methods for the estimation of LAI can be grouped into direct and indirect methods (Jonckheere et al., 2004; Zheng and Moskal, 2009). While the former are assumed to provide values closest to the true LAI (Chen et al., 1997), they are time-consuming and therefore only applicable on a small scale – especially in forest environments. By contrast the indirect methods which are mostly based on optical measurement of light transmission or attenuation within vegetation canopies allow for quick and easy LAI estimation, but rely on a number of theoretical assumptions (e.g. random distribution of foliage elements) that are not always fulfilled. Since the clumping of plant parts at various scales or the attenuation of light

by stems and branches need to be considered, the optical methods do not represent exact measurements of LAI (Jonckheere et al., 2004). To account for this, terms like Plant Area Index (PAI) and effective Plant Area Index (PAI_e) or effective Leaf Area Index (LAI_e) were coined (Weiss et al., 2004). Among the optical methods, digital hemispherical photography (DHP) has become a widely used tool for the ground-based estimation of LAI and related attributes. While there are clear advantages of using DHP (e.g. ease of measurement, flexibility and low costs, permanent record of canopy structure, ability to determine clumping), one major drawback of DHP is the lack of standardization, preventing consistent comparability with other indirect methods (e.g. the Licor LAI-2000 Plant Canopy Analyzer, hereafter referred to as LAI-2000). Since neither the Licor LAI-2000 measurements nor the hemispherical images acquired for this study allow the separation of the incoming radiation that is intercepted by woody elements from that intercepted by green tissue, the acronyms PAI and PAI_e (PAI not corrected for clumping) rather than LAI and LAI_e are used in this paper, except when referring to the basic LAI methodology and theory.

1.2. Hemispherical photography

This lack of standardization is due to many influences, which can be roughly grouped into uncertainties introduced at the stage of image acquisition and uncertainties introduced at the stage of processing the acquired images. During image acquisition factors like exposure (Chen et al., 1991; Macfarlane et al., 2000; Zhang et al., 2005), camera type, image format and size (Frazer et al., 2001; Inoue et al., 2004) as well as variable sky brightness (Clark, 2009; Zhang et al., 2005) all affect the calculation of gap fraction and hence the estimation of PAI_e. At the processing stage factors like gamma correction (Thimonier et al., 2010; Macfarlane et al., 2007), image sharpening (Walter, 2009; Macfarlane et al., 2000), image band selection for thresholding, type of thresholding (manual/automatic) and threshold algorithm (Nobis and Hunziker, 2005; Leblanc et al., 2005; Jonckheere et al., 2004, 2005) influence the determination of gap fraction and related attributes.

Of all the uncertainties associated with hemispherical photography, thresholding and exposure are two, if not the two, major influences for the estimation of forest structural attributes (Chen et al., 1991; Jonckheere et al., 2005). Both affect the discrimination of canopy elements from sky. However any threshold algorithm can only be as good as the ability of the hemispherical image to represent the true canopy structure. This ability is mainly controlled by exposure. Determining the correct exposure is however a difficult issue, particularly because hemispherical images tend to exhibit overexposure close to vertical directions and underexposure close to horizontal directions (Zhang et al., 2005). Another issue is the influence of exposure on the discrimination of gaps of different sizes. While large inter-crown gaps are relatively insensitive to changes in exposure, small intra-crown gaps are extremely sensitive to changes in exposure, i.e. getting over-proportionally lost upon underexposing. For this reason dense forest stands are much more affected by changing exposure than open stands. This issue of correct exposure was investigated by Zhang et al. (2005) who developed a protocol for determining the optimum exposure irrespective of forest stand density. They propose determining the sky exposure in a very large opening, acting as reference from which the in-stand exposure is attained by increasing the shutter speed by two stops with the aperture unchanged at F5.3 (or similar).

While the approach by Zhang et al. (2005) is theoretically sound, the most important drawback of the proposed protocol is the limited availability of very large openings for the determination of sky exposure in many forested areas. This is acknowledged by the authors who suggest (alternatively) measuring sky reference exposure through a large canopy gap using a tele-lens. However even

large canopy gaps can be difficult to find sometimes, especially for very dense forest patches. The remaining problem condenses to the basic difficulty of all LAI-methods which require reference measurements (LAI-2000, approach of Cescatti, 2007): Spatially and temporally variable sky brightness conditions can severely limit their application. Based upon the approach by Cescatti (2007), Lang et al. (2010) propose a promising method to overcome the lack of an above-canopy reference by combining a sky radiance model with radiance values obtained from gaps of the below-canopy image. Another constraint with regard to the approach by Zhang et al. (2005) is the fact that they based their analysis on specific camera and image processing settings, i.e. images were saved as 8-bit JPEGs and the blue band was selected for further processing. As pointed out by Jonckheere et al. (2005), high-dynamic range digital imagery has the potential to improve the discrimination of canopy elements from sky, thus yielding gap fractions potentially different from those resulting from low-dynamic range hemispherical images. Besides images saved in different file formats undergo a camera- and format-specific processing (compression, chroma subsampling, image sharpening, etc.) which potentially alters the distribution of DNs and hence influences any histogram-related analysis (i.e. thresholding). This raises the question whether, and if so how, the radiometric image resolution, file format and threshold algorithm affect the determination of the optimum in-stand exposure as suggested by Zhang et al. (2005). More generally the influence of exposure on forest structural attributes, namely gap fraction, PAI_e and clumping indices, as a function of the combined effects of the radiometric image resolution, file format and threshold algorithm should be investigated.

Thresholding of hemispherical images to derive gap fraction constitutes another issue of debate, in particular with regard to the choice of threshold type and algorithm. Even though the increased variability (i.e. uncertainty) which results from manual thresholding is widely acknowledged (Englund et al., 2000; Jonckheere et al., 2005; Leblanc et al., 2005; Korhonen et al., 2011; Zhao and Popescu, 2009), manual thresholding is nevertheless applied in many studies. This is due to the lack of an automatic algorithm that works satisfactorily for variable sky illumination conditions and for hemispherical images of forest stands of different structure. Jonckheere et al. (2005) extensively tested existing and easy-to-implement algorithms and were able to identify a few candidates. They were able to show that by applying a combination of global and local thresholds classification results can be improved, particularly in the case of variable sky brightness. Considering the liability of hemispherical photography to variations in hemispherical sky brightness, this approach constitutes a promising avenue for further research. Despite having been tested based on visual and quantitative analyses, the gap fraction and PAI_e values produced by the different automatic algorithms (Jonckheere et al., 2005) were not validated with independent data, such as LAI-2000 measurements. Another crucial issue which is to be considered is the fact that since a hemispherical image and its histogram are the outcome of a delicate interplay between a number of factors (exposure, sky brightness, canopy structure, camera settings, etc.), the choice of the threshold algorithm naturally affects the estimation of forest structural attributes. Conversely since threshold algorithms differ in their sensitivity to changes in the histogram, the effects of those factors on the estimation of canopy parameters should also vary. This is to be considered when assessing potential influences (such as the radiometric resolution or the file format) and determining the optimum exposure.

An additional problem is related to the appropriate image band selection for thresholding. Most research concerning hemispherical photography makes use of the blue band for producing the necessary binary images, since it is in the blue part of the visible spectrum that leaves exhibit maximum absorption and lowest

scattering, hence theoretically offering maximal contrast between sky and canopy (Jonckheere et al., 2005). Besides, using the blue band ensures compatibility with measurements made with the LAI-2000 which operates below 490 nm. However it is well known that the blue band usually suffers more from the effect of blooming near the zenith and in large openings than the red and green bands (Leblanc et al., 2005). Some studies have used more than one band to improve the discrimination between sky and canopy elements (Chapman, 2007; Kucharik et al., 1997). However this approach suffers from the drawback of the limited capability of most threshold algorithms and hemispherical image analysis software to handle multi-channel images. To our knowledge no systematic analysis of the influence of the image band selection on the estimation of forest structural attributes has been published so far. As in the case of the radiometric image resolution and file format this raises the questions how the image band selection in combination with different threshold algorithms affects the estimation of forest structural attributes and the determination of the optimum in-stand exposure.

Based on these unresolved research issues the following objectives for improving the standardized processing of hemispherical images emerged:

- Assess the influences of the radiometric image resolution, file format and image band selection on the estimation of forest structural attributes (gap fraction, PAI_e, clumping indices) and how these influences interact with the different threshold algorithms and the determination of optimum exposure.
- Develop a flexible approach to determine the optimum exposure independent of any reference exposure measurements.
- Further explore the potentials of multi-channel thresholding and develop a robust and objective approach to automatic image thresholding.

2. Materials and methods

2.1. Study site description

This study was carried out as part of a comprehensive data collection campaign which aims at estimating forest bio-physical and structural attributes from airborne hyperspectral and laser scanning data. This campaign serves as preparation for the German Hyperspectral satellite mission EnMAP and was located in the *Pfälzerwald* forest near Kaiserslautern, Germany, where the EnMAP Core Science Team forest research group at the University of Trier established one of its main research sites (Merzalben, 49°16′N, 7°48′E).

During an extensive field validation at the EnMAP core site *Merzalben* in August 2010 a total of 24 plots (30 m × 30 m) in mostly mixed beech-oak stands were sampled for key inventory parameters and PAI_e reference data, collected with the LAI-2000. Test plots were established across stands of different canopy structure in order to cover a wide range of PAI_e values (Table 1).

2.2. Experimental methods

At 16 of the 24 plots digital hemispherical images were acquired simultaneously to study the effects of the radiometric image resolution, file format and image band selection on the estimation of forest structural attributes.

Hemispherical images were taken with a Nikon D300 digital camera in combination with a Circular Fisheye lens (Sigma 4.5 mm F2.8 EX DC HSM). The camera was set to exposure-priority mode (metering method: matrix) with the aperture fixed at F6.3 and in order to re-evaluate the influence of exposure we adopted the following exposure scheme, utilizing the bracketing function of digital

cameras: Images were consecutively taken from automatic exposure to four stops of underexposure. Images were saved both as 16-bit RAW and as 8-bit JPEG (basic quality). Noise reduction was turned off and in order to minimize camera motion, automatic release was applied.

As far as the sampling scheme is concerned, 5 simultaneous measurements were obtained per plot, – one at the center of the plot and the other four located at the corners. To ensure maximum comparability between the simultaneous PAI_e measurements, both the digital camera and the LAI-2000 were mounted on tripods, horizontally leveled and measurements were taken at the same height (approx. 1.3 m) and sampling positions. The LAI-2000 was operated in remote mode without view restriction.

Since sky illumination is one of the most critical aspects of the indirect optical LAI methods, all measurements were taken under uniform sky conditions (i.e. either overcast sky or around sunset/sunrise). Due to technical problems with the LAI-2000 instrument data from 8 plots had to be excluded from the comparative analysis with the hemispherical images, leaving a total number of 40 simultaneous measurements, which still cover the full PAI_e range observed.

2.3. Threshold algorithms

One of the main goals of this study was to compare the influence of the file format (JPEG, RAW/TIFF) and the radiometric resolution (8-bit, 16-bit) on the estimation of forest structural attributes and how these effects relate to the threshold algorithm applied. The choice of threshold algorithms was, however, limited by the availability of software packages able to handle both 8-bit and 16-bit images. Due to the large amount of hemispherical images, another requirement for the software packages was to provide batch processing. The freeware ImageJ – Image Processing and Analysis in Java (http://rsbweb.nih.gov/ij/) along with the plugins Multi-Thresholder (Baler et al., 2009) and Auto Threshold (Landini, 2011) meets both requirements.

After pre-analysis on a subset of the hemispherical images (i.e. comparing the resulting values with LAI-2000 measurements), the three global threshold algorithms Isodata (Ridler), Minimum and Otsu were selected as candidates for further analysis. The Isodata algorithm by Ridler and Calvard (1978) constitutes an iterative clustering which increments the threshold (as the average of the background and foreground) until the thresholds of the iterations converge. The Minimum algorithm (Prewitt and Mendelsohn, 1966) is a histogram shape-based algorithm which assumes a bimodal distribution of digital numbers (DNs). The threshold is found at the minimum between the two local maxima which are searched for by smoothing the histogram with a running average of size 3. The Otsu algorithm (Otsu, 1979) is a clustering algorithm which searches for the threshold that minimizes the intra-class variance. For a more detailed treatment of threshold algorithms see the overview by Sezgin and Sankur (2004) and/or the assessment by Jonckheere et al. (2005).

Furthermore we tested the Isodata algorithm by Ball and Hall (1965) as it allows for multi-layer clustering. Based on iterative optimization Isodata represents a clustering approach for finding optimal data partitions. The main user input for the algorithm is the number of clusters. The algorithm starts by distributing cluster means evenly in the (multi-dimensional) data space. The remaining pixels are then iteratively clustered around these means using minimum distance techniques. In each iteration updated means are calculated and the clustering is repeated. The algorithm converges either when the maximum number of iterations is reached or when less than a specified fraction of pixels changes clusters between iterations. This clustering approach guarantees local but not necessarily global optimization as different starting points can lead

Table 1
Description of the subset of test stands used in this study.

Plot	Dominant species	Development stage	Storey description[a]	Layers	DBH mean [cm]	DBH StDev [cm]	Height mean [m]	Height StDev [m]	Stem Density [n ha^{-1}]
1	Beech/oak	Maturing	Single main storey	Main	38.6	10.6	25.8	6.0	300
2	Oak	Maturing	Second storey	Main	33.6	17.6	27.7	2.6	1278
	Beech	Dimensioning		2nd	13.2	10.4	15.5	4.9	
3	Oak	Maturing	Second storey	Main	44.2	10.4	29.3	5.2	933
	Beech	Dimensioning		2nd	13.2	4.8	16.0	5.3	
4	Oak	Maturing	Second storey	Main	43.0	9.0	30.7	2.0	967
	Beech	Dimensioning		2nd	13.2	5.3	14.7	5.7	
5	Oak	Maturing	Second storey	Main	42.4	10.2	28.2	6.5	1100
	Beech	Dimensioning		2nd	13.4	8.1	15.3	5.3	
6	Beech	Maturing	Single main storey	Main	41.1	10.9	32.0	3.7	300
7	Oak	Maturing	Second storey	Main	39.2	18.6	25.1	9.2	1011
	Beech	Dimensioning		2nd	13.4	6.1	14.4	5.4	
8	Oak	Qualification	Single main storey	Main	6.9	3.5	13.0	–	7644

[a] Storey description according to FutMon (2009). Mean site elevations range from 540 m to 560 m, mean site slopes from 2° to 8°.

to different solutions. Despite this limitation, the fact that computational requirements are bearable makes the approach attractive (Duda et al., 2001), in particular for our case where the objective solely aims at the identification of the cluster with the maximum brightness characteristics (i.e. sky). Besides its efficiency, another advantage of the Isodata algorithm is the fact that it is implemented in many standard spatial data analysis software packages. Since the threshold algorithm by Ridler and Calvard basically constitutes the Isodata algorithm run with two clusters, the former is hereafter referred to as the Ridler algorithm.

To allow for a fully automatic and objective processing of hemispherical images based on the Isodata algorithm, the selection of the cluster number as well as the allocation of clusters to the binary classes "sky" and "canopy" were dealt with as follows. Based on a sensitivity analysis, ten clusters were chosen for clustering (cf. Section 3.5). Binary images were then generated based on a simple decision rule where the cluster associated with the highest mean DN was assigned the value "1" (sky) while the remaining clusters were assigned the value "0" (canopy). In case that more than one cluster was associated with the class "sky", the respective clusters were manually assigned the value "1". This, however, solely occurred for images with a considerable variation of sky brightness, e.g. blue sky partly covered with clouds, conditions which are to be avoided for the acquisition of hemispherical images anyways. The procedure was implemented in a standard image processing environment (IDL/ENVI) which allows for batch processing.

2.4. Image processing and estimated canopy parameters

The images captured in Nikon's proprietary raw format (NEF) were saved as uncompressed 16-bit TIFFs using Nikon's software Capture NX 2.2.4. In order to isolate the effects of the radiometric resolution from the effects caused by the different file formats, the 16-bit TIFFs were rescaled to 8-bit TIFFs. To assess the differences in the estimation of forest structural attributes based on different image layers, the red and blue bands were selected for further image processing. As already pointed out the blue band is usually chosen for analysis even though it exhibits stronger blooming effects in the near-zenith and in large canopy gaps than the red and green bands (Leblanc et al., 2005). It is noteworthy that a large number of the hemispherical images acquired for this study exhibited a stronger blooming in the blue band over the full zenith angle range. The different aims of our comparative study resulted in the following combinations as input into the image processing chain: Blue band (8-bit JPEG), blue band (8-bit TIFF), blue band (16-bit TIFF), red band (8-bit JPEG), red band (8-bit TIFF) and red band (16-bit TIFF). For each of these combinations the five exposure levels (cf. Section 2.2) were processed with the previously mentioned threshold

algorithms. Furthermore a new approach to multi-channel thresholding was tested by stacking the differently exposed images and subjecting these stacks to the Isodata clustering algorithm by Ball and Hall (1965). The binary images derived from the thresholding were analyzed with the software WinScanopy to derive gap fraction, PAI$_e$ and clumping indices. To assess the differences in the estimates of these parameters based on different image layers, radiometric image resolutions and file formats, differences were tested for statistical significance with the Wilcoxon matched pairs signed rank test (as the differences are not normally distributed, a non-parametric test was chosen).

Since the number of mixed pixels as well as underexposure increase with higher zenith angle (Jonckheere et al., 2004; Leblanc et al., 2005), analysis of the hemispherical images was restricted to a zenith range of 0°–60°. For optimal comparability the fifth ring (61°–74°) of the LAI-2000 was excluded from further analysis and the same LAI calculation method (LAI-2000 method) was used. This method is based on the work of Miller (1967) who proposes an exact solution for the calculation of LAI (LI-COR, 1992):

$$LAI = 2 \int_0^{\frac{\pi}{2}} -\ln(T(\theta)) \cos\theta \sin\theta d\theta \tag{1}$$

$$LAI = 2 \sum_{i=1}^{5} -\ln(T(\theta_i)) \cos\theta_i \sin\theta_i d\theta_i \tag{2}$$

With the LAI-2000 method, equation 1 is integrated numerically by summing the weighted logarithms of the five individual zenith rings' average gap fractions (equation 2). This method is hereafter referred to as the linear LAI-2000 method (or linear averaging). In contrast to the LAI-2000, hemispherical images are able to capture gap fraction in zenithal and azimuthal direction and with a much higher resolution. This bi-directional resolving results in so-called gap fraction (sky grid) segments and enables applying a different approach to the calculation of LAI. Instead of taking the logarithm of the zenith rings' average gap fraction, the logarithms of the segments are taken first and then averaged over the respective zenith ring. This method is hereafter referred to as the logarithmic LAI-2000 method (or logarithmic averaging) and is commonly used for the determination of leaf clumping by relating the LAI derived from the linear averaging to the LAI derived from the logarithmic averaging (Lang and Xiang, 1986). The clumping index based on Lang and Xiang (1986) is hereafter referred to as CI-2000. Since a number of methods for the estimation of clumping exist, we included another widely used method (Chen and Cihlar, 1995) in the present study to test whether the potential influences (threshold algorithm, etc.) affect the estimation of clumping differently for the two methods. The Chen and Cihlar method compares the measured distribution of

gap lengths (or gap sizes) to the distribution that would be attained in case of randomly distributed foliage. In the present study the gap fraction distribution was determined based on gap size, an adaption of the Chen and Cihlar method implemented in WinScanopy. By manually selecting a threshold value, gaps are split into within-crown gaps and between-crown gaps, with the former assumed to being randomly distributed. Clumping is then found by relating the distribution of total gap sizes to the distribution of within-crown gaps. The clumping index based on the gap size distribution is hereafter referred to as CI-GSD.

3. Results and discussion

3.1. The influence of the radiometric image resolution and file format

In order to assess the influence of the radiometric image resolution on the estimation of forest structural attributes as a function of exposure and threshold algorithm and in order to isolate it from the effects caused by the file format, 200 hemispherical images (8 plots × 5 hemispherical images per plot × 5 exposure levels) were analyzed separately for each combination of file format and radiometric resolution. The median differences between these combinations are shown in Tables 2a and 2b. As can be seen the radiometric resolution has little effect on the estimated forest structural attributes – regardless of the selected image band and the threshold algorithm applied. By contrast the different file formats influence the estimation, however only with a significant magnitude for the images thresholded with the Isodata and Minimum algorithms – the reason for which will be discussed in connection with the comparison of the PAI_e estimates from the hemispherical images and the LAI-2000 (cf. Section 3.4). For these two algorithms the TIFFs yield higher gap fractions and as a consequence lower PAI_e values than the JPEGs (Tables 2a and 2b).

This is contrary to the study of Inoue et al. (2004) who found no significant differences in the gap fraction estimates between basic-quality JPEGs and high-quality TIFFs taken with a Nikon Coolpix 990. However, since the authors also showed that the camera type affects the estimation, the deviating findings can be attributed to the use of different cameras (Coolpix 990 vs. D300) in the two studies. The reason is most likely the use of different quantization tables in the quantization step of the JPEG compression. Since camera manufacturers choose an arbitrary "image quality" name for the different scale factors of the internal quantization, these names cannot be compared between makes or models by the same manufacturer (Hass, 2008). Frazer et al. (2001) compared fine-quality JPEGs and uncompressed TIFFs taken with a Nikon Coolpix 950 and found no significant differences in mean stand estimations of canopy openness, LAI_e and transmitted global PAR. However, the authors observed strong differences for a number of images and concluded that it is best not to use JPEG-compression ratios smaller than 1:4. The significant differences found in this study are most likely caused by the strong compression effects associated with the basic quality JPEG-compression of the D300.

Even though the conversion from the raw image data to a JPEG file includes a number of processing steps (color space conversion, chroma subsampling, block segmentation, discrete cosine transformation, quantization, etc.), quantization is the major source of error induced by the JPEG-compression (Hass, 2008). Quantization works such that the different frequency image components, resulting from the discrete cosine transformation, are ordered with ascending frequency and many of the high-frequency components, which are more likely to represent noise, are discarded by the algorithm. For the D300 and the basic quality JPEG setting, this results in lower gap fraction and thus higher PAI_e estimates for the JPEG than the TIFF images (Tables 2a and 2b).

The file format (i.e. the JPEG-compression) also affects the other canopy parameters, namely the number of zero gap fraction segments and the clumping indices. Even though the median differences for the clumping index values seem rather small (Tables 2a and 2b), their effect on the PAI values corrected for clumping is noticeable, especially for the PAI values corrected with the CI-2000. Based on the Isodata algorithm correcting the PAI_e with the CI-2000 increases the median differences by 68% (blue band) and 71% (red band). Using the CI-GSD, differences increase by 32% for the blue band and 35% for the red band. A similar trend can be observed for the Minimum algorithm – median differences increase by 63% (CI-2000/blue band), 66% (CI-2000/red band), 54% (CI-GSD/blue band) and 46% (CI-GSD/red band). Also noteworthy is the fact that the differences in the estimated canopy parameters between the TIFFs and JPEGs increase with decreasing exposure (data not shown) and that they are stronger for the red than the blue band images (Tables 2a and 2b). This is true for both the Isodata and the Minimum threshold algorithm, a fact which hints to a systematic influence of the image band selection (for a detailed analysis see Section 3.3).

3.2. The influence of exposure

Table 3 lists the mean values of the estimated canopy parameters as a function of exposure. Since the influence of exposure on the estimation behaves similar for both the blue and the red band images, the latter are omitted. Likewise since their median differences are marginal (cf. Tables 2a and 2b), the file formats TIFF 8-bit and JPEG 8-bit (Ridler and Otsu) as well as TIFF 8-bit (Isodata and Minimum) are omitted.

Since the acquisition and processing of hemispherical images is a delicate interplay between a number of factors (exposure, canopy structure, camera settings, threshold algorithm, etc.), this interdependency needs to be explicitly considered when assessing their influence on the estimation of forest structural attributes. Most noticeable, (1) the Ridler and Otsu algorithms yield the same mean values and (2) they differ strongly from the gap fraction and PAI_e/PAI estimates based on the Isodata and Minimum algorithms (30–65% difference depending on exposure level and parameter). Common to all four algorithms is the strong influence of exposure on the retrieval of the gap fraction and PAI_e (Table 3), corroborating the need to determine the optimum exposure regardless of the threshold algorithm applied. Fig. 1a and b highlights the impact of exposure and its interplay with the file format (Fig. 1a and b is intended to serve as a representative selection for the different threshold algorithms). They also highlight the variability in the estimates caused by the different canopy structure of the test stands.

Contrary to the gap fraction and PAI_e, the clumping indices do not follow a general trend as far as the influence of exposure is concerned. Based on the 16-bit TIFFs, the Lang and Xiang clumping index (CI-2000) is only weakly affected by exposure, however exhibiting a slight decline with exposure for all threshold algorithms (Table 3). This decline also causes only a small additional increase in the PAI values with decreasing exposure – small compared to the effect caused by exposure itself (the additional increase caused by the decreasing clumping index values makes up 8–28% of the PAI increase caused by exposure). By contrast to the 16-bit TIFFs, the Lang and Xiang clumping index calculated from the 8-bit JPEGs exhibits a stronger decrease with exposure (Table 3). This is due to the increase of zero gap fraction segments with decreasing exposure. Zero gap fraction segments strongly affect the calculation of PAI based on the logarithmic averaging and hence the Lang and Xiang clumping index, because the logarithm of zero cannot be computed and near-zero values result in unrealistically high PAI-values. This effect results in a stronger additional PAI increase

Table 2a
Median differences in the estimated canopy parameters based on different file format and radiometric resolution combinations (FF/RR) of the blue band images.

Algorithm	FF/RR	GF	PAI$_e$	ZGF	CI-2000	CI-GSD	PAI (2000)	PAI (GSD)
Ridler	TIFF 16bit–TIFF 8bit	−0.18***	0.02***	0	0.00	0.00***	0.02***	0.02***
	TIFF 16bit–JPEG 8bit	−0.38***	0.03***	0***	0.01***	0.03***	0.01	−0.07***
Otsu	TIFF 16bit–TIFF 8bit	−0.18***	0.02***	0	0.00	0.00***	0.02***	0.02***
	TIFF 16bit–JPEG 8bit	−0.36***	0.03***	0***	0.01***	0.03***	0.01	−0.07***
Isodata	TIFF 16bit–TIFF 8bit	−0.03***	0.01***	0	0.00	0.00***	0.01***	0.01***
	TIFF 16bit–JPEG 8bit	1.03***	−0.37***	−4***	0.02*	0.01*	−0.62*	−0.49***
Minimum	TIFF 16bit–TIFF 8bit	0.01***	0.00***	0	0.00	0.00	0.00*	0.00**
	TIFF 16bit–JPEG 8bit	0.86***	−0.31***	−4***	0.02***	0.02***	−0.51*	−0.48***

GF = gap fraction, PAI$_e$ = effective Plant Area Index, ZGF = zero gap fraction sky grid segments, CI-2000 = Lang and Xiang (1986) clumping index, CI-GSD = clumping index based on gap size distribution analysis. PAI (2000) = Plant Area Index corrected for clumping with the CI-2000 index, PAI (GSD) = Plant Area Index corrected for clumping with the CI-GSD index.
* Wilcoxon-Test: $p < 0.05$.
** Wilcoxon-Test: $p < 0.01$.
*** Wilcoxon-Test: $p < 0.001$.
Wilcoxon-Test: no asterisk indicates $p > 0.05$.

Table 2b
Median differences in the estimated canopy parameters based on different file format and radiometric resolution combinations (FF/RR) of the red band images.

Algorithm	FF/RR	GF	PAI$_e$	ZGF	CI (2000)	CI (GSD)	PAI (2000)	PAI (GSD)
Ridler	TIFF 16bit–TIFF 8bit	0.00***	0.00***	0	0.00	0.00	0.00	0.00
	TIFF 16bit–JPEG 8bit	−0.49***	0.06***	0***	0.01***	0.02***	0.03**	−0.02***
Otsu	TIFF 16bit–TIFF 8bit	0.00***	0.00***	0	0.00	0.00	0.00	0.00
	TIFF 16bit–JPEG 8bit	−0.48***	0.05***	0***	0.01***	0.02***	0.02**	−0.03***
Isodata	TIFF 16bit–TIFF 8bit	−0.01	0.00	0	0.00	0.00	0.01	0.00
	TIFF 16bit–JPEG 8bit	1.19***	−0.54***	−9***	0.04***	0.01***	−0.93***	−0.73***
Minimum	TIFF 16bit–TIFF 8bit	0.02***	−0.01***	0	0.00	0.00	−0.01	0.00
	TIFF 16bit–JPEG 8bit	1.02***	−0.44***	−6***	0.03***	0.02***	−0.73***	−0.64***

GF = gap fraction, PAI$_e$ = effective Plant Area Index, ZGF = zero gap fraction sky grid segments, CI-2000 = Lang and Xiang (1986) clumping index, CI-GSD = clumping index based on gap size distribution analysis. PAI (2000) = Plant Area Index corrected for clumping with the CI-2000 index, PAI (GSD) = Plant Area Index corrected for clumping with the CI-GSD index. For further annotations see Table 2a.

Table 3
Mean values of the estimated canopy parameters as a function of exposure based on the blue band images. FF/RR = file format-radiometric resolution combination, AE = automatic exposure, UE (1S)–UE (4S) = 1–4 stops of underexposure. For further annotations see Table 2a.

| Algorithm	FF/RR	Exposure	GF	PAI$_e$	ZGF	CI-2000	CI-GSD	PAI (2000)	PAI (GSD)
Ridler	TIFF 16bit	AE	27.9	2.0	1	0.90	0.74	2.2	2.6
		UE (1S)	20.4	2.5	1	0.90	0.81	2.7	3.0
		UE (2S)	15.3	2.9	1	0.90	0.85	3.2	3.4
		UE (3S)	11.2	3.4	2	0.89	0.88	3.8	3.9
		UE (4S)	8.2	3.9	3	0.88	0.89	4.5	4.4
Otsu	TIFF 16bit	AE	27.9	2.0	1	0.90	0.74	2.2	2.6
		UE (1S)	20.4	2.5	1	0.90	0.81	2.7	3.0
		UE (2S)	15.3	2.9	1	0.90	0.85	3.2	3.4
		UE (3S)	11.3	3.4	2	0.89	0.88	3.8	3.9
		UE (4S)	8.2	3.9	3	0.88	0.89	4.5	4.4
Isodata	JPEG 8bit	AE	10.9	3.5	4	0.88	0.92	3.9	3.8
		UE (1S)	7.7	4.1	6	0.88	0.93	4.6	4.4
		UE (2S)	5.3	4.7	9	0.86	0.92	5.5	5.1
		UE (3S)	3.6	5.4	14	0.83	0.91	6.5	6.0
		UE (4S)	1.8	6.6	28	0.81	0.91	8.3	7.4
	TIFF 16bit	AE	12.3	3.2	2	0.90	0.88	3.6	3.7
		UE (1S)	9.2	3.7	2	0.90	0.91	4.1	4.1
		UE (2S)	6.7	4.2	3	0.89	0.91	4.8	4.7
		UE (3S)	4.9	4.8	5	0.88	0.91	5.5	5.3
		UE (4S)	3.9	5.5	8	0.86	0.91	6.4	6.0
Minimum	JPEG 8bit	AE	13.7	3.1	3	0.89	0.84	3.5	3.7
		UE (1S)	9.4	3.7	5	0.88	0.87	4.2	4.3
		UE (2S)	6.3	4.4	7	0.87	0.89	5.1	5.0
		UE (3S)	4.2	5.3	12	0.84	0.89	6.3	5.9
		UE (4S)	3.2	6.2	22	0.82	0.90	7.6	6.9
	TIFF 16bit	AE	13.9	3.1	2	0.90	0.87	3.4	3.5
		UE (1S)	10.2	3.6	2	0.90	0.90	4.0	4.0
		UE (2S)	7.4	4.1	3	0.89	0.91	4.6	4.5
		UE (3S)	6.1	4.6	4	0.88	0.91	5.2	5.1
		UE (4S)	4.5	5.4	7	0.87	0.91	6.2	5.9
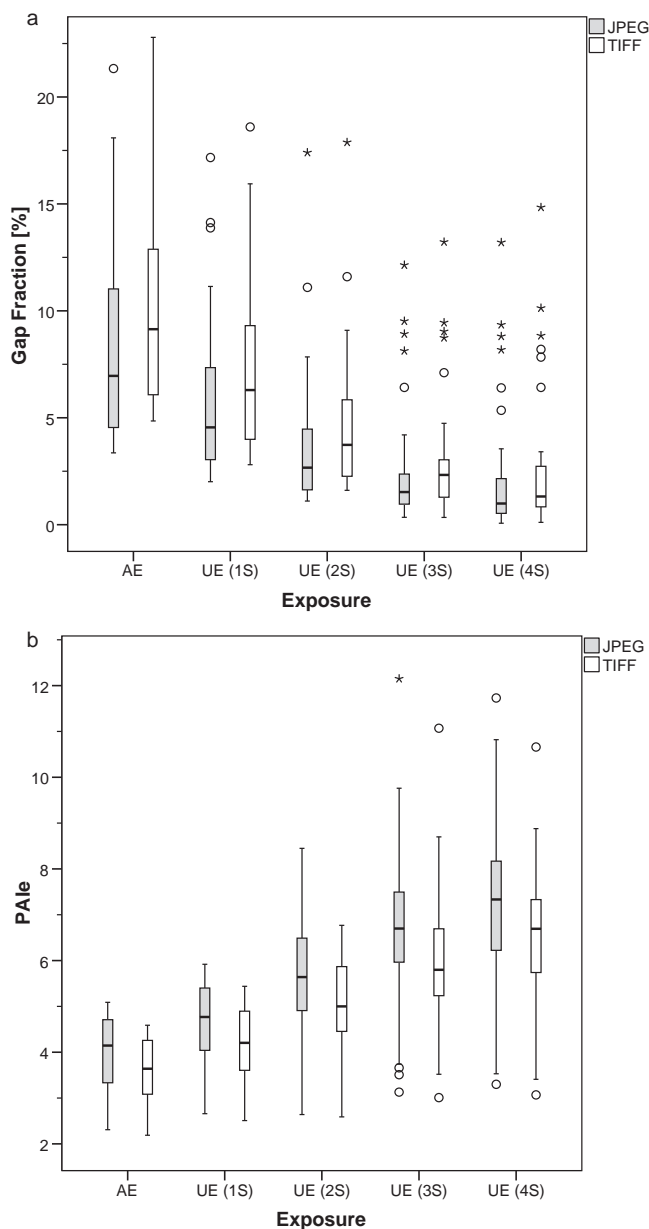
Fig. 1. a and b: Influence of the file format on the estimation of forest structural attributes as a function of exposure. Data based on the red band 16-bit TIFFs thresholded with the Isodata algorithm. AE = automatic exposure, UE (1S)–UE (4S) = 1–4 stops of underexposure. Circles indicate outliers greater than 1.5 × standard deviation, stars indicate outliers greater than 3 × standard deviation. Differences between TIFF- and JPEG-based estimates were tested with the Wilcoxon matched pairs signed rank test for each exposure level separately. All differences are statistically significant ($p < 0.001$).

(20–43% of the PAI increase caused by exposure) for the 8-bit JPEGs than for the 16-bit TIFFs.

To deal with the "zero gap fraction segment"-effect, different approaches have been proposed, most of which comprise substituting segments with zero gap fraction either by adding one sky pixel to the empty segments (van Gardingen et al., 1999) or by assigning a theoretical maximum PAI value (e.g. the default setting in the software WinScanopy is to assign a PAI of 10). Gonsamo et al. (2010) demonstrated that by using either one of these approaches, a systematic bias is introduced into the estimation of clumping and PAI. This bias is expressed in the above mentioned stronger additional PAI increase, however to isolate its exact proportion, a comparison with the values derived from the application of a less biased method

would be required. Nevertheless these findings carry important consequences for estimating clumping following the approach of Lang and Xiang (1986). Due to the bias introduced by the "zero gap fraction segment"-effect we recommend not to use JPEGs with a basic compression for the retrieval of the Lang and Xiang clumping index based on the Isodata and Minimum algorithms.

As far as the clumping index based on the gap size distribution (CI-GSD) is concerned, it reveals a completely different behavior toward the influence of exposure. This is to be expected since exposure in combination with the threshold algorithm may strongly alter the gap size distribution. By contrast to the CI-2000, the CI-GSD values increase with decreasing exposure, however with the magnitude differing for the different threshold algorithms and file formats (Table 3).

More interestingly than the general trend, however, is how the differences between the values of the two clumping index methods translate into PAI-differences. For the Ridler and Otsu algorithms the PAI-differences are greatest for automatic exposure (0.4) and decline with decreasing exposure (0.3, 0.2 and 0.1). For the Isodata and Minimum algorithms and based on the 16-bit TIFFs, the reverse is true: Differences are greatest for the 4-stops underexposure (0.4, 0.3, respectively) and decrease with increasing exposure (0.2, 0.1). As with the Lang and Xiang clumping index, the CI-GSD values based on the 8-bit JPEGs reveal a completely different behavior, both for the Isodata and for the Minimum algorithm (Table 3): Here differences in the PAI values caused by differences between the clumping methods strongly increase with decreasing exposure, particularly for the Isodata algorithm (0.1–0.9 PAI).

3.3. The influence of the image band selection

As far as the influence of the image band selection is concerned, the gap fractions retrieved from the blue band images are higher than the gap fractions based on the red band. This is true for all four threshold algorithms, file formats and exposure levels with the exception of the Ridler and Otsu algorithms applied to the automatically exposed 16-bit TIFFs (Table 4). The higher gap fractions are caused by a stronger blooming in the blue than the red band (Leblanc et al., 2005), which is supported by the general trend observed in the data (Table 4) that the differences decrease with a reduction in exposure (as it is known that decreasing exposure reduces blooming). The gap fraction differences translate into small PAI$_e$ differences (ranging from −0.29 to 0.12) for all four algorithms applied to the 16-bit TIFFs (Table 4). The 8-bit JPEGs thresholded with the Isodata and Minimum algorithms, however, reveal considerable PAI$_e$ differences between the blue and red bands (range: −0.27 to −0.91). Furthermore a higher number of zero gap fraction segments are observed for the red than for the blue band images (Table 4). As already explained this directly affects the determination of the Lang and Xiang clumping index and thus the PAI-2000 values. By contrast the differences in the clumping index values for the algorithms applied to the 16-bit TIFFs as well as their effect on the PAI estimations are marginal (Table 4).

Concluding the first part of this study, it was demonstrated that depending on the threshold algorithm applied, both the file format and the image band selection can have a strong impact on the estimated forest structural attributes. More precisely the 8-bit JPEGs (basic compression) that were thresholded with the Isodata and Minimum algorithms yielded canopy parameters significantly different from their 16-bit TIFF counterparts. Furthermore it could be shown that the choice of the threshold algorithm has a strong effect on the estimation, too. As a consequence, the threshold algorithm, file format and image band selection (as well as their interactions) should also affect the determination of optimum exposure as proposed by Zhang et al. (2005).

Table 4
Median differences between the estimated canopy parameters based on the blue and the red band images. FF/RR = file format-radiometric resolution combination, AE = automatic exposure, UE (1S)–UE (4S) = 1–4 stops of underexposure. For further annotations see Table 2a. Since the median differences for the file formats TIFF 8-bit and JPEG 8-bit (Ridler and Otsu) as well as TIFF 8-bit (Isodata and Minimum) deviate only marginally from the 16-bit TIFFs, the former are omitted.

Alg.	FF/RR	Exp.	GF	PAI_e	ZGF	CI (2000)	CI (GSD)	PAI (2000)	PAI (GSD)
Ridler	TIFF 16bit	AE	−2.42	0.12	0	0.00	−0.01	0.12	0.19
		UE (1S)	0.42	−0.02*	0	0.00	−0.02***	−0.04*	0.04
		UE (2S)	0.94***	−0.08***	0	0.00**	−0.02***	−0.10***	−0.03*
		UE (3S)	0.73***	−0.12***	0	0.00***	−0.02***	−0.11***	−0.05***
		UE (4S)	0.55***	−0.13***	0*	0.00***	−0.02***	−0.11***	−0.06***
Otsu	TIFF 16bit	AE	−2.42	0.12	0	0.00	−0.01	0.12	0.19
		UE (1S)	0.42	−0.02*	0	0.00	−0.02***	−0.04*	0.04
		UE (2S)	0.89***	−0.09***	0	0.00**	−0.02***	−0.10***	−0.03*
		UE (3S)	0.73***	−0.12***	0	0.00***	−0.02***	−0.11***	−0.05***
		UE (4S)	0.55***	−0.13***	0*	0.00***	−0.01***	−0.11***	−0.06***
Isodata	TIFF 16bit	AE	1.83***	−0.19***	0	0.00***	−0.01***	−0.31***	−0.21***
		UE (1S)	1.78***	−0.29***	0	0.00***	−0.01***	−0.40***	−0.33***
		UE (2S)	0.77***	−0.27***	0	0.00**	−0.01**	−0.29***	−0.27***
		UE (3S)	0.55	−0.29	0	0.00	−0.01	−0.31	−0.27*
		UE (4S)	0.16	−0.09	0***	0.00***	0.00	−0.09	−0.05
	JPEG 8bit	AE	2.05***	−0.37***	−1***	0.01***	0.03***	−0.48***	−0.65***
		UE (1S)	1.88***	−0.38***	−2***	0.02***	0.03***	−0.55***	−0.64***
		UE (2S)	1.08***	−0.53***	−6***	0.03***	0.01*	−0.91***	−0.87***
		UE (3S)	0.77**	−0.62***	−8***	0.01*	0.00	−0.86***	−0.74***
		UE (4S)	0.30	−0.44*	−4*	0.01	−0.01*	−0.73*	−0.35
Minimum	TIFF 16bit	AE	1.67***	−0.16***	0*	0.00**	−0.01**	−0.27***	−0.15***
		UE (1S)	1.64***	−0.27***	0*	0.00***	−0.01***	−0.36***	−0.24***
		UE (2S)	0.82***	−0.24***	0**	0.00***	−0.01***	−0.25***	−0.21***
		UE (3S)	0.96***	−0.28***	0	0.00*	−0.01**	−0.31***	−0.26***
		UE (4S)	0.22	−0.14*	0*	0.00	−0.01**	−0.14	−0.06
	JPEG 8bit	AE	2.10***	−0.27***	0**	0.01***	−0.02***	−0.38***	−0.26***
		UE (1S)	2.17***	−0.40***	−1***	0.01***	−0.01***	−0.61***	−0.46***
		UE (2S)	1.15***	−0.57***	−2***	0.02***	−0.01*	−0.65***	−0.58***
		UE (3S)	0.92*	−0.91***	−9***	0.02***	0.00	−1.43***	−0.98***
		UE (4S)	0.30	−0.40***	−5**	0.01	−0.01	−0.77***	−0.30**

3.4. Comparison of the PAI_e estimates derived from DHP and the LAI-2000

In order to better assess the differences in the estimates of gap fraction and PAI_e, the PAI_e derived from digital hemispherical photography were compared to simultaneous LAI-2000 measurements. The assessment is based upon the root mean squared error (RMSE) between the PAI_e estimates of the two methods and upon the slope of the linear regression (without an intercept). As already mentioned, the Ridler and Otsu algorithms yielded – in most cases – the same threshold values and thus same canopy parameter values. Consequently they are listed together in Table 5. Most noticeable, the PAI_e estimates based on the Ridler and Otsu algorithms underestimate the LAI-2000 measurements, independent of exposure, revealing the inadequacy of these algorithms for the PAI_e estimation (Table 5). By contrast, the Isodata and Minimum algorithms show a higher sensitivity and thus better agreement with the LAI-2000. One aspect which is also evident from Table 5 is that, regardless of the threshold algorithm applied, hemispherical images taken with automatic exposure underestimate the LAI-2000 measurements significantly. The degree of under-estimation is particularly pronounced for dense canopies and high PAI_e. With a decrease in exposure the underestimation declines, for medium to high PAI_e more so than for low PAI_e (Fig. 2), until the underestimation turns into an overestimation, revealing the sensitivity of the PAI_e estimation to exposure for dense canopies (Table 5). By contrast the PAI_e estimates derived from the open forest stands are much less affected by changing exposure and show a constantly good agreement with the LAI-2000 values.

These general trends apply to the PAI_e estimates based on both the Minimum and the Isodata algorithms and are independent of the selected image band and file format (Table 5, Fig. 2). The main difference between the image band and file format

Table 5
Comparison of the PAI_e estimates derived from DHP and the LAI-2000. Slope = slope of the regression of the form $y = ax$, AE = automatic exposure, UE (1S)–UE (4S) = 1–4 stops of underexposure.

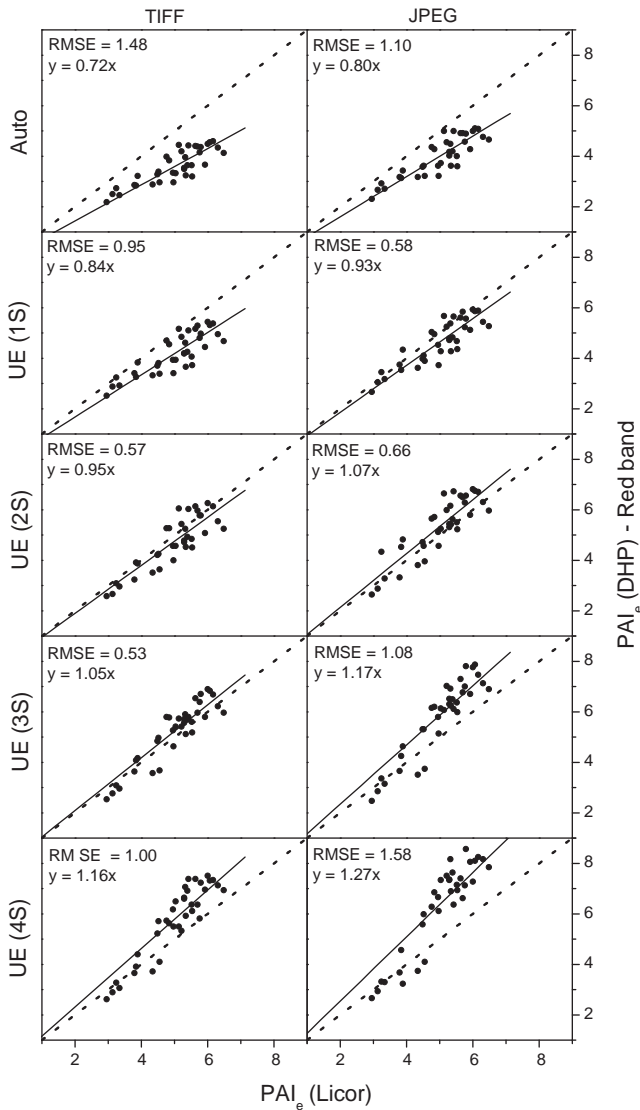| Algorithm	File format	Exposure	Blue band		Red band	
			Slope	RMSE	Slope	RMSE
Minimum	TIFF	AE	0.61	2.01	0.68	1.66
		UE (1S)	0.71	1.51	0.81	1.06
		UE (2S)	0.82	0.97	0.94	0.67
		UE (3S)	0.93	0.54	1.06	0.94
		UE (4S)	1.09	0.75	1.15	1.29
	JPEG	AE	0.62	1.95	0.71	1.51
		UE (1S)	0.74	1.37	0.88	0.80
		UE (2S)	0.88	0.71	1.06	0.70
		UE (3S)	1.05	0.52	1.37	2.59
		UE (4S)	1.27	1.51	1.53	3.40
Isodata	TIFF	AE	0.64	1.85	0.72	1.48
		UE (1S)	0.73	1.37	0.84	0.95
		UE (2S)	0.84	0.86	0.95	0.57
		UE (3S)	0.96	0.44	1.05	0.53
		UE (4S)	1.11	0.71	1.16	1.00
	JPEG	AE	0.69	1.63	0.80	1.10
		UE (1S)	0.81	1.08	0.93	0.58
		UE (2S)	0.93	0.57	1.07	0.66
		UE (3S)	1.06	0.58	1.17	1.08
		UE (4S)	1.20	1.14	1.27	1.58
Ridler/Otsu	TIFF	AE	0.39	3.11	0.38	3.16
		UE (1S)	0.49	2.61	0.51	2.48
		UE (2S)	0.58	2.16	0.62	1.94
		UE (3S)	0.67	1.68	0.72	1.44
		UE (4S)	0.78	1.14	0.83	0.92
	JPEG	AE	0.38	3.14	0.37	3.27
		UE (1S)	0.48	2.66	0.50	2.55
		UE (2S)	0.57	2.20	0.61	2.00
		UE (3S)	0.67	1.71	0.71	1.51
		UE (4S)	0.78	1.15	0.82	0.98

Fig. 2. Regression of the PAI$_e$ derived from the single red band images thresholded with the Isodata algorithm against the PAI$_e$ derived from Licor measurements. Auto = automatic exposure, UE (1S)–(4S) = 1–4 stops of underexposure.
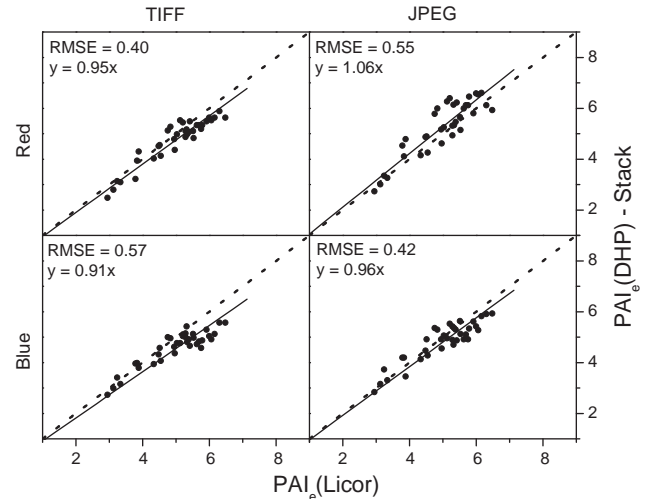

Fig. 3. Regression of the PAI$_e$ derived from the exposure-stacks against the PAI$_e$ derived from LAI-2000 measurements.

RMSE values, corroborating the suitability of the Isodata algorithm for thresholding hemispherical images to derive LAI.

The other main finding of the comparison between the PAI$_e$ estimates derived from the hemispherical images and the LAI-2000 measurements is that the determination of optimum exposure is dependent on the file format, the selected image band as well as the threshold algorithm applied. Hence these need to be implicitly accounted for when determining the exposure for hemispherical images. This affects the general applicability of the protocol proposed by Zhang et al. (2005). The main goal therefore is to develop an approach to the processing of hemispherical images independent of exposure and desirably less affected by the above mentioned influences.

3.5. A concept for the standardized processing of hemispherical images

Jonckheere et al. (2005) stressed the need for further research into the potentials of multi-channel thresholding. Considering the liability of hemispherical photography to a multitude of influences, incorporating as much valid information as possible into the segmentation process to constrain the variability induced by those influences, appears only a logical consequence. One method of enhancing the information basis which is for example routinely used for remote sensing applications is data or image fusion (Richards and Jia, 2006; Simone et al., 2002). Considering the strong influence of exposure on the estimation of forest structural attributes, we tested the potential of including the full exposure information by stacking the five differently exposed images taken at each sampling point (cf. Section 2.2). These image- or layer-stacks provide the basis for the Isodata algorithm which is at the heart of the proposed standardized image processing chain. As mentioned before the Isodata algorithm enables an efficient multi-layer clustering (Duda et al., 2001) and is therefore particularly attractive for the purpose of testing multi-channel or multi-layer thresholding. It has to be noted that the other algorithms tested in this study are basically capable of multi-layer thresholding, too. However, as these are not readily implemented in image processing software, the present assessment is limited to the Isodata algorithm.

Results show that the RMSEs of the image stacks either considerably decrease or match the RMSEs of the optimum exposure level for the different file format and image band combinations (Figs. 2 and 3), except for the blue band TIFF stacks which exhibit a slight RMSE increase. This is due to the systematic higher gap
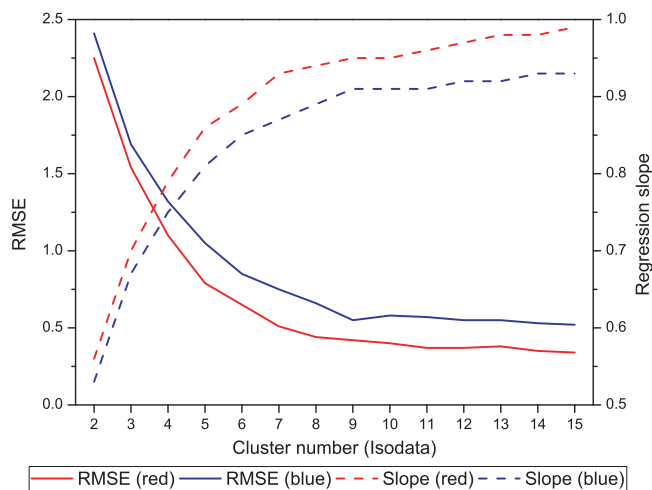
combination is a shift in magnitude as can be seen from the slope values (Table 5, Fig. 2). This shift is easily explained by the gap fraction and PAI$_e$ differences observed for the four combinations. What is more interesting, however, is how these differences pertain to the determination of optimum exposure. In terms of overall RMSE and unbiasedness of the regression, 3 stops of underexposure is the optimum exposure for the blue band TIFFs (Isodata/Minimum) and JPEGs (Minimum), respectively, 2 stops of underexposure for the blue band JPEGs based on the Isodata algorithm. For the red band images the optimum exposure is found at one lower stop of underexposure than compared to the blue band images. This trend is observed for both the Isodata and the Minimum algorithm and shows the influence of the image band selection on the determination of the optimum exposure. Furthermore the determination can also be affected by the file format as obvious from the Isodata values (Table 5, Fig. 2). By contrast, the influence of the file format and image band selection on the determination of the optimum exposure for the images thresholded with the Ridler and Otsu algorithms is marginal (Table 5). Comparing the two better performing algorithms, Isodata and Minimum, the former generally yields lower

Fig. 4. Influence of the number of Isodata clusters on the regression of the PAI$_e$ derived from the stacks (both of the blue and of the red band images) against the PAI$_e$ from LAI-2000 measurements and the respective RMSEs.

fractions of the blue band TIFFs which result in an underestimation of PAI$_e$ particularly for dense canopies. This underestimation is witnessed for both the single images and the image stacks (Table 5 and Fig. 3), which is why – in our case – the red band image stacks were used for the PAI$_e$ estimation.

These findings implicate two distinct advantages of the Isodata multi-layer clustering:

- The choice of the file format for the estimation of PAI$_e$ is less critical with the layer-stack approach. Nevertheless we recommend using the raw image data (saved as TIFFs) as basis for the stacking, particularly considering the influence of the file format on the estimation of clumping and PAI (as could be shown in this study).
- The selection of optimum exposure as a function of the file format and image band selection is no longer required which simplifies standardization of the acquisition and processing of hemispherical images based on the Isodata algorithm.

To allow for a fully automatic and standardized processing of hemispherical images based on the Isodata algorithm, the main user input (i.e. the selection of the cluster number) has to be replaced by some kind of automation rule. We therefore implemented a simple decision rule where the cluster with the highest mean DNs is assigned to the class "sky" and the remaining clusters are assigned to the class "canopy". Since the clustering of image pixels (in particular mixed pixels) depends on the number of clusters specified, its influence on the PAI$_e$ estimation was assessed (Fig. 4). As the use of raw image data as the basis for the stacking is recommended, the following analysis was based on the (exposure) stacks of the red and blue bands of the 16-bit TIFFs. These were successively clustered with 2–15 clusters, the resulting classifications were then binarised with the above mentioned decision rule, PAI$_e$ was calculated and compared to LAI-2000 measurements. The RMSE between the two methods as well as the regression slope served as quality criteria for the assessment.

Fig. 4 shows that with increasing the cluster number, the underestimation of LAI-2000 measurements decreases (i.e. increasing slope values). Simultaneously the RMSE declines until it stabilizes on a low level. This saturation effect occurs around the cluster numbers 9 and 10, both for the red and for the blue band stacks of the 16-bit TIFFs. Due to the blooming-induced higher gap fractions of the blue band stacks, the respective RMSEs are constantly higher than the RMSEs of the red band stacks (Fig. 4). More importantly,

however, is the stabilizing effect of the RMSEs, observed for both image bands, which enables a fully automatic and standardized processing of hemispherical images based on the Isodata algorithm.

Last but not least, potential weaknesses of the proposed standardized processing have to be addressed. One of the difficulties is the assignment of the clusters generated by the Isodata algorithm to the binary classes, "canopy" or "sky". If done manually an uncertainty similar to manual thresholding is introduced. To avoid this problem and allow for an automatic and objective assignment, we implemented a simple decision rule which worked well except in the case of extremely variable sky brightness (cf. Section 2.3). Alternatively the implementation of more complex decision criteria for cluster assignment or the implementation of a stratified Isodata clustering (local threshold approach) could solve the problem of variable sky brightness conditions (which however affect all global threshold algorithms).

Another difficulty which may be encountered is the possible motion of canopy elements while shooting the series of hemispherical images. This can result in blurring around the edges of leaves in the image stack thus increasing the number of mixed pixels. Compared to the single images taken with different exposure, however, one of the strengths of the multi-layer clustering based on the exposure stacks is the reduced influence of mixed pixels, i.e. a more certain assignment of pixels to the class "sky", a fact which shows in the lower RMSE values. As far as mixed pixels are generally concerned, their amount is clearly influenced by exposure, which is why the definition and assignment of mixed pixels is not straightforward. Leblanc et al. (2005) propose an interesting way of dealing with mixed pixels by linear interpolation – their approach however suffers from the drawback of having to determine two thresholds.

These influences show that it is crucial to take external factors such as sky brightness conditions or wind-driven motion of canopy elements into account when acquiring hemispherical images.

4. Summary and conclusions

The main goals of this study were to investigate the influences of the radiometric image resolution, file format and image band selection as well as their interaction with the threshold algorithm on the estimation of forest structural attributes (gap fraction, PAI$_e$, clumping indices) and to develop a more objective and robust approach to the processing of hemispherical images. Threshold algorithms tested in this study are the Ridler, Otsu and Minimum algorithms as well as a proposed new standardized processing based on the Isodata clustering algorithm.

With regard to the first goal, this study was able to demonstrate that, depending on the threshold algorithm applied, the file format and the image band selection can have a significant impact on the estimation of forest structural attributes. By contrast the radiometric resolution was found to affect the estimation only marginally. Raw images (saved as TIFFs) exhibited higher gap fractions than basic-compressed JPEG images due to the different steps that raw image data goes through when being compressed to the JPEG file format. Since any further analysis departs from the gap fraction, the determination of PAI$_e$/PAI and clumping are directly affected. One such effect is a systematic bias in the log-averaged PAI$_e$ values of the JPEG images which results from an increase in zero gap fraction segments (with decreasing exposure) combined with the method of substituting empty sky segments with a PAI$_e$ of 10 (cf. Section 3.2). Since the log-averaged PAI$_e$ are used to determine leaf clumping (Lang and Xiang method), this bias causes clumping index differences between JPEG and TIFF which, more significantly, translate into increasing differences in PAI corrected with the two different clumping index methods presented in this paper. For these reasons
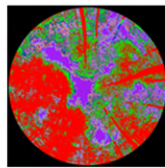
Input: 16-bit Raw single band* images taken with the exposure
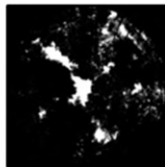settings: Auto, UE (1S), UE (2S), UE (3S), UE (4S)
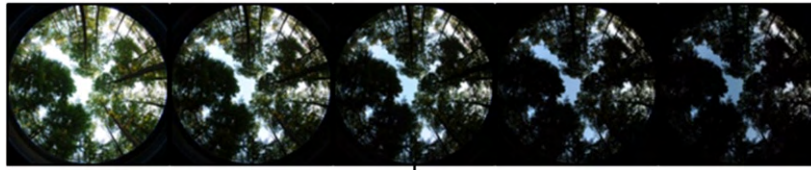
Layer-stacking the differently exposed images

Isodata multi-layer clustering: N° of clusters =10

Binarization based on the decision rule: Cluster with highest
mean DNs = Sky, remaining clusters= canopy

Calculation of forest structural attributes

Fig. 5. Proposed standardized batch processing of hemispherical images for the estimation of forest structural attributes based on the Isodata algorithm. * = depending on the degree of blooming either the red or blue band. Auto = automatic exposure, UE (1S) to UE (4S) = one to four stops of underexposure.

we recommend to use the raw instead of JPEG-compressed image data for the estimation of forest structural attributes.

With regard to the influence of the image band selection, special attention has to be paid to the effect of blooming, since it could be demonstrated that it causes significant differences in the estimates of canopy parameters, particularly for gap fraction and PAI_e. As far as clumping is concerned, its calculation is less affected by the image band selection than by the file format. It was shown that even though the blue band theoretically offers the best contrast for thresholding, due to better absorption, blooming can easily compensate this potential advantage. Hence the degree of blooming in the different bands, particularly the blue band, should always be examined. If blooming in the blue band is noticeably stronger than in the red band, we recommend using the latter.

The fact that the file format and the image band selection did not affect strongly the canopy parameter estimates derived from the images thresholded with the Ridler and Otsu algorithms does not imply that these are better suited for thresholding hemispherical images. On the contrary, by comparing results with LAI-2000 measurements this study revealed that, independent of exposure, these algorithms yield significantly higher gap fractions and thus lower PAI_e. As a consequence the Ridler and Otsu algorithms are not suitable for the estimation of gap fraction and PAI_e.

Since the file format and the image band selection significantly influence the estimation of forest structural attributes based on the Isodata and Minimum algorithms, an effect on the determination of the optimum exposure is also to be expected. This is a crucial point because regardless of the threshold algorithm applied, exposure constitutes the strongest influence on the estimation of forest structural attributes. As could be shown in the present study the optimum exposure is dependent on the file format as well as the image band selection, suggesting the need for an approach

which reduces this inter-dependence. We therefore propose a new approach to the standardized processing of hemispherical images. This approach represents a multi-layer clustering where the layers comprise of five differently exposed hemispherical images. These images are taken with automatic (below-canopy) exposure and 1–4 stops of underexposure. They are then stacked and passed to the Isodata clustering algorithm, which has proven to be an efficient and flexible method. Based on an assessment of the influence of the cluster number on the estimation of PAI$_e$, it could be shown that with the selection of 9–10 clusters the RMSEs between the LAI-2000 measurements and the PAI$_e$ derived from the image stacks reach a quasi-constant level. Increasing the number of clusters above this value does not significantly improve the correlation. This behavior is observed for both the red and the blue band image stacks, which gives us confidence in the use of a fixed cluster number. In the present study a value of 10 was chosen. Binary images are created from these 10 clusters based on a simple decision rule where the cluster with the highest mean DNs is assigned to the class "sky" while the remaining clusters are assigned to the class "canopy". Provided that hemispherical images are taken under homogenous sky brightness conditions, this automation rule performs consistently (Fig. 5).

The proposed approach provides a standardized and fully automatic processing of hemispherical images. Applying this processing scheme, excellent agreement with the LAI-2000 was achieved. Since the comparison was based on hemispherical images of deciduous forests of variable stand structure (cf. Table 1), we are confident that our approach is robust. To further assess its applicability the proposed standardized processing will be tested for coniferous forests, too. The standardization not only allows better comparability between research studies and field campaigns but also eliminates major uncertainties associated with using DHP for estimation of forest structural attributes. It has to be noted though that matching different indirect optical methods is not per se an indication of improved accuracy, rather it provides consistency between methods, which in the absence of a real LAI reference is a minimum requirement. The proposed approach to the processing of hemispherical images provides such consistency, which in turn provides the potential for DHP to replace the LAI-2000. DHP offers the advantage to calculate clumping and to provide a permanent record of the canopy structure. Besides being practical, easy-to-implement and comparatively cheap, DHP still bears a lot of potential, in particular considering the fast technical advances in the field of digital photography. We therefore believe that – if sufficiently standardized – hemispherical photography is the most efficient tool for estimating forest structural attributes.

Acknowledgements

References

Baler, K.G., Landini, G., Rasband, W., 2009. MultiThresholder (accessed 16.06.11) http://rsb.info.nih.gov/ij/plugins/multi-thresholder.html.

Ball, G.H., Hall, D.J., 1965. ISODATA, a Novel Method of Data Analysis and Pattern Classification. NTIS-AD-699616, Stanford Res. Inst., Menlo Park, Stanford, CA.

Cescatti, A., 2007. Indirect estimates of canopy gap fraction based on the linear conversion of hemispherical photographs: methodology and comparison with standard thresholding techniques. Agricultural and Forest Meteorology 143 (1–2), 1–12.

Chapman, L., 2007. Potential applications of near infra-red hemispherical imagery in forest environments. Agricultural and Forest Meteorology 143 (1–2), 151–156.

Chen, J.M., Black, T.A., 1992. Defining leaf area index for non-flat leaves. Plant, Cell & Environment 15 (4), 421–429.

Chen, J.M., Black, T.A., Adams, R.S., 1991. Evaluation of hemispherical photography for determining plant area index and geometry of a forest stand. Agricultural and Forest Meteorology 56 (1–2), 129–143.

Chen, J.M, Cihlar, J., 1995. Quantifying the effect of canopy architecture on optical measurements of leaf area index using two gap size analysis methods. IEEE Transactions on Geoscience and Remote Sensing 33 (3), 777–787.

Chen, J.M., Rich, P.M., Gower, S.T., Norman, J.M., Plummer, S., 1997. Leaf area index of boreal forests: theory, techniques, and measurements. Journal of Geophysical Research 102 (D24), 29429–29443.

Clark, J.A., 2009. Forest Biomass Estimation with Hemispherical Photography for Multiple Forest Types and Various Atmospheric Conditions. Oregon State University, Corvallis, OR.

Duda, O.D., Hart, P.E., Stork, D.G., 2001. Pattern Classification. John Wiley & Sons, New York/Chichester/Weinheim/Brisbane/Singapore/Toronto, 680 pp.

Englund, S.R., O'Brien, J.J., Clark, D.B., 2000. Evaluation of digital and film hemispherical photography and spherical densiometry for measuring forest light environments. Canadian Journal of Forest Research 30 (9), 1999–2005.

Frazer, G.W., Fournier, R.A., Trofymow, J.A., Hall, R.J., 2001. A comparison of digital and film fisheye photography for analysis of forest canopy structure and gap light transmission. Agricultural and Forest Meteorology 109 (4), 249–263.

FutMon, 2009. Forms and Explanatory Items Version 5.3 (accessed 16.06.11) http://www.futmon.org/data_submission/FutMon_ICPForestsForms2009_V5_3e.pdf.

Gonsamo, A., Walter, J.-M.N., Pellikka, P., 2010. Sampling gap fraction and size for estimating leaf area and clumping indices from hemispherical photographs. Canadian Journal of Forest Research 40 (8), 1588–1603.

Hass, C., 2008. Digital Photography (accessed 16.06.11) http://www.impulseadventure.com/photo/.

Inoue, A., Yamamoto, K., Mizoue, N., Kawahara, Y., 2004. Effects of image quality, size and camera type on forest light environment estimates using digital hemispherical photography. Agricultural and Forest Meteorology 126 (1–2), 89–97.

Jonckheere, I., Fleck, S., Nackaerts, K., Muys, B., Coppin, P., Weiss, M., Baret, F., 2004. Review of methods for in situ leaf area index determination: Part I. Theories, sensors and hemispherical photography. Agricultural and Forest Meteorology 121 (1–2), 19–35.

Jonckheere, I., Nackaerts, K., Muys, B., Coppin, P., 2005. Assessment of automatic gap fraction estimation of forests from digital hemispherical photography. Agricultural and Forest Meteorology 132 (1–2), 96–114.

Korhonen, L., Korpela, I., Heiskanen, J., Maltamo, M., 2011. Airborne discrete-return LIDAR data in the estimation of vertical canopy cover, angular canopy closure and leaf area index. Remote Sensing of Environment 115 (4), 1065–1080.

Kucharik, C., Norman, J.M., Murdock, L.M., Gower, S.T., 1997. Characterizing canopy nonrandomness with a multiband vegetation imager (MVI). Journal of Geophysical Research 102 (D24), 29455–29473.

Landini, G., 2011. Auto Treshold (accessed 16.06.11) http://pacific.mpi-cbg.de/wiki/index.php/Auto_Threshold.

Lang, A.R.G., Xiang, Y., 1986. Estimation of leaf area index from transmission of direct sunlight in discontinuous canopies. Agricultural and Forest Meteorology 37 (3), 229–243.

Lang, M., Kuusk, A., Mõttus, M., Rautiainen, M., Nilson, T., 2010. Canopy gap fraction estimation from digital hemispherical images using sky radiance models and a linear conversion method. Agricultural and Forest Meteorology 150 (1), 20–29.

Leblanc, S.G., Chen, J.M., Fernandes, R., Deering, D.W., Conley, A., 2005. Methodology comparison for canopy structure parameters extraction from digital hemispherical photography in boreal forests. Agricultural and Forest Meteorology 129 (3–4), 187–207.

LI-COR, 1992. LAI-2000 Plant Canopy Analyser. Instruction Manual. LICOR, Lincoln, NE, USA.

Macfarlane, C., Coote, M., White, D.A., Adams, M.A., 2000. Photographic exposure affects indirect estimation of leaf area in plantations of Eucalyptus globulus Labill. Agricultural and Forest Meteorology 100 (2–3), 155–168.

Macfarlane, C., Hoffman, M., Eamus, D., Kerp, N., Higginson, S., McMurtrie, R., Adams, M., 2007. Estimation of leaf area index in eucalypt forest using digital photography. Agricultural and Forest Meteorology 143 (3–4), 176–188.

Miller, J.B., 1967. A formula for average foliage density. Australian Journal of Botany 15 (1), 141–144.

Nobis, M., Hunziker, U., 2005. Automatic thresholding for hemispherical canopy-photographs based on edge detection. Agricultural and Forest Meteorology 128 (3–4), 243–250.

Otsu, N., 1979. A threshold selection method from gray-level histograms. IEEE Transactions on Systems, Man and Cybernetics 9, 62–66.

Prewitt, J.M.S., Mendelsohn, M.L., 1966. The analysis of cell images. Annals of the New York Academy of Sciences 128, 1035–1053.

Richards, J.A., Jia, X., 2006. Remote Sensing Digital Image Analysis – An Introduction. Springer, Berlin/Heidelberg/New York.

Ridler, W., Calvard, S., 1978. Picture thresholding using an iterative selection method. IEEE Transactions on Systems, Man and Cybernetics 8, 630–632.

Sezgin, M., Sankur, B., 2004. Survey over image thresholding techniques and quantitative performance evaluation. Journal of Electronic Imaging 13 (1), 146.

Simone, G., Farina, A., Morabito, F.C., Serpico, S.B., Bruzzone, L., 2002. Image fusion techniques for remote sensing applications. Information Fusion 3 (1), 3–15.

Thimonier, A., Sedivy, I., Schleppi, P., 2010. Estimating leaf area index in different types of mature forest stands in Switzerland: a comparison of methods. European Journal of Forest Research 129 (4), 543–562.

van Gardingen, P.R., Jackson, G.E., Hernandez-Daumas, S., Russell, G., Sharp, L., 1999. Leaf area index estimates obtained for clumped canopies using hemispherical photography. Agricultural and Forest Meteorology 94 (3–4), 243–257.

Walter, J.-M.N., 2009. Hemispherical Photography of Forest Canopies – Practice. CIMES-FISHEYE 2009 Jean-Michael Walter – Universite de Strasbourg France.

Weiss, M., Baret, F., Smith, G.J., Jonckheere, I., Coppin, P., 2004. Review of methods for in situ leaf area index (LAI) determination: Part II. Estimation of LAI, errors and sampling. Agricultural and Forest Meteorology 121 (1–2), 37–53.

Zhang, Y., Chen, J.M., Miller, J.R., 2005. Determining digital hemispherical photograph exposure for leaf area index estimation. Agricultural and Forest Meteorology 133 (1–4), 166–181.

Zhao, K., Popescu, S., 2009. Lidar-based mapping of leaf area index and its use for validating GLOBCARBON satellite LAI product in a temperate forest of the southern USA. Remote Sensing of Environment 113 (8), 1628–1645.

Zheng, G., Moskal, L.M., 2009. Retrieving Leaf Area Index (LAI) using remote sensing: theories. Methods and Sensors, 2719–2745.

Chapter III: Retrieval of gap fraction and effective plant area index from phase-shift terrestrial laser scans

Pyare Pueschel, Glenn Newnham, Joachim Hill

remote sensing

Article

Retrieval of Gap Fraction and Effective Plant Area Index from Phase-Shift Terrestrial Laser Scans

Pyare Pueschel [1,*], **Glenn Newnham** [2] **and Joachim Hill** [1]

[1] Department of Environmental Remote Sensing and Geoinformatics, University of Trier, D-54286 Trier, Germany; E-Mail: hillj@uni-trier.de

[2] CSIRO Land and Water, Private Bag 10, Clayton South, VIC 3169, Australia; E-Mail: glenn.newnham@csiro.au

* Author to whom correspondence should be addressed; E-Mail: p.pueschel@uni-trier.de; Tel.: +49-651-201-4593; Fax: +49-651-201-3815.

Abstract: The characterization of canopy structure is crucial for modeling eco-physiological processes. Two commonly used metrics for characterizing canopy structure are the gap fraction and the effective Plant Area Index (PAI_e). Both have been successfully retrieved with terrestrial laser scanning. However, a systematic assessment of the influence of the laser scan properties on the retrieval of these metrics is still lacking. This study investigated the effects of resolution, measurement speed, and noise compression on the retrieval of gap fraction and PAI_e from phase-shift FARO Photon 120 laser scans. We demonstrate that FARO's noise compression yields gap fractions and PAI_e that deviate significantly from those based on scans without noise compression and strongly overestimate Leaf Area Index (LAI) estimates based on litter trap measurements. Scan resolution and measurement speed were also shown to impact gap fraction and PAI_e, but this depended on leaf development phase, stand structure, and LAI calculation method. Nevertheless, PAI_e estimates based on various scan parameter combinations without noise compression proved to be quite stable.

1. Introduction

Information about forest canopy structure is crucial for understanding the significant role forest canopies play in global processes such as water and carbon cycling. Parker [1] gives a general definition of canopy structure as "the organization in space and time, including the position, extent, quantity, type and connectivity, of the above-ground components of vegetation". In addition to simple forest stand-based descriptors, such as stem density or mean tree height, descriptors related to the amount, distribution, and orientation of foliage within the canopy are vitally important for understanding plant physiology and growth [1]. These foliage metrics include the Leaf Area Index (LAI), commonly defined for flat leaves as half the total leaf area per unit ground surface area [2], and the foliage area volume density (FAVD), defined as the volume density function of foliage area [3].

Ground-based methods for the estimation of LAI are usually grouped into two categories; direct and indirect methods [4]. The direct methods include destructive sampling and litterfall collection [4]. The indirect methods include methods based on leaf contact, such as the inclined point quadrat [5], and passive optical methods, such as hemispherical photography or LI-COR's Plant Canopy Analyzer (PCA) [4]. As the direct methods are costly, labor intensive and time-consuming [4,6], indirect LAI methods are more commonly applied.

Indirect optical estimates of LAI are all based on a common theoretical framework that uses the probability of non-interception of light passing through the forest canopy to infer structural characteristics. They also rely on a number of theoretical assumptions about the canopy structure, specifically that the foliage elements are planar and distributed randomly within the canopy volume (according to a Poisson point process) [4,7]. In reality, the structure of forest canopies deviates from these assumptions. Forest canopies are a collection of foliage, twigs, and branches that are often clumped around branches and into discrete crown. Various researchers have proposed modifications of the Monsi and Saeki equations relating gap probability to LAI using correction factors that account for leaf and needle clumping or the contribution of woody vegetation components (see [8] for a detailed review). As these correction factors are difficult to measure directly, they are usually inferred from the indirect passive optical measurements. Additionally, passive optical methods are susceptible to specific hemispherical sky illumination conditions, in particular direct sunlight, that can impact apparent gap probability for a given canopy structure (e.g., [9–12]).

Light Detection and Ranging (LiDAR), sometimes referred to as laser scanning, has received increased attention in forestry in recent years as a means of overcoming the limitations of conventional indirect structural measurements. Depending on the platform that the scanner operates from, laser scanning is commonly categorized into airborne laser scanning (ALS), and terrestrial laser scanning (TLS) or terrestrial LiDAR (TLiDAR). LiDAR is based on the emission of a highly collimated laser pulse and registering its reflected signal from objects. This yields not only explicit 3-D information (range and location relative to the scanner position) but also information about the magnitude of the reflected signal in relation to the magnitude of the emitted pulse (*i.e.*, its apparent reflectance [3]).

Two common range measurement methods are used in commercial TLS instruments, phase-shift and time-of-flight [13]. Phase-shift scanners use the difference in phase between the emitted and received continuous laser beam with its power modulated at a series of frequencies. Time-of-flight scanners are based on a measurement of the time difference between the emission of a laser pulse and

the registering of a reflected return pulse. While phase-shift scanners record only a single range per measurement direction, time-of-flight scanners may record more than one range or even continuously record the return intensities as a waveform [14]. Range measurement methods can influence the resulting data properties (e.g., maximum range, ranging error and noise, measurement speed). In turn, these may influence the retrieval of vegetation structural metrics.

While phase-shift scanners are characterized by extremely high measurement speeds, their maximum range tends to be more restrictive than time-of-flight scanners [15]. Both, phase-shift and time-of-flight scanners, have been successfully used for the retrieval of structural and biophysical forest metrics. These include tree positions (e.g., [16,17]), tree height (e.g., [18,19]), diameter at breast height (e.g., [20,21]), stem volume (e.g., [22,23]), biomass (e.g., [24–26]).

Terrestrial laser scanning has been shown to be particularly useful in the retrieval of gap fraction and LAI. This is due to the low sensitivity to variable sky illumination conditions, and the enhanced information content captured within the 3-D data [27]. In particular the possibility of explicitly characterizing three-dimensional canopy structure is widely acknowledged as the major benefit of TLS (e.g., [3,7,28,29]). This is fundamental in the characterization of the orientation and 3-D distribution of vegetative elements (leaves, branches, stems) within the forest canopy (as defined by [1]), but also allows detailed analysis of the size and 3-D distribution of canopy gaps, leading to increased understanding of radiative transfer through the canopy [30,31]. The ability to measure the 3-D distributions of canopy gaps and vegetative elements also allows explicit analysis of clumping, which can only be indirectly inferred from passive-optical measurements, such as hemispherical photography [3,7,32].

Another advantage of the 3-D data provided by TLS is the possibility to more accurately measure leaf area [28,33,34]. Two general methods of estimating LAI using TLS have been identified [11]: gap fraction and voxel based methods. The voxel approach [27,29–31,35,36] divides the 3-D scanner environment into cubic volume elements (voxels), which are populated by canopy elements based upon ray-tracing of the scan data. Leaf area can then be estimated based on the number and location of voxels, which are shown to contain vegetation. More sophisticated 3-D approaches have also been demonstrated, such as the tree reconstruction by Côté *et al.* [37], or the geometrical crown depth method of Huang and Pretzsch [38].

By comparison, the gap fraction approach uses the numbers of laser returns in given zenith angle ranges to an estimate of gap probability. These gap probability measurements are subsequently used to determine LAI, in a similar manner to methods well known in hemispherical photography [6,10,11,39–42]. However, the 3-D information from the scanner can be further utilized to determine the vertical distribution of this LAI in the form of vertical foliage profiles [3,9,12,32].

The gap fraction methods that solely rely on the angular gap fraction information (2D methods) have two main disadvantages: (1) they lose the 3-D information [10] and (2) they are limited in their application to single scans. This is in contrast to the 3-D methods, which are mostly based upon merged scan point clouds from multiple scans acquired at different locations. Although the merging of scans from different viewpoints is associated with higher computational demands, as well as a time-consuming scan data acquisition and registration, it is, thus far, the most effective method for reducing the effect of occlusion.

Both 3-D and 2-D based LAI estimation methods are influenced by the so-called edge effect [28], where partial interception of the beam occurs at the edge of objects, and the remaining pulse travels further to hit other objects or travel through canopy gaps. While the intensity information recorded by full waveform scanners allows an accurate assessment of the proportion of the beam intercepted, and thus the true within beam gap fraction [12], complete interception or gap must be assumed with the discrete return time-of-flight and phase-shift scanners. Partial interceptions in phase-shift scanner data may also produce artifacts caused by range averaging which can confuse gap filtering and result in the total disregard of partial interceptions in gap probability calculations [39].

Of significant concern in vegetation structure assessment is also the inability of phase-shift scanners to unambiguously record non-interception of the beam. This results in randomly distributed points within canopy gaps that need to be addressed through firmware filtering or post processing. Both the artifacts caused by range averaging and the beam non-interceptions need to be filtered. Traditionally in TLS, filtering is applied to reduce noise, which usually refers to the ranging noise defined as the standard deviation of the distances about the best-fit plane of the points on a planar target [43]. This type of noise depends on a number of factors including the targets' reflectivity and can be minimized by noise compression (*i.e.*, increase the signal-to-noise ratio usually achieved by averaging of multiple returns within a pulse window) [43]. In vegetation structure assessment noise is important as it contains information about the size and distribution of gaps within the canopy. In many cases, filtering is based on both the inferred location and intensity of laser returns. As return intensities are the result of complex interactions of a number of factors including scanner properties such as beam divergence, beam spot size, range, return response threshold [29], and target properties such as orientation, surface texture, and bidirectional reflectance characteristics [27,37,40], the estimation of gap fraction and LAI from phase-shift scanner data is heavily influenced by the filtering methods applied.

This paper investigates the effects of scanner and scan properties on the retrieval of gap fraction and PAI_e derived from phase-shift scanner data. The application of phase-shift scanners for the retrieval of gap fraction and related metrics has not been investigated when compared to discrete return time-of-flight scanners (e.g., [10,11,28,29–31,33,37–42]) and time-of-flight full waveform scanners (e.g., [3,9,12,33,34,44]). This study tries to bridge this gap by investigating the effects of the main phase-shift scan properties of scan resolution (angular step size) and measurement speed (pulses per second), as well as a scanner-specific noise compression and firmware based data filtering using a phase-shift FARO Photon 120 terrestrial laser scans.

2. Materials and Methods

2.1. Study Site

The study site (49°16′N, 7°48′E) is located in the Pfälzerwald forest near Kaiserslautern, Germany. The study was carried out at two test plots within stands where permanent forest monitoring is carried out. This monitoring has produced a large pool of *in situ* biophysical and structural measurements including litterfall. One test plot was established at a pure beech (*Fagus sylvatica*) stand, which is characterized by a distinct overstorey of dominant trees around 50 years old and a layer of emerging trees younger than 50 years. The other test plot was established at a mixed stand of 200-year-old oak

(*Quercus petraea*) trees in the overstorey and young beech (*Fagus sylvatica*) trees in the understorey. Mean diameter at breast height (DBH) and mean tree height for the beech stand were 16.4 cm (σ = 7.3) and 18.5 m (σ = 5.7). The stem density of the beech stand was 1032 trees per ha. Mean DBH and mean tree height for the oak-beech stand were 34 cm (σ = 17.1) and 30.7 m (too few height measurements available for reliable standard deviation for tree height). The stem density of the oak-beech stand was 283 trees per ha. Both stands were characterized by consistent slopes (~3°) and mean elevations of around 522 m.

2.2. Data Acquisition and Scanner Characteristics

Terrestrial Laser Scanning was carried out with a FARO Photon 120 phase shift instrument [43]. This scanner operates at a wavelength of 785 nm, with measurement speeds of up to 976,000 points per second, and with variable angular step sizes. The beam diameter (at exit) is 3.3 mm and beam divergence is 0.16 mrad [43]. The height above ground of the instruments beam emission point was set to 1.75 m and scans were performed at single locations with a field-of-view of 360° horizontal and 310° vertical, providing an almost complete spherical capture of the scanner's surroundings.

Table 1. FARO Photon 120 scanner parameter sets used at each of the two study plots (modified from table in [43]). Resolution refers to the ratio of the maximum resolution of 40,000 pts/360° for each rotation of the scan head. Noise compression factors 2× and 4× refer to the averaging of ranges within two by two and four by four laser pulse windows respectively. Durations of the hardware filtering are approximate.

Resolution	Angular Step Size (°)	Point Spacing (cm/10 m)	Scan Speed (kpt/s)	Noise Compression	Scanning Time (min)	Filtering Time (min)
1/2	0.018	0.3	976	-	03:24	03:25
			488	-	06:49	03:15
			244	-	13:39	02:30
1/4	0.036	0.6	488	-	01:42	01:06
			244	-	03:24	01:01
			122	-	06:49	01:01
			244	2×	13:39	16:02
1/8	0.072	1.3	244	-	00:51	00:30
			122	-	01:42	00:26
			244	2×	03:24	04:16
			122	2×	06:49	04:18
			244	4×	13:39	14:20
1/16	0.144	2.5	244	2×	00:51	01:15
			122	2×	01:42	01:10
			244	4×	03:24	03:45

To assess the effects on gap fraction and PAI$_e$ retrieval, scans were performed with different angular step size, measurement speed, and noise compression (Table 1). Scan parameters were chosen to provide comparable datasets at each plot while not exceeding scanning times of 15 min. Each scan setting was tested at the centre points of the two test plots and on four different dates (24 April 2013,

2 May 2013, 10 May 2013, 7 June 2013). Dates were chosen to cover the phenology of leaf development. Leaf development took place predominantly between the second and third measurement dates. As such, the first two dates can be characterized as leaf-off, while the latter two dates can be characterized as leaf-on.

All scans were performed with the FARO Photon 120 hardware filters, "clear sky" and "clear contour", activated. The "clear sky" filter removes scan points with low intensity, which result from intercepting no object, *i.e.*, mainly when the scanner views open sky. The "clear contour" filter removes scan points with large separation to surrounding points, which can be the result of intercepting multiple objects, mainly at the edges of foreground objects [43]. In addition to these hardware filters, three different levels of noise compression can be set prior to scanning with the FARO Photon 120: no compression, noise compression by averaging neighboring scan points in a two by two window, and noise compression by averaging scan points in a four by four window [43].

LAI measurements obtained by collection of leaf litter were used as reference. As litterfall LAI for the year laser scans were recorded (2013) were not yet available, long-term averages for the test sites [45] were used in this study. As the beech stand was thinned shortly before the last scan date, the long-term average for the beech stand was not included.

2.3. Scan Data Pre-Processing

The scan data was collected in the proprietary FARO format and exported to PTX, an ASCII-based format that orders the scan points (Cartesian coordinates relative to the instrument optical center and laser return intensities) according to measurement time while recording non-returns as zero for all Cartesian axes. Spherical coordinates (zenith, azimuth, and range) are then computed from the Cartesian coordinates. In cases where a zero range was recorded (*i.e.*, sky points) zenith and azimuth angles were interpolated from valid (non-zero) neighboring returns. The coordinate system conversion allows projecting the scan data as 2D raster images with azimuth and zenith representing x and y. The original Cartesian coordinates, as well as the range and intensity information, were stored as separate image bands. Figure 1 shows a subset of range images for the different scan parameter sets applied in this study. The difference in the visual appearance of these subsets demonstrates the influence of the scan parameters, particularly apparent in the level of noise within the canopy gaps.
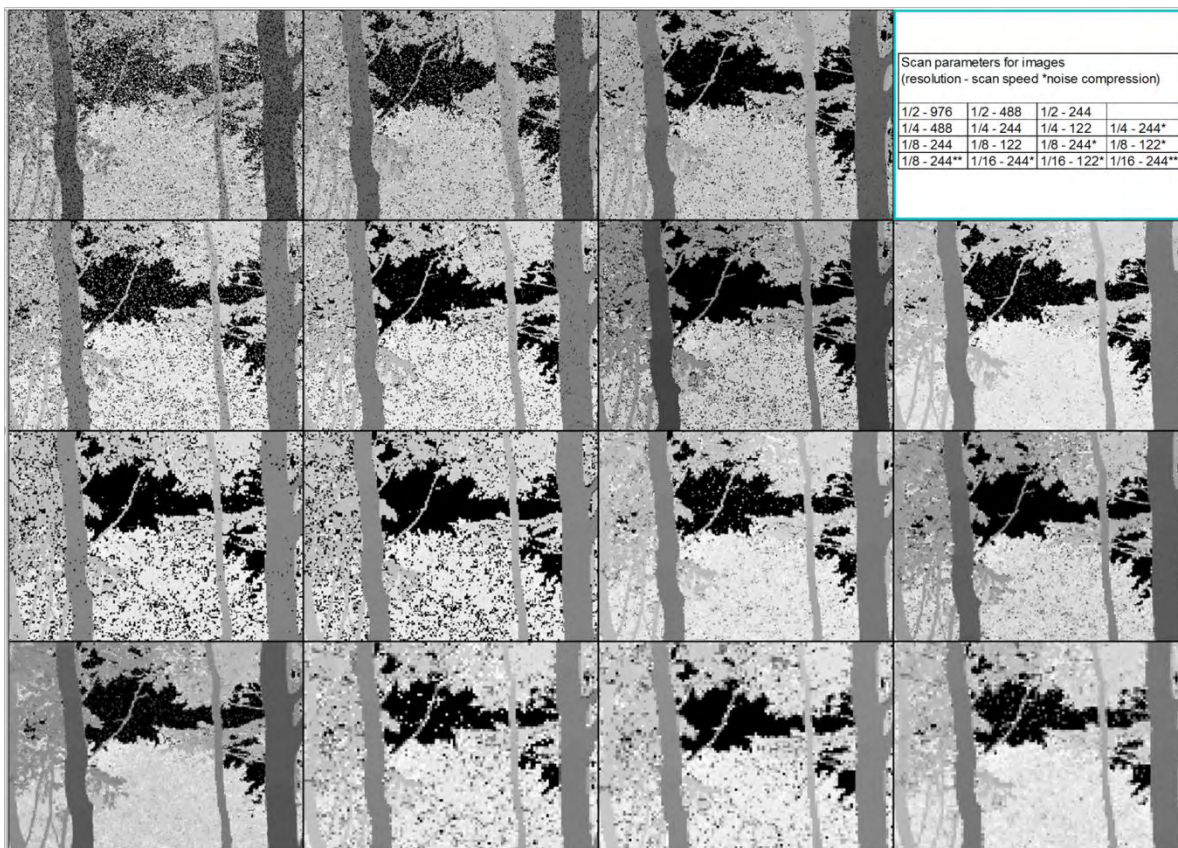
2.4. Scan Data Filtering

Phase shift scanners, such as the FARO Photon 120 are known to suffer from noise (see Section 1). While for traditional applications of terrestrial laser scanning noise is mostly treated as unwanted data and simply removed from the point cloud, noise is important in vegetation structural analysis as it contains information about the size and distribution of gaps within the canopy.

To develop a data processing scheme for a consistent and accurate detection of canopy gaps, the effects of FARO's hardware filtering were studied in detail based on two sets of test scans: The first set included scans performed with and without the "clear sky" filter and with "clear contour" activated in both cases. The second set includes scans performed with and without the "clear contour" filter and with "clear sky" activated in both cases. Constant intensity thresholds were used to separate

sky returns from the "clear sky" and "clear contour" filtered scan returns. In addition, the sensitivity of the gap fraction and PAI_e estimates to threshold changes was assessed by varying the threshold by ±5%.

Figure 1. Scan range images based on the different scan parameter sets applied in this study. Legend: Scan resolution is displayed as the fraction of the full resolution (40,000 points per 360°). Scan speed is displayed in kilo-points per second. The single asterisk denotes scans performed with 2× noise compression and the double asterisk denotes scans performed with 4× noise compression.

Scan parameters for images
(resolution - scan speed *noise compression)

1/2 - 976	1/2 - 488	1/2 - 244	
1/4 - 488	1/4 - 244	1/4 - 122	1/4 - 244*
1/8 - 244	1/8 - 122	1/8 - 244*	1/8 - 122*
1/8 - 244**	1/16 - 244*	1/16 - 122*	1/16 - 244**

To deal with the noise that results from beam non-interceptions (see Section 1 and Figure 1), we applied a kernel-based majority filter (kernel of 3 × 3 pixels) to the 2D scan images, *i.e.*, each image pixel which is not classified as sky is checked for its 8 surrounding pixels. If the majority of these are classified as sky, the centre pixel is assumed to be noise and consequently reclassified as sky. To assess the effect of this type of noise on the retrieval of gap fraction and PAI_e, the scan data was analyzed both with and without applying the majority filtering.

2.5. Gap Fraction and PAIe Calculation

The indirect optical methods of estimating gap fraction and Leaf Area Index are mainly based on modeling the radiation transmission through the canopy (see [46]). Assuming a random azimuthal foliage distribution and using Beer's Law, this gap probability is modeled as a function of foliage projection function G toward a zenith angle θ, LAI, and path length through the canopy (the cosine of θ) such that:

$$Pgap(\theta) = e^{-G(\theta)LAI/\cos(\theta)} \tag{1}$$

The clumping of canopy elements, particularly into individual tree crows can lead to an increase in the gap probability for a given LAI. In this case, the term effective LAI is often used in the above equation [47]. In addition, since the distinction between foliage and woody material can often not be made with the passive-optical instruments, the estimated leaf area is truly a Plant Area Index (PAI). Hence in this study the term effective Plant Area Index (PAI_e) is used. For active-optical instruments such as TLS, various approaches to the estimation of gap fraction and LAI exist (see Section 1). In this study the gap fraction based approach was followed. In this approach gap fraction is inferred from the number of laser pulses with no returns from the canopy within some zenith angle range $d\theta$ (N_{gap}) as a proportion of the total number of pulses emitted by the instrument within $d\theta$ (N_{pulses}). Note that this is the complement to fractional cover based on canopy hits N_{canopy}:

$$Pgap(d\theta) = N_{gap}(d\theta)/N_{pulses}(d\theta) = (1 - N_{canopy}(d\theta))/N_{pulses}(d\theta) \tag{2}$$

Miller [48] proposed the following solution for Equation (1):

$$LAI = 2 \int_{0}^{\pi/2} -\ln\big(Pgap(\theta)\big)\cos\theta\sin\theta d\theta \tag{3}$$

Based on gap fractions averaged over zenith angle ranges $d\theta_i$, e.g., LI-COR PCA measurements [49], Equation (3) can be integrated numerically by summing the weighted logarithms of the individual zenith angle ranges' gap fractions (Equation (4)).

$$LAI = 2 \sum_{i=1}^{n} -\ln\big(Pgap(d\theta_i)\big)\cos\theta_i\sin\theta_i d\theta_i \tag{4}$$

With the LI-COR PCA, five zenith angle ranges (0–13°, 16–28°, 32–43°, 47–58°, 61–74°) are used. The weights $\sin\theta_i d\theta_i$ are based on the centre angles of these ranges. The weights are then normalized to sum to one [49]. Sometimes only ranges 1–4 with a stronger weighting of the fourth range are used in the calculation of LAI to reduce the effects of multiple scattering which is strongest in the higher zenith angles resulting in a frequent underestimation of LAI [50]. Leblanc and Chen [51] also showed that while the fifth range is least sensitive to changes in canopy LAI, the third and fourth ranges are most stable in case of variable sky radiation. The strong weighting of the fourth range is based on the theory that for an idealized random foliage distribution and a view angle of 57.5°, the projection coefficient G (~0.5) is independent of the mean leaf angle [52]. This is used to determine LAI directly from gap fraction measurements at this angle [3]:

$$LAI = -1.1\ln\big(Pgap(57.5°)\big) \tag{5}$$

In this study, in order to assess the effects of resolution, measurement speed, and noise compression on the retrieval of gap fraction, and hence their influence on the calculation of PAI_e, the numerical integration of Equation (4) based on ranges 1–4 and based on ranges 1–5 was used. These are, hereafter, referred to as PAI_e (0–58°) and PAI_e (0–74°). In addition, the gap fraction retrieved from a small zenith range (±2.5°) centered on 57.5° was used in accordance with Equation (5) to calculate PAI_e, hereafter referred to as the PAI_e (57.5°).

3. Results and Discussion

3.1. Data Filtering

One of the key challenges in the use of phase-shift laser scanners for vegetation structural assessment is the correct and unambiguous identification of canopy gaps. This requires different filtering methods to those employed for application in built structures such as engineering and mining. Figure 2 depicts the intensity and range images of the set of test scans filtered (hereafter referred to as the filtered scan) and unfiltered (hereafter referred to as the raw scan) with the FARO "clear sky" filter. To analyze the range and intensity distribution of sky points, scan regions visually identified as sky were subset and statistics calculated. The corresponding histograms are depicted in Figure 3. While the range values of the sky points from the raw scan show a uniform random distribution, the intensity distribution shows a distinct bimodal pattern which spans almost the full value range. From these observations it is obvious that for raw scans, sky points cannot be separated from non-sky points based on the range and intensity distributions alone (*i.e.*, a simple thresholding is not applicable).

> **Figure 2.** Range and intensity images of the test scans without "clear sky" filtering (**Left**) and with "clear sky" filtering (**Right**). Intensity images are displayed above their respective range image. The images' grayscales were stretched to maximize the contrast between sky and canopy, with black and white corresponding to minimum and maximum values respectively.
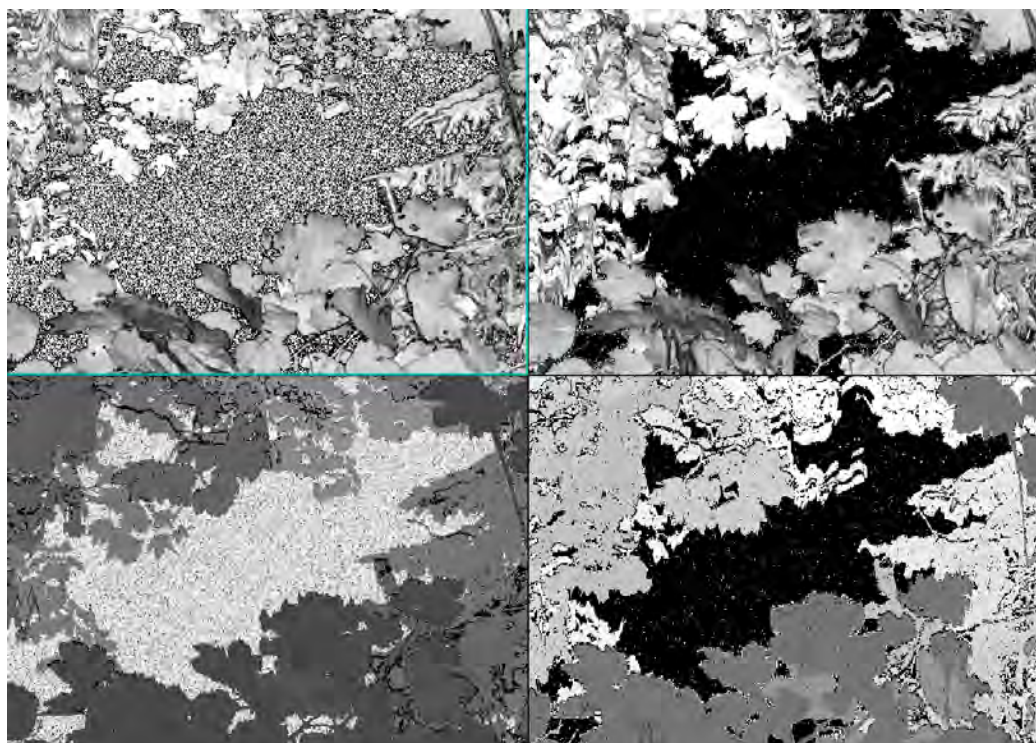
As mentioned, scan points identified by the "clear sky" filter are assigned zero range (Figure 3b). The presence of a number of non-zero values in Figure 3b reveals that the "clear sky" filter does not detect all sky points. These also show in Figure 3d as the small number of high intensities protruding from an otherwise normal distribution. As the histograms are based on sky points retrieved from the

same image regions of the raw and the filtered scan, another interesting observation to note is that the "clear sky" algorithm obviously rescales the intensity values of sky points to achieve this normal distribution (see Figure 3b,d).

Figure 3. Range and intensity histograms of sky points retrieved from the images' canopy gaps displayed in Figure 2. (**a**) Range histogram of the unfiltered scan, (**b**) Range histogram of the filtered scan, (**c**) Intensity histogram of the unfiltered scan, (**d**) Intensity histogram of the filtered scan.
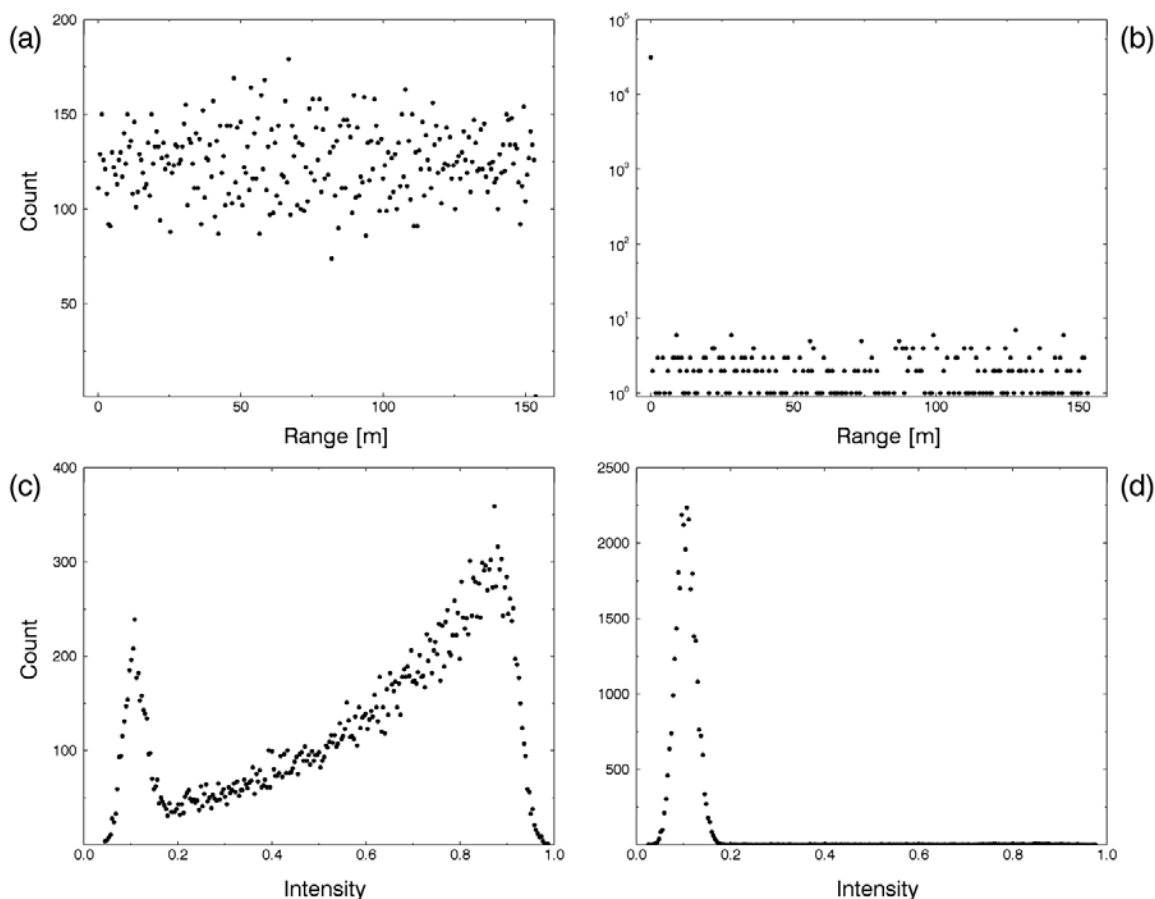
To further analyze hardware filter interactions, the second test set was used to plot the intensity distribution of all scan points which were assigned zero range by the hardware filters (Figure 4). As higher intensity values are assumed to be not sky, the bimodal shape of the histogram from the scan without the "clear contour" filter reveals that the "clear sky" algorithm erroneously filters non-sky points (Figure 4a). Their occurrence increases strongly in case of additionally applying the "clear contour" filter (Figure 4b). These erroneously filtered non-sky points can also be visually identified in the range images as the random black pixels spreading over the foliage (Figure 2).

While the peak centered on the intensity value of 0.6 in Figure 4b can be explained by beam interceptions of multiple targets with high intensities such as stems or branches, the increase in the peak centered at 0.15 may be explained by partial interceptions of the beam. Clearly, the removal of these non-sky points by the hardware filtering will result in an overestimation of gap fraction.

Figure 4. Intensity histograms of all filtered scan points retrieved from the second set of test scans. (**a**) Scan filtered only with "clear sky". (**b**) Scan filtered with "clear sky" and "clear contour".
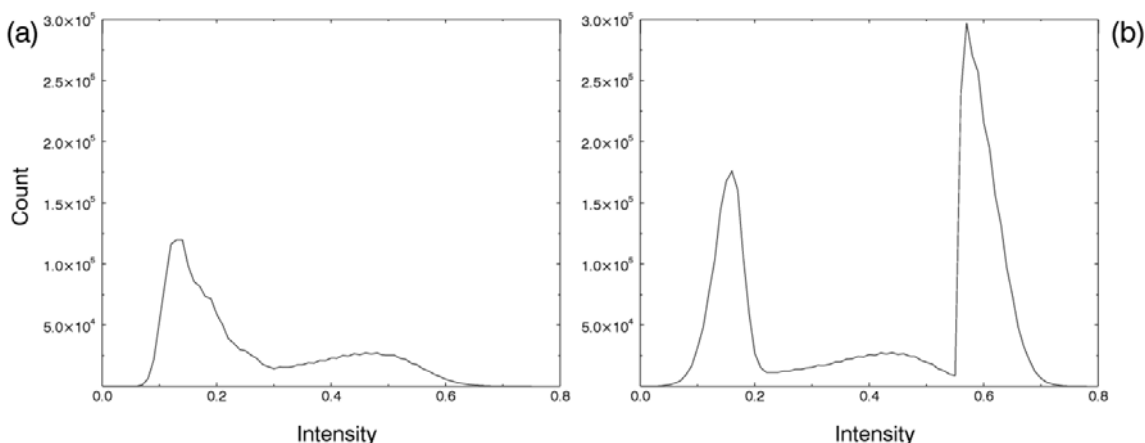
To deal with errors of omission in the detection of sky points we applied a three by three pulse window kernel-based majority filter. This was run and resulted in complete removal of unfiltered points from the sky region of the test scan. To deal with errors of commission, where true and partial vegetation returns were considered sky, a simple intensity threshold was applied, such that all points with an intensity value greater than a threshold were considered true vegetation returns. However, since histograms represent scene-dependent statistics, the histogram-based intensity thresholding is not straightforward. This is obvious from Figure 5 which shows the intensity histograms of sky points for scans of different scan resolution and measurement speed. Based on these observations from the test scan regions we applied a constant intensity threshold of 0.3.

Figure 5. Intensity histograms of sky points retrieved from test scan regions with different scan parameters (scan resolution and measurement speed).
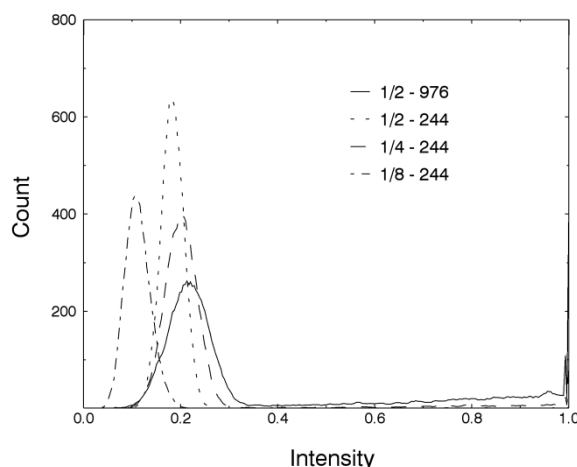

3.2. Gap Fraction

To investigate whether the effects of the scan parameters on the retrieval of gap fraction exhibit a dependency on zenith angle, leaf development phase, and stand structure, the retrieved gap fractions

were plotted separately for zenith rings of 10 ° width, for leaf-off and leaf-on development phases, and for the two test plots of different stand structure (Figures 6 and 7). The most striking feature of Figures 6 and 7 are the strong differences in the gap fractions retrieved from scans, with and without noise compression. Gap fractions from noise-compressed scans are much lower than those from non-compressed scans. This effect is independent of zenith, leaf development phase, stand structure, and the other parameters (*i.e.*, scan resolution and measurement speed) investigated. The differences are less pronounced for high to medium zenith angles (0–55 °) than low zenith angles (>55 °), in particular for leaf-on scans (Figures 6 and 7).

Figure 6. Average gap fractions of the scans collected at the Beech plot with different scan parameters. Legend (scan parameters): Scan resolution is displayed as the fraction of the maximum scan resolution. Scan speed is displayed in kpts/s. The single and double asterisks denote scans performed with the 2-factor and 4-factor noise compression.
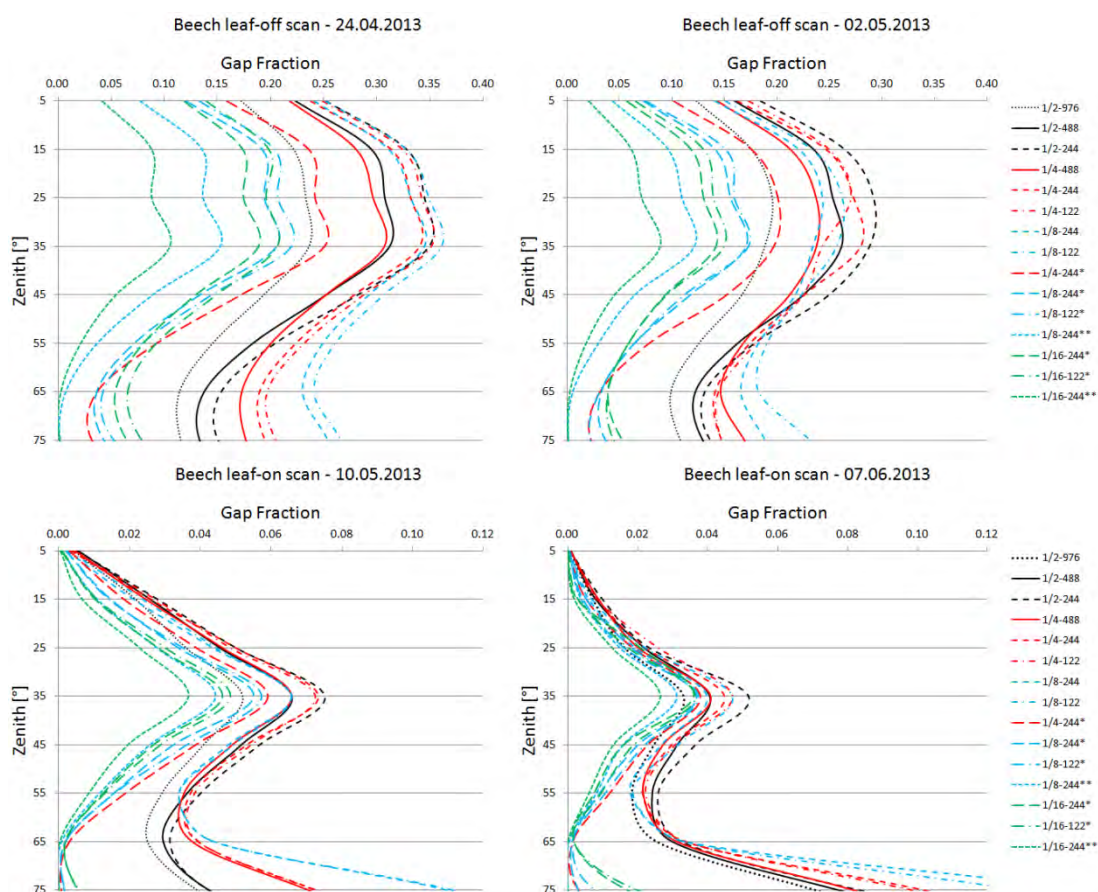
This can be explained by the combined effects of stand structure, laser beam divergence, scan resolution (point density), range, and the noise compression algorithm (see Section 2.2). Due to the increasing laser beam spot size and point spacing with range (spot sizes of 0.45 cm, 0.97 cm, and 1.85 cm for ranges of 10 m, 30 m, and 60 m; for a list of point densities achieved see Table 1), and the larger canopy path lengths for low zenith angles, the probability of hitting only gaps is reduced strongly for low zenith angles and in case of a general decrease of gaps with canopy closing.

Figure 7. Average gap fractions of the scans collected at the Oak-beech plot with different scan parameters. Legend (scan parameters): Scan resolution is displayed as the fraction of the maximum scan resolution. Scan speed is displayed in kpts/s. The single and double asterisks denote scans performed with the 2-factor and 4-factor noise compression.
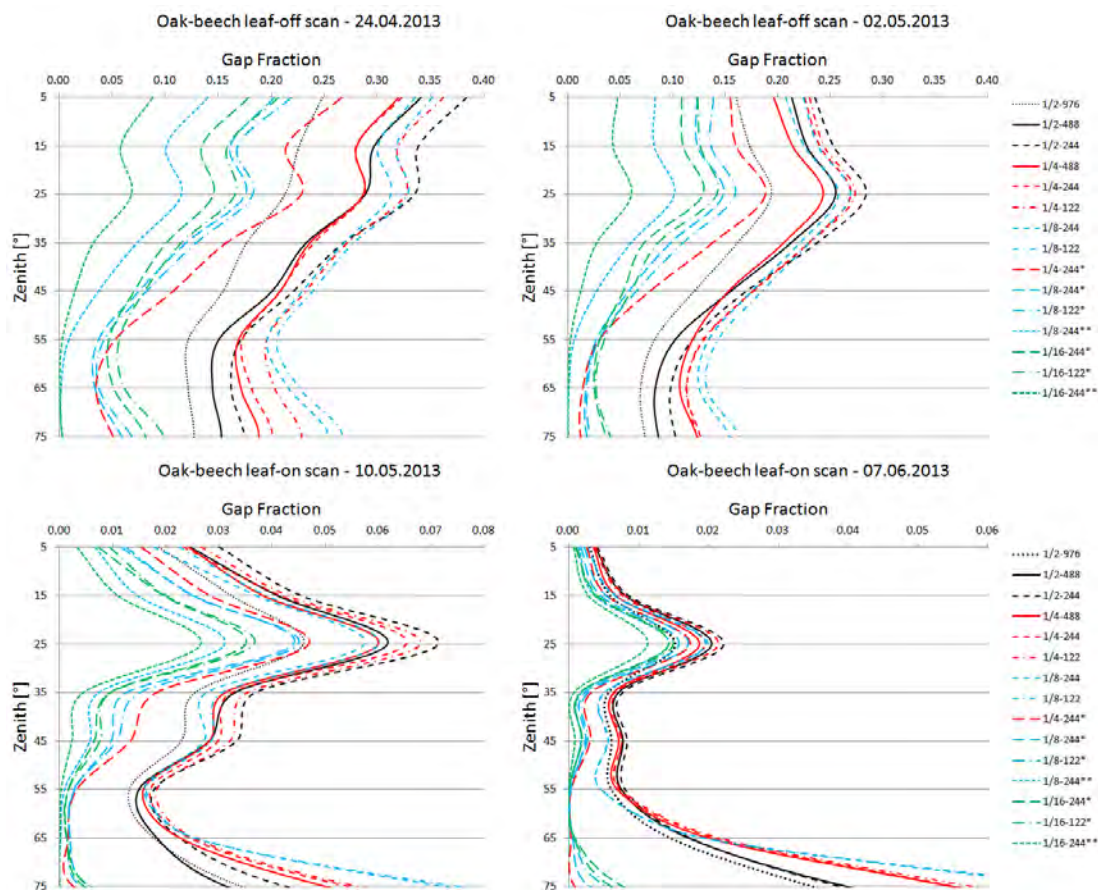
With regard to the level of noise compression, the 4-factor noise compression results in smaller gap fractions compared to the 2-factor noise compression, due to the stronger spatial averaging. However, absolute gap fraction differences between the two noise compression factors are smaller for leaf-on scans and for low zenith angles (Figures 6 and 7). While for leaf-on scans this is caused by the general decrease of large gaps with canopy closing, the smaller differences for low zenith angles is the result of stand structure, laser beam divergence, scan resolution, and range. Based on these results it is clear that stand structure is a key factor in determining the magnitude of the noise compression effect. For low-density stands with a large proportion of between-canopy gaps, the spatial averaging of scan points should influence the gap fraction estimation a lot less compared to dense stands with a large proportion of smaller within-canopy gaps.

With regard to the effects of the scan resolutions and measurement speeds applied in combination with the noise compression, the different measurement speeds result in marginal differences, which however seem to be larger for high zenith angles and for leaf-off scans. This is observed for both test plots and both the 1/8 and 1/16 scan resolutions (Figures 6 and 7). By contrast, the scan resolutions have a stronger effect on the gap fraction estimates, yielding larger gap fractions for high zenith angles with increasing scan resolution. This effect is less pronounced for leaf-on scans. For low zenith angles

(>55°) this pattern is reversed, *i.e.*, gap fraction increase with decreasing resolution. This can be observed for the different leaf development phases and for both plots (Figures 6 and 7). Given the decreasing probability of hitting only gap within the low zenith angle range for scans with decreasing resolution due the spatial averaging of larger scan point spacing, this reversal is difficult to explain. A possible explanation might be that with decreasing resolution an increasing proportion of low zenith scan points is erroneously filtered and removed by the hardware filters.

With regard to the effect of the scan parameters on the gap fractions derived from the scans without noise compression, a similar dependency on zenith angle can be observed for the scan resolution. For angles greater than 55°, gap fractions increase with decreasing resolution, an effect which is independent of leaf development phase and stand structure (Figures 6 and 7). Again, this might be attributed to the fact that scan points are disproportionally filtered out from lower resolution scans. Gap fractions retrieved from zenith angles smaller than 55° exhibit no systematic pattern as a function of scan resolution. Scans performed with the resolutions 1/4 and 1/8 also show gap fraction differences between the two measurement speeds 244 and 122 kpts/s which appear to be random, rather than systematic. By contrast, a distinct effect of measurement speed can be observed for the scans with resolution 1/2, *i.e.*, an increase in gap fraction with decreasing scan speed. This effect is independent of leaf development phase and stand structure, and it is more pronounced for high to medium zenith angles (0–55°) and for leaf-off scans (Figures 6 and 7). The reason for this effect is the higher noise level (*i.e.*, larger number of undetected sky points) present within canopy gaps with increasing measurement speed (see Figure 1). Since there is, (a) a larger number of gaps within the high to medium zenith canopy regions compared to the low zenith angles; and (b) a general larger number of gaps during the leaf-off phase, the magnitude of this noise is more pronounced for high to medium zenith angles and for leaf-off scans.

3.3. PAIe

To investigate how the differences in the retrieved gap fractions resulting from the different scan parameters translate into differences in PAI_e, in particular accounting for the effects of using different LAI calculation methods, PAI_e was calculated with three methods (see Section 2.5) for the two plots and the four different acquisition dates (Figures 8 and 9). As was to be expected from the gap fraction results, the strong effect of the noise compression is clearly reflected in the PAI_e results. For the scans with parameter combinations 1/4-244, 1/8-244, and 1/8-122, which allow a direct comparison of the magnitude of this effect (see Table 1), PAI_e increases by 54%, 73%, and 76% (mean of the three LAI methods and in the order of the above-mentioned parameter combinations) for the leaf-off beech scans, by 27%, 30%, and 28% for the leaf-on beech scans, by 64%, 84%, and 83% for the leaf-off oak-beech scans, and by 44%, 42%, and 41% for the leaf-on oak-beech scans.
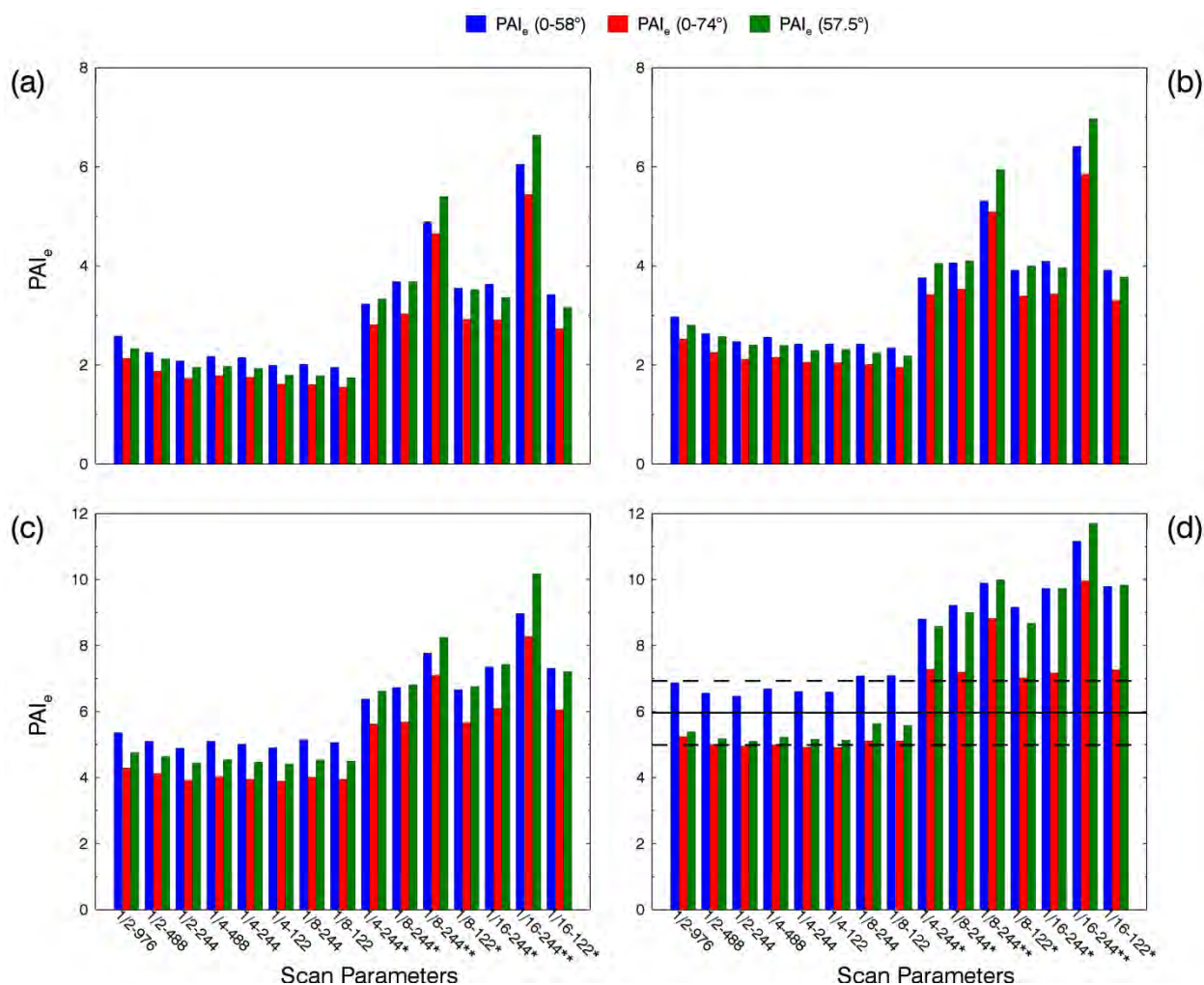
The effect of the noise compression level itself can be observed from the scans with parameter combinations 1/8-244 and 1/16-244 (see Table 1). Compared to the 2-factor compression, applying the 4-factor noise compression increases the PAI_e by 32% and 55% (mean of the three LAI methods and in the order of the above-mentioned parameter combinations) for the leaf-off beech scans, by 9% and 17% for the leaf-on beech scans, by 42% and 76% for the leaf-off oak-beech scans, and by 17% and 28% for the leaf-on oak-beech scans.

Figure 8. Effective PAI based on the scans collected at the Beech plot with different scan parameters. Leaf-off dates: (**a**) 24 April 2013. (**b**) 2 May 2013. Leaf-on dates: (**c**) 10 May 2013. (**d**) 7 June 2013. Scan parameters: Scan resolution is displayed as the fraction of the maximum scan resolution. Scan speed is displayed in kpts/s. The single and double asterisks denote scans performed with the 2-factor and 4-factor noise compression.
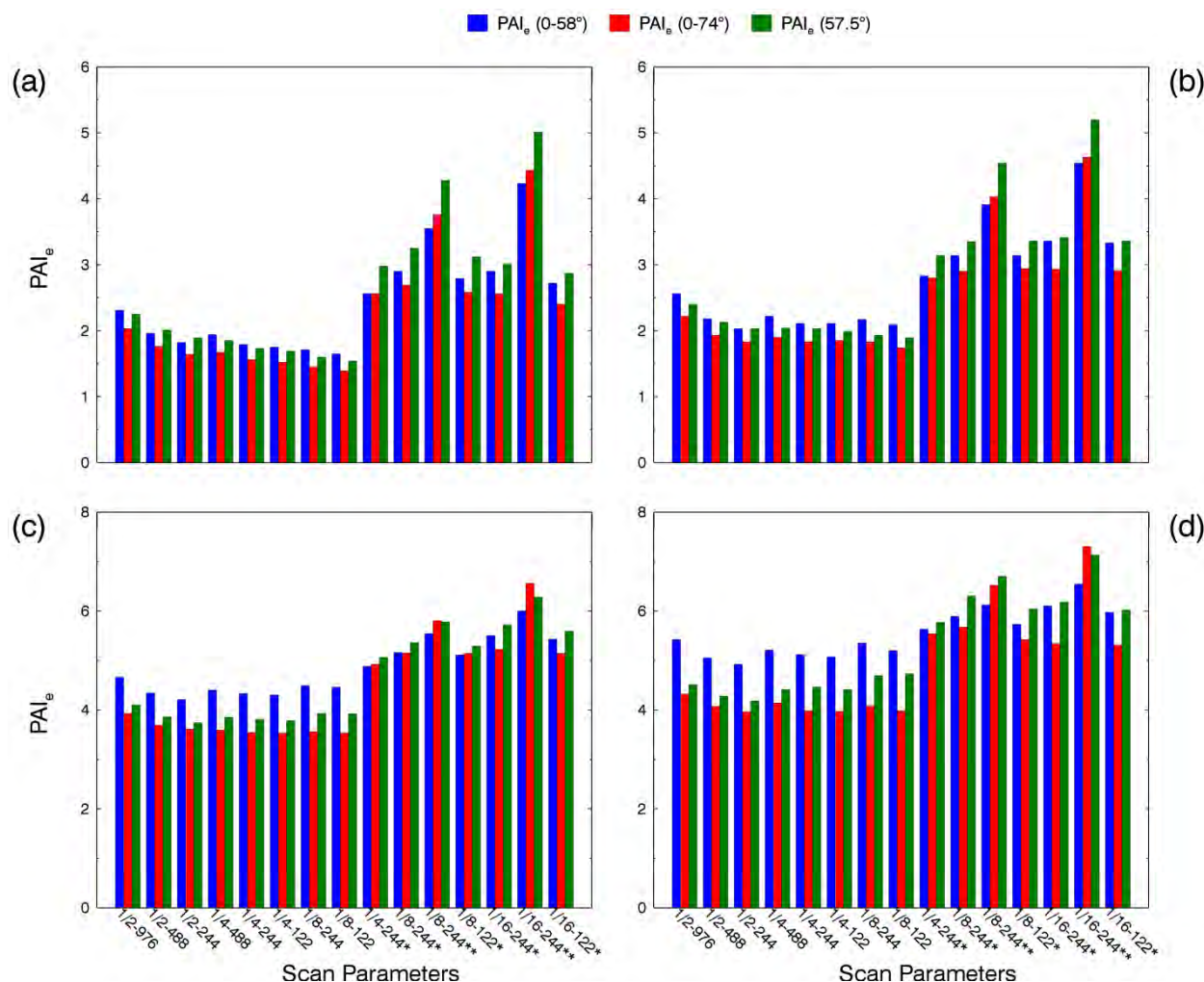
The stronger effect for the leaf-off scans can be attributed to the larger number of gaps with noise (*i.e.*, undetected sky points) present. Since noise compression particularly affects the gap fraction retrieved from low zenith angles (see Section 3.2), the LAI calculation methods with a stronger weighting of gap fractions from these zenith regions, PAI_e (0–58°) and PAI_e (57.5°), are affected by noise compression more strongly than the PAI_e (0–74°): PAI_e increase by 69% and 81% compared to 52% (leaf-off beech), by 76% and 88% compared to 68% (leaf-off oak-beech), by 41% and 33% compared to 12% (leaf-on beech), and by 42% and 55% compared to 30% (leaf-on oak-beech). These averages are based on the percentage deviations in PAI_e of all scan pairs with comparable parameter combinations and the 2-factor noise compression. The 4-factor noise compressed scans confirm this trend. By contrast, the resolutions and measurement speeds applied in combination with the noise compression only have a marginal influence on the PAI_e (Figures 8 and 9).

Figure 9. Effective PAI based on the scans collected at the Oak-Beech plot with different scan parameters. Leaf-off dates: (**a**) 24 April 2013. (**b**) 2 May 2013. Leaf-on dates: (**c**) 10 May 2013. (**d**) 7 June 2013. Scan parameters: Scan resolution is displayed as the fraction of the maximum scan resolution. Scan speed is displayed in kpts/s. The single and double asterisks denote scans performed with the 2-factor and 4-factor noise compression. The lines in 9 (d) depict the mean (solid line) and standard deviations (dashed lines) of the litterfall LAI for the period 2004–2008.

With regard to the effect of the scan parameters applied without noise compression, a pattern of decreasing PAI_e with decreasing measurement speed and with decreasing scan resolution can be observed, in particular for the leaf-off scans. This effect is also more pronounced for the 1/2 resolution than resolutions 1/4 and 1/8, as a consequence of the observed gap fraction pattern (see Section 3.2). Concerning the different LAI calculation methods applied, the PAI_e derived from the uncompressed scans decrease in the order of methods, PAI_e (0–58 °), PAI_e (57.5 °), and PAI_e (0–74 °). This effect is enhanced with gradual canopy closing (Figures 8 and 9). In spite of the various scan resolutions and measurement speeds applied, the PAI_e estimates based on the scan parameter combinations without noise compression are quite stable, in particular taking into account the variability induced by the use of different LAI calculation methods: The mean PAI_e standard deviations (standard deviations of the PAI_e values from all parameter combinations without noise compression averaged for the three LAI

methods) are 0.22, 0.15, 0.13, 0.16 for the beech scans, and 0.20, 0.19., 0.13, 0.19 for the oak-beech scans (in ascending order of dates). By comparison, the mean PAI_e range of the LAI methods (range of the PAI_e calculated with the three LAI methods averaged for all parameter combinations without noise compression) are 0.24, 0.29, 0.77, and 1.11 for the beech scans, and 0.39, 0.39, 1.05, and 1.72 for the oak-beech scans (again in ascending order of dates).

To assess whether the PAI_e based on the scans with our without noise compression are closer to the "true" LAI, the mean and standard deviations of litterfall LAI for the oak-beech plot was included in the analysis (Figure 9d). As actual 2013 litterfall LAI are not yet available, and litterfall can vary considerably from year to year, the comparison with litterfall LAI is supposed to allow for an indication of trend rather than a rigorous validation. In addition, whereas litterfall actually yields a measure of foliage mass and area, the LAI derived from terrestrial laser scanning in this study represents an effective Plant Area Index (*i.e.*, not accounting for clumping and the proportion of woody components). Based on a study of estimating LAI, clumping, and woody area index from digital hemispherical photography [45], which was carried out at a number of permanent forest monitoring sites including the two where the present study was carried out, we used an average clumping index of 0.84 along with an average woody area index of 0.2 to derive an approximate multiplication factor of 0.95 for the conversion from PAI_e to LAI. Hence, LAI derived from TLS in this study are only slightly smaller than their corresponding PAI_e. Despite the approximate nature of this comparison, the litterfall LAI indicate that the "true" LAI is overestimated strongly by applying noise compression, in particular considering the unrealistically high PAI_e for the scans acquired during the leaf-off period (see Figures 8 and 9).

3.4. Majority Filtering

To assess the magnitude of the error of omission caused by the "clear sky" filter, an image-based majority kernel filtering was applied to all scans (see Sections 2.4 and 3.1). PAI_e derived from this filtering were then compared to PAI_e derived without applying the majority filtering (Table 2).

The results reflect the visual impression of the different scans' range images in Figure 1 with respect to the major trend: The higher the measurement speed the greater the amount of undetected sky points. Hence, PAI_e differences increase with increasing speed. This can be observed for the scans performed without noise compression during both the leaf-off and the leaf-on phase. Differences are, however, more pronounced during leaf-off due to the higher amount of gaps and therefore a higher amount of undetected sky points. The fact that the uncompressed scans with scan resolution 1/8 yield the highest PAI_e differences are noteworthy, in particular considering their visual appearance (Figure 1). This might be explained by a potential erroneous removal of valid scan points at the border regions of branches and sky by the applied majority filter. This effect might be particularly enhanced for leaf-off scans with low scan resolution where a large number of coarsely depicted border regions are present.

Another trend, which can be observed in the results, is that PAI_e differences are smaller for the scans with FARO's noise compression compared to those without noise compression (Table 2). This is an indication of the efficiency of the noise compression to reduce the error of omission. With regard to the different LAI methods used, PAI_e differences based on the PAI_e (0–58°) and PAI_e (0–74°) methods were shown to be larger than those based on the PAI_e (57.5°) method (Table 2). This is easily

explained by the fact that the former also include gap fractions from high zenith angles in their calculation. As these have a larger proportion of gaps compared to the zenith range around 57.5 °, the PAI_e (0–58 °) and PAI_e (0–74 °) are affected more strongly by the "clear sky" filter's error of omission.

Table 2. Percentage deviation in Plant Area Index (PAI_e) caused by the majority filtering ("filtered") in relation to the PAI_e derived from the unfiltered scans ("raw"). Percentage deviation = (PAI_e (filtered)—PAI_e (raw))/PAI_e (raw).

Site	Parameters	Leaf-Off			Leaf-On		
		Percentage Deviation (%)			Percentage Deviation (%)		
		PAI_e (0–58 °)	PAI_e (0–74 °)	PAI_e (57.5 °)	PAI_e (0–58 °)	PAI_e (0–74 °)	PAI_e (57.5 °)
	1/2—976	−5.8	−4.9	−3.0	−3.4	−2.7	−1.4
	1/2—488	−4.2	−3.8	−2.7	−2.0	−1.6	−0.9
	1/2—244	−1.5	−1.8	−1.7	−0.4	−0.4	−0.3
	1/4—488	−5.5	−5.1	−4.1	−2.1	−1.8	−1.1
	1/4—244	−3.7	−3.6	−3.6	−0.7	−0.7	−0.6
	1/4—122	−3.4	−3.4	−3.6	−0.5	−0.6	−0.6
	1/8—244	−7.8	−7.2	−7.1	−1.4	−1.6	−1.5
Beech	1/8—122	−8.0	−7.6	−7.7	−1.1	−1.3	−1.4
	1/4—244—2×	−1.4	−1.1	−0.8	−0.8	−0.5	−0.6
	1/8—244—2×	−1.4	−1.1	−0.9	−0.8	−0.5	−0.5
	1/8—244—4×	−2.6	−1.7	−1.2	−2.1	−1.3	−1.1
	1/8—122—2×	−1.0	−0.8	−0.7	−0.2	−0.1	−0.2
	1/16—244—2×	−1.8	−1.5	−0.7	−0.8	−0.5	−0.7
	1/16—244—4×	−2.3	−1.5	−1.1	−1.8	−1.0	−0.8
	1/16—122—2×	−1.6	−1.4	−0.8	−0.3	−0.2	−0.5
	1/2—976	−4.3	−4.2	−2.5	−1.6	−1.6	−0.6
	1/2—488	−3.6	−3.5	−2.6	−1.0	−1.0	−0.4
	1/2—244	−2.0	−2.1	−2.3	−0.4	−0.4	−0.3
	1/4—488	−5.1	−4.9	−4.0	−1.4	−1.4	−0.9
	1/4—244	−4.8	−4.7	−4.2	−0.8	−0.8	−0.7
	1/4—122	−3.9	−3.9	−4.0	−0.8	−0.7	−0.7
	1/8—244	−7.7	−7.5	−6.8	−2.1	−1.9	−1.9
Oak-beech	1/8—122	−7.8	−7.6	−7.1	−2.0	−1.9	−2.0
	1/4—244—2×	−1.0	−0.8	−0.7	−0.4	−0.3	−0.2
	1/8—244—2×	−0.9	−0.8	−0.5	−0.3	−0.3	−0.1
	1/8—244—4×	−1.0	−0.8	−0.4	−0.6	−0.7	0.0
	1/8—122—2×	−0.9	−0.7	−0.6	−0.1	−0.2	−0.1
	1/16—244—2×	−1.0	−1.0	−0.5	−0.2	−0.2	0.0
	1/16—244—4×	−0.6	−0.7	−0.2	−0.3	−0.3	0.0
	1/16—122—2×	−1.3	−1.2	−0.7	−0.1	−0.1	0.0

Overall, PAI_e differences between the majority filtered and unfiltered scans are relatively small (on average less than 5%), which hints at a rather marginal effect of the omission error on the PAI_e estimates. However, the small differences may very well be partly due to an inefficient removal of the undetected sky points by the applied majority filter, in particular considering the dense occurrence of

these points within canopy gaps of scans with very high measurement speeds (see Figure 1). An iterative filtering might help to solve this problem, however, this may also increase the potential erroneous removal of valid scan points at the border regions of branches and sky by the majority filter. Alternative approaches to deal with the "clear sky" filter's error of omission might be devised, e.g., based on the additional color information from a simultaneous acquisition of canopy photos.

3.5. Threshold Variation

To assess the sensitivity of the PAI_e estimates to changes in the intensity threshold used to separate correctly filtered sky points from falsely filtered scan points (see Sections 2.4 and 3.1), the default threshold used in this study was varied by ±5%. Results are presented separately for the leaf-off and leaf-on scans (Table 3a,b). In general, decreasing the threshold has a stronger effect on PAI_e than increasing the threshold, regardless of scan parameters, LAI method, and stand structure (Table 3a,b). This is due to the characteristic low intensity distribution of sky points (see Figures 4b and 5). However, this effect seems to be dependent on the leaf development phase with much larger PAI_e differences for leaf-off scans than for leaf-on scans, which indicates that for open canopies with higher ambient noise the intensity distribution of sky points tends to shift to a higher value range.

Furthermore noise compressed scans tend to be less sensitive to threshold changes than uncompressed scans. This is most likely due to the strong general reduction in "clear contour" filtered scan points and erroneously "clear sky" filtered scan points as a result of the noise compression algorithm, and which results in unimodal rather than bimodal intensity histograms that are typical for the uncompressed scans (see Figure 4a,b in Section 3.1).

Another trend, which can be observed is that for the leaf-off scans the applied resolutions influence the sensitivity to threshold changes, *i.e.*, PAI_e differences increase with decreasing resolution. For the leaf-on scans this trend is less pronounced and influenced by stand structure, too. This observation hints at a combined effect of scan resolution and ambient noise on the intensity distribution of filtered scan points and therefore a different sensitivity to threshold changes. By contrast, the measurement speed exhibited no systematic sensitivity to threshold changes.

With regard to the different LAI calculation methods applied, the PAI_e estimates based on the PAI_e (57.5 °) method and the leaf-on scans without noise compression are more sensitive to threshold variations compared to PAI_e (0–58 °) and PAI_e (0–74 °) methods (Table 3a,b). This pattern, however, could not be observed for the compressed leaf-on scans and the leaf-off scans in general. This might be explained by the fact that during the leaf-off phase, gap fractions of the lower zenith angles are generally larger compared to the leaf-on phase, and therefore less influenced by threshold changes. In addition, applying noise compression might disproportionately reduce "clear sky" and "clear contour" filtered scan points for low zenith angles, resulting in such small gap fractions that relatively small threshold variations have little effect.

Including the gap fractions of higher zenith angles into the LAI calculation seems to have a stabilizing effect with regard to the sensitivity of the PAI_e estimates to threshold changes: On average (mean of the different scan parameter combinations), PAI_e based on the PAI_e (0–58 °) and PAI_e (0–74 °) methods vary from −4.8% to 6.5% for the leaf-on beech scans, and from −6.1% to 7.7% for the leaf-on oak-beech scans (Table 3b). By comparison, PAI_e based on the PAI_e (57.5 °) method vary from −11.1%

to 11.2% for the leaf-on beech scans, and from −8.9% to 11.5% for the leaf-on oak-beech scans (Table 3b). This variability in the PAI_e estimation induced by threshold changes shows that the threshold selection is a critical part of the proposed approach of extracting gap fraction and PAI_e from phase shift FARO laser scans.

Table 3. (**a**) The effect of threshold variation on the PAI_e calculated from the leaf-off scans and with different LAI calculation methods. (**b**) The effect of threshold variation on the PAI_e calculated from the leaf-on scans and with different LAI calculation methods.

Site	Parameters	% Deviation (Decrease of Threshold by 5%)			% Deviation (Increase of Threshold by 5%)		
		PAIe (0–58°)	PAIe (0–74°)	PAIe (57.5°)	PAIe (0–58°)	PAIe (0–74°)	PAIe (57.5°)
Beech	1/2—976	7.0	6.8	8.0	−3.0	−2.6	−3.5
	1/2—488	6.2	5.8	7.2	−2.4	−1.9	−2.8
	1/2—244	8.5	6.9	7.3	−3.0	−2.0	−2.6
	1/4—488	13.2	13.1	14.3	−6.6	−5.4	−6.9
	1/4—244	11.8	10.3	12.7	−5.6	−4.3	−6.1
	1/4—122	10.7	10.0	11.4	−5.8	−4.9	−5.8
	1/8—244	16.1	15.6	22.1	−10.8	−9.1	−12.2
	1/8—122	19.7	18.7	26.3	−11.7	−9.9	−13.8
	1/4—244—2×	4.0	2.4	2.9	−0.9	−0.5	−0.4
	1/8—244—2×	5.7	4.3	5.3	−1.2	−0.9	−1.3
	1/8—244—4×	2.6	1.9	1.6	−0.5	−0.2	−0.2
	1/8—122—2×	4.4	4.1	3.4	−1.7	−1.3	−0.8
	1/16—244—2×	10.7	10.9	11.0	−4.2	−3.5	−4.0
	1/16—244—4×	1.5	1.7	0.8	−0.4	−0.2	−0.2
	1/16—122—2×	7.5	7.8	9.6	−4.6	−3.3	−4.2
Oak-beech	1/2—976	10.8	9.5	9.1	−4.3	−3.7	−3.9
	1/2—488	10.3	8.6	8.9	−3.7	−3.1	−3.3
	1/2—244	9.5	7.8	8.7	−3.4	−2.7	−2.4
	1/4—488	14.4	12.0	13.2	−6.6	−5.5	−6.0
	1/4—244	14.4	12.1	13.9	−6.3	−5.4	−6.0
	1/4—122	10.8	9.1	11.4	−5.4	−4.8	−5.2
	1/8—244	16.4	15.1	16.9	−9.9	−8.9	−9.6
	1/8—122	18.4	16.9	18.7	−10.5	−9.5	−10.1
	1/4—244—2×	5.5	3.2	4.2	−0.9	−0.7	−0.3
	1/8—244—2×	3.9	3.2	3.6	−1.3	−1.2	−1.1
	1/8—244—4×	0.5	0.3	0.5	−0.2	−0.1	0.0
	1/8—122—2×	3.1	2.4	3.4	−1.0	−0.9	−1.0
	1/16—244—2×	10.1	9.0	10.7	−4.6	−4.0	−4.1
	1/16—244—4×	1.4	0.6	1.8	−0.2	−0.1	−0.2
	1/16—122—2×	12.8	11.3	10.3	−4.9	−4.4	−3.9

(**a**)

Table 3. *Cont.*

Site	Parameters	% Deviation (Decrease of Threshold by 5%)			% Deviation (Increase of Threshold by 5%)		
		PAIe (0–58°)	PAIe (0–74°)	PAIe (57.5°)	PAIe (0–58°)	PAIe (0–74°)	PAIe (57.5°)
	1/2—976	6.2	6.8	9.6	−4.3	−3.9	−7.1
	1/2—488	4.9	5.8	9.9	−3.9	−3.4	−6.9
	1/2—244	5.7	6.2	10.4	−4.0	−3.2	−7.0
	1/4—488	4.6	6.6	10.8	−4.8	−4.8	−11.4
	1/4—244	5.2	7.9	12.1	−5.1	−5.1	−12.4
	1/4—122	5.5	7.8	11.4	−4.8	−4.8	−12.2
	1/8—244	6.8	11.5	12.8	−6.0	−6.9	−16.1
Beech	1/8—122	4.3	8.6	12.4	−5.1	−6.2	−15.8
	1/4—244—2×	0.6	1.0	0.4	−0.2	−0.4	−0.4
	1/8—244—2×	2.6	2.7	0.5	−0.4	−1.3	−0.9
	1/8—244—4×	0.7	0.8	3.0	0.0	0.0	−0.1
	1/8—122—2×	0.5	2.6	0.4	−0.3	−1.4	−1.1
	1/16—244—2×	3.5	6.7	1.2	−1.3	−2.8	−1.7
	1/16—244—4×	0.8	0.7	1.2	0.0	0.0	0.0
	1/16—122—2×	0.8	5.4	1.2	−0.5	−2.5	−2.1
	1/2—976	6.9	6.3	8.5	−4.8	−4.1	−6.3
	1/2—488	5.4	4.8	7.9	−4.3	−3.6	−6.0
	1/2—244	5.9	5.2	8.4	−4.4	−3.6	−6.0
	1/4—488	7.9	7.6	11.4	−6.8	−6.1	−9.3
	1/4—244	7.8	7.7	11.5	−6.8	−6.1	−9.4
	1/4—122	7.6	7.5	12.1	−6.7	−6.0	−9.5
	1/8—244	10.1	10.3	15.4	−8.8	−8.4	−12.5
Oak-beech	1/8—122	10.7	11.0	16.6	−9.1	−8.6	−12.5
	1/4—244—2×	0.8	1.3	1.3	−0.5	−0.7	−1.3
	1/8—244—2×	1.5	2.6	3.5	−1.1	−1.7	−3.3
	1/8—244—4×	2.6	2.6	1.5	0.0	0.0	0.0
	1/8—122—2×	1.6	2.8	3.7	−1.3	−1.7	−3.0
	1/16—244—2×	2.5	4.6	3.1	−2.4	−3.2	−6.1
	1/16—244—4×	0.4	0.2	0.0	0.0	0.0	0.0
	1/16—122—2×	2.4	4.6	4.3	−2.5	−3.3	−6.3

(**b**)

The results indicate that applying a constant threshold value for scans with different scan parameters and collected for stands with different structure and leaf development phase is not the optimal solution, as histograms represent scene-dependent scan statistics. The implementation of an automated threshold selection based on the intensity distribution of filtered scan points retrieved for each scan separately might be a potential solution. However, due to the lack of true reference data this approach cannot be validated in the present study. Besides such a validation would have to be based on the retrieved gap fraction instead of PAI$_e$, and reference data for the size and distribution of gaps in the canopy is generally hard to obtain [3,37].

Approaches for the identification of scan pulses from canopy gaps based on the variance of neighboring scan points (with regard to range, intensity, and color information) from phase shift scans without the use of hardware filtering could be an alternative [53]. Yet again, the rigorous assessment of any such approach is hardly possible without the availability of true gap fraction reference data. When comparing the above-mentioned PAI_e variability induced by changing the threshold to the variability induced by using different LAI calculation methods (see Section 3.3), threshold changes have a smaller effect than the LAI calculation itself. If, in addition the low variability induced by the different scan parameters applied without noise compression is considered, PAI_e estimates based on using a constant intensity threshold of 0.3 yield reasonable values when compared to the mean long-term litterfall LAI (see Section 3.3).

4. Conclusions

This study investigated the effects of scan resolution, measurement speed, and noise compression on the retrieval of gap fraction and effective Plant Area Index from phase-shift FARO Photon 120 terrestrial laser scans. It could be demonstrated that FARO's noise compression algorithm yields gap fractions and PAI_e which deviate significantly from those based on scans without noise compression. Mean litterfall LAI were also strongly overestimated by the scans performed with noise compression.

We, therefore, conclude that while noise compression might generally help to reduce the noise in phase-shift terrestrial laser scans without affecting the retrieval of structural forest metrics such as stem diameter [54], FARO's noise compression should not be applied for retrieving gap fraction and related structural metrics such as the PAI_e. The parameters, scan resolution and measurement speed, were shown to influence the retrieval of these metrics, too. However, the magnitudes of these effects proved to be smaller than the effect of noise compression, and proved to depend on zenith, leaf development phase, stand structure, and LAI calculation method.

Nevertheless, the overall PAI_e estimates based on the scan parameter combinations without noise compression exhibited a relative stability, in spite of the various scan parameter combinations applied. This conclusion was drawn from the fact that the variation in the PAI_e estimation induced by the scan resolutions and measurement speeds applied without noise compression was significantly lower than the variation induced by applying different LAI calculation methods. This gives confidence in using phase-shift TLS for a reliable and consistent retrieval of gap fraction as the base for estimating PAI_e.

It could also be demonstrated that scans performed with high measurement speeds (978 and 488 kpt/s) are especially prone to noise when FARO's "clear sky" and "clear contour" filters are applied. The post-processing filtering approach applied in this study could reduce this noise to some effect, but, due to the lack of a true gap fraction reference, it could not be properly assessed. Unless any such post-processing approach is proven to be effective and working, we suggest performing phase-shift FARO scans with lower measurement speeds (244 and 122 kpt/s) to reduce this type of noise.

While the proposed approach of identifying sky points from hardware filtered FARO scans by using a constant intensity threshold yielded reasonable PAI_e when compared to the mean long-term litterfall LAI, the implementation of a variable threshold selection based on each scan's specific intensity distribution might be a better solution. Considering that the hardware filters are mostly company secret and were not developed for specialized applications, such as vegetation structural

analysis, developing specialized filters for raw scan data would probably be most appropriate. However, the availability of gap fraction reference data is crucial for the rigorous assessment of any such approach, including 3-D based approaches.

Above all, more research is required to investigate the effects of scan parameters for different phase-shift laser scanners as well as the effects of different scanner properties, most notably the ranging principle, on the retrieval of gap fraction and LAI. Compared to the passive-optical instruments such as the LI-COR PCA or digital hemispherical photography, TLS offers a number of advantages, e.g., the improved characterization of clumping due to the 3D information, or the lower sensitivity to variable sky illumination.

Due to the technical progress in the field of terrestrial and mobile laser scanning, the information content provided by the laser scanners is steadily increasing (e.g., multi-spectral lasers, UAV-based applications), which will greatly enhance the retrieval of structural forest metrics, such as the separation of woody from non-woody vegetation components. With decreasing costs, increasing scanner operability (reduction in size and weight, longer battery lives, *etc.*), and with increasing research corroborating the reliable and consistent retrieval of structural forest metrics, there is a good chance that TLS will be routinely applied in forest inventory and as a tool for collecting reference data to, e.g., validate airborne and satellite based remote sensing data.

Acknowledgments

Author Contributions

Pyare Pueschel is the principal author of this manuscript responsible for the research concept, the collection, analysis and interpretation of the data, and for writing major portions of the manuscript. Glenn Newnham provided IDL code for the processing of raw scan data, contributed to the discussion and interpretation of results, and contributed some portions of the written manuscript. Joachim Hill contributed to the research concept and to the discussion of results.

Conflicts of Interest

The authors declare no conflict of interest.

References

1. Parker, G.G. Structure and Microclimate of Forest Canopies. In *Forest Canopies: A Review of Research on a Biological Frontier*; Lowman, M., Nadkarni, N., Eds.; Academic Press: San Diego, CA, USA, 1995; pp. 73–106.
2. Chen, J.M.; Black, T.A. Defining leaf area index for non-flat leaves. *Plant Cell Environ.* **1992**, *15*, 421–429.

3. Jupp, D.L.B.; Culvenor, D.S.; Lovell, J.L.; Newnham, G.J.; Strahler, A.H.; Woodcock, C.E. Estimating forest LAI profiles and structural parameters using a ground-based laser called Echidna®. *Tree Physiol.* **2008**, *29*, 171–181.

4. Jonckheere, I.; Fleck, S.; Nackaerts, K.; Muys, B.; Coppin, P.; Weiss, M.; Baret, F. Review of methods for *in situ* leaf area index determination: Part I. Theories, sensors and hemispherical photography. *Agric. For. Meteorol.* **2004**, *121*, 19–35.

5. Warren Wilson, J. Inclined point quadrats. *New Phytol.* **1960**, *59*, 1–8.

6. Seidel, D. Terrestrial Laser Scanning: Applications in Forest Ecological Research. PhD Thesis, Georg-August Universität, Göttingen, Germany, 2011.

7. Zheng, G.; Moskal, L.M. Retrieving leaf area index (LAI) using remote sensing: Theories, methods and sensors. *Sensors* **2009**, *9*, 2719–2745.

8. Weiss, M.; Baret, F.; Smith, G.J.; Jonckheere, I.; Coppin, P. Review of methods for *in situ* leaf area index (LAI) determination: Part II. Estimation of LAI, errors and sampling. *Agric. For. Meteorol.* **2004**, *121*, 37–53.

9. Strahler, A.H.; Jupp, D.L.B.; Woodcock, C.E.; Schaaf, C.B.; Yao, T.; Zhao, F.; Yang, X.; Lovell, J.; Culvenor, D.; Newnham, G. Retrieval of forest structural parameters using a ground-based lidar instrument (Echidna®). *Can. J. Remote Sens.* **2008**, *34*, S426–S440.

10. Guang, Z.; Moskal, L.M.; Soo-Hyung, K. Retrieval of effective leaf area index in heterogeneous forests with terrestrial laser scanning. *IEEE Trans. Geosci. Remote Sens.* **2013**, *51*, 777–786.

11. Ramirez, F.; Armitage, R.; Danson, F. Testing the application of terrestrial laser scanning to measure forest canopy gap fraction. *Remote Sens.* **2013**, *5*, 3037–3056.

12. Zhao, F.; Yang, X.; Schull, M.A.; Román-Colón, M.O.; Yao, T.; Wang, Z.; Zhang, Q.; Jupp, D.L.B.; Lovell, J.L.; Culvenor, D.S. Measuring effective leaf area index, foliage profile, and stand height in New England forest stands using a full-waveform ground-based lidar. *Remote Sens. Environ.* **2011**, *115*, 2954–2964.

13. Dassot, M.; Constant, T.; Fournier, M. The use of terrestrial lidar technology in forest science: Application fields, benefits and challenges. *Ann. For. Sci.* **2011**, *68*, 959–974.

14. Newnham, G.; Armston, J.; Muir, J.; Goodwin, N.; Tindall, D.; Culvenor, D.; Püschel, P.; Nyström, M.; Johansen, K. *Evaluation of Terrestrial Laser Scanners for Measuring Vegetation Structure: A Comparison of the Faro Focus 3D 120, Leica C10, Leica HDS7000 and Riegl VZ100a*; CSIRO: Melbourne, Australia, 2012.

15. Van Genechten, B. *Theory and Practice on Terrestrial Laser Scanning: Training Material Based on Practical Applications*; Santana Quintero, M., Lerma, J.L., Heine, E., van Genechten, B., Eds.; Universidad Politecnica de Valencia Editorial: Valencia, Spain, 2008.

16. Simonse, M.; Aschoff, T.; Spiecker, H.; Thies, M. Automatic Determination of Forest Inventory Parameters Using Terrestrial Laserscanning. In Proceedings of the ScandLaser Scientific Workshop on Airborne Laser Scanning of Forests, Umea, Sweden, 3–4 September 2003.

17. Aschoff, T.; Spiecker, H. Algorithms for the automatic detection of trees in laser scanner data. *Int. Arch. Photogramm. Remote Sens. Spat. Inf. Sci.* **2004**, *XXXVI-8/W2*, 66–70.

18. Maas, H.G.; Bienert, A.; Scheller, S.; Keane, E. Automatic forest inventory parameter determination from terrestrial laser scanner data. *Int. J. Remote Sens.* **2008**, *29*, 1579–1593.

19. Antonarakis, A.S. Evaluating forest biometrics obtained from ground lidar in complex riparian forests. *Remote Sens. Lett.* **2011**, *2*, 61–70.

20. Bienert, A.; Scheller, S.; Keane, E.; Mullooly, G.; Mohan, F. Application of Terrestrial Laser Scanners for the Determination of Forest Inventory Parameters. In Proceedings of the ISPRS Commission V Symposium "Image Engineering and Vision Metrology", Dresden, Germany, 25–27 September 2006.

21. Lovell, J.L.; Jupp, D.L.B.; Newnham, G.J.; Culvenor, D.S. Measuring tree stem diameters using intensity profiles from ground-based scanning lidar from a fixed viewpoint. *ISPRS J. Photogramm. Remote Sens.* **2011**, *66*, 46–55.

22. Tansey, K.; Selmes, N.; Anstee, A.; Tate, N.J.; Denniss, A. Estimating tree and stand variables in a Corsican pine woodland from terrestrial laser scanner data. *Int. J. Remote Sens.* **2009**, *30*, 5195–5209.

23. Pueschel, P.; Newnham, G.; Rock, G.; Udelhoven, T.; Werner, W.; Hill, J. The influence of scan mode and circle fitting on tree stem detection, stem diameter and volume extraction from terrestrial laser scans. *ISPRS J. Photogramm. Remote Sens.* **2013**, *77*, 44–56.

24. Yao, T.; Yang, X.; Zhao, F.; Wang, Z.; Zhang, Q.; Jupp, D.; Lovell, J.; Culvenor, D.; Newnham, G.; Ni-Meister, W. Measuring forest structure and biomass in New England forest stands using Echidna ground-based lidar. *Remote Sens. Environ.* **2011**, *115*, 2965–2974.

25. Holopainen, M.; Vastaranta, M.; Kankare, V.; Räty, M.; Vaaja, M.; Liang, X.; Yu, X.; Hyyppä, J.; Hyyppä, H.; Viitala, R. Biomass Estimation of Individual Trees Using Stem and Crown Diameter TLS Measurements. In Proceedings of the 2011 ISPRS Workshop Laser Scanning, Calgary, AB, Canada, 29–31 August 2011; Volume XXXVIII-5/W12.

26. Kankare, V.; Holopainen, M.; Vastaranta, M.; Puttonen, E.; Yu, X.; Hyyppä, J.; Vaaja, M.; Hyyppä, H.; Alho, P. Individual tree biomass estimation using terrestrial laser scanning. *ISPRS J. Photogramm. Remote Sens.* **2013**, *75*, 64–75.

27. Béland, M.; Baldocchi, D.D.; Widlowski, J.-L.; Fournier, R.A.; Verstraete, M.M. On seeing the wood from the leaves and the role of voxel size in determining leaf area distribution of forests with terrestrial lidar. *Agric. For. Meteorol.* **2014**, *184*, 82–97.

28. Eitel, J.U.H.; Vierling, L.A.; Long, D.S. Simultaneous measurements of plant structure and chlorophyll content in broadleaf saplings with a terrestrial laser scanner. *Remote Sens. Environ.* **2010**, *114*, 2229–2237.

29. Henning, J.G.; Radtke, P.J. Ground-based laser imaging for assessing three-dimensional forest canopy structure. *Photogramm. Eng. Remote Sens.* **2006**, *72*, 1349–1358.

30. Van der Zande, D.; Stuckens, J.; Verstraeten, W.W.; Muys, B.; Coppin, P. Assessment of light environment variability in broadleaved forest canopies using terrestrial laser scanning. *Remote Sens.* **2010**, *2*, 1564–1574.

31. Bittner, S.; Gayler, S.; Biernath, C.; Winkler, J.B.; Seifert, S.; Pretzsch, H.; Priesack, E. Evaluation of a ray-tracing canopy light model based on terrestrial laser scans. *Can. J. Remote Sens.* **2012**, *38*, 619–628.

32. Zhao, F.; Strahler, A.H.; Schaaf, C.L.; Yao, T.; Yang, X.; Wang, Z.; Schull, M.A.; Román, M.O.; Woodcock, C.E.; Olofsson, P. Measuring gap fraction, element clumping index and LAI in Sierra forest stands using a full-waveform ground-based lidar. *Remote Sens. Environ.* **2012**, *125*, 73–79.

33. Clawges, R.; Vierling, L.; Calhoon, M.; Toomey, M. Use of a ground-based scanning lidar for estimation of biophysical properties of western larch (larix occidentalis). *Int. J. Remote Sens.* **2007**, *28*, 4331–4344.

34. Yang, X.; Strahler, A.H.; Schaaf, C.B.; Jupp, D.L.B.; Yao, T.; Zhao, F.; Wang, Z.; Culvenor, D.S.; Newnham, G.J.; Lovell, J.L. Three-dimensional forest reconstruction and structural parameter retrievals using a terrestrial full-waveform lidar instrument (Echidna®). *Remote Sens. Environ.* **2013**, *135*, 36–51.

35. Moskal, L.M.; Zheng, G. Retrieving forest inventory variables with terrestrial laser scanning (TLS) in urban heterogeneous forest. *Remote Sens.* **2011**, *4*, 1–20.

36. Hosoi, F.; Omasa, K. Voxel-based 3-D modeling of individual trees for estimating leaf area density using high-resolution portable scanning lidar. *IEEE Trans. Geosci. Remote Sens.* **2006**, *44*, 3610–3618.

37. Côté, J.-F.; Widlowski, J.-L.; Fournier, R.A.; Verstraete, M.M. The structural and radiative consistency of three-dimensional tree reconstructions from terrestrial lidar. *Remote Sens. Environ.* **2009**, *113*, 1067–1081.

38. Huang, P.; Pretzsch, H. Using terrestrial laser scanner for estimating leaf areas of individual trees in a conifer forest. *Trees* **2010**, *24*, 609–619.

39. Danson, F.; Armitage, R.; Bandugula, V.; Ramirez, F.; Tate, N.; Tansey, K.; Tegzes, T. Terrestrial Laser Scanners to Measure Forest Canopy Gap Fraction. In Proceedings of the 8th SilviLaser, Edinburgh, Scotland, 17–19 September 2008.

40. Danson, F.M.; Hetherington, D.; Morsdorf, F.; Koetz, B.; Allgower, B. Forest canopy gap fraction from terrestrial laser scanning. *IEEE Geosci. Remote Sens. Lett.* **2007**, *4*, 157–160.

41. Zheng, G.; Moskal, L.M. Spatial variability of terrestrial laser scanning based leaf area index. *Int. J. Appl. Earth Obs. Geoinf.* **2012**, *19*, 226–237.

42. Calders, K.; Verbesselt, J.; Bartholomeus, H.; Herold, M. Applying Terrestrial Lidar to Derive Gap Fraction Distribution Time Series During Bud Break. In Proceedings of the SilviLaser 2011, 11th International LiDAR Forest Applications Conference, Hobart, Australia, 16–20 October 2011.

43. FARO. *Faro Laser Scanner Photon 20/120 User's Manual*; FARO: Korntal-Münchingen, Germany, 2010.

44. Hilker, T.; Leeuwen, M.; Coops, N.; Wulder, M.; Newnham, G.; Jupp, D.B.; Culvenor, D. Comparing canopy metrics derived from terrestrial and airborne laser scanning in a Douglas-fir dominated forest stand. *Trees* **2010**, *24*, 819–832.

45. Greve, M. Vergleich von Methoden zur Erhebung des Blattflächenindex in Wäldern (In German)/Comparison of Methods for the Estimation of Leaf Area Index in Forests. M.Sc. Thesis, University of Trier, Trier, Germany, 2010.

46. Ross, J.K. *The Radiation Regime and Architecture of Plant Stands*; Junk Publishers: The Hague, The Netherlands, 1981; p. 391.

47. Black, T.A.; Chen, J.-M.; Lee, X.; Sagar, R.M. Characteristics of shortwave and longwave irradiances under a Douglas-fir forest stand. *Can. J. For. Res.* **1991**, *21*, 1020–1028.

48. Miller, J.B. A formula for average foliage density. *Aust. J. Bot.* **1967**, *15*, 141–144.

49. LI-COR Inc. *LAI-2000 Plant Canopy Analyzer. Instruction Manual*; LICOR Inc: Lincoln, NE, USA, 1992.

50. Chen, J.M.; Govind, A.; Sonnentag, O.; Zhang, Y.; Barr, A.; Amiro, B. Leaf area index measurements at Fluxnet-Canada forest sites. *Agric. For. Meteorol.* **2006**, *140*, 257–268.

51. Leblanc, S.G.; Chen, J.M. A practical scheme for correcting multiple scattering effects on optical LAI measurements. *Agric. For. Meteorol.* **2001**, *110*, 125–139.

52. Wilson, J.W. Analysis of the spatial distribution of foliage by two-dimensional point quadrats. *New Phytol.* **1959**, *58*, 92–101.

53. Newnham, G.; Mashford, J.; Püschel, P.; Armston, J.; Culvenor, D.; Siggins, A.; Nyström, M.; Goodwin, N.; Muir, J. Non-Parametric Point Classification for Phase-Shift Laser Scanning. In Proceedings of the SilviLaser 2012, Vancouver, BC, Canada, 16–19 September 2012.

54. Pueschel, P. The influence of scanner parameters on the extraction of tree metrics from faro photon 120 terrestrial laser scans. *ISPRS J. Photogramm. Remote Sens.* **2013**, *78*, 58–68.

Chapter IV: The influence of scan mode and circle fitting on tree stem detection, stem diameter and volume extraction from terrestrial laser scans

Pyare Pueschel, Glenn Newnham, Gilles Rock, Thomas Udelhoven, Willy Werner, Joachim Hill
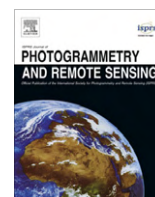
The influence of scan mode and circle fitting on tree stem detection, stem diameter and volume extraction from terrestrial laser scans

Pyare Pueschel [a,*], Glenn Newnham [b], Gilles Rock [a], Thomas Udelhoven [a], Willy Werner [c], Joachim Hill [a]

[a] Department of Environmental Remote Sensing and Geoinformatics, University of Trier, D-54286 Trier, Germany
[b] CSIRO Land and Water, Private Bag 10, Clayton South, Vic 3169, Australia
[c] Department of Geobotany, University of Trier, D-54286 Trier, Germany

A B S T R A C T

Terrestrial laser scanning (TLS) has been used to estimate a number of biophysical and structural vegetation parameters. Of these stem diameter is a primary input to traditional forest inventory. While many experimental studies have confirmed the potential for TLS to successfully extract stem diameter, the estimation accuracies differ strongly for these studies – due to differences in experimental design, data processing and test plot characteristics. In order to provide consistency and maximize estimation accuracy, a systematic study into the impact of these variables is required. To contribute to such an approach, 12 scans were acquired with a FARO photon 120 at two test plots (Beech, Douglas fir) to assess the effects of scan mode and circle fitting on the extraction of stem diameter and volume. An automated tree stem detection algorithm based on the range images of single scans was developed and applied to the data. Extraction of stem diameter was achieved by slicing the point cloud and fitting circles to the slices using three different algorithms (Lemen, Pratt and Taubin), resulting in diameter profiles for each detected tree. Diameter at breast height (DBH) was determined using both the single value for the diameter fitted at the nominal breast height and by a linear fit of the stem diameter vertical profile. The latter is intended to reduce the influence of outliers and errors in the ground level determination. TLS-extracted DBH was compared to tape-measured DBH. Results show that tree stems with an unobstructed view to the scanner can be successfully extracted automatically from range images of the TLS data with detection rates of 94% for Beech and 96% for Douglas fir. If occlusion of trees is accounted for stem detection rates decrease to 85% (Beech) and 84% (Douglas fir). As far as the DBH estimation is concerned, both DBH extraction methods yield estimates which agree with reference measurements, however, the linear fit based approach proved to be more robust for the single scan DBH extraction (RMSE range 1.39–1.74 cm compared to 1.47–2.43 cm). With regard to the different circle fit algorithms applied, the algorithm by Lemen showed the best overall performance (RMSE range 1.39–1.65 cm compared to 1.49–2.43 cm). The Lemen algorithm was also found to be more robust in case of noisy data. Compared to the single scans, the DBH extraction from the merged scan data proved to be superior with significant lower RMSE's (0.66–1.21 cm). The influence of scan mode and circle fitting is reflected in the stem volume estimates, too. Stem volumes extracted from the single scans exhibit a large variability with deviations from the reference volumes ranging from −34% to 44%. By contrast volumes extracted from the merged scans only vary weakly (−2% to 6%) and show a marginal influence of circle fitting.

© 2012 International Society for Photogrammetry and Remote Sensing, Inc. (ISPRS) Published by Elsevier B.V. All rights reserved.

1. Introduction

Even though terrestrial laser scanning (TLS) is not a new technology, its application for forest inventory and research is still relatively new, mainly because of high scanner costs and hardware limitations to the data processing. However with the rapid technical progress in this field, terrestrial laser scanners and associated hardware have become affordable which – also encouraged by the promising results of pilot studies (e.g. Simonse et al., 2003; Thies and Spiecker, 2004, Hopkinson et al., 2004) – boosted research and their use in forestry. Moreover, due to considerable reductions in size and weight, scanners and their equipment have become manageable in terms of their practical use in the field. TLS has been used to estimate a number of biophysical and structural vegetation parameters including tree location (e.g. Simonse et al., 2003; Aschoff and Spiecker, 2004), tree height (e.g. Maas et al., 2008, Tansey et al., 2009), diameter at breast height (e.g. Bienert

* Corresponding author. Tel.: +49 651 2014593; fax: +49 651 201 3815.
E-mail address: p.pueschel@uni-trier.de (P. Pueschel).

et al., 2006; Lovell et al., 2011), stem volume (Tansey et al., 2009), biomass (Yao et al., 2011; Holopainen et al., 2011), chlorophyll (Eitel et al., 2010), Leaf Area Index and gap fraction (e.g. Henning and Radtke, 2006; Clawges et al., 2007; Danson et al., 2007; Jupp et al., 2009; Strahler et al., 2008). A large number of these experimental studies have confirmed the potential for TLS to successfully extract these parameters; however a systematic study of the factors which influence the information extraction from TLS data is still lacking, even though the need for such analyses was already formulated at quite an early stage (cf. Thies and Spiecker, 2004). The following potentially influence the accuracy of the information extraction from TLS data:

- Ranging method: Time-of-flight discrete return, time-of-flight waveform, continuous wave phase-shift.
- Scanner characteristics: Ranging errors, laser wavelength and beam divergence.
- Scan settings: Angular resolution (scan geometry), integration time.
- Scan mode: Single or multiple (merged) scans.
- Data processing: Filtering, higher level algorithms for deriving tree metrics.

These attributes also exhibit interdependencies which affect structural metrics derived from TLS data. For forest applications these interdependencies are further complicated by the influence of stand and plot characteristics (e.g. tree species composition and age, canopy layering, degree of undergrowth, stem density and slope). As a consequence of the combined effects of these influences, the existing studies yield widely different results, even for such seemingly simple tasks as stem detection and diameter extraction (see Table 1). Note that Table 1 is not intended to provide a complete overview; rather it is to highlight the differences in the studies which contribute to the wide range of results found and which make it difficult to objectively compare the proposed methodologies and algorithms. Above all, this calls for a more systematic study into the TLS-related influences. The present study is intended to contribute to such an approach by assessing the influences of circle fitting and scan mode on stem diameter and volume extraction from TLS data. To date, both have received relatively little attention in the TLS literature. To our knowledge only Thies and Spiecker (2004) and Maas et al. (2008) specifically address the influence of scan mode and Tansey et al. (2009) as well as Brolly and Király (2009) specifically address the influence of circle fitting. However, except for Brolly and Király (2009), all studies are based on relative small sample sets (see Table 1), reported results and drawn conclusions should therefore be cautiously judged and need to be supported by further research. While studies on the influence of scan mode on stem diameter and volume extraction are scarce, the effects on stem detection are well documented (e.g. Watt and Donoghue, 2005; Bienert et al., 2007; Litkey et al., 2008; Liang et al., 2009; Lovell et al., 2011). The main disadvantage of using single scans for stem detection is the shadowing of background objects by foreground objects, i.e. the shadowing of stems by branches, leaves, and other stems. By contrast multiple (merged) scans have the advantage of providing a better 3D tree coverage (Thies and Spiecker, 2004; Bienert et al., 2006). While it is widely acknowledged that the use of merged scans for stem detection is the most effective means to reduce the effect of shadowing, single scan mode is often preferred due to its higher sampling efficiency. Therefore, one of the aims of this study was to develop a stem detection algorithm based on single scan mode which minimizes the effects of shadowing.

As far as the stem diameter and volume extraction is concerned, particular consideration has to be given to the issue of noise in TLS data. In this context, noise refers both to laser scan returns without physical meaning and to returns with physical meaning but which, depending on the purpose of the data analysis, represent unwanted data. The separation of unwanted from wanted data is considered to be one of the most important steps in successfully extracting meaningful information from TLS data, and which may be achieved either by filtering of the raw data or by applying more robust modeling techniques (cf. Maas et al., 2008; Litkey et al., 2008). For example Aschoff et al. (2004) use linear regression to check the validity of diameter measurements and Bienert et al. (2007) introduce a so-called reliability factor to prevent over- or underestimated diameters from circle fitting to noisy data. To account for the influence of noise on the extraction of stem diameter and volume from TLS data, we implemented a robust stem diameter extraction algorithm and compared three different circle fit algorithms and two different methods of determining diameter at breast height (DBH).

2. Materials and methods

2.1. Study site

This study was carried out as part of a comprehensive campaign for calibration of forest biophysical and structural parameters derived from airborne hyperspectral and laser scanning data. This campaign serves as preparation for the German hyperspectral satellite mission EnMAP (http://www.enmap.org/) and was located in the *Pfälzerwald* forest near Kaiserslautern, Germany, where our research group established one of its main research sites (*Merzalben*, 49°16′N, 7°48′E). This research site consists of a number of permanent forest monitoring plots providing a large pool of in situ biophysical and structural measurements, which makes the site ideal for validating remote sensing derived parameters and calibrating remote sensing driven models. The present study was carried out at the main forest monitoring plot, a mixed Beech Douglas fir stand, which is characterized by two zones of pure Beech and pure Douglas fir and one zone where these species are evenly mixed. During a field campaign in August 2011 representative areas of the pure zones were scanned with a total of 12 terrestrial laser scans. The pure zones differ not only in tree species but also in stand structure and topology (Figs. 1a and 1b and Table 2).

2.2. Data acquisition

The TLS scans were acquired in August 2011 with a FARO Photon 120, a phase-shift laser scanner with 360° × 320° field of view and a minimum horizontal and vertical step size of 0.009° (approximately 40,000 laser pulses for a full hemispherical scan). The scanner settings used for this study were an angular resolution of 0.036° (point spacing of 6.28 mm/10 m) and a measurement speed of 122 kpt/s. In addition hardware filters were set to remove ghost points. These settings resulted in a scan time of 6:49 min and yielded compressed scan sizes of approximately 185 MB. Reference objects (highly reflecting targets) were placed in positions where they could be viewed from multiple scan locations in order to post-process the single scans into one merged scan with a common coordinate system. Tree locations and diameter at breast height (DBH) tape measurements were extracted from an existing database. DBH is measured annually on a sub-sample of trees (464 trees) and every 4 years on all 922 trees of the plot. Reference data for the DBH measurements were recorded in April 2012, which potentially introduces a systematic bias due to the time lag between the scan acquisition and DBH collection. Additionally six Beech stem diameter profiles with a step size of 20 cm and a maximum height of 10 m were recorded in Mai 2012 with a mobile lift in order to validate the stem volume estimates. Due to inaccessibil-

Table 1
Experimental design, scanner settings and methodologies of selected studies on automatic stem detection and DBH extraction from TLS data. Man. = managed, nat. = natural, SD = stem detection, DBH = diameter at breast height, PS = phase-shift, TF = time-of-flight, WF = waveform, S = single scan mode, M = multiple (merged) scan mode.

Study	Tree species	Stem density (n/ha)	Plot size (ha)	Sample Size (n)	Scanner type	Scan mode	Scan resolution (°)	Stem detection	Detection rate (%)	DBH extraction	Algorithm	DBH RMSE (cm)	DBH bias (cm)
Simonse et al. (2003)	Douglas and silver fir	–		28	Z + F Imager 5003 (PS)	M	–	2D-Slice Hough-transform	93[a]	Circle fitting	Algebraic	–	1.7
Thies and Spiecker (2004)	Beech, oak, silver-fir	556[a]	0.09	50 (SD) 11 (DBH)	Z + F Imager 5003 (PS)	S, M	–	2D-Slice Hough-transform	22 (S), 52 (M)	Circle fitting	Algebraic	3.48 (S)[a], 3.22 (M)[a]	0.75 (S)[a], −0.32 (M)[a]
Litkey et al. (2008)	Pine	–	0.07 (DBH)	10 (DBH), 52 (SD)	Faro 880 HE80 (PS)	S	0.034	Range image clustering	85	Circle fitting	Least squares (Nelder-Mead)	3	–
Maas et al. (2008)	Spruce, beech, larch, fir	212–410[a]	0.05–0.07	14–29	Riegl LMS-Z420i (TF), Faro LS 800 HE80 (PS)	S, M	–	2D-Slice clustering	97.5	Circle fitting	Similar to Henning and Radtke (2006)	1.80–3.25 (S), 1.48 (M)	−0.67–1.58 (S), 0.93 (M)
Brolly and Király (2009)	Oak, hornbeam, beech, larch, spruce, birch	761[a]	0.28	213	Riegl LMS-Z420i (TF)	S	0.055	2D-Slice clustering	72 (circle), 63 (cylinder)	Circle & cylinder fitting	Least squares	3.4–4.2 (circle), 7 (cylinder)	−0.8, −1.6 (circle), 0.5 (cylinder)
Liang et al. (2009)	Scots pine, Norway spruce	533–1500[a]	0.03	16–45	Leica HDS6000 (PS)	S	0.18	Classification/ clustering	53–89	Circle fitting	Least squares (Nelder-Mead)	–	–
Tansey et al. (2009)	Corsican pine	1000	0.05	66 (SD) 8 (DBH)	Riegl LMS-Z420i (TF)	M	0.12	2D-Slice Hough-transform	100	Circle & cylinder fitting, Hough transform	Least squares (Gauss–Newton)	3.7 (cylinder), 1.9 (circle), 2.3 (Hough)	3.6 (cylinder)[a], 1.7 (circle)[a], 1.6 (Hough)[a]
Antonarakis (2011)	Black poplar, hybrid poplar	255 (man.), 950 (nat.)	0.5 (man.), 0.1 (nat.)	166 (man.), 95 (nat.)	Leica HDS 3000 (TF)	M	–	Semi-automated	100 (man.), 60 (nat.)	Cylinder fitting	Similar to Hopkinson et al. (2004)	–	0.3 (nat.), 0.4 (man.)
Lovell et al. (2011)	Ponderosa pine, Monterey pine	123–477	0.13–0.79	60–97	Echidna® (WF)	S	0.29	Reflectance-based	54–68	Angular stem width	Intensity-based angular-diameter relation	–	4.3–9.1
Yao et al. (2011)	Hemlock, white pine, red oak, red maple, red spruce, yellow birch, beech	1017–3281	0.13–0.20	–	Echidna® (WF)	S	0.23	Reflectance-based	42	Angular stem width	Intensity-based angular-diameter relation	7 (conifers), 8 (broadleaf)	–

[a] Values calculated based on data provided in the publication.

ity, stem profiles could not be collected for the Douglas fir zone. As far as the data pre-processing is concerned, the individual scan data were first registered to produce merged point clouds for each of the zones scanned. The registration had to be carried out manually using FARO Scene and is therefore more time-consuming than the automated processing of the single scan data which converts the point clouds to raster images containing the x, y, z range, intensity, azimuth and zenith information for each scan point.

2.3. Stem detection

Our approach to automated tree stem detection or tree location mapping is similar to the approach of Forsman and Halme (2005). It utilizes range differences between neighboring pixel of the single scan range image as the basis for stem detection. While the Forsman and Halme approach aims at object segmentation of the whole range image based on consecutive pixel of similar range, our approach is based on range differences between neighboring pixels of a 2D-slice taken from the range image. To minimize the shadowing of stems by branches and leaves, our approach utilizes multiple slices extracted from different heights:

Scanner returns are assessed in multiple slices $L_i(\theta)$ each of zenithal thickness 0.36° and azimuthal coverage of 360°. Slices are separated by a zenithal offset of 0.9°. Within each slice and for each vertical scan line $L_i(\varphi)$ at azimuth φ the range variance $\sigma_r^2(i, \varphi)$ and mean $\mu_r(i, \varphi)$ are computed. If $\mu_r(i, \varphi)$ falls below the mean range threshold τ_{range} and $\sigma_r^2(i, \varphi)$ falls below the range variance threshold $\tau_{\sigma2}$ then $L_i(\varphi)$ is considered to be a possible stem return. Consecutive (possible) stem returns with range differences below the range difference threshold τ_{diff} and which cover a minimum azimuthal span $\delta(\varphi)$ provide the primary evidence of a tree stem. The locations of stem centers as specified by their central azimuth detected in each slice $L_i(\theta)$ are then compared to determine if they correspond to a single tree stem or to different stems.

The parameter set used in the present study is: τ_{diff} = 10 cm, τ_{range} = 30 m, $\tau_{\sigma2}$ = 0.0002, $\delta(\varphi)$ = 0.18°. τ_{diff} and $\tau_{\sigma2}$ were chosen based on a sensitivity analysis (Fig. 2). τ_{range} is an optional parameter. The number of slices $L_i(\theta)$ used is nine for the Beech scans and five for the Douglas fir scans. These slices are centered at zenithal heights i = {−3.6°, −2.7°, −1.8°, −0.9°, 0°, 0.9°, 1.8°, 2.7°, 3.6°} and i = {−3.6°, −2.7°, −1.8°, −0.9°, 0°} with i = 0° representing the scanner height. The reason for using different slice numbers is the lower stem density of the Douglas fir zone compared to the Beech zone
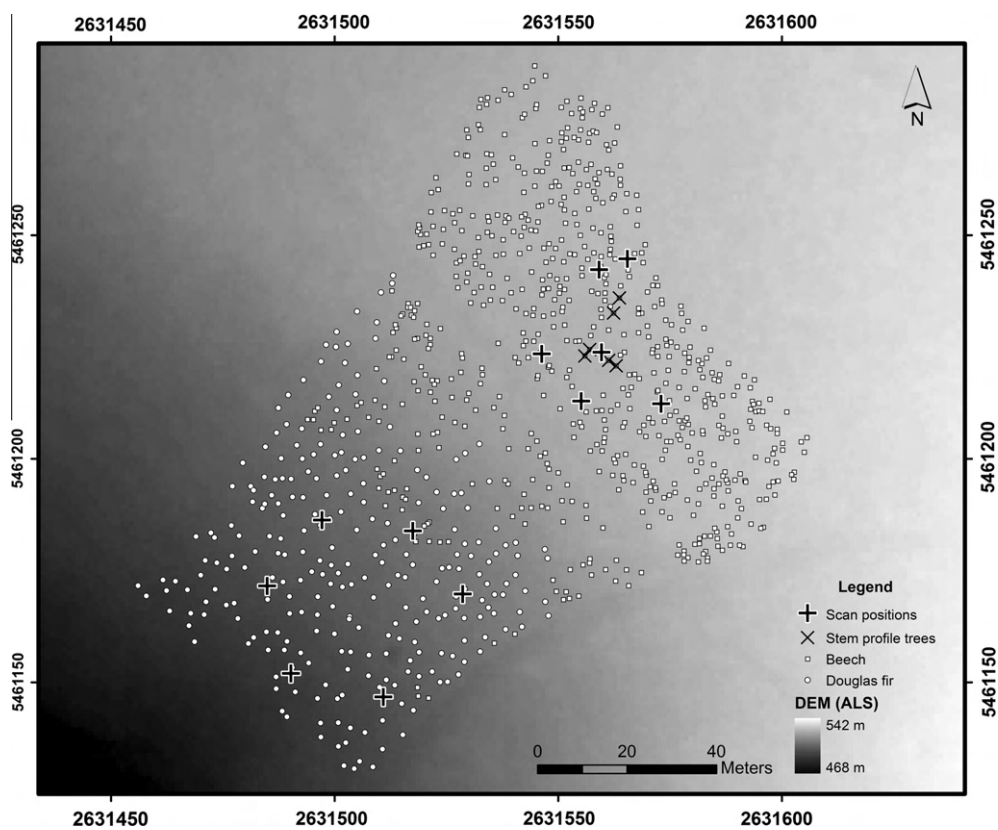
Fig. 1a. Research site *Merzalben*. Digital elevation model (DEM) derived from airborne laser scanning. Tree locations were determined using a tachymeter and dGPS.
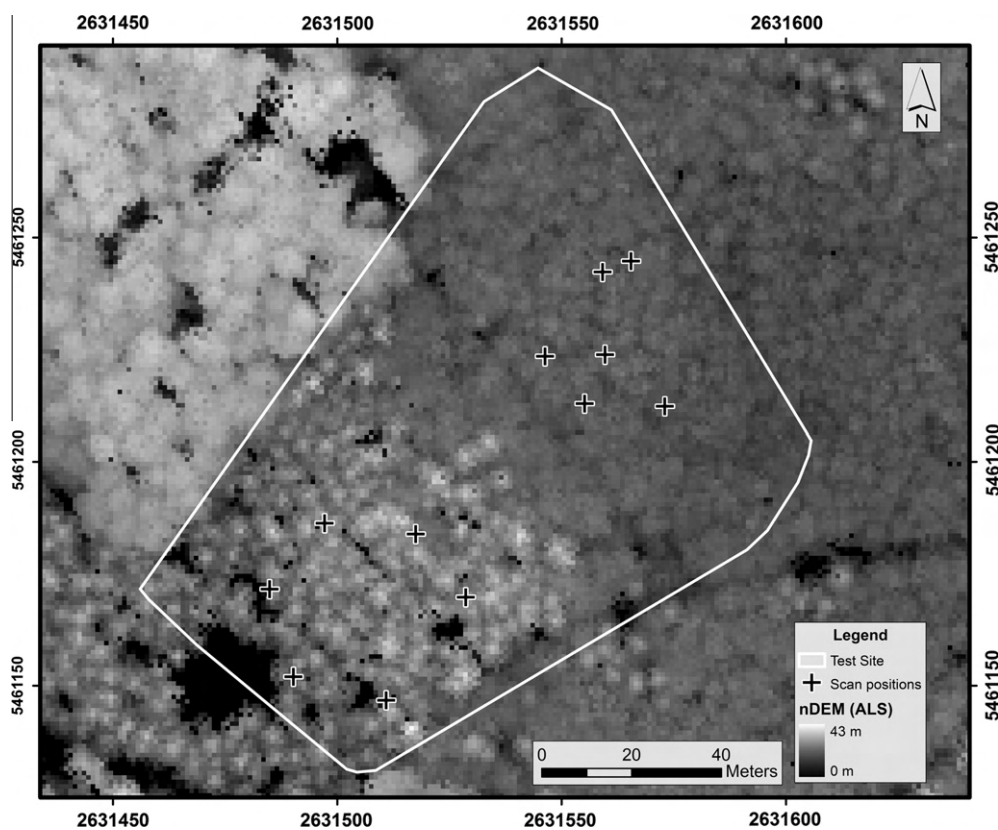

Fig. 1b. Research site *Merzalben*. Normalized height model (nDEM) derived from airborne laser scanning.

Table 2
Structural attributes and stand characteristics of the research site *Merzalben*. DBH and height statistics are based on the full sample (No. of trees = 922). Stem density (SD), total area and slope relate to the zones of pure Beech and pure Douglas fir.

	DBH (cm)				Height (m)				SD (No./ha)	Area (ha)	Slope (°)
Species	Min	Max	Mean	Std	Min	Max	Mean	Std	Total	Total	Total
Beech	1.4	34.7	16.4	7.3	3.4	28	18.5	5.7	1032	0.5	3.1
Douglas fir	3.7	51.2	28.7	7.5	8	36.1	27.1	4	579	0.5	6.5

(see Section 2.1). Based on the scan resolution applied in this study, the azimuthal span $\delta(\varphi) = 0.18°$ corresponds to stem diameters of 3.14 cm, 6.28 cm, and 9.24 cm for ranges of 10 m, 20 m, and 30 m respectively. $\delta(\varphi)$ was determined based on the DBH distribution of our research site where less than 5% of the trees within the range used in this study (30 m) have DBH below 10 cm.

2.4. Stem diameter and volume extraction

2.4.1. Circle fit algorithms

In order to assess the effects of the circle fit algorithm on the extracted stem diameters and volumes, three different circle fit algorithms were tested: A geometric algorithm implemented by Lemen (1991) and two algebraic algorithms (Pratt, 1987, and Taubin, 1991) as implemented by Chernov (2009a,b). Geometric and algebraic fits are the two general approaches to fitting a circle to a set of given points. The geometric fit aims at minimizing the sum of the squares (SS) of a set of points $(x_1, y_1), (x_2, y_2), \ldots, (x_n, y_n)$ that a circle, represented by the equation $(x - a)^2 + (y - b)^2 = r$, is fitted to (Umbach and Jones, 2003):

$$SS(a, b, R) = \sum_{i=1}^{n} (R - \sqrt{(x_i - a)^2 + (y_i - b)^2})^2 \quad (1)$$

where a and b denote the center of the circle and R its radius. There exist various numerical algorithms to minimize SS over a, b and R (Gander et al., 1996). These approaches are considered to be accurate, as the geometric fit corresponds to the Maximum Likelihood estimate of a, b and R (Al-Sharadqah and Chernov, 2009). However, a major concern in geometric fits is that the respective minimization algorithms have no closed solution and, thus, they usually require iterative and computationally intensive numeric schemes such as a general Gauss–Newton or Levenberg–Marquardt. Their performance among others strongly depends on the choice of the initial guess (Al-Sharadqah and Chernov, 2009). Algebraic fits on the other hand use an algebraic equation to represent a circle (Pratt, 1987):

$$A(x^2 + y^2) + Bx + Cy + D = 0 \quad (2)$$

Constrained by $B^2 + C^2 - 4AD = 1$ \quad (3)

This equation describes all circles and with $A = 0$ also lines. Corresponding fits are non-iterative and thus faster than Geometric fits. One of the most popular algebraic fits is the Kåsa algorithm (Kåsa, 1976) which aims at finding the circle that minimizes the function.

$$F_K = \sum f_i^2 = \sum_{i=1}^{n} (r_i^2 - R^2)^2$$

$$= \sum_{i=1}^{n} (x_i^2 + y_i^2 - 2ax_i - 2ay_i + a^2 + b^2 - R^2)^2 \quad (4)$$

where $f_i = r_i^2 - R^2$ denotes the algebraic distance from the point (x_i, y_i) to the circle.

However, it has been found that the accuracy of the Kåsa fit suffers in cases when the observed points do not represent complete circular arcs (Al-Sharadqah and Chernov, 2009). Thus, several modifications of the F_K-function were developed to overcome this limitation, e.g. by Pratt (1987) and by Taubin (1991). To account for the incomplete circular representation of tree stems in single scan mode we tested the circle fit algorithms by Pratt and Taubin and in order to compare between the performances of the general approaches, algebraic and geometric, we included a geometric fit (Lemen, 1991).

2.4.2. Methodology

Our approach to automated stem diameter extraction is based upon a step-wise vertical slicing of the point cloud and circle fitting to extracted stem points, similar to Bienert et al. (2006). Our approach applies equally to single and merged scan data. First, points which fall within the boundaries of a bounding box of size 60 cm × 60 cm, centered at the stem centroid derived from the stem detection, are extracted and define a set of stem points. The height minimum of this set is then searched for which represents the ground level, provided that there is no occlusion. Since it has been found that the phase-shift FARO scans suffer from so-called ghost points below ground level which affect the determination of the exact ground level (Bienert et al., 2006; Maas et al., 2008), we implemented a histogram-based outlier detection and removal. The height maximum is implemented as a user-definable parameter which is constrained by the height maximum found by the
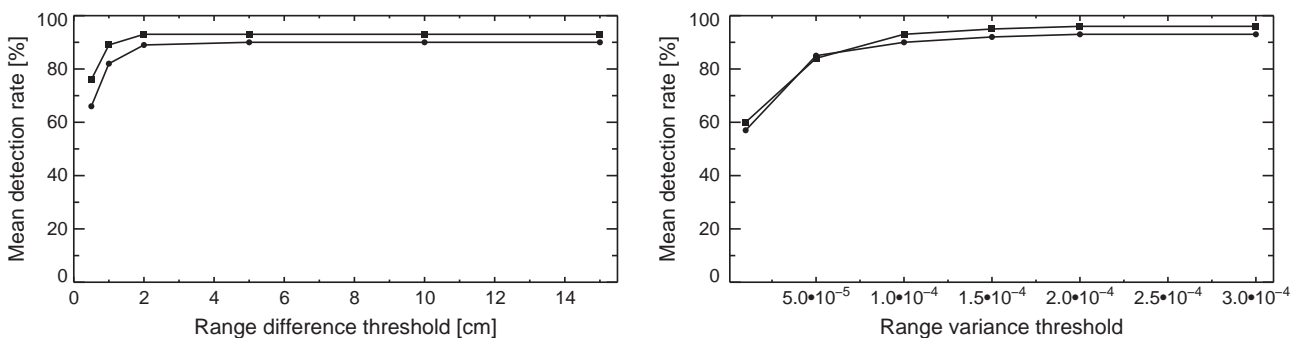

Fig. 2. Sensitivity analysis of the stem detection algorithm parameters range difference threshold and range variance threshold. Mean stem detection rates based on the 6 single scans for each of the pure zones. Squares = Douglas fir, circles = Beech. Remaining parameters according to Section 2.3

algorithm. Starting from the stem centroid, stem points which fall within the boundaries of a slice of 5 cm vertical thickness are extracted and circle fitting is applied. Since the set of stem points also includes points which represent branches and leaves and which affect the circle fitting, an exclusion of these outliers is mandatory. We therefore implemented a range-based outlier test based on a fixed buffer added to the radius of the circle fitted for the previous slice (buffer = ¼ of the previous circle's radius). To prevent further errors in the circle fitting (e.g. fitting too large of a circle due to point clouds with circle arcs smaller than semi circles) an upper radius threshold of 0.3 m is set in our algorithm. If this value is exceeded, the radius of the circle fitted for the previous slice is used instead. The basic steps of the algorithm are performed for all slices from the starting point to the local minimum and maximum. In a final step DBH is extracted both directly as the stem diameter at the nominal height of 1.3 m and indirectly based on a robust linear fit of the stem diameter profile.

2.4.3. Volume extraction

Stem volume was extracted based on the stem diameter profiles. In order to achieve the same vertical slice width of the TLS derived stem profiles (5 cm), the reference stem profiles were interpolated with a cubic spline. Stem volume was then calculated for both TLS derived and reference stem profiles by summing the volumes calculated for each slice approximated as a conical frustum:

$$V_{stem} = \sum_{z=0}^{10m} t_{slice} \times \frac{\pi}{3} \times (r_1^2 + r_1 \times r_2 + r_2^2) \qquad (5)$$

with t_{slice} is the slice thickness and r_1 and r_2 are the top and base radii.

Due to uncertainties in the exact determination of the local tree minima (e.g. due to ghost points and/or occlusion effects) and uncertainties in the exact height determination of the single reference stem profile measurements (e.g. due to buckled stems), which result in an offset between the TLS derived and reference stem profiles, volumes were compared rather than stem diameter measurements.

3. Results

3.1. Stem detection

Depending on the number of slices used for stem detection, mean detection rates vary from 56% to 94% for Beech and from 68% to 96% for Douglas fir. This demonstrates that shadowing strongly affects the single scan based stem detection if only a small part of the data is used. Raising the number of slices and therefore enhancing the visibility, mean detection rates also increase (Table 3). However, fewer slices are required for the Douglas fir compared to the Beech scans to achieve similar mean detection rates, which shows the influence of stem density. Based on one slice the algorithm detects 12% more of the trees in the lower density Douglas fir zone than in the higher density Beech zone. Based on five slices the algorithm detects 96% of the trees in the lower density zone, whereas for the higher density zone only 81% are detected. However, overall detection rates are above 90% for both zones and – equally important – false detection rates are low (Table 3). It has to be noted though that the high detection rates achieved relate to trees which are visible to the scanner and thus potentially detectable (i.e. non-occluded and partially occluded trees). If occluded trees are accounted for, mean detection rates reduce to 85% for Beech and 84% for Douglas fir. These effective detection rates are mainly determined by the shadowing effect which constitutes an inherent limitation of the single scan based

stem detection (see Section 1). Since the magnitude of this effect depends on stand structure and site characteristics, it is important to report detection rates based on potentially detectable trees instead of effective detection rates in order to provide for an objective comparison with other single scan based methods.

3.2. DBH extraction

3.2.1. Single scans

In order to test the influence of the scan mode and circle fitting on the stem diameter extraction, diameter at breast height (DBH) was extracted from both single and merged TLS scan data and based on three different circle fit algorithms and two different extraction methods (see Section 2.4). DBH extracted from the single scans generally show a good agreement with reference DBH with RMSE's ranging from 1.39 to 2.43 cm (Fig. 3 and Table 4). However, results reveal that DBH extracted at the nominal breast height differ significantly from those estimated based on a linear fit of the diameter profile (Table 4). This observation is backed by the error histograms (Fig. 4). The slight overestimation for the direct extraction DBH and the underestimation for the linear fit DBH compared to reference DBH are found for both Beech and Douglas fir and for all three circle fit algorithms. Due to the time lag between the TLS scan acquisition and the DBH reference collection (August 2011–April 2012), a slight underestimation of in situ DBH is to be expected which indicates that the linear fit DBH yield values closer to the true values; a fact which is supported by the lower RMSE values (Table 4). This can be attributed to the fact that the linear fit extraction method is less prone to errors in the determination of the ground level and thus the exact breast height. The overestimation observed for the DBH directly extracted at breast height may therefore be caused by a negative bias in the determination of the ground level, possibly as a result of remaining ghost points below ground level (see Section 2.4.2).

As far as the influence of the circle fitting is concerned, mean differences between the three algorithms do only differ marginally, which is reflected in the error histograms (Fig. 4). Nevertheless, RMSE's are higher for the algebraic-based algorithms Pratt and Taubin than for the parametric-based Lemen algorithm (Table 4). This can be observed for both Beech and Douglas fir and to a lesser degree for both DBH extraction methods, which consolidates the better performance of the Lemen algorithm. The lower RMSE's observed for the linear fit DBH estimates suggest that a robust modeling and/or removal of outliers (e.g. ghost points) is more important than the choice of the circle fit algorithm. In addition the DBH estimation errors show no dependence on range (Fig. 5) for the range and scan settings used in this study. However, a range effect (i.e. increasing estimation errors with increasing range) might be expected for longer ranges and/or lower scan resolutions.

3.2.2. Merged scans

DBH extracted from the merged scans generally show a very good agreement with reference DBH with RMSE's ranging from 0.66 to 1.21 cm (Fig. 6 and Table 5). Similar to the single scan DBH, linear fit DBH underestimate and direct extraction DBH overestimate reference measurements (Table 5). However, contrary to the single scans, differences in RMSE between the two methods are smaller (Tables 4 and 5), which suggests a reduced influence of outliers for the merged scan data. Based on the RMSE's, the Lemen algorithm performs slightly better than the Pratt and Taubin algorithms for the direct extraction DBH. This effect is negligible for the linear fit DBH (Table 5). The biggest difference compared to the single scan DBH, however, is an improved accuracy which is reflected in the considerably lower RMSE's irrespective of the DBH extraction method, tree species and circle fit algorithms (Tables 4 and 5 and Figs. 3 and 6).

Table 3

Mean stem detection rates. Reported values are mean values of the six single scans for each of the pure zones. L_i = horizontal slices at different zenithal offsets from the scanner height (0°). Visible trees relate to non-occluded and partially occluded trees.

No. of slices used for stem detection	Beech (%)	Douglas fir (%)
1: L_i (0°)	56	68
2: L_i (0°, −0.9°)	68	83
3: L_i (0°, −0.9°, −1.8°)	75	89
4: L_i (0°, −0.9°, −1.8°, −2.7°)	78	92
5: L_i (0°, −0.9°, −1.8°, −2.7°, −3.6°)	81	96
6: L_i (0°, −0.9°, −1.8°, −2.7°, −3.6°,+0.9°)	84	
7: L_i (0°, −0.9°, −1.8°, −2.7°, −3.6°,+0.9°,+1.8°)	87	
8: L_i (0°, −0.9°, −1.8°, −2.7°, −3.6°,+0.9°,+1.8°,+2.7°)	90	
9: L_i (0°, −0.9°, −1.8°, −2.7°, −3.6°, +0.9°, +1.8°, +2.7°, +3.6°)	94	
False detection rate	2	1
Detection rate visible trees	94	96
Detection rate visible and occluded trees[a]	85	84

[a] Since the initial stem detection range of 30 m exceeded for some of the scans the test site boundaries where no tree location information was available, a radius of approximately 21 m was used to calculate this statistic.
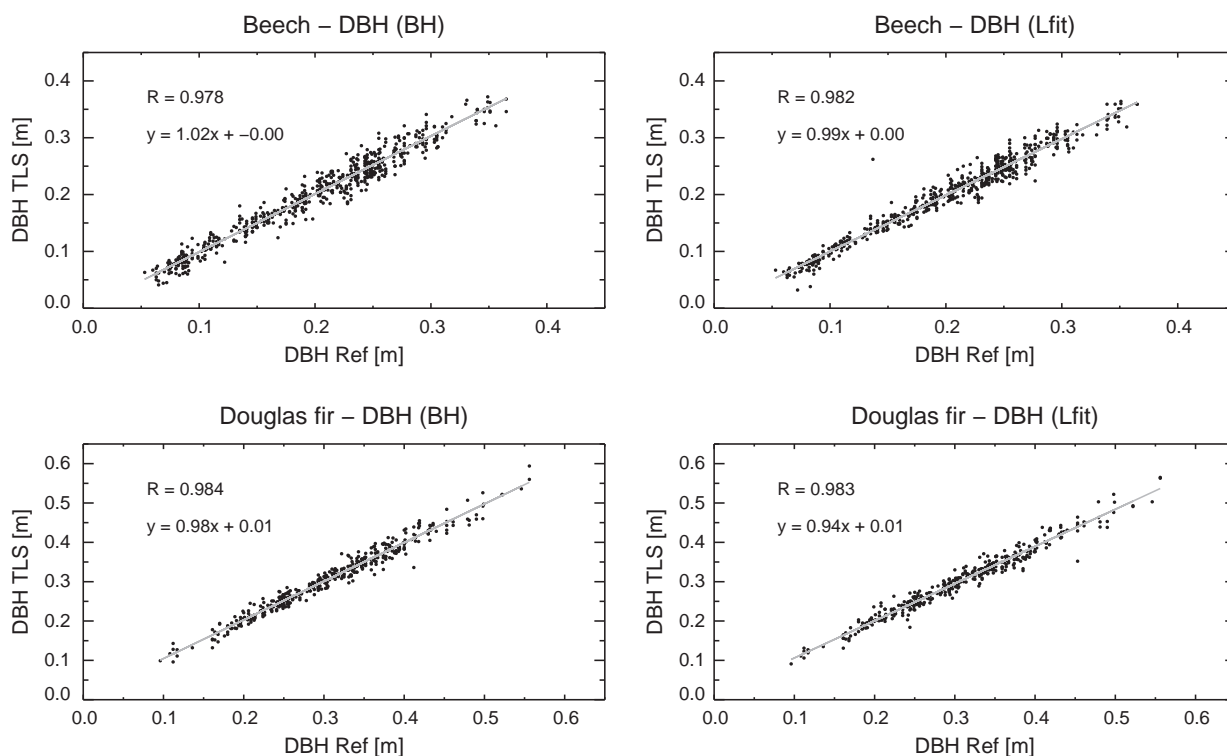

Fig. 3. Comparison of reference DBH and DBH derived from the single TLS scans. Comparison is exemplified by TLS-DBH based on the Lemen circle fitting and two DBH extraction methods: DBH extracted at the nominal breast height (BH) and DBH estimated based on fitting a line to the diameter profile (Lfit).

Table 4

Statistics for the automated stem diameter extraction from the single scans. n (Trees) = unique number of trees detected in all six single scans. n (Total) = multiple detections are accounted for, i.e. individual trees are scanned from different angles and hence detected in more than one single scan. Mean difference = Mean (Reference DBH − TLS derived DBH). DBH (BH) = DBH extracted at the nominal breast height, DBH (Lfit) = DBH estimated based on fitting a line to the diameter profile.

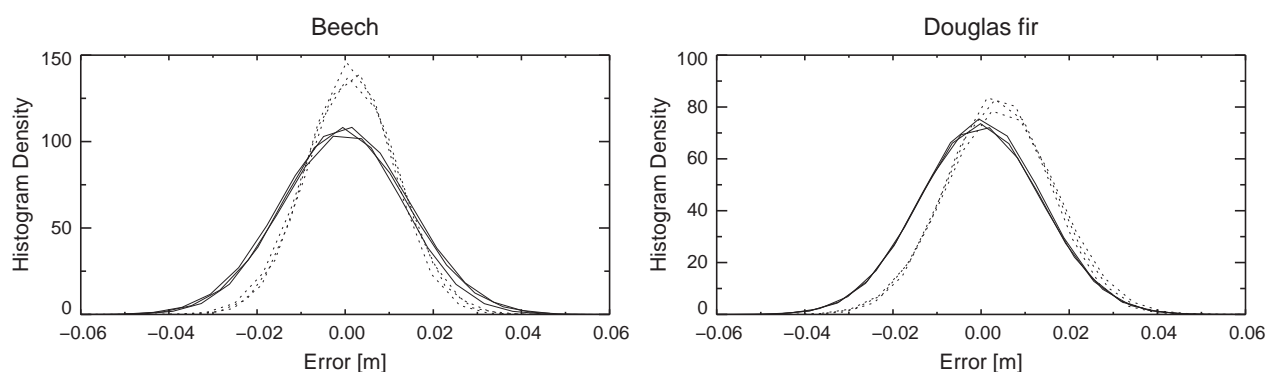| Plot	n (Trees)	n (Total)	Algorithm	Mean difference (cm)		RMSE (cm)	
				DBH (BH)	DBH (Lfit)	DBH (BH)	DBH (Lfit)
Beech	289	820	Lemen	−0.07	0.14	1.58	1.39
			Pratt	−0.18	0.16	2.20	1.49
			Taubin	−0.21	0.22	2.43	1.57
Douglas fir	213	536	Lemen	−0.13	0.47	1.47	1.65
			Pratt	−0.19	0.46	2.04	1.68
			Taubin	−0.18	0.51	2.02	1.74

Fig. 4. Distribution of the DBH estimation errors for the different DBH extraction methods and circle fit algorithms. Dotted lines = Circle fit errors based on the linear fit DBH extraction. Solid lines = Circle fit errors based on the direct DBH extraction.

The improved accuracy can be attributed to a more stable and accurate circle fit which results from the full coverage of stem cross-sections and the reduced influence of outliers due to this improved coverage. This is demonstrated by the reduced influence of the DBH extraction methods and circle fit algorithms on the model performance (Tables 4 and 5). Since sampling efficiency is an important consideration in forest inventory, estimation errors were analyzed as a function of the number of scans contributing to the stem diameter modeling. Results show that for the Beech zone at least three scans contributed to the stem diameter modeling of each of the 82 trees within the overlap of the six scans (Fig. 7). Also, roughly equal number of trees were observed from four, five, and six scan locations. By contrast, most Douglas fir trees within the scan overlap could only be observed from two or three scan locations (Fig. 7). This is due to the positioning of the scans in combination with the steeper slope of the Douglas fir zone (see Fig. 1a). Therefore only Douglas fir trees observed from two or three scan locations were taken into account for this analysis. While estimation errors for Beech show no distinct dependence on the number of scans, estimation errors for Douglas fir trees observed from two locations yield a slightly higher mean error compared to trees observed from three locations. However, their relative error ranges are similar. We therefore conclude that two respectively three merged scans are sufficient to achieve good estimation accuracies.

Another aspect which so far has received little attention in the TLS literature is to relate stem diameter estimation errors to the magnitude of radial growth (increment). For TLS to become an effective and reliable inventory tool for determining increment and consequently growth, the estimation error has to be lower than the increment. At our research site DBH has been measured annually since 2008 which allows the calculation of radial growth for a four year period and the comparison with the DBH estimation errors based on the single and merged scans (Fig. 8). Results show that RMSE's for Beech and Douglas fir are on a similar level and are also relatively constant over the DBH range observed, except for a slight increase of Douglas fir RMSE's for the DBH classes 0.3–0.4 m and 0.4–0.5 m. As already mentioned merged scan RMSE's are significantly lower than single scan RMSE's. While increment of both Beech and Douglas fir exceeds the merged scan RMSE's already for DBH greater 0.1–0.2 m, radial growth exceeds the single scan RMSE's not until DBH greater than 0.2–0.3 m.

3.3. Stem form and volume extraction

The automated stem diameter extraction proposed in the present study yields stem diameter vertical profiles (taper curves) which are then used to determine stem volume and form (see Section 2.4). Both metrics are of particular interest in forestry. TLS derived stem diameter profiles show good agreement with in situ measured profiles for mean single scan and merged scan profiles (Figs. 9 and 10). By contrast single scan profiles can exhibit both a strong systematic under- or overestimation of stem diameters, depending on scan location (Fig. 9). Merged scan profiles are less prone to such biases and show that the stem form, which can vary strongly between trees of different species as well as trees of the same species, can be determined quite well allowing the extraction of information such as the height of the crown base (Fig. 10).

The results for the stem profile extraction are reflected in the stem volume estimates, too. Volumes extracted from the merged scan data show an excellent agreement with reference volumes with deviations ranging from −2% to 6% (Table 6). By contrast stem
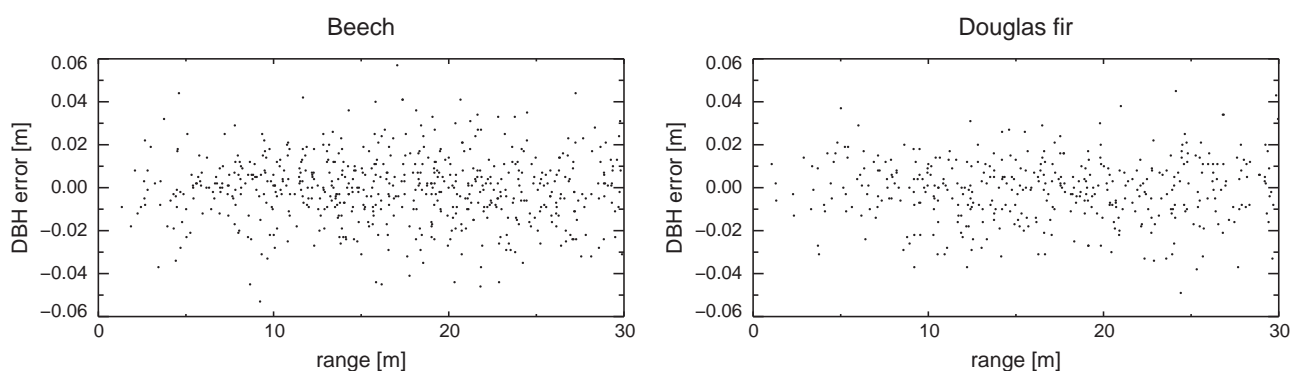

Fig. 5. DBH estimation errors as a function of range. Range independence is exemplified by TLS-DBH based on the Lemen circle fitting and the direct DBH extraction. Error-range patterns are similar for the different circle fit algorithms and DBH extraction methods.
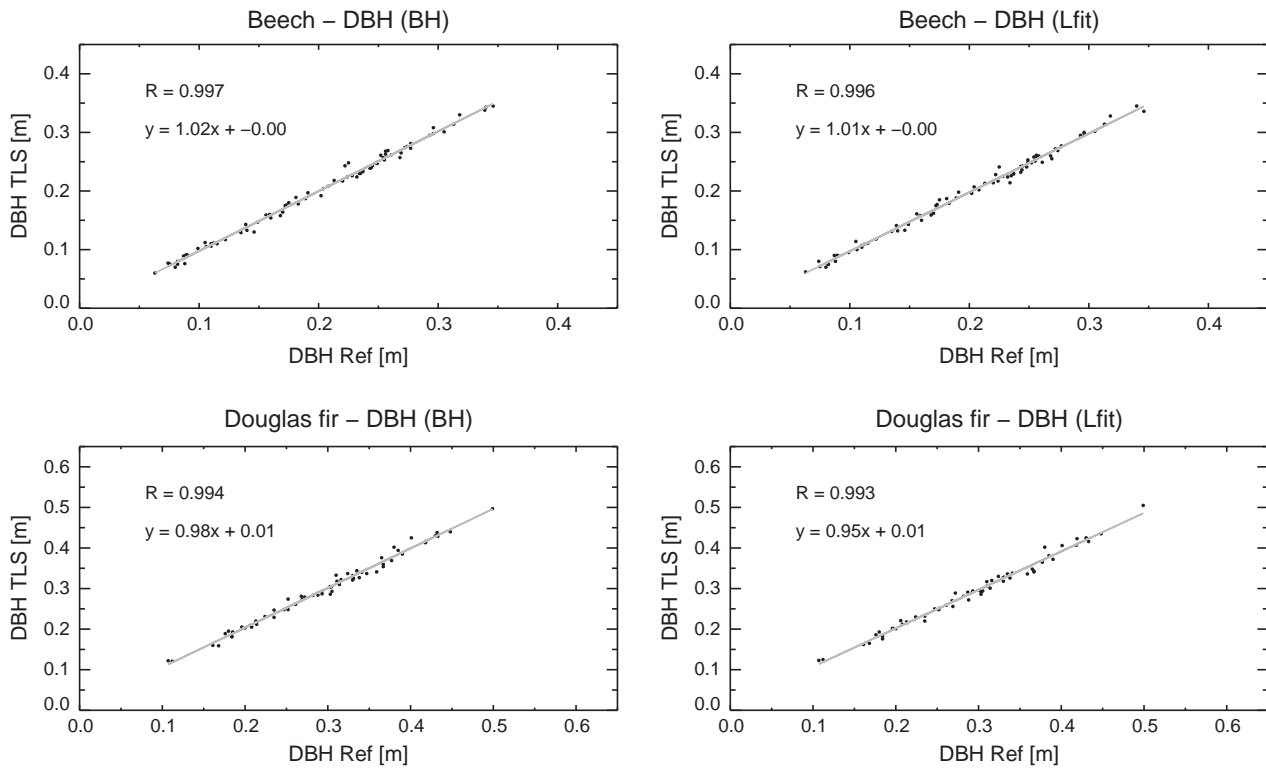
Fig. 6. Comparison of reference DBH and DBH derived from the merged TLS scans. TLS-DBH is based on the Lemen circle fitting and two DBH extraction methods: DBH extracted at the nominal breast height (BH) and DBH estimated based on fitting a line to the diameter profile (Lfit).

Table 5
Statistics for the automatic stem diameter extraction from the merged scans. Mean difference = Mean (Reference DBH − TLS derived DBH). DBH (BH) = DBH extracted at the nominal breast height, DBH (Lfit) = DBH estimated based on fitting a line to the diameter profile.

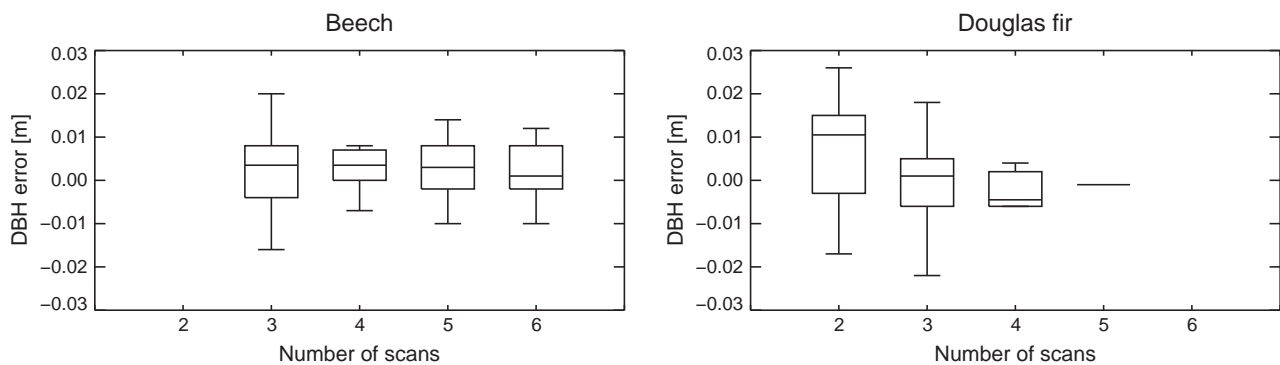| Plot	n (Trees)	Algorithm	Mean difference (cm)		RMSE (cm)	
			DBH (BH)	DBH (Lfit)	DBH (BH)	DBH (Lfit)
Beech	82	Lemen	0.00	0.23	0.66	0.67
		Pratt	−0.18	0.24	0.90	0.64
		Taubin	−0.09	0.24	0.79	0.66
Douglas fir	67	Lemen	−0.16	0.25	0.97	1.06
		Pratt	−0.32	0.21	1.21	1.15
		Taubin	−0.29	0.25	1.20	1.14

Fig. 7. DBH estimation errors as a function of the number of scans in merged scan mode. DBH error = DBH (Reference) − DBH (TLS). Analysis based on the DBH resulting from the Lemen circle fitting and the linear fit extraction method.

volumes extracted from the single scan data vary from −34% to 44%. This large variability mainly results from the inferior single scan stem diameter extraction (see Section 3.2). However, the results also show that depending on scan location and visibility it is possible to achieve good stem volume estimates for single scans with errors as low as −2% to 4% (Table 6). Also, quite a large variability can be observed for the single scan volume estimates based on different circle fit algorithms despite the fact that only a
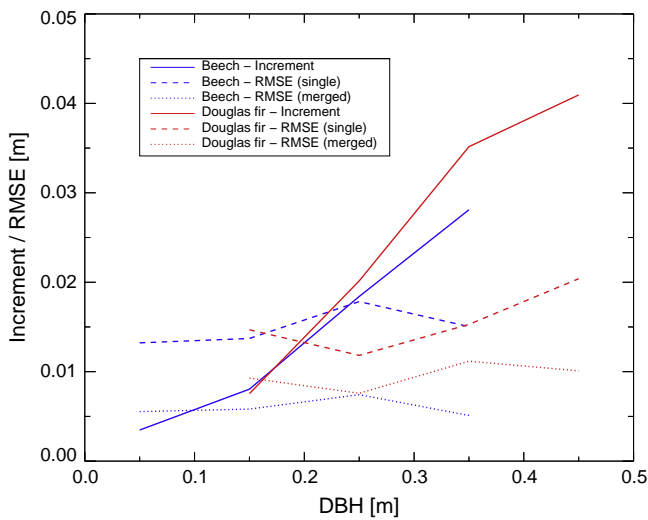
Fig. 8. Comparison of mean DBH increment and DBH estimation errors based on single and merged TLS scans. DBH increment = mean DBH class radial growth over the period 2008–2012 at the *Merzalben* research site.

marginal effect of circle fitting could be observed for the extracted DBH (see Section 3.2). This might be explained by the step-wise vertical slicing and diameter modeling of the stem point clouds (see Section 2.4.2). Random errors in the circle fitting for the different algorithms potentially propagate from slice to slice which is then strongly reflected in the volume estimates. Another important consideration for a TLS-based estimation of stem volume which is reflected in the results is the fact that due to complete or partial shadowing by stems and branches only 1/3–2/3 of the single scans could effectively be used to extract stem form and volume (Table 6).

4. Discussion

4.1. Stem detection

For TLS to be routinely applied in forest inventory, an automated, efficient and accurate extraction of forest metrics from TLS data is required. In this context, the detection of trees is of particular importance as it provides for basic inventory variables such as stem density and stem locations, which constitute the base for higher level algorithms for deriving tree metrics (stem diameter, volume, etc.). An efficient and effective stem detection algorithm is therefore mandatory. A number of different approaches have

been proposed (e.g. Aschoff and Spiecker, 2004; Forsman and Halme, 2005; van Leeuwen et al., 2011), most of which are based on single scans as their collection and processing is less time-consuming compared to multiple (merged) scans. By contrast merged scans provide for a much better 3D coverage of trees which reduces shadowing effects most effectively (see Section 1). While the shadowing of background objects by foreground objects is an inherent limitation of the use of single scans for stem detection, partial occlusion of stems by branches and leaves is something that can be minimized by utilizing either the whole point cloud information or significant parts of it. The approach to stem detection proposed in the present study is based on the latter by running the stem detection algorithm for multiple slices extracted from the range image of a single TLS scan (see Section 2.3). To test its robustness we conducted a sensitivity analysis of parameters and applied the approach to scans collected at two zones of our study site which significantly differ in stem density (see Sections 2.1 and 2.3). The results demonstrate that our approach yields high detection rates – the number of range image slices required to achieve these rates however depends on the stem density and degree of branching of the area scanned, i.e. nine slices were required for the higher density Beech zone compared to five slices for the lower density Douglas fir zone (see Section 3.1). Currently the number of slices used in our algorithm is set to a fixed number as determined by the number of slices required to achieve mean detection rates of around 95% in this study. Since this kind of information is normally difficult to obtain a priori, the choice of slice numbers could be implemented as an iterative process with the iteration terminating if the change in detection rate falls below a user-defined threshold. Alternatively, since the algorithm is fast and efficient (computing time is in the range of seconds), the initial slice numbers could be set relatively high to guarantee good results. Also, it would be worth considering the relation between the overlaying circles of the multiple slices, which are for now only used to avoid output of multiple stem detections. There is potential in including this relation for minimizing false detections and/or assessing the degree of branching (occlusion effects). Differences in the circles' coordinates could also be used to yield improved tree locations and/or rough estimates of the stem form, which could then be used as input to more complex single-tree based models.

4.2. DBH extraction

With regard to the extraction of stem diameters, this study demonstrated that estimation accuracies for merged scan data are significantly higher than compared to single scan data, corroborating earlier studies (Thies and Spiecker, 2004; Maas et al., 2008). By contrast to these studies, however, the present analysis is based
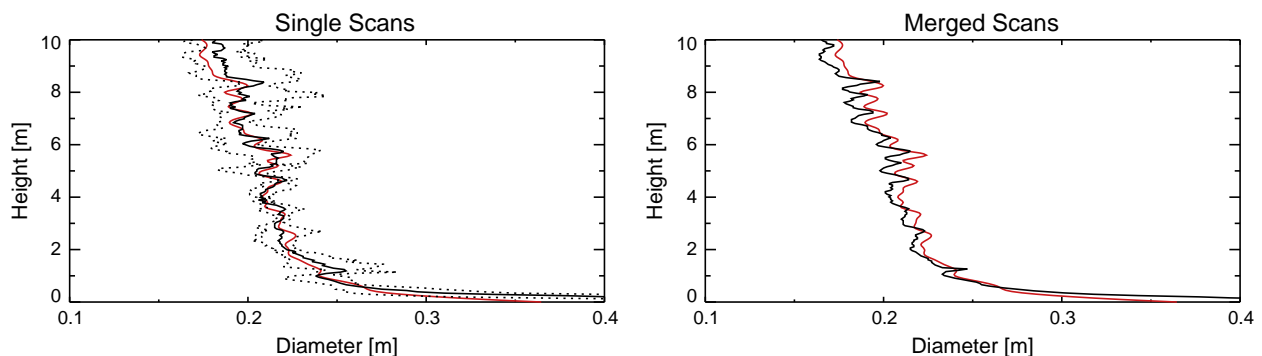

Fig. 9. Comparison of reference and stem profiles derived from the single and merged TLS scans. Example: Tree No. 543. Red line = reference profile, dotted lines = min. and max. of single scan profiles, solid line = stem diameter profiles derived from the single (mean) and merged scans.
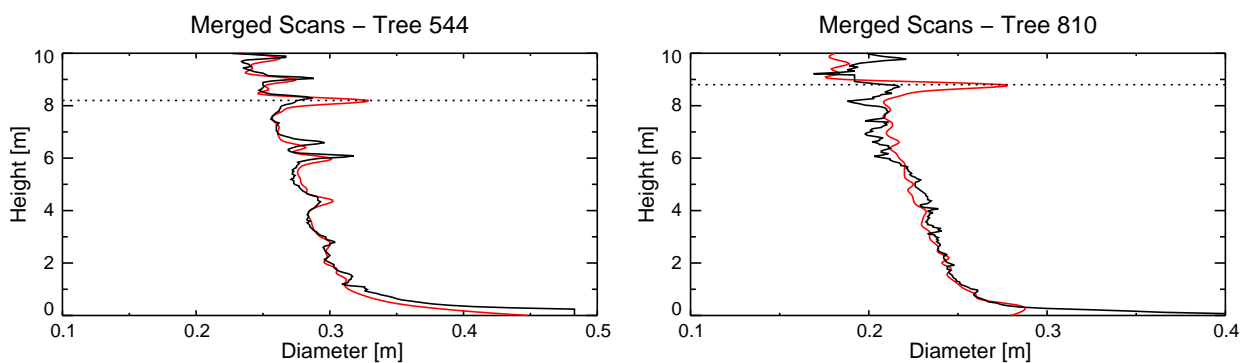
Fig. 10. Comparison of reference and stem diameter profiles derived from the merged TLS scans. Example: Red line = reference profile, black line = TLS derived profile, dotted line = crown base height.

Table 6
Stem volume deviations in % of the reference volume (m³). The plus indicates an incomplete stem profile due to partial occlusion, the dash indicates non-visibility to the scanner.

Tree	Algorithm	Scan 1	Scan 2	Scan 3	Scan 4	Scan 5	Scan 6	Merged scans	Reference
542	Lemen	–	16	+	13	+	−9	0	0.44
	Pratt	–	16	+	12	+	−18	1	
	Taubin	–	15	+	12	+	−15	1	
543	Lemen	−5	4	17	9	–	–	−2	0.36
	Pratt	−7	5	17	11	–	–	0	
	Taubin	−7	5	17	9	–	–	−1	
544	Lemen	+	+	19	20	+	+	3	0.66
	Pratt	+	+	28	14	+	+	3	
	Taubin	+	+	27	25	+	+	3	
546	Lemen	+	+	−9	6	14	–	0	0.39
	Pratt	+	+	−9	5	18	–	1	
	Taubin	+	+	−9	5	14	–	1	
810	Lemen	+	+	18	−2	21	−34	1	0.41
	Pratt	+	+	17	−22	17	−13	3	
	Taubin	+	+	15	−16	17	−7	2	
823	Lemen	20	–	–	+	+	5	5	0.30
	Pratt	44	–	–	+	+	20	6	
	Taubin	4	–	–	+	+	20	6	

on large sample sets of two different tree species, Beech and Douglas fir, which gives more robust results. This study could also show that properly dealing with noise in TLS data (see also Section 1) is crucial for improving the estimation accuracies. This was demonstrated by the lower RMSE's based on a robust linear fit of the stem diameter profile compared to the direct extraction of stem diameter at breast height. The linear fit method has the advantage of being more robust against errors in the determination of the ground level and therefore the exact breast height and/or against errors in the circle fitting at breast height as a result of unwanted data (i.e. scanner returns from branches and leaves). However, RMSE differences between the two DBH extraction methods are smaller for the merged scan data, which suggests a reduced influence of noise as a result of a more stable and accurate circle fit from the full coverage of stem cross-sections for the merged scan data. Alternatively, filtering of the raw data can be used to minimize noise and therefore estimation errors, e.g. by assessing the RMSE of the circle fit. However, care should be taken in using this measure, because the goodness-of-fit is not necessarily an indication of the accuracy of the model (Litkey et al., 2008) and is influenced by a number of factors such as the circularity of the stem cross-section (Brolly and Király, 2009). Non-circularity is certainly a major factor contributing to the estimation errors from circle fitting, with varying magnitude depending on tree species. As far as the influence of circle fitting in general is concerned, this study demonstrated that a robust modeling and/or filtering of noise has a

stronger influence on estimation accuracies than the choice of the circle fit algorithm. Litkey et al. (2008) suggest that a proper removal of outliers even allows for applying different models including circle and cylinder fitting. This is in contradiction to the study of Tansey et al. (2009) which found circle fitting to be more accurate and efficient than cylinder fitting even though the latter performed better in case of leaning stems. With regard to the different modeling of stem diameters, the modeling success in terms of agreement with true diameters is less dependent on range than on stem visibility from the scanner's viewpoint and on the presence of outliers (Litkey et al., 2008). From our experience and based on the analysis of measurement error as a function of range (see Section 3.2.1), this hypothesis can be confirmed; at least for the scan settings applied in these studies.

Regarding the use of merged scan data, Maas et al. (2008) reported lower RMSE's for merged time-of-flight scan data compared to phase-shift single scan data and concluded that the number of scans has a larger influence on DBH accuracy than scanner type. Our study showed that the number of merged scans which contribute to the stem diameter modeling does not influence the estimation accuracies significantly (see Section 3.2.2). This is due to the fact that the stems in the overlap of the scans were well covered from multiple angles which resulted in a complete coverage of the stems' cross-sections in most cases. Thus we conclude that the coverage of a tree stem's circumference is the key issue for a reliable and successful modeling of stem diameters, rather than

the exact number of scans that contribute to its coverage (cf. also Bienert et al., 2007, and Litkey et al., 2008). Besides providing more accurate DBH estimates, merged scan data also allows for the application of advanced modeling techniques such as ellipse fitting (Aschoff and Spiecker, 2004) or B-splines (Pfeifer and Winterhalder, 2004). This would help to reduce the error which results from fitting circles to non-circular stem cross sections observed for many tree species.

However, the use of merged scan data also has its drawbacks, the main ones being the time-consuming collection and registration of multiple scans (Bienert et al., 2006) as well as the reduced efficiency in terms of sampling number (cf. Tables 4 and 5). The latter is an important consideration if TLS is to be routinely used in forest inventory, since forest inventory aims at maximizing its sampling while minimizing costs (Lovell et al., 2011). In the context of a TLS-based forest inventory, the benefit of obtaining objective and repeatable measurements of vegetation structure for growth (or more general for biomass change) monitoring is emphasized by a number of studies (e.g. Watt & Donoghue, 2005, Tansey et al., 2009). TLS clearly has the potential to provide such information, however in order to establish TLS for this purpose one key aspect, which so far has received little attention in the TLS literature is to relate stem diameter estimation errors to the magnitude of radial growth (increment). For TLS to become an effective and reliable inventory tool for determining increment and consequently growth, the estimation error has to be lower than the increment. Our study demonstrated that if TLS is to be used for determining stem growth, tree species specific growth rates, the growth period and the estimation errors, which may significantly differ between scan settings, have to be taken into account for properly assessing the reliability of such measurements (see Section 3.2.2).

4.3. Stem form and volume extraction

As far the extraction of stem volume from TLS data is concerned, the estimation of stem volume is a main objective in forest inventory, in particular from a commercial point of view (Bienert et al., 2007). Another variable of interest is the stem form (Gaffrey et al., 1998; Holopainen et al., 2011). Both stem volume and form cannot be measured efficiently with traditional methods, hence allometric equations with DBH and tree height as input variables are mainly used. By contrast, TLS potentially allows for a direct measurement of stem form and volume and therefore could be a valuable tool for forest inventory. Our study could show that stem form and volume can be successfully extracted from TLS data for stem parts which are not too heavily occluded by branches and leaves. As stem form and volume are based on the extraction of stem diameters, the results reflect the findings from the stem diameter extraction that merged scan data provide for a more stable and accurate estimation. It could also be shown that information such as the height of the crown base can be extracted from TLS data. However the major challenge of determining whole stem volumes remains. This is due to the shadowing of background objects by foreground objects which particularly affects stem parts within the canopy. For example Watt and Donoghue (2005) stated that tree taper can be measured reliably below the canopy but not within the canopy due to dense branching. Tansey et al. (2009) tried to extract stem volume with no success, a fact which they attributed to the uncertain stem height estimation from TLS data. The shadow effect strongly depends on stand structure and may be minimized by the use of multiple scans (Lovell et al., 2011). However even the improved 3D-coverage of merged scan data may be negligible in very dense forest stands (Antonarakis, 2011) and in case of dense branching. Maas et al. (2008) observed an overall RMSE of 4.7 cm for a single tree profile, however with larger errors in the lower and upper

stem parts. The latter were attributed mainly to branching. For the same reason Bienert et al. (2007) were not able to retrieve reliable diameter measurements above a height of 7.8 m. Based on the comparison of 22 trees with harvester data they achieved reliable diameters with a standard deviation of 2.48 cm. We conclude that shadowing constitutes an inherent limitation for the use of TLS to derive stem form and volume for complete stems. However, the findings in this study show that both metrics can be extracted with good accuracy for stem parts which are not too heavily occluded by branches and leaves. Depending on tree species and their degree of branching this might coincide with the merchantable volume and therefore very well be of value in forest inventory.

5. Conclusions

Research in recent years has proven that terrestrial laser scanning (TLS) is a valuable tool to assess vegetation structure, in particular with regard to traditional forest inventory parameters (e.g. Maas et al., 2008; Litkey et al., 2008). However, while most studies focused on assessing the general potential of TLS for a successful retrieval of vegetation parameters, less attention was paid to assess the factors which influence the scan data and hence the parameter retrieval. The fact that potential influences are numerous and interconnected necessitates a more systematic approach to further research in this field, in particular if TLS is to be routinely used in forest inventory (cf. Thies and Spiecker, 2004). While the present study could show that scan mode has a considerable influence on the accuracy of an automated extraction of stem diameter, form, and volume from TLS data, a number of potential influences remain to be assessed, including scan resolution (point cloud density) and integration time. These will be addressed in a follow-up study. Also, for TLS to be routinely and effectively used in forest inventory, the sampling design (number and positioning of scans) has to be optimized with respect to the basic inventory parameters and with respect to the variability in stand structure. This may include the design of parameter-specific and data integration sampling schemes. The latter is required to deal with the limitations of TLS, most notably the uncertain tree height estimation (cf. Maas et al., 2008; Tansey et al., 2009), and to scale the sampling from the plot to stand scale. Another key issue for successfully integrating TLS in forest inventory is the automatization of the scan data processing (Thies and Spiecker, 2004). Despite the rapid development in computer hardware and scanner technology in recent years, the automated processing of TLS data is still a challenge, in particular with regard to the efficient storage and analysis of voluminous merged scan data, the filtering of noise and unwanted data, and methods to deal with partial and complete occlusion. It is to be expected that these issues will be resolved in due time. In the advent of multi-wavelength laser scanners, the potential of TLS to improve the assessment of vegetation structure is immense. In order to fully exploit this potential the scan data influences have to be properly dealt with in such a way as to lay a sound basis for an automated information extraction from TLS data.

References

Al-Sharadqah, A., Chernov, N., 2009. Error analysis for circle fitting algorithms. Electronic Journal of Statistics 3, 886–911.

Antonarakis, A.S., 2011. Evaluating forest biometrics obtained from ground lidar in complex riparian forests. Remote Sensing Letters 2 (1), 61–70.

Aschoff, T., Spiecker, H., 2004. Algorithms for the automatic detection of trees in laser scanner data. International Archives of Photogrammetry, Remote Sensing and Spatial Information Sciences 36 (Part 8/W2), 66–70.

Aschoff, T., Thies, M., Spiecker, H., 2004. Describing forest stands using terrestrial laser-scanning. International Archives of Photogrammetry, Remote Sensing and Spatial Information Sciences 35 (Part B), 237–241.

Bienert, A., Scheller, S., Keane, E., Mullooly, G., Mohan, F., 2006. Application of terrestrial laser scanners for the determination of forest inventory parameters. International Archives of Photogrammetry, Remote Sensing and Spatial Information Sciences 36 (Part 5), on CD-ROM.

Bienert, A., Scheller, S., Keane, E., Mohan, F., Nugent, C., 2007. Tree detection and diameter estimations by analysis of forest terrestrial laserscanner point clouds. International Archives of Photogrammetry, Remote Sensing and Spatial Information Sciences 36 (Part 3/W52), 50–55.

Brolly, G., Király, G., 2009. Algorithms for stem mapping by means of terrestrial laser scanning. Acta Silvatica & Lignaria Hungarica 5, 119–130.

Chernov, N., 2009. Circle fit (Pratt method), MATLAB CENTRAL. <http://www.mathworks.com/matlabcentral/fileexchange/22643-circle-fit-pratt-method> [accessed 26.07.12].

Chernov, N., 2009. Circle Fit (Taubin method), MATLAB CENTRAL. <http://www.mathworks.com/matlabcentral/fileexchange/22678> [accessed 26.07.12].

Clawges, R., Vierling, L., Calhoon, M., Toomey, M., 2007. Use of a ground-based scanning lidar for estimation of biophysical properties of western larch (*Larix occidentalis*). International Journal of Remote Sensing 28 (19), 4331–4344.

Danson, F.M., Hetherington, D., Morsdorf, F., Koetz, B., Allgower, B., 2007. Forest canopy gap fraction from terrestrial laser scanning. IEEE Geoscience and Remote Sensing Letters 4 (1), 157–160.

Eitel, J.U.H., Vierling, L.A., Long, D.S., 2010. Simultaneous measurements of plant structure and chlorophyll content in broadleaf saplings with a terrestrial laser scanner. Remote Sensing of Environment 114 (10), 2229–2237.

Forsman, P., Halme, A., 2005. 3-D mapping of natural environments with trees by means of mobile perception. IEEE Transactions on Robotics 21 (3), 482–490.

Gaffrey, D., Sloboda, B., Matsumura, N., 1998. Representation of tree stem taper curves and their dynamic, using a linear model and the centroaffine transformation. Journal of Forest Research 3 (2), 67–74.

Gander, W., Golub, G.H., Strebel, R., 1996. Least squares fitting of circles and ellipses. Bulletin of the Belgian Mathematical Society 3, 63–84.

Henning, J.G., Radtke, P.J., 2006. Ground-based laser imaging for assessing three-dimensional forest canopy structure. Photogrammetric Engineering & Remote Sensing 72 (12), 1349–1358.

Holopainen, M., Vastaranta, M., Kankare, V., Räty, M., Vaaja, M., Liang, X., Yu, X., Hyyppä, J., Hyyppä, H., Viitala, R., Kaasalainen, S., 2011. Biomass estimation of individual trees using stem and crown diameter TLS measurements. International Archives of Photogrammetry, Remote Sensing and Spatial Information Sciences 38 (Part 5/W12), on CD-ROM.

Hopkinson, C., Chasmer, L., Young-Pow, C., Treitz, P., 2004. Assessing forest metrics with a ground-based scanning lidar. Canadian Journal of Remote Sensing 34 (3), 573–583.

Jupp, D.L.B., Culvenor, D.S., Lovell, J.L., Newnham, G.J., Strahler, A.H., Woodcock, C.E., 2009. Estimating forest LAI profiles and structural parameters using a ground-based laser called Echidna®. Tree Physiology 29 (2), 171–181.

Kåsa, I., 1976. A curve fitting procedure and its error analysis. IEEE Transactions on Instrumentation and Measurement 25 (1), 8–14.

Lemen, J.R., 1991. Fit circle. Astronomy Department, University of Washington. <http://www.astro.washington.edu/docs/idl/cgi-bin/getpro/library32.html?FIT_CIRCLE> [accessed 26.07.12].

Liang, X., Litkey, P., Hyyppä, J., Kaartinen, H., Vastaranta, M., Holopainen, M., 2009. Automatic stem location mapping using TLS for plot-wise forest inventory. In: Proc. SilviLaser Conference, College Station, Texas, 14–16 October, pp. 314–323.

Litkey, P., Liang, X., Kaartinen, H., Hyyppä, J., Kukko, A., Holopainen, M., 2008. Single-scan TLS methods for forest parameter retrieval. In: Proc. SilviLaser Conference, Edinburgh, 17–19 September, pp. 295–304.

Lovell, J.L., Jupp, D.L.B., Newnham, G.J., Culvenor, D.S., 2011. Measuring tree stem diameters using intensity profiles from ground-based scanning lidar from a fixed viewpoint. ISPRS Journal of Photogrammetry and Remote Sensing 66 (1), 46–55.

Maas, H.G., Bienert, A., Scheller, S., Keane, E., 2008. Automatic forest inventory parameter determination from terrestrial laser scanner data. International Journal of Remote Sensing 29 (5), 1579–1593.

Pfeifer, N., Winterhalder, D., 2004. Modelling of tree cross sections from terrestrial laser scanning data with free-form curves. International Archives of Photogrammetry, Remote Sensing and Spatial Information Sciences 36 (Part 8/W2), 76–81.

Pratt, V., 1987. Direct least-squares fitting of algebraic surfaces. Computer Graphics 21 (4), 145–152.

Simonse, M., Aschoff, T., Spiecker, H., Thies, M., 2003. Automatic determination of forest inventory parameters using terrestrial laser scanning. ScandLaser Scientific Workshop on Airborne Laser Scanning of Forests, Umea, Sweden.

Strahler, A.H., Jupp, D.L.B., Woodcock, C.E., Schaaf, C.B., Yao, T., Zhao, F., Yang, X., Lovell, J., Culvenor, D., Newnham, G., Ni-Miester, W., Boykin-Morris, W., 2008. Retrieval of forest structural parameters using a ground-based lidar instrument (Echidna®). Canadian Journal of Remote Sensing 34 (S2), S426–S440.

Tansey, K., Selmes, N., Anstee, A., Tate, N.J., Denniss, A., 2009. Estimating tree and stand variables in a Corsican Pine woodland from terrestrial laser scanner data. International Journal of Remote Sensing 30 (19), 5195–5209.

Taubin, G., 1991. Estimation of planar curves, surfaces, and nonplanar space curves defined by implicit equations with applications to edge and range image segmentation. IEEE Transactions on Pattern Analysis and Machine Intelligence 13 (11), 1115–1138.

Thies, M., Spiecker, H., 2004. Evaluation and future prospects of terrestrial laserscanning for standardized forest inventories. International Archives of Photogrammetry, Remote Sensing and Spatial Information Sciences 36 (Part 8/W2), 192–197.

Umbach, D., Jones, N., 2003. A few methods for fitting circles to data. IEEE Transactions on Instrumentation and Measurement 52 (6), 1881–1885.

van Leeuwen, M., Coops, N.C., Newnham, G.J., Hilker, T., Culvenor, D.S., Wulder, M.A., 2011. Stem detection and measuring DBH using terrestrial laser scanning. In: Proc. SilviLaser Conference, Hobart, 16–20 October. 6 p. (on CD-ROM).

Watt, P.J., Donoghue, D.N.M., 2005. Measuring forest structure with terrestrial laser scanning. International Journal of Remote Sensing 26 (7), 1437–1446.

Yao, T., Yang, X., Zhao, F., Wang, Z., Zhang, Q., Jupp, D., Lovell, J., Culvenor, D., Newnham, G., Ni-Meister, W., Schaaf, C., Woodcock, C., Wang, J., Li, X., Strahler, A., 2011. Measuring forest structure and biomass in New England forest stands using Echidna ground-based lidar. Remote Sensing of Environment 115 (11), 2965–2974.
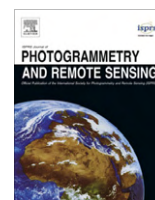
Chapter V: The influence of scanner parameters on the extraction of tree metrics from FARO Photon 120 terrestrial laser scans

Pyare Pueschel

Contents lists available at SciVerse ScienceDirect

ISPRS Journal of Photogrammetry and Remote Sensing

The influence of scanner parameters on the extraction of tree metrics from FARO Photon 120 terrestrial laser scans

Pyare Pueschel *

Department of Environmental Remote Sensing and Geoinformatics, University of Trier, D-54286 Trier, Germany

ARTICLE INFO

ABSTRACT

In the present study the influence of the scanner parameters, scan resolution (angular step size), scan speed (number of laser pulses per second), and pulse duration, on tree stem detection, stem diameter and volume extraction from phase-shift FARO Photon 120 TLS data was assessed. Additionally the effects of a data post processing (filtering of raw scan data) were investigated. All analyses were carried out based on single and merged scan data. It could be shown that scan speed, pulse duration and data filtering only marginally affect stem detection rates and stem diameter and volume estimation accuracies. By contrast scan resolution was found to have an effect, the magnitude of which, however, is range-dependent. For example mean stem detection rates for the three different scan resolutions tested were found to be equal in near range, but decreased more strongly for the lower scan resolutions in far range. With regard to the stem diameter extraction, scan resolution did not affect stem diameter at breast height (DBH) estimation accuracy, but limited the range within which DBH could be reliably extracted. The root mean squared error (RMSE) for DBH extracted from the single scan data was found to be significantly larger compared to the RMSE for DBH extracted from the merged scan data. Single scan data yielded stem volume estimates with lower accuracies, too. This study demonstrated that it is possible to maximize sampling efficiency by using scanner parameter sets with low scanning times (i.e., low scan resolution, high scan speed) without significantly losing estimation accuracy. If maximum accuracy is desired for both DBH and stem volume, the acquisition of multiple scans with a subsequent data merging is required.
© 2013 International Society for Photogrammetry and Remote Sensing, Inc. (ISPRS) Published by Elsevier B.V. All rights reserved.

1. Introduction

Terrestrial laser scanning (TLS) has become a valuable tool for assessing vegetation structure due to its capability to provide objective and consistent, though not necessarily unbiased, measurements. Additionally, TLS offers the benefit of extracting structural metrics which cannot be measured cost-efficiently by traditional methods such as caliper or tape. Examples are the stem form and merchantable volume which are both of particular interest in forest inventory (Holopainen et al., 2011). While a number of studies have shown that some of the basic inventory metrics can be extracted from TLS data with sufficient accuracy, e.g., tree location and stem density (e.g., Simonse et al., 2003; Aschoff and Spiecker, 2004; Hopkinson et al., 2004), diameter at breast height (e.g., Bienert et al., 2006; Maas et al., 2008), other important metrics such as tree height (e.g., Maas et al., 2008) or stem volume (e.g., Tansey et al., 2009) have so far not been retrieved with sufficient accuracy. This is mainly due to shadowing, i.e., the occlusion of

background objects by foreground objects, which currently constitutes one of the major obstacles to an effective and accurate extraction of structural tree metrics from TLS data. Shadowing depends on scan location and on factors which control the stand structure, e.g., stem density, stem size, (spatial) stem distribution, canopy layering, degree of undergrowth, and forest management practices. While statistical methods have been proposed to deal with partial occlusion of objects (Lovell et al., 2011), complete shadowing can only be dealt with by scanning objects from different locations. Even then a complete coverage may not be possible, in particular for complex structures such as forest canopies. The use of multiple (merged) TLS scans for improving the retrieval of structural metrics implies another important consideration in forest inventory: Sampling efficiency, i.e., minimizing costs while maximizing sampling and preserving parameter estimation accuracy. While TLS has proven to provide good estimation accuracy, its efficiency in terms of scan acquisition (scanner positioning, set-up and scan duration), in particular in case of scanning from multiple locations, has so far not been the focus of interest. Of the factors contributing to the scan acquisition efficiency, scan duration has the strongest influence. Scan duration is controlled by the basic scanner parameters, scan resolution (angular step

* Tel.: +49 651 2014593; fax: +49 651 201 3815.
E-mail address: p.pueschel@uni-trier.de

size), scan speed (number of laser pulses per second), pulse duration, and scan field-of-view. It has to be noted that these factors influence each other, hence they do not per se increase the scan duration. For example, scanning with a small field of-view and high scan resolution may yield a similar scan time compared to scanning with a large field-of-view and low scan resolution. Also, the ranging method (phase-shift vs. time-of-flight) has some effect, e.g., phase-shift scanners allow for higher scan speeds, but exhibit smaller effective scan ranges compared to time-of-flight scanners. Since it is desirable to increase the scan acquisition efficiency while preserving the estimation accuracy, the present study focused on assessing the influence of scan resolution, scan speed, and pulse duration (i.e., signal-to-noise ratio) on the accuracies of stem detection, stem diameter and volume extraction from phase-shift TLS data (a FARO Photon 120 was chosen as an exemplary phase-shift scanner in this study). Since phase-shift scanning of vegetation structure suffers from noise, particular consideration has to be given to the issue of noise removal. In this context, noise refers both to laser scan returns without physical meaning and to returns with physical meaning but which, depending on the purpose of the data analysis, represent unwanted data. The separation of unwanted from wanted data is considered to be one of the most important steps in successfully extracting structural metrics from TLS data, usually achieved by data filtering and/or robust data modeling (e.g., Aschoff et al., 2004; Maas et al., 2008; Litkey et al., 2008). The data filtering and robust modeling which were applied in this study are described in Section 2 along with the material of this study. Results are presented in Section 3 and discussed in detail in Section 4. Last but not least, conclusions are given (Section 5).

2. Materials and methods

2.1. Study area

The study area is located in the Pfälzerwald forest near Kaiserslautern, Germany, where a number of permanent forest monitoring plots lie in close vicinity, providing a large pool of in situ biophysical and structural measurements. The study was carried out at a pure Beech (Fagus sylvatica) stand (Fig. 1). The stand is characterized by a main storey of Beech trees around the age of 50 yrs and a second storey (understorey) of Beech trees, which may be younger than or the same age as the main storey trees (Werner, personal communication). Stem density is 1032 stems/ha, mean and standard deviation are 16.4 cm and 7.3 cm for diameter at breast height (DBH) and 18.5 m and 5.7 m for tree height. Stand area is roughly 0.5 ha, mean slope is 3.1°, and mean elevation is 522 m.

2.2. Data collection

During a field campaign in May 2012, three terrestrial laser scans were performed within the Beech stand. For these measurements a FARO Photon 120 phase-shift scanner was used (FARO, 2009b). The height above ground of the instruments beam emission point was 1.75 m and scans were performed with a field-of-view of 360° (Hz) by 310° (V). In order to assess the influence of the basic scanner parameters, scan resolution, scan speed, and pulse duration, scans were performed with different parameter sets at each of the three viewpoints (Fig. 1, Table 1). Since sampling efficiency (i.e., scan duration) is crucial in forest inventory, scanner parameters were chosen such as not to exceed a scan time of
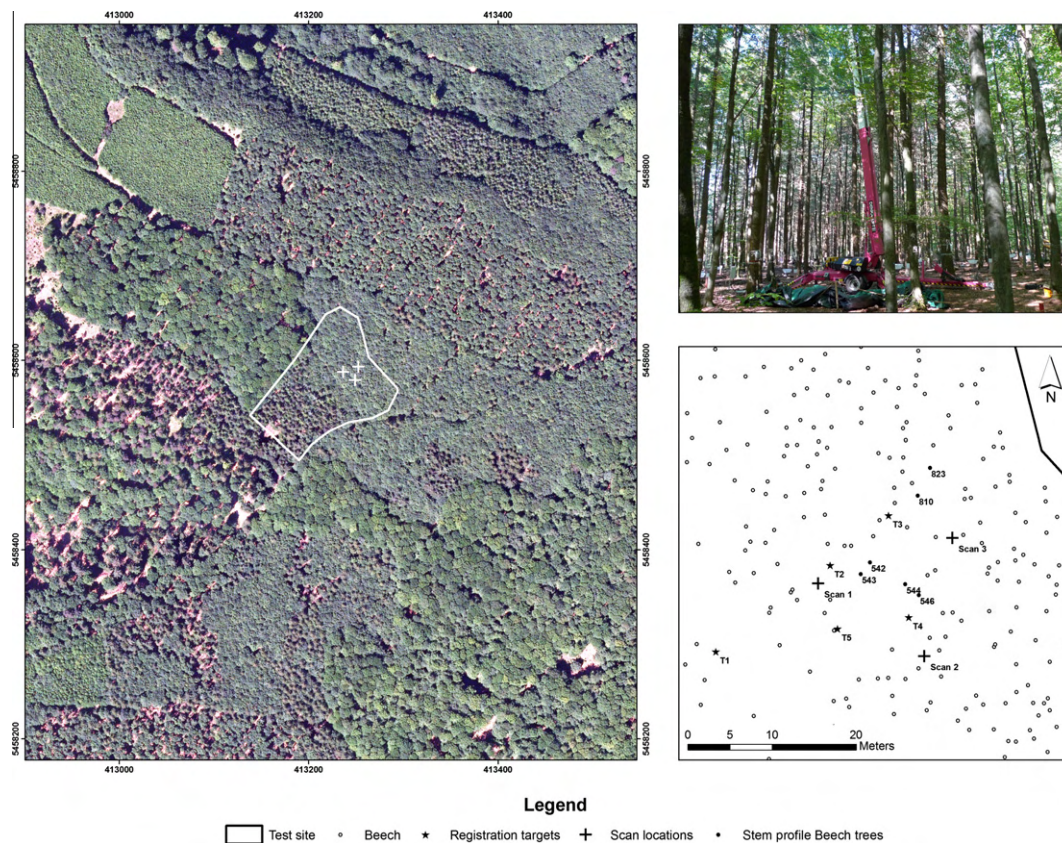

Fig. 1. Study area. Left: aerial imagery of the study area depicting the scan locations and the boundaries of the test site. Projected coordinate system: UTM. Upper right: image of the Beech stand at the test site. The mobile lift aiding the measurement of upper stem diameters is visible in the image center. Lower right: Experimental set-up of this study showing locations of scans, registration targets, and stem profile trees.

30 min. In order to register the single scans, resulting in merged scan data with a common coordinate system, registration reference targets were placed in positions visible from all three scan locations (Fig. 1). Targets included four spherical targets (FARO laser scanner reference sphere set) and one planar target (Table 2). Reference DBH measurements (measured with tape at 1.3 m height above ground) were recorded in April 2012 and tree locations were extracted from an existing database in order to validate the TLS derived stem locations. Additionally six stem diameter profiles with a step size of 20 cm and a maximum height of 10 m were recorded during the field campaign with the purpose of validating the TLS derived stem volume estimates. Profile diameters were measured with tape; upper stem parts could be accessed using a mobile lift (upper right picture in Fig. 1). However, due to the size of the lift the sampling of trees was restricted to trees along the track of the test site (lower right picture in Fig. 1). For the same reason (and due to heavy branching), stem parts could only be accessed up to a height of 10 m. The sampling area is also limited by the size of the available registration targets. This is because these targets have to be visually identified in the 2D-projected images of the scans for the registration process; depending on target size and scan resolution there is a maximum distance which can be set between target and scanner for the target to be still clearly identified in the image. According to FARO (2010), the maximum distance is 18 m when scanning with a resolution of ¼. Based on the scan resolutions tested in this study (Table 1), the scanner and target locations had to be subjectively chosen (Lower right picture in Fig. 1, Table 2). Due to these restrictions in the experimental set-up, the sampling of stem profile trees for the estimation of stem volume is not random; results reported in this study may therefore not necessarily be achieved by sampling schemes such as those traditionally applied in forest inventory. It has to be noted, though, that

Table 1
FARO Photon 120 scanner parameter sets applied in the present study (modified from Tables 1 and 2 in FARO (2009a). Noise compression reduces raw data noise by a factor of two. Resolution refers to ratios of the maximum angular resolution (40,000 3D points/360° = step size 0.009°). The vertical step size equals the horizontal step size. Additionally the FARO Photon 120 specific hardware filters, clear sky and clear contour, were set.

Resolution	Scan speed (kpt/s)	Repetition rate (Hz)	Pulse duration (ms)	Noise compression	Scan time (min)	Scan size (MB)
1/4	244	24	0.93	–	03:24	185
	122	12	1.87	–	06:49	183
	244	12	1.87	2×	13:39	670
	122	6	3.74	2×	27:18	662
1/8	244	49	0.47	–	00:51	56
	122	24	0.93	–	01:42	56
	244	24	0.93	2×	03:24	185
	122	12	1.87	2×	06:49	183
1/10	244	61	0.37	–	00:32	38
	122	31	0.75	–	01:05	38
	244	31	0.75	2×	02:11	121
	122	15	1.50	2×	04:22	120

Table 2
Reference targets used for the registration of the single scans.

Target			Distance (m) from scan location		
Nr.	Type	Size (m²)	Scan 1	Scan 2	Scan 3
T1	Plane	1	14.3	24.8	31.4
T2	Sphere	0.07	5.7	10.8	17.6
T3	Sphere	0.07		17.4	8.1
T4	Sphere	0.07	11.6	5.1	10.9
T5	Sphere	0.07	2.8	15.4	15.1

Table 3
Mean registration errors of the single scan registration fits. The different numbers of registration targets is due to the non-detection of these targets in the 2D-projected scan images as a result of the combined effects of scan resolution, target size and distance scanner-target.

Scan res.	Scan speed (kpt/s)	Noise comp.	Point distance[a] (mm)	Point drift[b] (mm)	Long. mismatch[c] (mm)	Orth. mismatch[d] (mm)	No. of targets
1/4	244	–	2.16	0.34	−0.50	1.67	6
	122	–	1.75	0.30	−0.50	1.27	6
	244	2×	1.61	0.15	0.15	1.17	6
	122	2×	1.53	0.23	0.28	1.00	6
1/8	244	–	0.83	0.10	−0.32	0.51	4
	122	–	0.26	0.03	−0.01	0.17	4
	244	2×	2.09	0.13	0.04	1.77	4
	122	2×	1.72	0.29	0.28	1.31	5
1/10	244	–	2.20	0.00	−0.05	2.16	3
	122	–	0.05	0.02	0.01	0.03	3
	244	2×	0.69	0.10	−0.03	0.38	4
	122	2×	1.62	0.16	0.15	1.22	4

[a] The standard deviation of the distance between the local reference points and their corresponding references.
[b] The mean value of the deviations between the local reference points and their corresponding references.
[c] The standard deviation of the longitudinal distance between the local reference points and their corresponding references. The longitudinal distance is the difference between the distance values to the scanner.
[d] The standard deviation of the orthogonal distance between the local reference points and the corresponding references (FARO, 2010).

the present study is intended not only to assess the effects of different scanner parameters, but also to identify potential limitations to the application of TLS for forest inventory, including the sampling design.

2.3. Data pre-processing

The individual scans were first registered manually to produce merged point clouds for each of the different scanner parameter sets applied in this study. Mean registration errors are listed in Table 3. In order to assess the effects of noise on the stem detection, stem diameter and volume extraction, scans were performed with different pulse durations which affect the signal-to-noise ratio (see noise compression in Table 1). In addition a post-filtering of the raw (single and merged) scan data was applied. For this purpose, the default FARO Scene 4.8 software filtering was used (FARO, 2010). This filtering comprises of a kernel-based stray point filtering and a reflectance filtering. For each scan point, the range differences between the neighboring scan points of the kernel and the scan point currently in the center of the kernel are checked. If a certain percentage of kernel scan points (specified by the allocation threshold) exhibit range differences below the range threshold, the central kernel scan point remains in the scan, otherwise it is removed (FARO, 2010). By contrast the reflectance threshold simply removes scan points with 11-bit scaled reflectance values below the default threshold of 300 (also scaled). Default parameter values for the stray point filtering are a square kernel of size 3 by 3 pixels, a range threshold of 2 cm, and an allocation threshold of 50% (i.e., half the number of kernel pixels minus the kernel center). The unfiltered and filtered (i.e., above-mentioned software filtering) single scan data was then converted from a Cartesian to a spherical coordinate representation, yielding 2D-projected raster images (Fig. 2), where the x- and y-axes represent the azimuth and zenith values (range determined by the user selected field-of-view). These raster images contain the x, y, z, range, intensity, azimuth and zenith information for each scan point (=raster pixel) as separate bands of the same image. The range band is required as input to the automated stem detection.

2.4. Stem detection

Automated tree stem detection is based on the approach by Pueschel et al. (2012) which utilizes range differences between neighboring pixels of a 2D-horizontal slice from the single scan range image to separate tree stems from other image components. To minimize occlusion of stems by branches and leaves the algorithm is iterated for multiple slices:

Scanner returns are assessed in multiple slices $L_i(\theta)$ each of zenithal thickness 0.36° and azimuthal coverage of 360°. Slices are separated by a vertical offset of 0.9°. Within each slice and for each vertical scan line $L_i(\varphi)$ at azimuth φ the range variance $\sigma_r^2(i, \varphi)$ is computed. If $\sigma_r^2(i, \varphi)$ falls below the range variance threshold $\tau_{\sigma2}$ then $L_i(\varphi)$ is considered to be a possible stem return. Consecutive (possible) stem returns with range differences below the range difference threshold τ_{diff} and which cover a minimum azimuthal span $\delta(\varphi)$; provide the primary evidence of a tree stem. The locations of stem centers as specified by their central azimuth detected in each slice $L_i(\theta)$ are then compared to determine if they correspond to a single tree stem or to different stems.

The parameter set used in the present study is: $\tau_{diff} = 10$ cm, $\tau_{\sigma2} = 0.0002$, $\delta(\varphi) = 0.18°$, $L_i(\theta) = 9$. τ_{diff} and $\tau_{\sigma2}$ were chosen based on a parameter sensitivity analysis. $\delta(\varphi)$ and $L_i(\theta)$ were chosen based on the results of a previous study (Pueschel et al., 2012). Slices $L_i(\theta)$ are centered at vertical heights $i = \{-3.6°, -2.7°, -1.8°, -0.9°, 0°, 0.9°, 1.8°, 2.7°, 3.6°\}$ with $i = 0°$ representing the scanner height (see horizontal line in Fig. 2). The azimuth span $\delta(\varphi) = 0.18°$ corresponds to theoretical stem diameters of 3.1 cm, 6.3 cm, and 9.2 cm for ranges of 10 m, 20 m, and 30 m respectively.

2.5. Stem diameter and volume extraction

Automated stem diameter extraction is based on the approach by Pueschel et al. (2012) which can be applied to rasterized single scan data as well as point clouds acquired by merged scans. Centered at the locations of stem centroids derived from the TLS-based stem detection (the centroids themselves are located at the stem fronts which face the scanner and do not correspond to stem centers), 3D-sets of potential stem points are extracted for each tree using a horizontal bounding box of size 60 cm by 60 cm. The main purpose of this step is to reduce the data volume; hence these dimensions were set arbitrarily. To avoid the omission of tree stem parts in case of leaning stems, the size of the bounding box may need to be increased (which was not the case in the present study). However, this affects only the processing time and not the process of extracting stem diameter itself. The height minimum of this set is then searched for which represents the ground level, provided that there is no occlusion. Since it has been found that the phase-shift FARO scans suffer from so-called ghost points below ground level which affect the determination of the exact ground level (Bienert et al., 2006; Maas et al., 2008), we implemented a histogram-based outlier detection and removal. The height maximum is implemented as a user-definable parameter (set to 10 m in this study) which is constrained by the height maximum found by the algorithm. Starting from the stem centroid, stem points which fall within the boundaries of a slice of 5 cm vertical thickness are extracted and circle fitting is applied. A geometric-based circle fit algorithm (Lemen, 1991) was used, which proved to be superior to two other algorithms tested in a previous study (Pueschel et al., 2012). Since the set of stem points also includes points which represent branches and leaves and which affect the circle fitting, an exclusion of these outliers is mandatory. We therefore implemented a range-based outlier test based on a fixed buffer added to the radius of the circle fitted for the previous slice (buffer = ¼ of the previous circle's radius). To prevent further errors in the circle fitting (e.g., fitting too large of a circle due to point clouds with circle arcs smaller than semi-circles) an upper stem diameter threshold is set (based on the stem size distribution at the test site, the threshold was set to 0.6 m). If this value is exceeded, the radius of the circle fitted for the previous slice is used instead. The basic steps of the algorithm are performed for all slices from the starting point to the local minimum and maximum. In case a tree stem splits up in two separate stems, the algorithm usually continues along the thicker stem. The algorithm produces stem diameter vertical profiles which are used to estimate DBH by applying a robust linear fit to the profile. Compared to extracting DBH directly at the nominal breast height, this method proved to be more stable against errors as a result of an uncertain ground level determination and of outliers (Pueschel et al., 2012). Based on the extracted diameter profiles, stem volume is calculated by approximating the stem point slices as conical frustums and summing up their volumes (Eq. (1)). Reference volumes were calculated equivalently for the in situ measured stem profiles. Due to heavy branching, stem diameter reference measurements could only be carried out

Fig. 2. Panoramic range image (2D-projection of single scan data). The yellow horizontal dash indicates the height above ground of the scanners' beam emission point. (For interpretation of the references to color in this figure legend, the reader is referred to the web version of this article.)

for stem heights up to 10 m, hence both the reference and TLS-extracted volume calculation were restricted accordingly (Section 2.2):

$$V_{stem} = \sum_{z=0}^{10m} t_{slice} \times \frac{\pi}{3} \times (r_1^2 + r_1 \times r_2 + r_2^2) \qquad (1)$$

with t_{slice} = slice thickness, r_1 and r_2 = top and base radii.

3. Results

3.1. Stem detection

Results for the automated stem detection show that stem detection is dependent on range, i.e., detection rates decrease with increasing distance from the scanner (Table 4, Fig. 3). The decrease results from the combined effects of an increasing shadowing and a systematic bias in the stem detection algorithm which omits trees with diameter spans smaller than 0.18° (cf. Section 2.4). While the effect of shadowing mainly depends on stem density, stem diameter distribution, and scanner location, the systematic bias solely depends on the stem diameter distribution within the effective scan range. Based on the spatial DBH distribution at the study site, 1%, 9%, and 18% of all trees within 10 m, 30 m, and 60 m range from the single scan locations are potentially omitted by the stem detection algorithm. If shadowing of these stems is accounted for (e.g., based on multiple scan locations combined with a spatial analysis of the distribution of stem sizes), the omission rates reduce to 1%, 3%, and 4%. Since the focus of our study was to assess the overall (i.e., effective) performance of the stem detection approach, detection rates reported are the results of the combined effects mentioned above. By contrast to the stem detection rates, false detection rates only slightly decrease with range (Fig. 3). False detection rates mainly depend on the degree of branching and distribution of leaves, the main source for errors, within the zenith range used for stem detection. Scan speed and pulse duration (i.e., noise compression), has a marginal effect on both stem detection and false detection rates (Fig. 3). The same applies to the effect of raw data filtering which yielded detection rates differing by a mean of 0.6% (standard deviation: 0.6%) and false detection rates differing by a mean of 0.2% (standard deviation: 0.8%). By contrast the scan resolution significantly affects the stem detection, the magnitude of which however is dependent on range (Fig. 3). This effect is easily explained if converting the scan resolution into point spacing: A scan resolution of 1/4 (10 kpt/360°) translates to

a point spacing of 0.6 cm, 1.9 cm, and 3.8 cm for ranges of 10 m, 30 m, and 60 m. These values increase to 1.3 cm, 3.8 cm, and 7.5 cm for a resolution of 1/8 (5 kpt/360°), respectively to 1.6 cm, 4.7 cm, and 9.4 cm for a resolution of 1/10 (4 kpt/360°). For ranges up to 10 m, scan resolutions 1/8 and 1/10 yield stem detection rates which only differ marginally from the scan resolution 1/4 (0.5% and 0.9%). For ranges up to 20 m, the differences increase to 6.4% and 10.3% and from 30 m on they reach near constant levels (mean differences 8.8% and 16.4%). The latter reflects the increasing shadowing of stems with increasing distance from the scanner which equally affects the different parameter sets applied in this study.

3.2. DBH extraction

3.2.1. Single scans

In order to test the influence of the scanner parameters on the stem diameter extraction, DBH was extracted from the single scans for each of the parameter sets. Analysis is based on the sum of all detected trees from all three single scans, yielding 387, 198, and 144 trees for the scan resolutions 1/4, 1/8, and 1/10. This constitutes a 49% difference between the resolutions 1/4 and 1/8, and a 63% difference between the resolutions 1/4 and 1/10 (percentages are the same for filtered and unfiltered data). These apparent disparities cannot be solely explained by the reduced stem detection rates of scan resolutions 1/8 and 1/10 which only account for mean differences of 8.8% and 16.4% (cf. Section 3.1). Rather they can be explained by the fact that not every tree detected by the algorithm provides stem point clouds with a sufficient representation of the stem form required for a successful modeling of stem diameters. This is mainly the result of shadowing. The scan resolutions 1/8 and 1/10 obviously yield a smaller number of such whole stem point clouds. This is also clearly range dependent (Fig. 4). While DBH was successfully extracted for ranges up to 45 m from the scans with 1/4 resolution, DBH could only be extracted for ranges up to 30 m for scans with resolution 1/8 and up to 25 m for scans with resolution 1/10. The reason might be that the corresponding scan point densities provide a coverage of the stem semi-circles (i.e., tree stems observed in single scan mode represent semi-circles when their scan points are projected on a horizontal plane) which is insufficient for a stable circle fitting, in particular considering that it is more likely to yield stem point clouds which represent circle arcs smaller than semi-circles with increasing range due to the shadow effect. The reduced scan point densities may also result in a circle fitting more prone to the influence of outliers

Table 4
Statistics for the stem detection based on rasterized single TLS scans. No. of reference and detected trees are mean numbers of the three single scan viewpoints. TLS-detected trees are based on the raw scan data (i.e., no software filtering applied).

| Scan res.	Scan speed (kpt/s)	Noise comp.	Mean no. of trees detected within range					
			10 m	20 m	30 m	40 m	50 m	60 m
1/4	244	–	27	93	150	171	178	179
	122	–	28	92	149	171	177	179
	244	2×	28	91	146	165	171	171
	122	2×	28	92	147	170	176	177
1/8	244	–	28	87	136	152	153	153
	122	–	27	88	137	150	153	153
	244	2×	28	84	129	144	147	147
	122	2×	28	84	130	144	146	146
1/10	244	–	28	84	124	133	135	135
	122	–	27	84	123	131	133	133
	244	2×	28	79	118	128	128	128
	122	2×	28	79	117	126	127	127
			Mean reference no. of trees within range					
			28	104	203	276	316	328
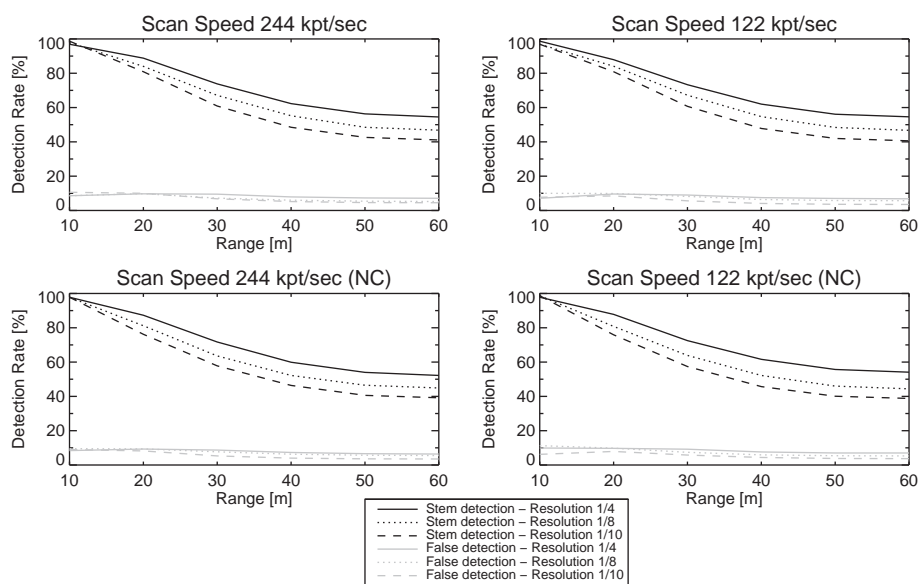
Fig. 3. Stem detection and false detection rates as a function of range, scan resolution, scan speed, and pulse duration (NC = noise compression according to Table 1). Analysis based on the raw scan data (i.e., no software filtering applied) of all three single scans.

(i.e., noise). While the scan resolutions applied in this study affected the range within which DBH could be successfully extracted, DBH estimation errors are neither dependent on scan resolution nor on range (Fig. 4). Similar to the stem detection, scan speed, noise compression, and data filtering do not influence the observed DBH extraction capabilities and the range function of estimation errors (Fig. 4). DBH estimation errors are also normally distributed irrespective of scan resolution, scan speed, noise compression, and data filtering (Fig. 5), however with slight variations in mean bias of the different scanner parameter sets (Table 5). The RMSE (root mean squared error) values resulting from the scans with noise compression are slightly higher than for the scans without noise compression both for the raw and to a lesser degree for the filtered scan data (Table 5). This effect, however, seems to diminish for scan resolution 1/10, as can be seen from the estimation error distribution (Fig. 5). Scans recorded with a measurement speed of 244 kpt/s yield RMSE's slightly higher than the scans with a speed of 122 kpt/s (Table 5), possibly due to the higher signal-to-noise ratio of the latter. This is supported by the fact that this observation does not apply to the noise-compressed scans. RMSE's based on the raw data are slightly higher than those based on the filtered data, and RMSE's tend to increase with decreasing scan resolution (Table 5). However, the estimation error distributions suggest that RMSE differences may be random rather than systematic, in particular considering that the RMSE is not a robust statistical measure. This leads to the conclusion that the DBH estimation accuracy is not significantly affected by scan resolution, scan speed, noise compression, and data filtering.

3.2.2. Merged scans

DBH was extracted from the merged scans for trees which yielded stem point clouds covering at least ¾ of the stems' circumference. This resulted in a total of 27 trees for the analysis. DBH estimation errors are range-independent, which based on the results from the single scans and the fact that the effective range for merged scans is smaller compared to single scans (approximately 20 m in our case) was to be expected. Another similarity between the two scan modes is that scans without noise compression yield smaller RMSE's compared to the scans with noise compression (Table 6). Overall, however, RMSE's do not seem to follow any systematic trend or to be a distinct function of the scan resolution, scan speed, and data filtering (Table 3). Also, there is no

apparent correlation between the mean errors of the single scan registration and the DBH estimation errors (Tables 3 and 6). As for the single scans, this leads to the conclusion that the scan resolution, scan speed, noise compression, and data filtering do not significantly influence the DBH estimation accuracy from merged scan data. However, they yield significantly lower RMSE's compared to the single scans, irrespective of the scanner parameters tested (Tables 5 and 6), which confirms the findings of a previous study (Pueschel et al., 2012). The improved DBH estimation accuracy is attributed to a more stable circle fitting as a result of an enhanced coverage of the tree stems' circumference.

3.3. Stem volume extraction

Stem volume was extracted for the four stem profile trees which lay within the triangle spanned by the three scan locations (Fig. 1). Stem volumes (for 0–10 m stem height) are 0.44 m^3, 0.36 m^3, 0.66 m^3, and 0.39 m^3 for trees with ID 542, 543, 544, and 546. These trees had to be chosen in close range to the scan locations due to restrictions in the experimental set-up (cf. Section 2.2). Results show that the TLS-derived stem volumes are independent of scan resolution, scan speed and pulse duration for the merged scan data (Fig. 6). By contrast single scan derived stem volumes can exhibit quite some variation from the reference volumes (e.g., Tree 544 in Fig. 6). Data filtering has only a marginal effect: Stem deviations from the reference volumes based on the raw and filtered data differ with a mean of 0.5% and a standard deviation of 4.4% for the single scans and with a mean of 0.7% and a standard deviation of 1.2% for the merged scans. These results reflect the findings of the DBH extraction, not only with regard to the influence of the scanner parameters, but also with regard to the superior performance of the tree metric extraction based on the merged scans. Stem volumes extracted from the merged scans deviate from the reference volumes by 1–9%, while mean stem volumes extracted from the single scans deviate by −1% to 35%. Additionally the single scan derived volumes exhibit a high variability as a result of scanner location and thus differing stem coverage (Fig. 6). This is in line with the observations by Bienert et al. (2007) and Litkey et al. (2008) that the coverage of stem cross-sections is crucial for a reliable and successful modeling of stem diameters. Since the extraction of stem volume is based on the modeling of stem diameters, model errors directly affect the
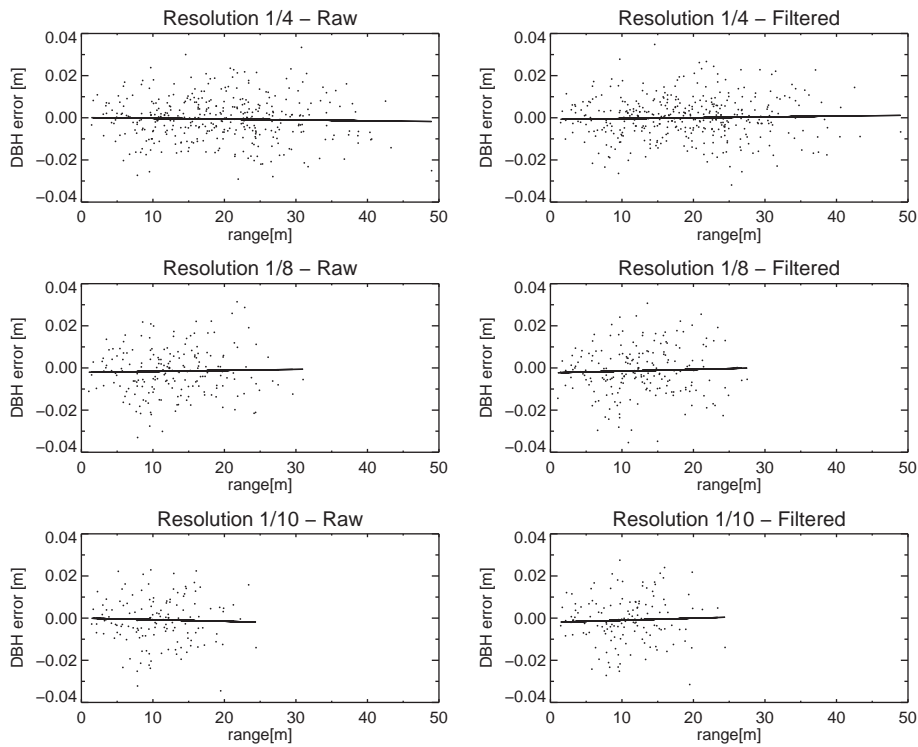
Fig. 4. DBH estimation errors as a function of range. Extracted DBH are based on all single scans performed with a scan speed of 244 kpt/s and without noise compression. Scans with a speed of 122 kpt/s and scans with noise compression yielded results which closely resemble the plots shown above. Solid lines represent the best fit of a simple linear regression.
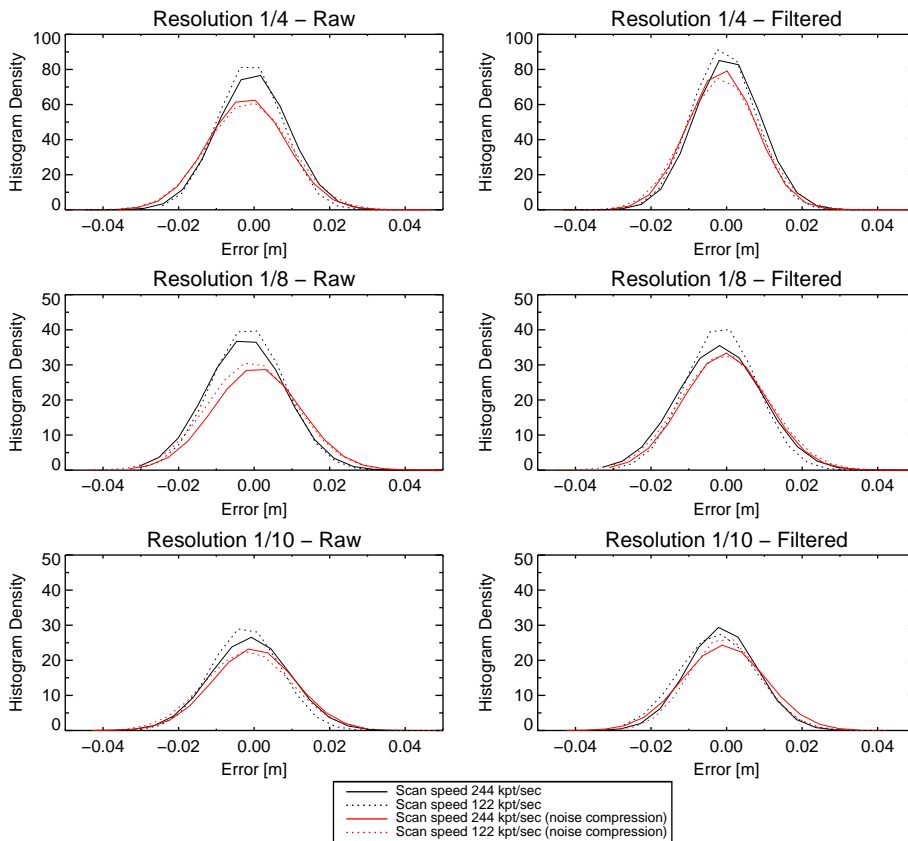

Fig. 5. Distribution of the DBH estimation errors as a function of scan resolution, scan speed, pulse duration (noise compression), and software filtering.

Table 5
Statistics for the DBH extracted from the single scans. Bias = Mean difference (Reference DBH – TLS derived DBH). NC = noise compression.

Scanner parameters			Raw scan data		Filtered scan data	
Resolution	Scan Speed	NC	Bias (cm)	RMSE (cm)	Bias (cm)	RMSE (cm)
1/4	244	–	−0.1	1.1	0.0	1.0
1/4	122	–	0.0	1.0	0.0	1.0
1/4	244	2×	−0.2	1.4	−0.1	1.2
1/4	122	2×	−0.2	1.3	−0.1	1.2
1/8	244	–	−0.2	1.2	−0.1	1.2
1/8	122	–	−0.1	1.1	−0.1	1.1
1/8	244	2×	0.1	1.7	0.0	1.3
1/8	122	2×	0.1	1.5	0.1	1.4
1/10	244	–	−0.1	1.4	−0.1	1.3
1/10	122	–	−0.2	1.2	−0.1	1.2
1/10	244	2×	−0.1	1.3	−0.1	1.3
1/10	122	2×	−0.0	1.5	0.0	1.3

Table 6
Statistics for the DBH extracted from the merged scans. Bias = Mean difference (Reference DBH – TLS derived DBH). NC = noise compression.

Scanner parameters			Raw scan data		Filtered scan data	
Resolution	Scan speed	NC	Bias (cm)	RMSE (cm)	Bias (cm)	RMSE (cm)
1/4	244	–	0.2	0.5	0.1	0.6
1/4	122	–	0.3	0.6	0.1	0.6
1/4	244	2×	0.0	0.8	0.0	0.7
1/4	122	2×	−0.1	0.8	−0.1	0.8
1/8	244	–	0.1	0.5	0.1	0.5
1/8	122	–	0.2	0.5	0.2	0.6
1/8	244	2×	0.0	0.8	0.0	0.9
1/8	122	2×	−0.2	0.7	0.0	0.7
1/10	244	–	0.0	0.6	0.0	0.6
1/10	122	–	0.2	0.8	0.2	0.9
1/10	244	2×	−0.1	0.8	0.0	0.9
1/10	122	2×	0.2	0.7	0.1	0.6

volume calculation. It is therefore important to quality-check TLS-derived volumes, e.g., by visual inspection of the stem diameter vertical profile, in particular as under- and overestimated diameters may cancel each other and result in pseudo-accurate measurements. Corroborating the findings of a previous study (Pueschel et al., 2012), the results also demonstrate that, depending on stem visibility, it is possible to achieve stem volume estimates from single scans with similar accuracy as those from the merged scans, provided trees are in close range to the scanner (in this study: max. 12 m). For trees observed further away from the scanner, the single scan based estimation may yield stem volumes with lower accuracy compared to the merged scans.

4. Discussion

The aims of this study were to assess the effects of the scanner parameters, scan resolution, scan speed and pulse duration (i.e., signal-to-noise ration), and a raw data filtering on stem detection, stem diameter and volume extraction from phase-shift TLS data. The scan resolution, scan speed, and pulse duration control the scan time, which is an important consideration for the application of TLS in forest inventory because of the demand to minimize costs while maximizing the sampling (cf. Lovell et al., 2011). Ideally increasing the efficiency should not decrease the parameter estimation accuracy. Since the use of TLS for deriving structural forest

metrics has the disadvantage of a time-consuming scanner set-up, in particular in case of multiple scan acquisition with the purpose of data merging, the reduction of scan time while preserving estimation accuracy is crucial. In the present study scanner parameters were chosen such as not to exceed a scan time of 30 min (Table 1). Besides the scan time another important consideration for the extraction of structural forest metrics from terrestrial laser scans is the specific scan file size (Table 1). The scan data which is usually saved in the scanner manufacturers' proprietary file format have to be exported to more accessible file formats for input into an automated data processing. This procedure roughly tripled the specific scan sizes in this study. In case of merging single scans, resulting scan sizes can easily exceed 5 GB. The feature extraction from such large point clouds can be quite tedious and time-consuming. Taking the requirement of forest inventory to maximize sample sizes into consideration, it is evident that the TLS data processing has to be automated, in particular for the merging (i.e., registration) of multiple single scans. It has to be noted though that the approach of using reference targets for the registration is quite time-consuming and tedious itself. Therefore new approaches to an effective and efficient scan registration are required. Since the raw scan data does not contain thematic information, the first step in such a processing need to be a scan point classification of sorts. A number of parametric and non-parametric methods have been proposed for this purpose (e.g., Liang et al., 2008; Park et al., 2010; Newnham et al., 2012). With regard to forest applications the major aim of these methods is the separation of vegetation from non-vegetation (ground, sky) scanner returns and the separation of woody from non-woody vegetations components. With regard to forest inventory, the identification of tree stems from the woody components forms the basis for any subsequent extraction of structural metrics from TLS data. An efficient and effective stem detection is therefore crucial. A number of different approaches have been proposed for stem detection (e.g., van Leeuwen and Nieuwenhuis, 2010). Most of the underlying studies focused on demonstrating the general applicability of the respective approaches, and paid less attention to assessing the influence of external factors such as scanner parameters or stem density. However, such an assessment is required both to warrant the robustness of the approach and to optimize the TLS scan data acquisition and processing for forest inventory.

In the present study, stem detection was achieved by applying the approach of Pueschel et al. (2012). Scan resolution was found to have a range-dependent effect on detection rates: For 10 m range the unfiltered single scan data with resolutions 1/4, 1/8, and 1/10 yielded same mean detection rates of 98%. For 30 m and 60 m range these dropped to 73%, 65%, 59%, and to 54%, 46%, 40% (in the order of decreasing resolution). The differences were attributed to an increase in the point density differences between the scan resolutions with increasing range (cf. Section 3.1). Scan speed, pulse duration (i.e., noise compression), and data filtering was found to have only a marginal effect on detection as well as false detection rates. By contrast to stem detection rates, false detection rates only slightly decrease with range: For 10 m range the scan resolutions yielded mean rates of 9%, 10%, and 8%. For 30 m and 60 m range these reduced to 9%, 8%, 6%, and to 7%, 5%, 4% respectively (again in the order of decreasing resolution). As for the stem detection rates, the differences between the scan resolutions are caused by increasing point density differences with range. Since clumped leaves are the main source of false detections, the observed rates could be reduced by scanning during the leaf-off phase. In case of coniferous trees, alternative checks for false detections, e.g., based on texture and/or simultaneously acquired color pictures, could be used. Pueschel et al. (2012) reported similar false detection rates for both Beech and Douglas fir, but rates may deviate for tree species with dense branching
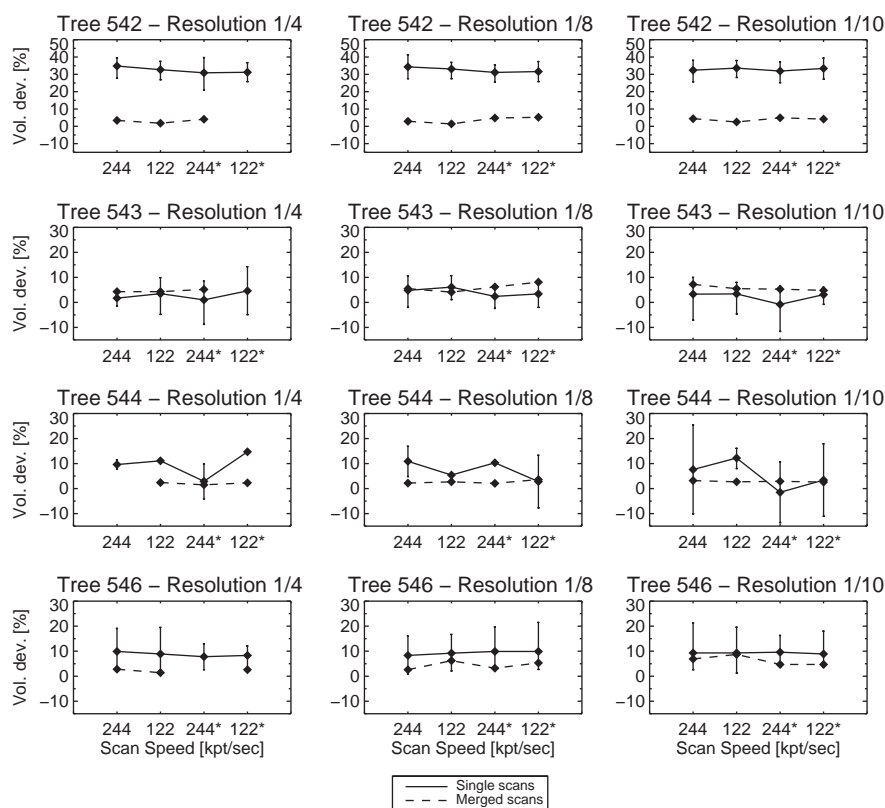
Fig. 6. Deviations from the reference stem volumes based on the volume extraction from the single and merged scan data. Error bars indicate min. and max. deviations of the single scan based volume estimates. The asterisk indicates scans with noise compression (Table 1). Analysis based on the raw scan data (i.e., no software filtering applied).

down to the lower stem parts. The strong decrease in stem detection rates with range resulted mainly from a combination of the effects stand density, scan geometry, shadowing, and systematic stem detection bias (cf. Section 3.1). Lovell et al. (2011) also observed a distinct range dependency of stem detection due to shadowing. Shadowing is caused by trees, in particular in close range, and constitutes a major and inherent drawback of using single scans for stem detection (e.g., Watt and Donoghue, 2005; Liang et al., 2009). The use of merged scans for stem detection has the advantage of a multi-angular coverage (Thies and Spiecker, 2004; Bienert et al., 2006), potentially increasing stem detection rates, but suffers from a much more time-consuming scanner set-up and data processing (i.e., positioning and registration of multiple scans) as well as from a smaller range which can be effectively used for stem detection. A hybrid single and merged scan based method might help to overcome this drawback, e.g., stem detection might be improved by assessing multiple stem detections in single scans based on a rough scan registration without the use of registration targets.

As far as the effects of scanner parameters on the DBH extracted from the single scans are concerned, it could be shown that the scanner parameter settings applied in this study did not significantly affect DBH estimation accuracies. Errors are normally distributed with slight variations in mean bias of the different scanner parameter sets. RMSE's range from 1 cm to 1.7 cm (raw scan data) and from 1 cm to 1.4 cm (filtered scan data). Estimation errors also proved to be independent on range. The most striking effect which could be observed is a reduced capability of the scans with resolutions 1/8 and 1/10 to model stem diameters with increasing range. This was attributed to the decreasing coverage of tree stems due to decreasing scan point densities resulting in an unstable circle fitting. DBH extracted from the merged scans

also proved to be independent of the scanner parameters applied in this study. Compared to the single scans, however, the enhanced coverage of stem cross-sections by merged scans resulted in a more stable and accurate circle fitting which yielded significantly lower RMSE's (ranging from 0.5 cm to 0.8 cm for the raw scan data and from 0.5 cm to 0.9 cm for the filtered scan data). This is in line with the observations by Bienert et al. (2007) and Litkey et al. (2008) that the coverage of stem cross-sections is crucial for a reliable and successful modeling of stem diameters. Another advantage of using merged scan data is that techniques can be applied which might be able to model tree stem forms more realistically, e.g., ellipse fitting (Aschoff and Spiecker, 2004) or B-splines (Pfeifer and Winterhalder, 2004). The influence of non-circularity on model fitting has been pointed out by a number of studies (e.g., Maas et al., 2008; Litkey et al., 2008; Brolly and Király, 2009).

Stem volumes extracted from the single and merged scans reflect the findings of the stem diameter extraction, i.e., the improved estimation accuracy for the merged scans, which is a logical consequence as stem volume is calculated based on the extracted stem diameter profile (cf. Section 2.5). This means that errors in the stem diameter modeling directly affect the volume determination. Negative and positive errors (under- and overestimation of diameter) may even cancel each other yielding pseudo-accurate volumes. It is therefore important to carefully check the derived volumes. Stem volumes deviations from the reference volumes range from −1% to 35% for the single scans and from 1% to 9% for the merged scans. While for trees with unobstructed view to the scanner stem volumes could be extracted from the single scans with similar accuracy compared to the merged scans, stem volumes of trees with partial occlusion vary strongly for the single scans, due to different stem coverage from the single scan locations. These results suggest that shadowing and therefore scan location are critical is-

sues for the extraction of stem volume from TLS data. By contrast the scanner parameters (scan resolution, scan speed, and pulse duration) were found to have only a marginal influence. However, it has to be noted that the sampling of trees for the stem volume analysis had to be restricted to the near range ($\sim$12 m); drawn conclusions are therefore only valid for these ranges. The reason for this restriction is that the reference targets used for the single scan registration had to be placed within a maximum range from all three scan locations, otherwise the low scan resolutions applied in this study would have caused these targets to be unrecognizable in the panoramic scan images (cf. Section 2.2). This aspect of the reference target based scan registration is a major drawback to the stem diameter and volume estimation from merged scans with low scan resolutions. A solution might be to increase the size of the reference targets, however at the expense of manageability. An alternative might be to develop scan registration approaches which do not require external reference targets.

5. Conclusion

Terrestrial laser scanning offers a number of advantages over traditional, manual measurements in forest inventory. Besides being objective and reproducible, TLS allows access to the measurement of forest metrics, e.g., stem volume, which are not feasible with traditional methods. While the general potential to retrieve forest metrics with high accuracy has been demonstrated, the effects of different scanner parameters on the estimation accuracy and sampling efficiency has received relatively little attention. Both are important considerations if TLS is to be routinely applied in forest inventory. For this reason the present study focused on assessing the effects of scanner parameters and data filtering on stem detection, stem diameter and volume extraction from phase-shift TLS data. Scanner parameter sets were chosen such as not to exceed a scan time of 30 min. This study could demonstrate that scan speed, pulse duration (i.e., noise compression), and data filtering only have a marginal influence on stem detection rates as well as on DBH and stem volume accuracies, which means that scans can be acquired with low scan quality and corresponding short scan times without significantly losing parameter estimation accuracy. For example based on a scan resolution of 1/4, choosing the lower scan quality setting, the scan time can be reduced from 27 min to 3½ min. A further reduction in scan time can be achieved by decreasing the scan resolution. While the scan resolutions tested in this study did not affect the DBH and stem volume estimation accuracies, they affected stem detection rates and more importantly the range within which stem diameter could be reliably extracted. For ranges up to 25–30 m scan resolutions 1/8 and 1/10 proved to be sufficient which would further reduce scan times from 3½ min to 1 min, respectively ½ min. For greater ranges a scan resolution of at least 1/4 is required. With regard to the scan mode, the results confirmed the findings of a previous study (Pueschel et al., 2012) that using merged instead of single scans significantly improves the DBH and stem volume estimation accuracies. However, depending on stem density the acquisition of multiple scans with the purpose of data merging is much more time-consuming compared to the single scan acquisition, mainly due to positioning scanner and reference targets with unobstructed line-of-sights to each other. Consequently the scan mode can be considered the bottleneck to increasing the sampling efficiency. While the lower estimation accuracy based on the single scans may be acceptable in case of DBH, the present study demonstrated that the variability in the stem volumes extracted from the single scans is too large for reliably estimating stem volume. Since the biggest potential of TLS for forest inventory lies exactly in retrieving forest metrics such as stem volume, the sampling design of a TLS-based

inventory has to be optimized to warrant sampling efficiency, i.e., the variability in stand structure has to be taken into account.

References

Aschoff, T., Spiecker, H., 2004. Algorithms for the automatic detection of trees in laser scanner data. International Archives of Photogrammetry, Remote Sensing and Spatial Information Sciences 36 (Part 8/W2), 66–70.

Aschoff, T., Thies, M., Spiecker, H., 2004. Describing forest stands using terrestrial laser-scanning. International Archives of Photogrammetry, Remote Sensing and Spatial Information Sciences 35 (Part B), 237–241.

Bienert, A., Scheller, S., Keane, E., Mohan, F., Nugent, C., 2007. Tree detection and diameter estimations by analysis of forest terrestrial laserscanner point clouds. International Archives of Photogrammetry, Remote Sensing and Spatial Information Sciences 36 (Part 3/W52), 50–55.

Bienert, A., Scheller, S., Keane, E., Mullooly, G., Mohan, F., 2006. Application of terrestrial laser scanners for the determination of forest inventory parameters. International Archives of Photogrammetry, Remote Sensing and Spatial Information Sciences 36 (Part 5) (on CD-ROM).

Brolly, G., Király, G., 2009. Algorithms for stem mapping by means of terrestrial laser scanning. Acta Silvatica and Lignaria Hungarica 5, 119–130.

FARO, 2010. FARO Laser Scanner Software SCENE Version 4.8 – User Manual.

FARO, 2009a. Laser Scanner Photon – User's Manual (Revised version: July 23, 2009).

FARO, 2009b. Laser Scanner Photon 120/20 – Specifications Sheet, <http://www.faro.com/adobe_pdf_mgr.aspx?item=969&pdfTitle=FARO_Photon_en_pdf> (accessed 12.12.12.).

Holopainen, M., Vastaranta, M., Kankare, V., Räty, M., Vaaja, M., Liang, X., Yu, X., Hyyppä, J., Hyyppä, H., Viitala, R., Kaasalainen, S., 2011. Biomass estimation of individual trees using stem and crown diameter TLS measurements. International Archives of Photogrammetry, Remote Sensing and Spatial Information Sciences 38 (Part 5/W12) (on CD-ROM).

Hopkinson, C., Chasmer, L., Young-Pow, C., Treitz, P., 2004. Assessing forest metrics with a ground-based scanning lidar. Canadian Journal of Remote Sensing 34 (3), 573–583.

Lemen, J.R., 1991. Fit circle. Astronomy Department, University of Washington, <http://www.astro.washington.edu/docs/idl/cgi-bin/getpro/library32.html?FIT_CIRCLE> (accessed 26.07.12.).

Liang, X., Litkey, P., Hyyppä, J., Kaartinen, H., Vastaranta, M., Holopainen, M., 2009. Automatic stem location mapping using TLS for plot-wise forest inventory. In: Proc. SilviLaser Conference, College Station, Texas, 14–16 October, pp. 314–323.

Liang, X., Litkey, P., Hyyppa, J., Kukko, A., Kaartinen, H., Holopainen, M., 2008. Plot-level trunk detection and reconstruction using one-scan-mode terrestrial laser scanning data. In: Proc. International Workshop on Earth Observation and Remote Sensing Applications, Beijing, June 30–July 2, pp. 136–140.

Litkey, P., Liang, X., Kaartinen, H., Hyyppä, J., Kukko, A., Holopainen, M., 2008. Single-scan TLS methods for forest parameter retrieval. In: Proc. SilviLaser Conference, Edinburgh, 17–19 September, pp. 295–304.

Lovell, J.L., Jupp, D.L.B., Newnham, G.J., Culvenor, D.S., 2011. Measuring tree stem diameters using intensity profiles from ground-based scanning lidar from a fixed viewpoint. ISPRS Journal of Photogrammetry and Remote Sensing 66 (1), 46–55.

Maas, H.G., Bienert, A., Scheller, S., Keane, E., 2008. Automatic forest inventory parameter determination from terrestrial laser scanner data. International Journal of Remote Sensing 29 (5), 1579–1593.

Newnham, G., Mashford, J., Pueschel, P., Armston, J., Culvenor, D., Siggins, A., Nyström, M., Goodwin, N., Muir, J., 2012. Non-parametric point classification for phase-shift laser scanning. In: Proc. SilviLaser Conference, Vancouver, 16–19 September, 7p. (on CD-ROM).

Park, H., Lim, S., Trinder, J., Turner, R., 2010. 3D Surface Reconstruction of Terrestrial Laser Scanner Data for Forestry. In: Proc. IEEE International Geoscience and Remote Sensing Symposium, Honolulu, 25–30 July, pp. 4366–4369.

Pfeifer, N., Winterhalder, D., 2004. Modelling of tree cross sections from terrestrial laser scanning data with free-form curves. International Archives of Photogrammetry, Remote Sensing and Spatial Information Sciences 36 (Part 8/W2), 76–81.

Pueschel, P., Newnham, G., Rock, G., Udelhoven, T., Werner, W., Hill, J., 2012. The influence of scan mode and circle fit algorithms on the extraction of stem diameter and volume from TLS data. In: Proc. SilviLaser Conference, Vancouver, 16–19 September, 9p. (on CD-ROM).

Simonse, M., Aschoff, T., Spiecker, H., Thies, M., 2003. Automatic determination of forest inventory parameters using terrestrial laserscanning. In: Proc. ScandLaser Scientific Workshop on Airborne Laser Scanning of Forests, Umeå, 3–4 September, pp. 251–257.

Tansey, K., Selmes, N., Anstee, A., Tate, N.J., Denniss, A., 2009. Estimating tree and stand variables in a Corsican Pine woodland from terrestrial laser scanner data. International Journal of Remote Sensing 30 (19), 5195–5209.

Thies, M., Spiecker, H., 2004. Evaluation and future prospects of terrestrial laserscanning for standardized forest inventories. International Archives of Photogrammetry, Remote Sensing and Spatial Information Sciences 36 (Part 8/W2), 192–197.

van Leeuwen, M., Nieuwenhuis, M., 2010. Retrieval of forest structural parameters using LIDAR remote sensing. European Journal of Forest Research 129, 749–770.

Watt, P.J., Donoghue, D.N.M., 2005. Measuring forest structure with terrestrial laser scanning. International Journal of Remote Sensing 26 (7), 1437–1446.

Chapter VI: Calibration of a forest growth model based on ground-based remote sensing measurements and long-term growth data

Not submitted for publication

Pyare Pueschel

1   Introduction

1.1   Forest growth modelling

The prediction of forest development and growth in particular has a long history in forestry dating back to the 19th century (Pretzsch, 2009). While early attempts at growth prediction were focused primarily on establishing empirical relationships between total volume yield and stand height-age development, forming the basis for the so-called yield tables, forest growth research has rapidly developed over the past few decades to include complex matter balance models. They simulate the physiological processes of growth and the underlying cause-effect relationships with environmental factors and are therefore also referred to as mechanistic or process-based eco-physiological growth models. Lately, a third class of growth models has received increased attention (Mäkelä et al., 2000); so-called hybrid models that incorporate both empirical and mechanistic relationships of forest growth. In addition to this broad model type classification, growth models can be classified according to the temporal and spatial resolution of the modelled processes, ranging from seconds to centuries, and from the individual tree to landscape level (Pretzsch, 2009). The most common spatial scales of the eco-physiological models are the individual tree-based and the stand-based scales. Both can be spatially explicit or position-independent, i.e. trees and stands are described by statistical averages and/or statistical distributions of structural parameters without explicitly accounting for their spatial distribution.

While eco-physiological models have become important tools for research and decision support in forest management, the importance of long-term forest growth monitoring has not diminished; due to the valuable information that this data provides about the fundamental interactions between forest structure, growth and yield, and environmental factors. Long-term growth data is also crucial for the calibration and validation of growth models. However, the availability of such reference data is limited and sites are often assumed to be representative for broad regions. As a consequence, this data cannot reflect small scale growth variability. Artificial time series of forest growth are therefore often used instead. These are based on the inventory of forest stands with similar site growing conditions and representing different stand development phases. Alternatively, inventory data collected from sites encompassing the full range of site growing conditions observed within a certain spatial extent (e.g. a

region) can provide lower and upper growth limits. These are especially useful for model calibration and validation (Pretzsch, 2009).

Remote sensing, airborne and satellite remote sensing in particular, has received an increased attention for assessing forest structure and growth on a large scale since traditional forest inventory is laborious, time-consuming and spatially limited. By comparison, the potential of ground-based remote sensing to evaluate forest growth has not been investigated so far. The present study is therefore intended to investigate the use of ground-based remote sensing by comparing model simulations calibrated with (a) long-term growth data, (b) artificial time series constructed from traditional forest inventory, and (c) artificial time series constructed from ground-based remote sensing measurements. The growth model 3-PG (Landsberg and Waring, 1997) is used for this purpose because of its flexible spatial scale and the possibility to incorporate remote sensing data.

1.2   The growth model 3-PG

3-PG (acronym stands for Physiological Processes Predicting Growth) can be applied both on a point-based scale (3-PG) and on a spatial scale (3-PG-Spatial). The spatial version can also be used in combination with remote sensing data (Coops et al., 1998). 3-PG is based on modelling the physiological processes of tree growth. As it includes empirical relationships to infer some of its model parameters it can be considered a hybrid model. It is also generic, i.e. 3-PG can be applied to various tree species provided that it is parameterized for these tree species. 3-PG assumes forest stands to be homogeneous with regard to tree species and age (Sands, 2004).

3-PG is built on five core modules: Biomass production, biomass partitioning, soil water balance, stocking and tree mortality, and stand inventory data (Landsberg & Sands, 2011). The model is driven by monthly meteorological observations of precipitation, temperature, frost days, and solar insolation. In addition to being tree species-specific, 3-PG is also site-specific. The required site data is site latitude, initial stocking, soil class, maximum plant-available soil water, site fertility, and initial values for the three biomass pools foliage, stem and roots. Based on its climatic and site input 3-PG calculates monthly values of gross and net primary productivity (GPP/NPP).

A key property of 3-PG is that it accounts for environmental factors that affect tree growth. The simulated NPP is partitioned into the three biomass pools according to specific allocation rules. The monthly increment in growth is linked to the volume growth and the stem mortality modules, and allows the calculation of common forest inventory parameters such as stocking, basal area, and diameter at breast height (DBH). In the following, the five modules of 3-PG and their main processes are shortly described. As a detailed description of 3-PG is beyond the scope of this study, the reader is referred to the publications of Landsberg and Waring (1997), and Landsberg and Sands (2011).

1.2.1 Soil water balance

The module water balance is based on a simple one-layered soil water model, i.e. the soil is assumed to be made up of one single homogenous layer. The soil water input is calculated from the precipitation reduced by interception and evapotranspiration. Potential irrigation can also be accounted for. The soil water pool is filled up by the input water up to a defined maximum water storage capacity. If this threshold is exceeded, the excessive input water is drained out of the system. Interception is modelled as a tree species-specific maximum loss rate that is regulated by LAI. Evapotranspiration is modelled by using a modified version of the Penman-Monteith equation, which takes into account environmental constraints (e.g. soil water stress, vapour pressure deficit) on canopy conductance. This bulk canopy conductance is calculated by reducing a species-specific maximum canopy conductance using the more limiting factor and using the proportion of simulated to maximum LAI. The maximum LAI is assumed to correspond to the maximum canopy conductance.

1.2.2 Biomass production

The biomass production is the core module of 3-PG and is based on the light use efficiency concept, i.e. primary productivity is proportional to the intercepted solar radiation with the light use efficiency ($g_{DryMatter}$ MJ^{-1}) as the slope of this linear relationship. The potential of plants to convert absorbed photosynthetically active solar radiation (APAR) into biomass is also commonly expressed by the term quantum efficiency (mol_{DM} mol^{-1}). Photosynthetically active radiation (PAR) is inferred from the model input of solar radiation by using a constant factor of 2.3 mol MJ^{-1}. The fraction of PAR that is absorbed (fAPAR) is calculated based on a modified Lambert-Beer law modelling light interception within the canopy as an exponential

function of LAI, a light extinction coefficient, and fractional canopy cover. LAI is calculated from the simulated foliage biomass and a species-specific leaf area (SLA).

One of the key properties of 3-PG is explicitly accounting for the effects of environmental factors on growth. In 3-PG these factors include temperature, water vapour pressure deficit, soil water, soil salinity, frost, site fertility, stand age, and atmospheric CO_2. These factors or modifiers are implemented in the model as dose-effect curves normalized between 0 (maximum constraining effects) and 1 (no constraints). For a detailed description see Landsberg and Waring (1997), and Landsberg and Sands (2011). The combined effect of modifiers on the canopy quantum efficiency is modelled as multiplicative with the exception of soil water and water vapour pressure deficit where only the more limiting factor of the two is included. GPP is calculated from APAR and the modified (i.e. reduced) canopy quantum efficiency. NPP is calculated from GPP assuming a constant respiration factor of 0.47.

1.2.3   Biomass partitioning

The simulated NPP is partitioned into the above-ground biomass pools, stem and foliage, and the below-ground root biomass pool according to user-defined allocation ratios. These ratios sum to one and are implemented based on linking root allocation primarily to available soil water and site fertility (within the range given by user-defined minimum and maximum root allocation ratios). The rationale is that trees react to environmental constraints by investing in growth such as to counteract these constraints, e.g. if soil water is the limiting factor, root growth is boosted to increase the trees' rooting zone and hence the potential uptake of water. The above-ground allocation ratio is derived from 1 minus the below-ground allocation ratio.

As the allocation into the above-ground biomass pools depends on tree development, the above-ground allocation is modelled as a function of stem diameter, i.e. it is expressed as the ratio of the foliage allocation ratio and the stem allocation ratio, arbitrarily specified for DBH 2 cm and 20 cm. DBH itself is derived from an allometric relationship with tree stem biomass. The monthly increments in growth of the three biomass pools are calculated from multiplying NPP with the allocation ratios minus a monthly loss rate (e.g. litterfall, root turnover) and minus the fractions lost from the biomass pools in case of tree mortality.

1.2.4   Stocking and tree mortality

Stocking is determined from the modelled stand development by explicitly accounting for tree mortality, either as the result of stress-related events (e.g. windbreak, insect calamity) or as the result of within-stand resource competition (i.e. self-thinning). In both cases the fractions lost from the biomass pools per dead tree needs to be specified. These fractions are assumed equal for both types of stem mortality. Self-thinning is implemented as a continuous process (i.e. mathematically expressed as a negative exponential function) during stand development using a species-specific maximum stand basal area.

1.2.5   Stand inventory data

3-PG provides the calculation of common forest inventory parameters including DBH, basal area, stem and stand volume, and volume increment. DBH is derived from an allometric relationship to stem mass. Basal area is calculated from stocking and DBH. Stem volume is modelled primarily using a wood density and a branch and bark ratio, which are both species-specific. Alternatively, stem volume can be calculated using an allometric relationship with DBH. Likewise mean stand height can be calculated. As the key model parameter DBH is itself derived from an allometric relationship and tree allometry is generally species- and site-specific, hence of limited spatial transferability, choosing an appropriate allometric equation is crucial for the calibration and application of 3-PG.

2 Materials and methods

2.1 Study area

The study area was the *Hoch- und Idarwald* forest, which is part of the *Hunsrück*, a low mountain range located south-west of the German Federal State of Rhineland-Palatinate. Predominant tree species in the *Hoch- und Idarwald* are Beech (*Fagus sylvatica*) and Norway spruce (*Picea Abies*). Large areas of the *Hoch- und Idarwald* forest will be converted into a national park, therefore, assessing the transition from managed to natural forest will be of particular interest to forest monitoring and growth modelling.
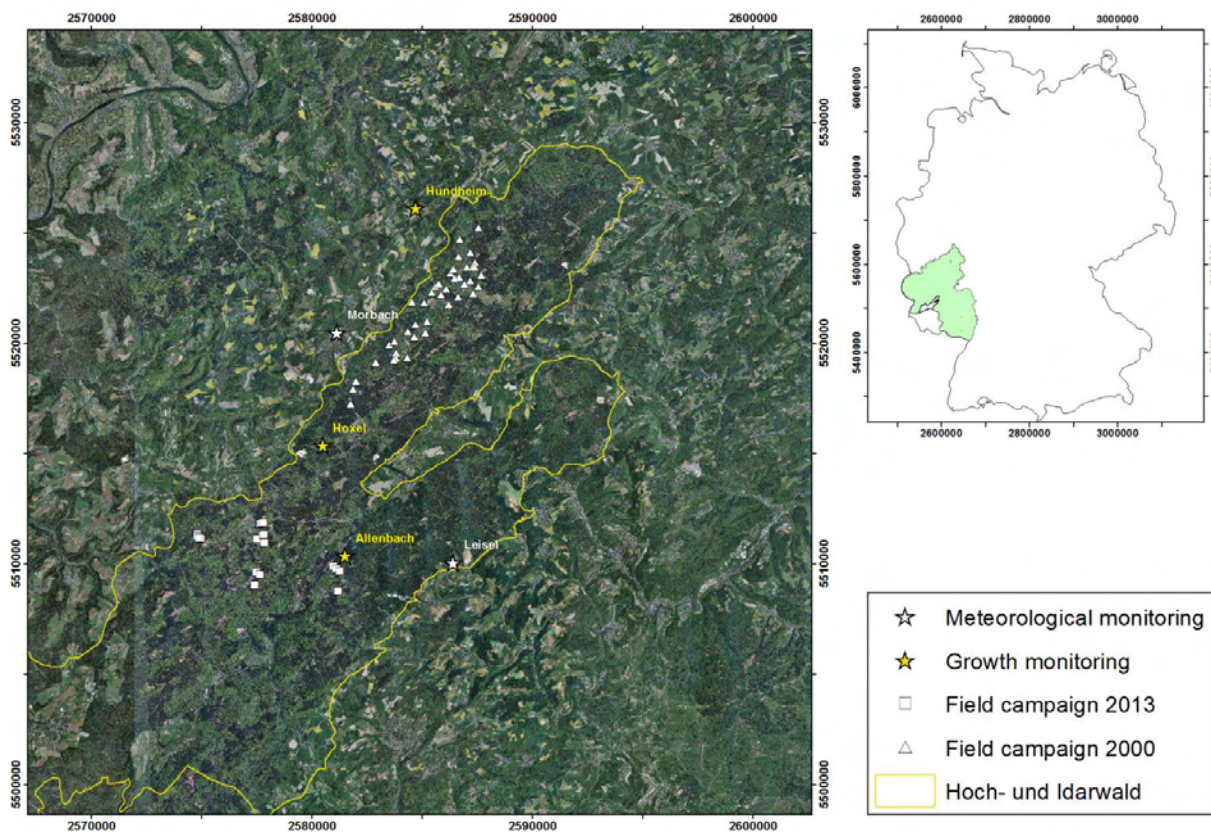

Figure 1: Study area *Hoch- und Idarwald* forest. Test plot locations of the field campaigns 2000 and 2013 and locations of the monitoring sites within the study area are shown in the large map. The location of the study area within the German federal state of Rhineland-Palatinate is shown in the small map. Projection coordinate system: Universal Transverse Mercator (UTM) based on WGS-84.

The main data collection was carried out at 21 Norway spruce test plots within the study area during a field campaign in August 2013. In addition, LAI data of an earlier field campaign within the area (Schlerf et al., 2004) was included in this study. Long-term forest growth data was available for two monitoring sites located within the *Hoch- und Idarwald* and for one

monitoring site located on the western border of the study area. Long-term meteorological observations were available from two weather stations (see Figure 1 for a detailed map of the study area).

2.2   Data collection and processing

2.2.1   Ground-based reference data

During the campaign in August 2013 test plots were established at pure Norway spruce stands of various stand ages and densities (Table 1). The stands were chosen to cover the forest stand development phases qualification (thickets), dimensioning (crop tree definition and selective thinning), and maturing (timber stage).

Table 1: Description of the Norway spruce test plots sampled in this study. Phase refers to the development phases qualification (Qua.), dimensioning (Dim.), and maturing (Mat.).

ID	X	Y	Phase	Stand age	Stand density	DBH mean	DBH std.	Height mean	Height std.
	UTM	UTM		yrs	trees/ha	[cm]	[cm]	[m]	[m]
4	364659.5	5509208.6	Mat.	65	962	28.4	9.6	21.3	5.4
15a	361192.8	5509133.9	Mat.	110	311	59.6	7.1	41.6	4.7
15b	361154.5	5509102.7	Mat.	110	269	63.2	8.5	39.6	9
16	361040.8	5508522.7	Dim.	65	523	35.4	5.9	23.8	2.4
20	364787.5	5509106.4	Mat.	65	665	34.2	8.9	23.7	5.2
21	364941.3	5508997.9	Mat.	65	764	29.1	6.6	21.6	3.8
32	361428.9	5509171.3	Dim.	65	580	34.8	5	31.4	5.1
67	361571.8	5510387.9	Dim.	65	509	29.2	6.9	21.3	3.2
68	361496.6	5510520.0	Dim.	65	477	32.5	9.6	23	5.8
69	361302.6	5510520.0	Dim.	48	1878	20.8	8.6	18.3	3.1
70	361241.5	5510610.0	Qua.	48	1655	20.6	7.4	19.2	1.7
79	361516.7	5510739.8	Dim.	67	509	39.4	4.9	27.2	1.8
80	361573.9	5510778.4	Dim.	67	509	37.6	5	26.3	1.6
107	364823.5	5508094.3	Qua.	35	1966	19.6	5.7	15.4	2.3
112	358553.5	5510947.7	Mat.	78	668	38.8	7.9	27.1	3.1
114	358538.9	5510830.2	Mat.	89	700	40.9	7.6	27.8	2.4
115	358612.7	5510757.1	Dim.	49	828	22.8	7.1	19.3	4.4
116	358690.6	5510728.3	Dim.	51	859	20	5.6	17.4	2.5
518	361561.9	5511323.8	Mat.	67	477	43.1	12.2	26.6	5.8
519	361491.4	5511301.1	Qua.	38	2069	17.5	5.2	16.3	3.3
520	361425.5	5511290.5	Qua.	38	3056	13.1	6.8	14.6	2.9

The test plots were circular with radii of 10–15 m. All trees (living and dead) within the plot radii were subjected to measurements of stem diameter at breast height (DBH), crown base

and tree height. DBH was measured with tape and tree height was measured with a Haglöf Vertex clinometer. Tree positions relative to the plot centre were also recorded. Stand ages and development phases were extracted from the forestry management database *Wöfis*. With regard to the ground-based remote sensing, terrestrial laser scans (TLS) and hemispherical photos were acquired at the plot centres. The single TLS scan mode was chosen to simulate the radial sampling design commonly applied in German forest inventory (*Winkelzählprobe*).

2.2.2   Ground-based remote sensing data

Terrestrial laser scanning was carried out with a FARO Photon 120 phase shift instrument (FARO, 2010). This scanner operates at a wavelength of 785 nm, with measurement speeds of up to 976,000 pulses per second and with variable angular step sizes. The beam diameter (at exit) is 3.3 mm and beam divergence is 0.16 mrad (FARO, 2010). The height above ground of the scanner's optical centre was set to approximately 1.75 m. Scans were performed with an angular step size of 0.036° (this corresponds to a scan point spacing of 0.6 cm at 10 m distance from the scanner) and a measurement speed of 244,000 pulses per second. In addition, the FARO hardware filters "clear sky" and "clear contour" were activated (FARO, 2010). The terrestrial laser scans were processed according to Pueschel et al. (2013a) and Pueschel et al. (2014) to derive the forest structural parameters stem density (stocking), DBH, and LAI. Tree heights could not be extracted reliably with TLS in this study.

Digital hemispherical photos were acquired with a Nikon D300 digital camera in combination with a Sigma Circular Fisheye lens. The camera was mounted on a tripod, levelled and set to the same height as the terrestrial laser scanner's optical centre (1.75 m). Aperture-priority mode with the aperture fixed at f/6.3 was set and using the camera's bracketing function five photos were taken at each plot centre with the exposure stops +2, +1, AE, -1, -2 (AE = automatic exposure, ± = F stops above/below AE). Photos were saved as 8-bit TIFF. To derive gap fraction, the photos were processed according to the Isodata-based approach of Pueschel et al. (2012) and with the Minimum threshold algorithm (Landini, 2011).

2.2.3   Stand volume retrieval

Mean stem volume was estimated from the mean plot DBH using a Norway spruce specific allometric equation (Zianis et al., 2005, Equation N° 88). Since height measurements could not be extracted from the TLS scans, an equation was chosen that only includes DBH. Mean

stand volume per hectare was estimated from the mean stem volume and the stand density. Stem and stand volumes were estimated separately for the manual and TLS measurements.

2.2.4   LAI retrieval

Based on the assumption of a random azimuthal foliage distribution and using Beer's Law, gap probability (fraction) is modelled as a function of foliage projection function G toward a zenith angle θ, LAI, and path length through the canopy (the cosine of θ) such that:

$$\text{Pgap}(\theta) = e^{-G(\theta)\text{LAI}/\cos(\theta)} \qquad\qquad (1)$$

LAI is derived from gap probability based on Miller (1967):

$$\text{LAI} = 2 \int_0^{\pi/2} -\ln\big(\text{Pgap}(\theta)\big) \cos\theta\sin\theta d\theta \qquad\qquad (2)$$

Based on mean gap probabilities for discrete zenith angle ranges $d\theta_i$, e.g. LI-COR LAI-2000 measurements (LI-COR, 1992), Equation (2) can be integrated numerically by summing the weighted logarithms of the individual zenith angle ranges' gap fractions:

$$\text{LAI} = 2 \sum_{i=1}^{n} -\ln\big(\text{Pgap}(d\theta_i)\big) \cos\theta_i\sin\theta_i d\theta_i \qquad\qquad (3)$$

With the LAI-2000, 5 zenith angle ranges (0–13°, 16–28°, 32–43°, 47–58°, 61–74°) are used. The weights $\sin\theta_i d\theta_i$ are based on the centre angles of these ranges. The weights are then normalized to sum to one (LI-COR, 1992).

Equation (3) was used in combination with the discrete zenith angle ranges of the LAI-2000 to calculate LAI based on the gap probabilities derived from the hemispherical photos and the terrestrial laser scans in this study. In addition, LAI-2000 measurements acquired at Norway spruce stands within the study area during an earlier field campaign were also used to derive LAI. As the clumping of canopy elements, particularly into individual tree crows can lead to an increase in the gap probability for a given LAI, the term effective LAI is often used instead (e.g. Jonckheere et al., 2004).

The distinction between foliage and woody material can also often not be made with the optical LAI instruments; therefore the LAI derived from the measurements obtained in this study represents an effective Plant Area Index (PAI_e). As the 3-PG model outputs leaf area, it was necessary to convert from PAI_e to LAI in order to calibrate the model with the ground-

based remote sensing measurements. PAI_e was converted to LAI based on mean values of clumping, wood area index (WAI), and needle-to-shoot area ratio provided by Greve (2010) for Norway spruce.

2.3   Long-term forest growth monitoring

Forest growth and yield data for calibrating the model 3-PG for Norway spruce was provided by the forestry administration for the three long-term monitoring sites located within the study area. These sites are *Hoxel*, *Hundheim*, and *Allenbach* (Table 2). The *Hundheim* site includes three separate growth plots (*Hundheim* 1-3), the data of which were averaged for the model calibration. The growth data consists of various structural parameters including stocking, mean and top height, mean DBH, and stem volume. To better assess the growth at these sites, the growth data was compared to empirically derived yield tables for Norway spruce (Fig. 2)
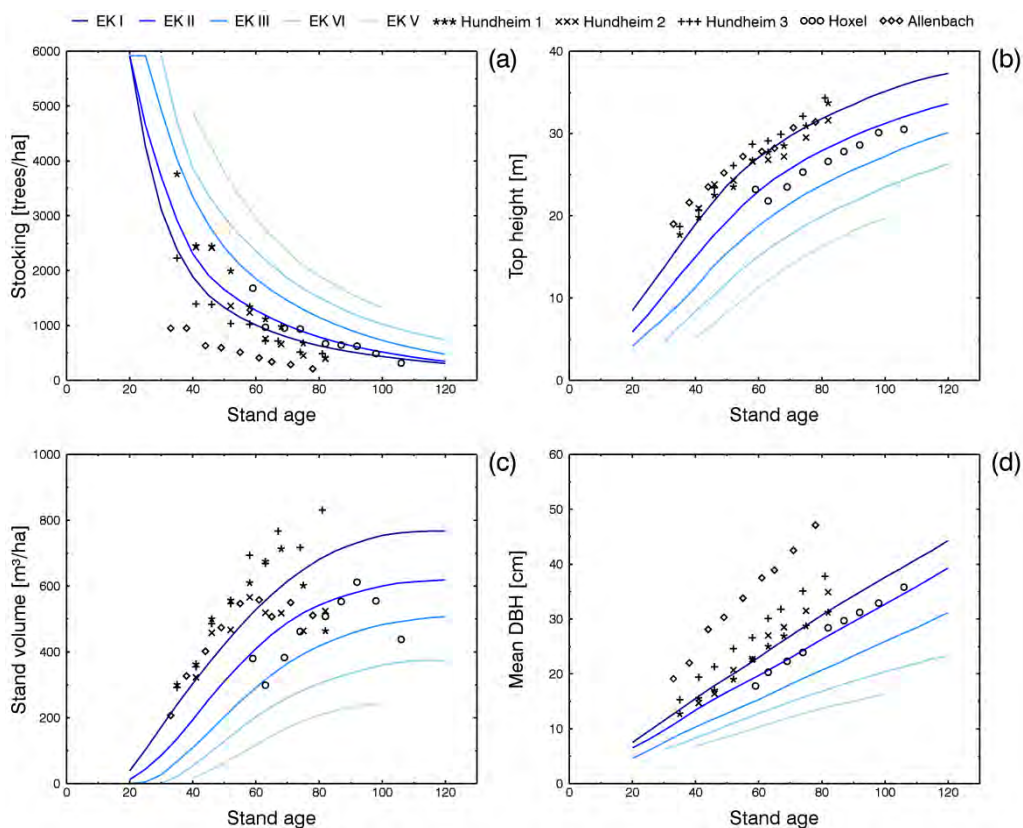
Figure 2: Comparison of the long term forest growth data used for model calibration in this study with growth data from empirical Norway spruce yield tables which account for medium stand thinning: *Ertragstafeln Fichte (mäßige Durchforstung) nach Wiedemann* (Schober, 1995). EK I-V represent different yield classes.

Table 2: Description of the forest growth monitoring sites. [a]Stand age at the time of the last inventories in 2006 (Allenbach) and 2007 (Hoxel/Hundheim). [b]According to Forstliche Standortsaufnahme (2003). [c]According to the World Reference Base for Soils (WRB). The site form mainly relates to the soil water regime; forms I-IV are not affected by logged water or groundwater, forms VII-X are affected by logged water or groundwater.

Forestry district	Section	Stand age[a]	Elevation	Slope	Exposition	Site form[b]	Soil type[c]
Dhronecken	Hoxel	106 yrs	640 m	4°	West	III	Dystric Cambisol
Dhronecken	Hundheim	82 yrs	515 m	3°	West	III	Gleyic Cambisol
Idarwald	Allenbach	78 yrs	670 m	4°	North-West	IX	Gleysol

2.4   Model calibration and simulations

2.4.1   Basic model calibration

3-PG is a generic forest growth model based on simulating the physiological processes of tree growth as well as the environmental factors affecting growth. As the capability of tree species to adapt to environmental growing conditions varies and the growing conditions vary with site conditions, 3-PG needs to be parameterized separately for different tree species and forest sites (see Section 1). 3-PG has been parameterized mainly for evergreen species, including Douglas fir (*Pseudotsuga menziesii*), ponderosa pine (*Pinus ponderosa*), and Scots pine (*Pinus sylvestris*). 3-PG has not been extensively parameterized for Norway spruce. Where available own measurements of physiological processes and site conditions were used for the parameterization. Where not available, values taken from the literature were preferred over default model values (see Table A-1 in the Appendix for a detailed list of model parameter values and their reference).

The main model parameters of the biomass allocation, the stem-to-foliage partitioning ratios at DBH 2 cm and 20 cm, and the main site parameters, site fertility and initial stocking, were estimated based on calibrating the model to the growth data of the three long-term monitoring sites. This model calibration was achieved by adjusting the model outputs of the structural parameters LAI, stocking, stand volume, and mean DBH to the measured time-series of these parameters (see Section 2.3). As measurements of LAI are not part of the long-term growth monitoring at these sites, artificial times-series were constructed from the LAI measurements obtained during the field campaigns (see Sections 2.1 and 2.2). For the model calibration, these LAI measurements were averaged over the stand age classes 20–40 yrs, 40–60 yrs, 60–80 yrs, and 80–110 yrs. The LAI derived from the hemispherical photos based on the two

11

different approaches used in this study were averaged for the same purpose. A model calibration was considered to be realistic when the simulated LAI was within the boundaries of the artificially constructed LAI curves. In addition, the simulated values of net primary productivity were checked for plausibility.

The site parameters soil class and maximum available soil water (ASW) were inferred from the site information provided by the forestry administration (Table 2). Based on this data and the geology of the study area, a clay-loam was chosen from the four general soil classes available in 3-PG. Based on the classification of utilizable water holding capacity of the rooting zone (Forstliche Standortsaufnahme, 2003), a medium water holding capacity of 105 mm was chosen as maximum available soil water (Table 3). Site fertility which results from the interaction of different site factors, and therefore difficult to measure directly, was estimated by taking the available site information into account. For the sites *Allenbach*, *Hoxel*, and *Hundheim* site fertilities of 0.3, 0.3, and 0.45 were set respectively (Table 3).

Table 3: Stand initialization and site factor data used for the model simulations.

	Unit	Allenbach	Hoxel	Hundheim	Mean model	Reference
Year planted	yr	1928	1901	1926	1901	Growth data
Initial year	yr	1	1	1	1	
Initial month	-	January	January	January	January	
End age	yr	100	120	100	110	
Initial foliage biomass	t/ha	1	1	1	1	Landsberg & Waring (1997)
Initial root biomass	t/ha	3	3	3	3	Landsberg & Waring (1997)
Initial stem biomass	t/ha	6	6	6	6	Landsberg & Waring (1997)
Initial stocking	trees/ha	3000	7000	6000	5000	Estimated
Initial ASW	mm	100	100	100	100	Estimated
Fertility rating	-	0.3	0.3	0.45	0.4	Estimated
Soil class	-	Clay-loam	Clay-loam	Clay-loam	Clay-loam	Estimated
Maximum ASW	mm	105	105	105	105	Estimated
Minimum ASW	mm	0	0	0	0	Estimated

Regarding the climate data required for running 3-PG, long-term meteorological observations were available from two weather stations within the study area (Fig. 1). These included hourly observations of temperature, rainfall, and solar radiation, available for the *Morbach* station of the German Weather Service for the years 1988–2002 and for the *Leisel* station of the *ZIMEN* network for the years 1991–2006. From these observations, mean monthly values required by 3-PG (see Section 1) were averaged over the available periods. The *Morbach* data was used for running 3-PG for *Hoxel* and *Hundheim*. The *Leisel* data was used for the *Allenbach* site.

Based on these long-term averages and the stand ages of the monitoring sites up to which growth data was available, basic 3-PG simulations were run for 100 years for the *Allenbach* and *Hundheim* sites and for 120 years for *Hoxel*. The Microsoft Excel based implementation of 3-PG by P. Sands (2010) was used for all model simulations in this study (available from http://booksite.elsevier.com/9780123744609/).

2.4.2 Extended model calibration

In addition to the basic model simulations, extended simulations were run accounting for tree removal, either as a consequence of natural disturbances or silvicultural events (e.g. stand thinning). Both causes can be explicitly accounted for in 3-PG by specifying the number of removed trees and the corresponding fraction of biomass lost from each of the three biomass pools (see Section 1). As the stand history of the growth monitoring sites was unknown, tree removal was accounted for by fitting the simulated stocking and stand volume curves to the measured data. This resulted in the following stocking specifications for the sites, i.e. the model was forced to reduce its simulated stem density to the following stem densities at the specified ages: 337 trees/ha at age 65 (*Allenbach*), 968 trees/ha at age 60 (*Hoxel*), and 600 trees/ha at age 68 (*Hundheim*). These were the only changes made compared to the basic 3-PG model simulations.

2.4.3 Parameter sensitivity study

As the majority of parameters of the stand initialization and site factor data were inferred from the scarce stand and site information available for the three growth monitoring sites (see Tables 2 and 3), a parameter sensitivity study was carried out to assess the influence of the main stand initialization and site parameters. The common practice of varying one parameter while the remaining parameters are kept constant was used for this purpose. It is to be noted that this approach is not capable of accounting for interactions between model parameters which inevitably exist within such a complex model. Based on the basic model calibration, site fertility was varied by $\pm\ 0.1$, and initial stocking was varied by $\pm\ 1000$ trees per hectare (Table 4). For the maximum available soil water, the mean values of the classes "low", "medium", and "high" were taken from the classification of utilizable water holding capacity of the rooting zone (Forstliche Standortsaufnahme, 2003).

Table 4: Stand initialization and site parameter combinations used for the model sensitivity study. ASW = maximum available soil water [mm]

Allenbach			Hoxel			Hundheim		
Stocking	Fertility	ASW	Stocking	Fertility	ASW	Stocking	Fertility	ASW
2000	0.30	105	6000	0.30	105	5000	0.45	105
3000	0.30	105	7000	0.30	105	6000	0.45	105
4000	0.30	105	8000	0.30	105	7000	0.45	105
3000	0.30	75	7000	0.30	75	6000	0.45	75
3000	0.30	150	7000	0.30	150	6000	0.45	150
3000	0.20	105	7000	0.20	105	6000	0.35	105
3000	0.40	105	7000	0.40	105	6000	0.55	105

2.4.4   Mean model calibration using artificial time series of forest structural parameters

To assess whether 3-PG can be calibrated with artificial time series of forest structural parameters derived both from ground-based remote sensing measurements and traditional manual inventory measurements, the data collected during the field campaign in 2013 was used to generate artificial time series of stocking, LAI, mean DBH, and stand volume. The aim of this assessment was not to achieve a calibration of the species parameterization sheet different to the one from the basic model calibration, but to assess the potential of these time-series to provide a local mean model calibration of stand initialization and site parameters. In this study, such a mean model calibration was tested for the *Hoch- und Idarwald* forest by comparing the artificial times series to model simulations based on an average initial stocking and site fertility. These were derived from averaging the values of the three monitoring sites (Table 3).

3   Results

3.1   Ground-based measurements of forest structural parameters

The ground-based measurements of the forest structural parameters used in this study are depicted in Figure 3. The LAI reveal the variability in stand structure which can be observed for Norway spruce stands in the study area, in particular for stands of the development phase dimensioning. This variability results from thinning activities adding to the natural variability observed during this development phase. The variability witnessed in the LAI for the stand age class 40-60 yrs, which corresponds to the dimensioning phase, seems to be dependent on the measurement method, too. The LAI derived from the terrestrial laser scanning exhibit the largest variability followed by the hemispherical photos and the LAI-2000. The mean TLS-LAI is also distinctly higher than the LAI derived from the passive optical methods, which themselves agree rather well (Fig. 3a). In addition, the effects of using different approaches to the extraction of gap probability from hemispherical photos are clearly visible.

Regarding the mean DBH, stem numbers, and stem densities retrieved from the TLS scans, the values agree well with the reference measurements for the stands of development phases dimensioning and maturing, but deviate strongly from the reference for qualification stands (Figs. 3b–d). While reference DBH is overestimated by the TLS, reference stem numbers and densities are underestimated by TLS. Both are the consequence of the occlusion effect that is inherent in terrestrial laser scans, in particular in single scan mode, i.e. scanning from a single location. Occlusion refers to the shadowing of background objects by foreground objects both lying in the same laser beam path. Occlusion can be partial or complete depending on object dimension, distance to scanner, and laser beam divergence. The underestimation of plot stem numbers is caused by the strong occlusion effects found in dense stands, which are especially characteristic for the qualification development phase. The result is a high degree of partial occlusion affecting the mathematical circle-fitting routine of the DBH retrieval algorithm in such a way as to overestimate the true diameter of these partially occluded stems.
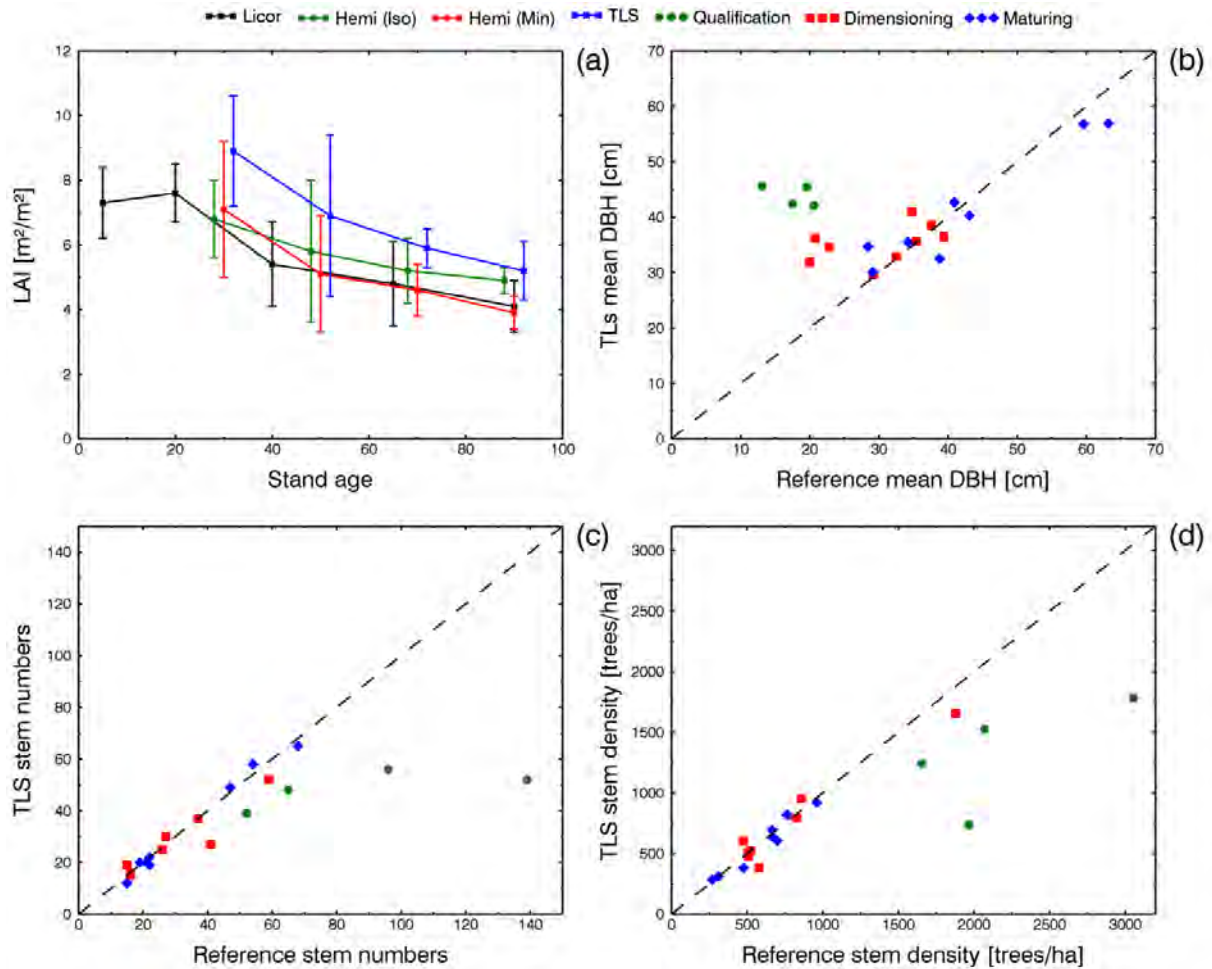
Figure 3. Ground-based plot measurements of forest structural parameters used in this study. (a) LAI, (b) Mean DBH, (c) Stem numbers, (d) Stem density. The LAI curves and error bars represent the mean and standard deviation of the LAI for the stand age classes 0–20 yrs, 20–40 yrs, 40–60 yrs, 60–80 yrs, and 80–110 yrs. Hemi (Iso) refers to the LAI derived from the hemispherical photos based on the approach of Pueschel et al. (2012). Hemi (Min) refers to the LAI derived from the hemispherical photos based on the Minimum algorithm. The Hemi (Iso) and TLS curves are offset by +/- 2 years on the x-axis for a better visibility. For a description of the stand development phases qualification, dimensioning and maturing see Section 2.2.1.

3.2   Basic model calibration

The basic model calibration based on the growth data of the three monitoring sites shows that the potential growth at these sites can be simulated well with the 3-PG model (Figs. 4–6; as the figures in the following sub sections all have the same layout, a detailed caption is only provided for Fig. 4). This applies to the simulated LAI and stocking for stand ages greater than 20–40 years and for the simulated mean DBH and stand volume up to stand ages of 60–80 years. The reason for the increasing differences between simulated and observed parameter values with increasing stand age is that the basic model calibration is statically simulating the

potential growth without explicitly accounting for biomass losses as a result of tree removal. As the growth monitoring at these sites is not intended to monitor the potential natural growth but the growth (or better the yield) that is achieved through active forest management (e.g. selective thinning), the measured growth data reflect the effects of such a controlled growth. This is particularly evident for the mature phase when harvesting starts and trees are removed. As a consequent, the stand volume is either reduced (*Hoxel, Hundheim*) or reaches a plateau (*Allenbach*) and the mean DBH curves concavely compared to the convex simulated mean DBH (Figs. 4–6). The latter results from the removal of large diameter trees and therefore a reduction in mean DBH and from the 3-PG model structure assuming forest stands to be made up of trees even-aged and with even stem diameters. In reality, the DBH within forest stands are of course far from being evenly distributed.
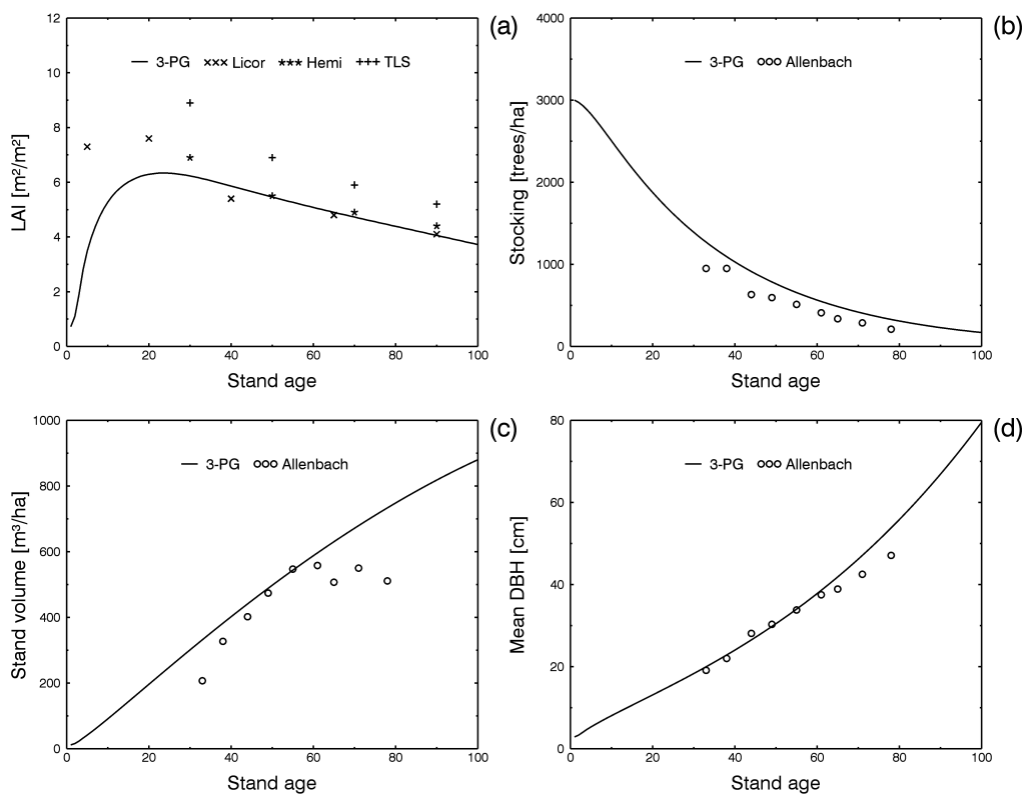
Figure 4. Basic model calibration for the forest growth monitoring site *Allenbach*. (a) LAI, (b) Stocking, (c) Stand volume, (d) Mean DBH. The LAI represent the mean LAI of the stand age classes 0–20 yrs, 20–40 yrs, 40–60 yrs, 60–80 yrs, and 80–110 yrs.
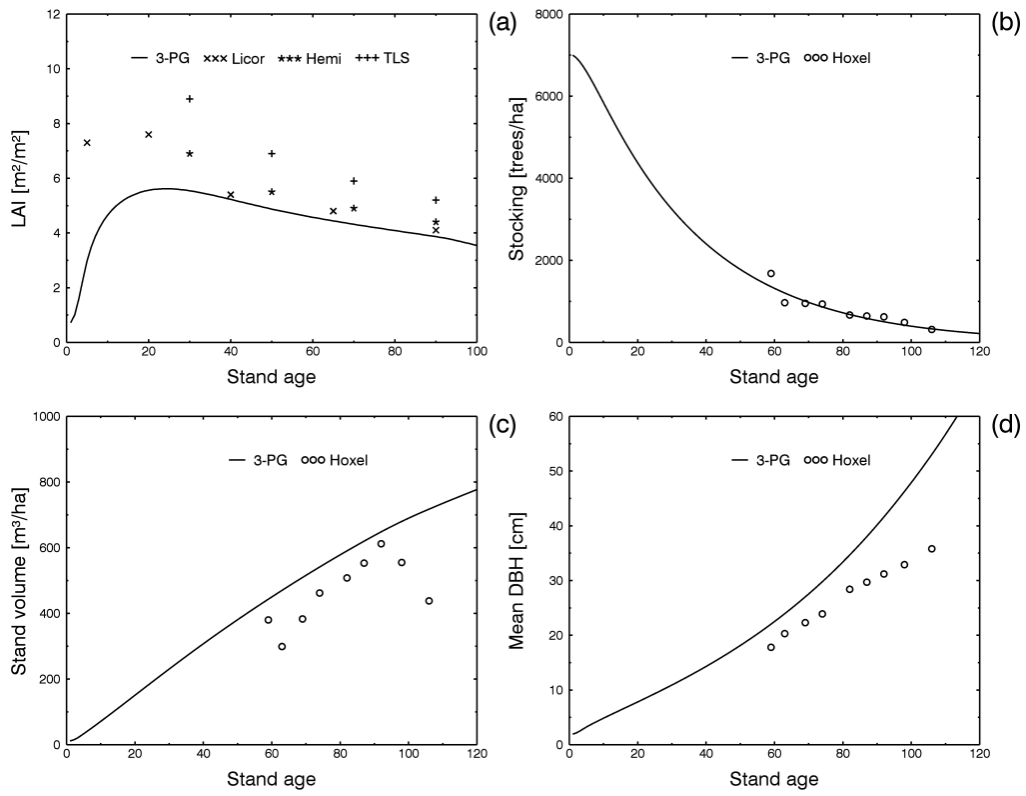
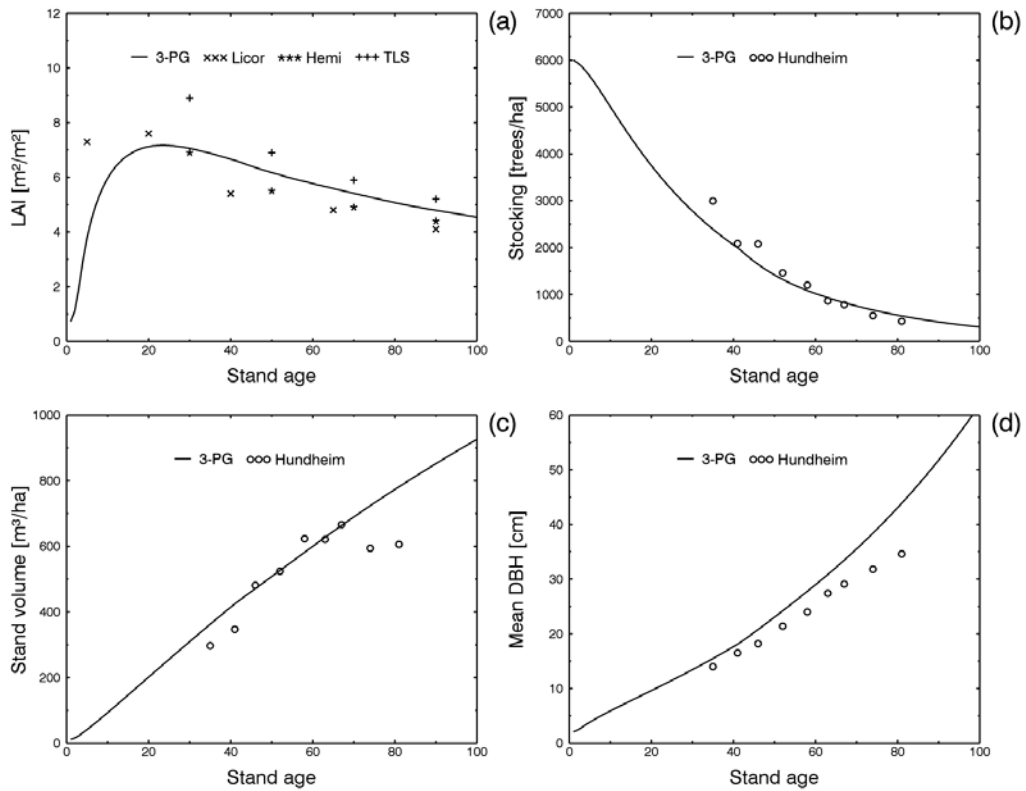**Figure 5. Basic model calibration for the forest growth monitoring site *Hoxel*.**

Figure 6. Basic model calibration for the forest growth monitoring site *Hundheim*.

3.3   Extended model calibration

The extended model calibration shows that explicitly accounting for tree removal in 3-PG results in more realistic simulations of stocking and stand volume (Figs. 7–9). However, extrapolating the calibrated model to other sites would require the knowledge of stand history; information that in reality is not available on a large scale and would need to be inferred. While stocking and stand volume may be more realistically simulated, the effects of removing a specified fraction from the biomass pools through tree removal seems to impact the LAI development in an unrealistic way (Figs. 7–9). This is acknowledged by the model developers who therefore advise cautious use of this sort of forced model setting (Sands, 2001). The results also reveal that the model does not react dynamically to these settings; instead the biomass is merely reduced by the specified fractions and 3-PG continues to simulate statically the potential growth thereafter. Potential effects of tree removal on the development of the remaining trees, e.g. an increase in biomass allocation to foliage through the increased light availability, cannot be accounted for in 3-PG.
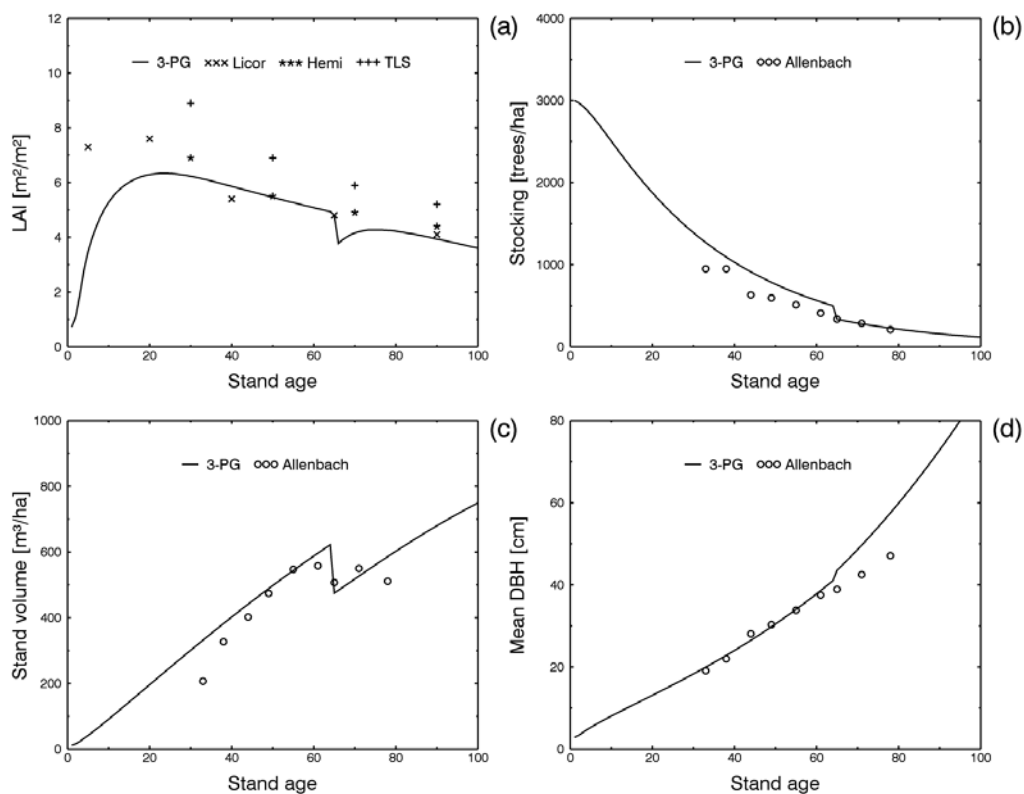

Figure 7. Extended model calibration for the forest growth monitoring site *Allenbach*.
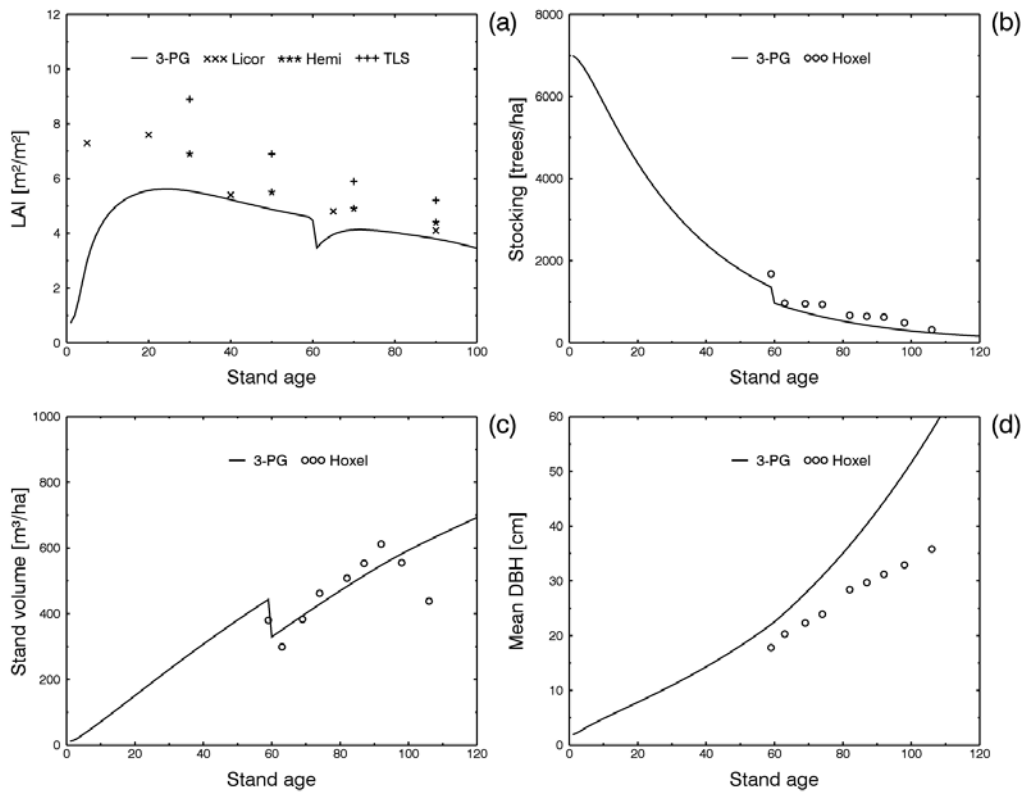
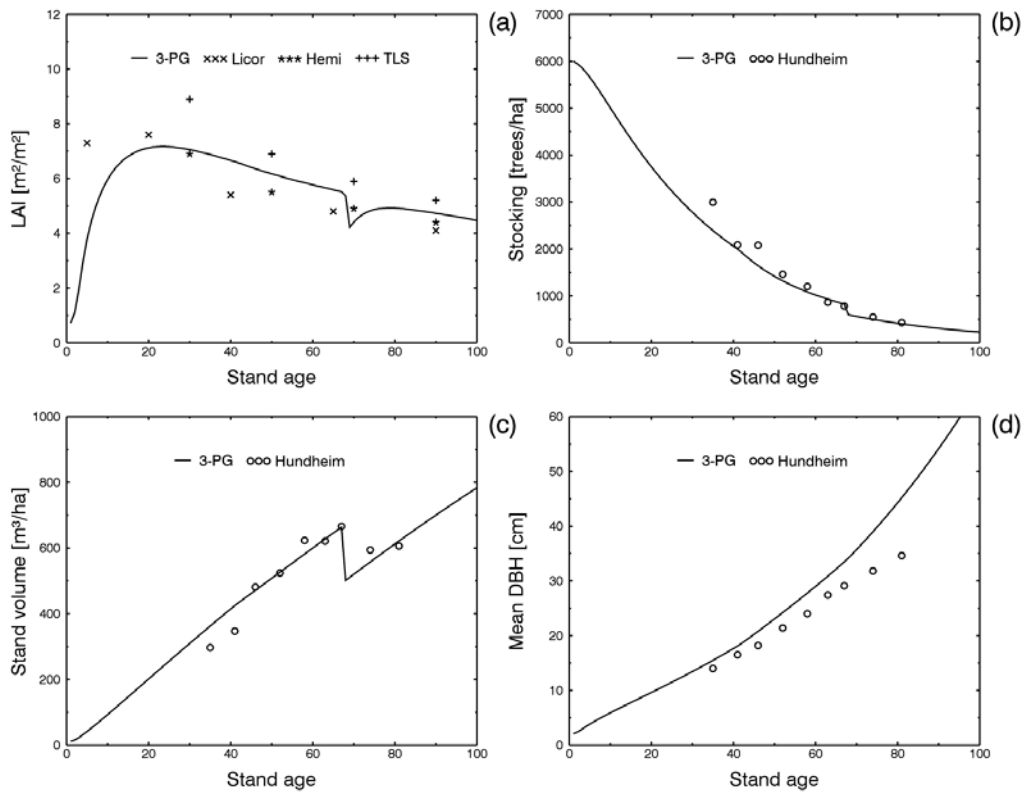**Figure 8. Extended model calibration for the forest growth monitoring site *Hoxel*.**

Figure 9. Extended model calibration for the forest growth monitoring site *Hundheim*.

3.4   Model parameter sensitivity

The parameterization of the model input, stand initialization and site factor data, is a critical issue in the general application of the 3-PG model, due to the limited availability of detailed forest stand and soil data on a large scale. The spatial heterogeneity of soil physical properties and related soil water processes makes it especially difficult to determine these at forest stand level. Based on the available site information for the growth monitoring sites, the main site parameters initial stocking, site fertility, and maximum available soil water were estimated in this study (see Section 2.4.1). To evaluate this parameter estimation, a sensitivity study of these model parameters was carried out (see Section 2.4.3). Varying the available soil water had a small effect on the simulated LAI, stocking, stand volume, and mean DBH for all three sites (Figs. 10, 13, 16). This might be due to the selected clay-loam soil class which generally exhibits favourable soil physical properties. The more extreme soil classes sand and clay should be affected more strongly by varying the maximum available soil water.

By comparison, varying the site fertility had a strong effect on simulated LAI, stand volume, and mean DBH for all three sites (Figs. 11, 14, 17). As the site fertility simply represents a linear scaling factor for the canopy quantum efficiency this was to be expected (see Section 1). The results also demonstrate the importance of calibrating the model with time-series of both leaf and woody biomass, as fitting the simulations as closely as possible to only one of the variables may result in estimation errors for the other variable which, however, could be compensated for by errors in the allocation fractions (Sands, 2004). Varying the site fertility by ± 0.1 had little effect on the simulated stocking, which can be explained by the way stand self-thinning is modelled in 3-PG (see Section 1). For the three sites, the simulated stocking was affected noticeably only when site fertility was increased by more than 0.2 fertility units (results not shown).

Varying the initial stocking by ± 1000 trees per hectare showed to have little effect on the simulated LAI and stand volume for all three sites (Figs. 12, 15, 18). With the exception of *Allenbach*, the simulated stocking and mean DBH were also only affected weakly, indicating that the initial stocking is not such a critical parameter provided a good initial estimate can be made. However, considering that the measured stocking varied strongly for the three sites (see Section 2.3, Fig. 2), determining an appropriate initial stocking might prove to be difficult for sites of unknown stand history.
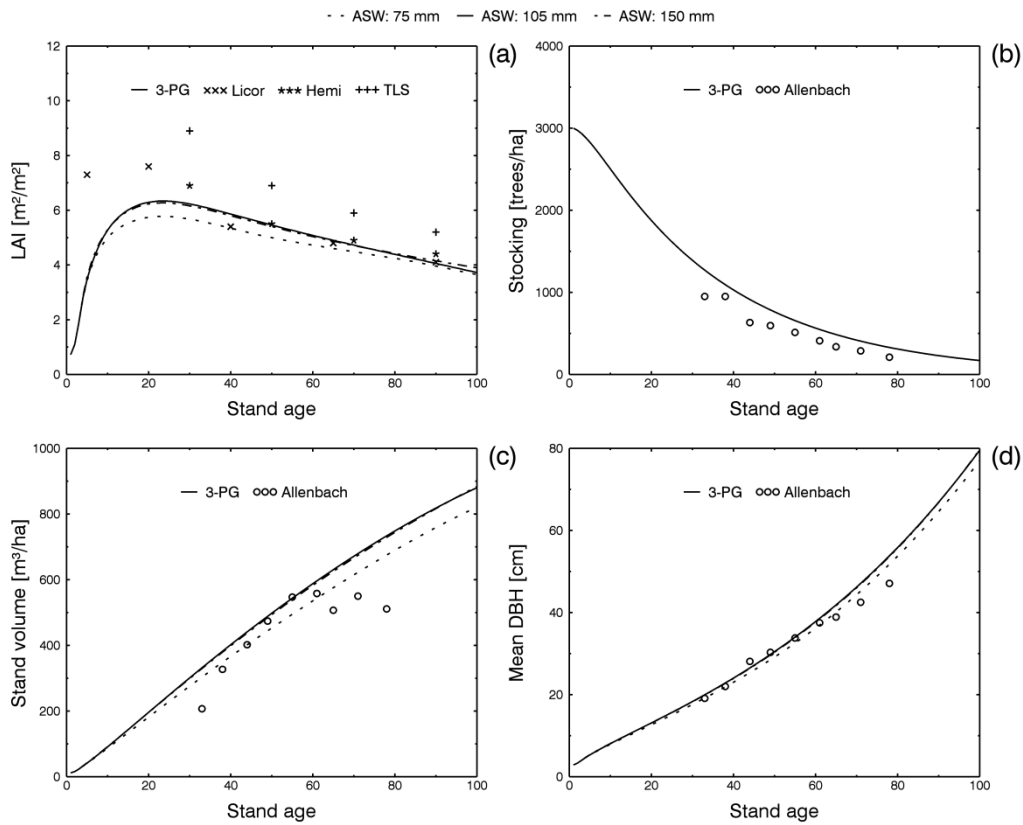
Figure 10. Basic model calibration parameter sensitivity for *Allenbach*. Parameter: Maximum available soil water (ASW).
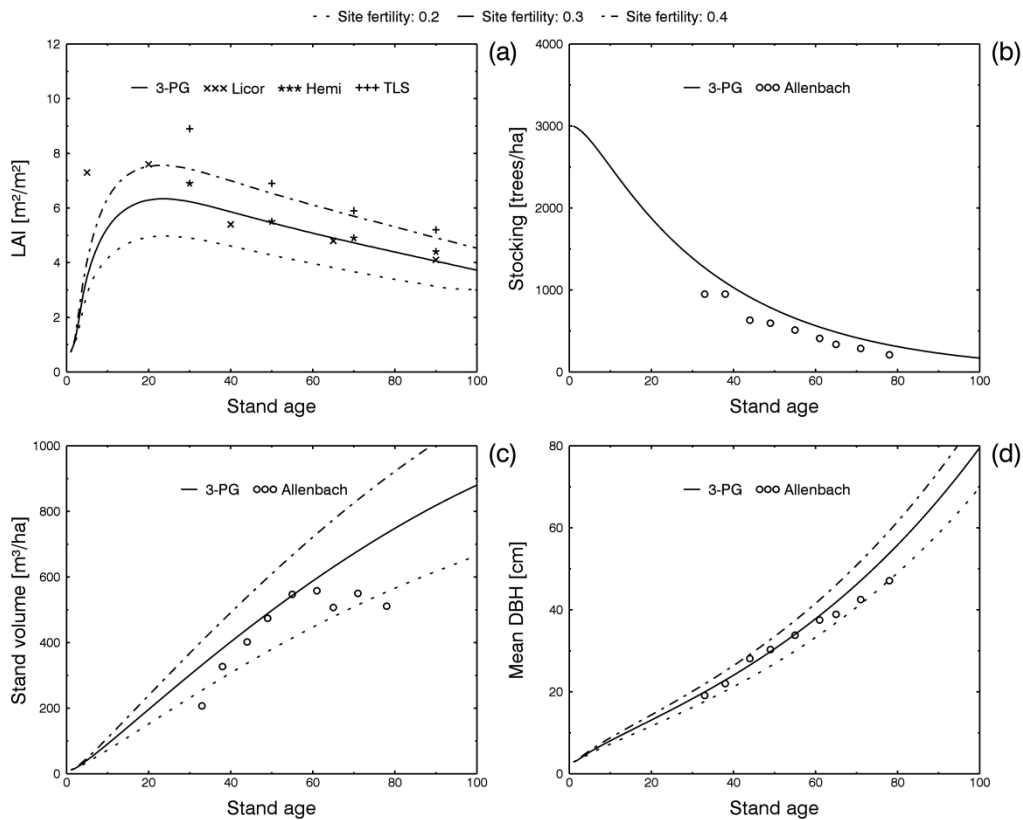

Figure 11. Basic model calibration parameter sensitivity for *Allenbach*. Parameter: Site fertility.
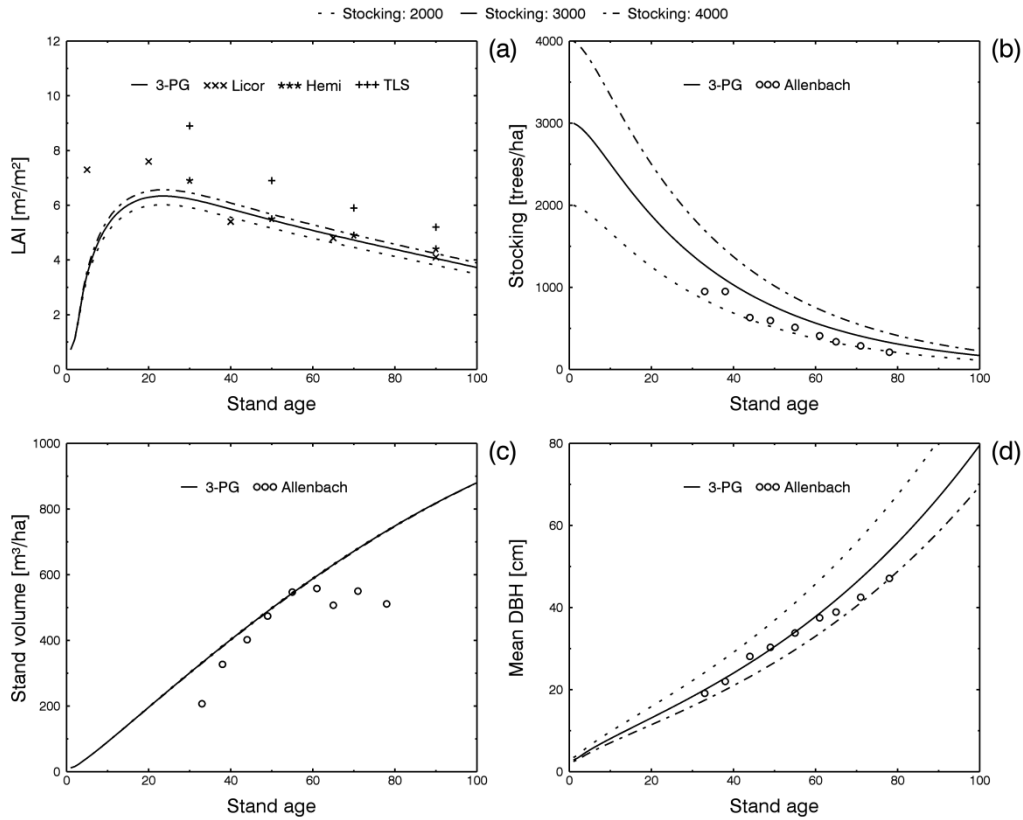
Figure 12. Basic model calibration parameter sensitivity for *Allenbach*. Parameter: Initial stocking.
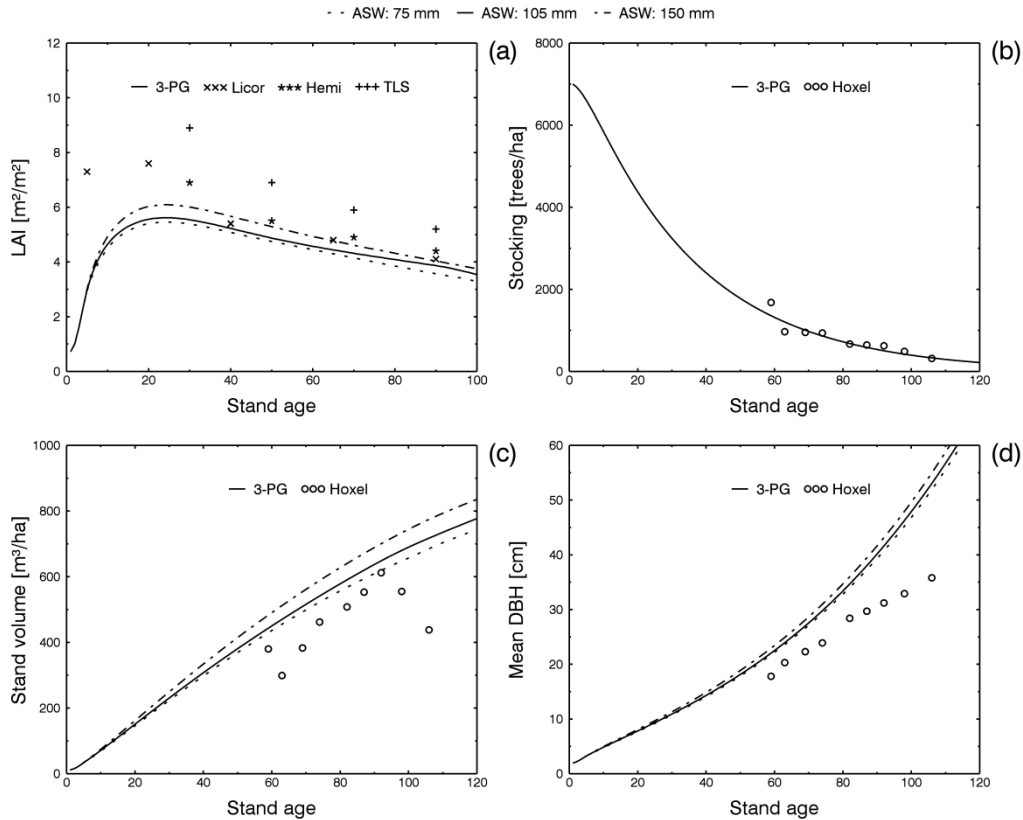

Figure 13. Basic model calibration parameter sensitivity for *Hoxel*. Parameter: Maximum available soil water (ASW).
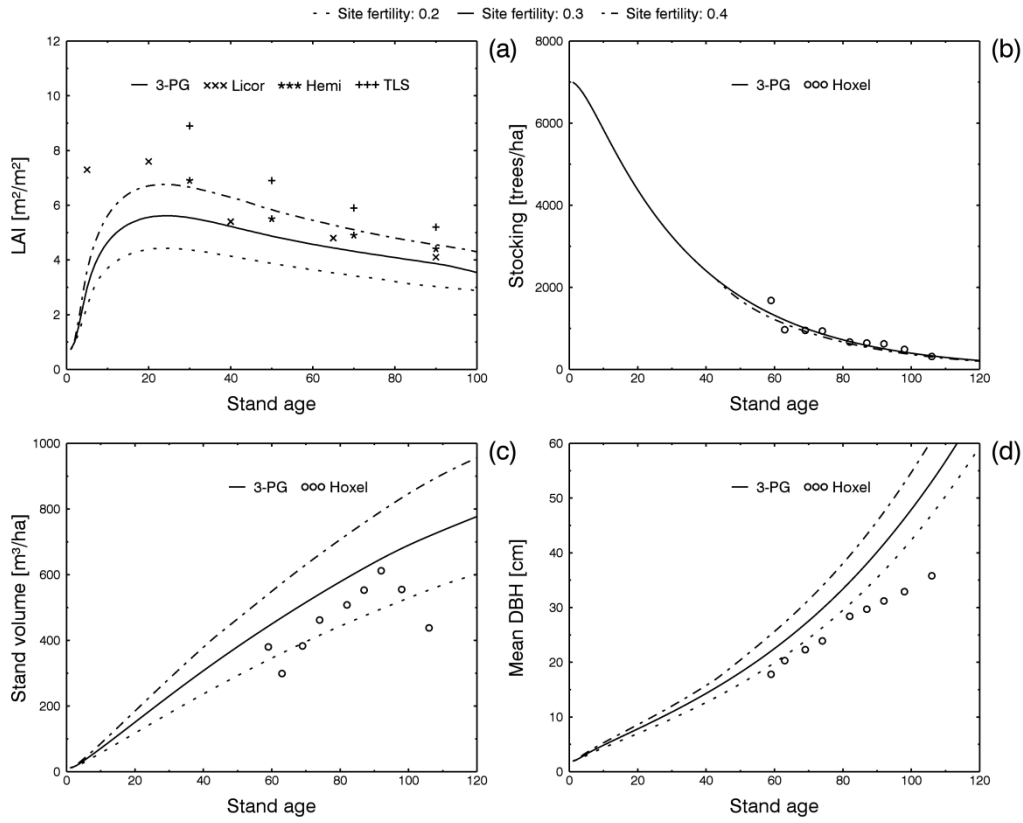
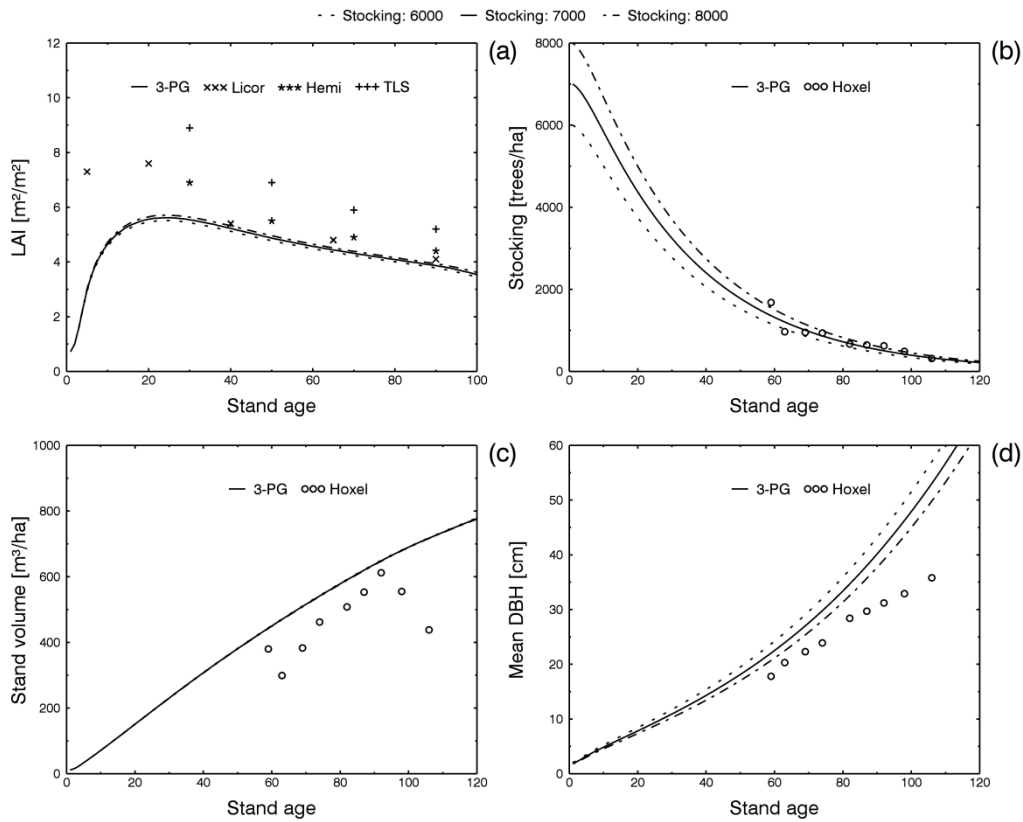**Figure 14. Basic model calibration parameter sensitivity for *Hoxel*. Parameter: Site fertility.**

Figure 15. Basic model calibration parameter sensitivity for *Hoxel*. Parameter: Initial stocking.
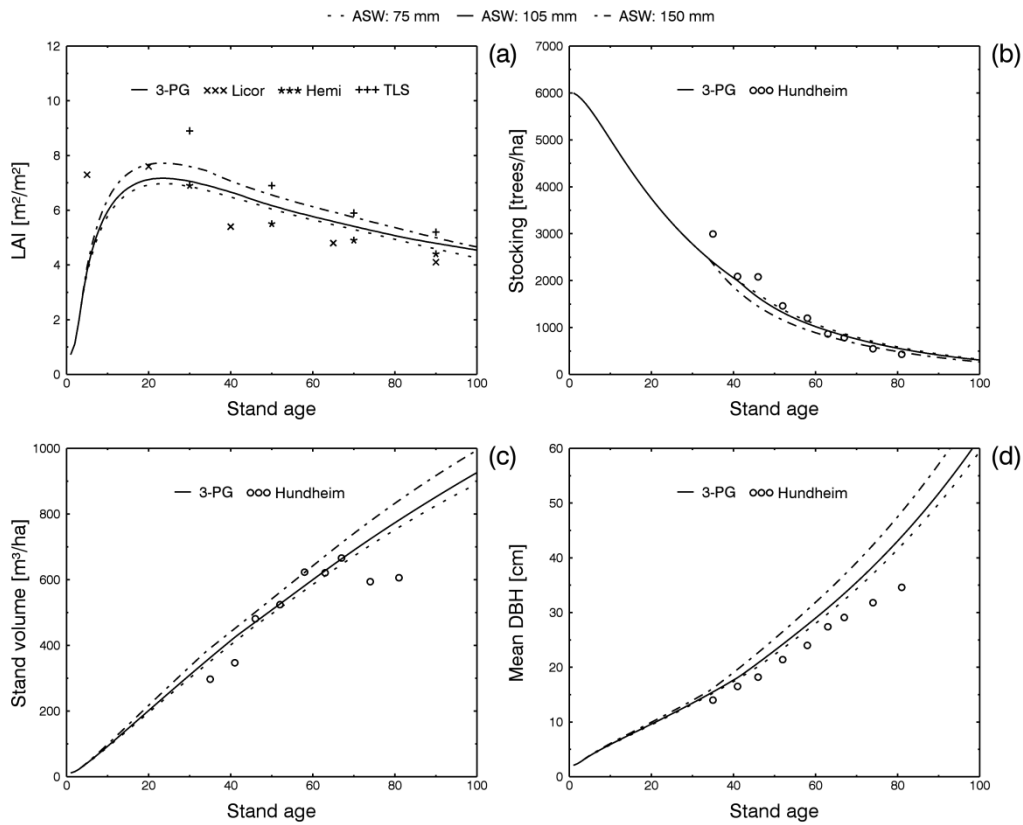
Figure 16. Basic model calibration parameter sensitivity for *Hundheim*. Parameter: Maximum available soil water (ASW).
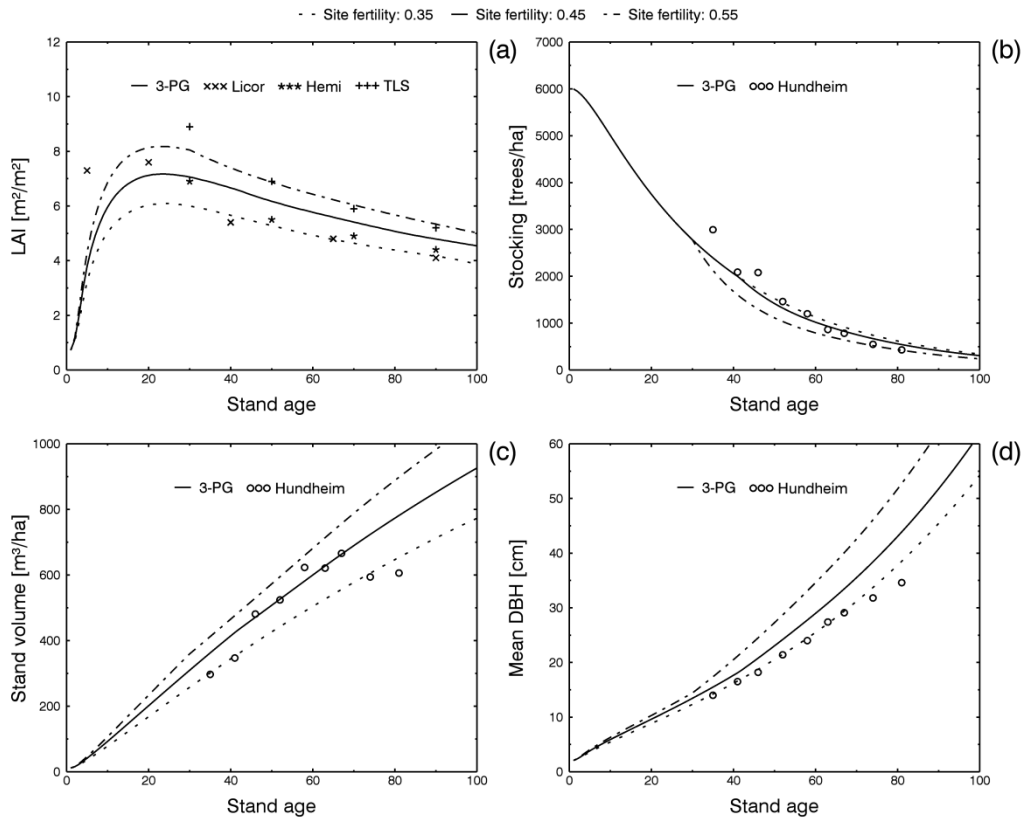

Figure 17. Basic model calibration parameter sensitivity for *Hundheim*. Parameter: Site fertility.
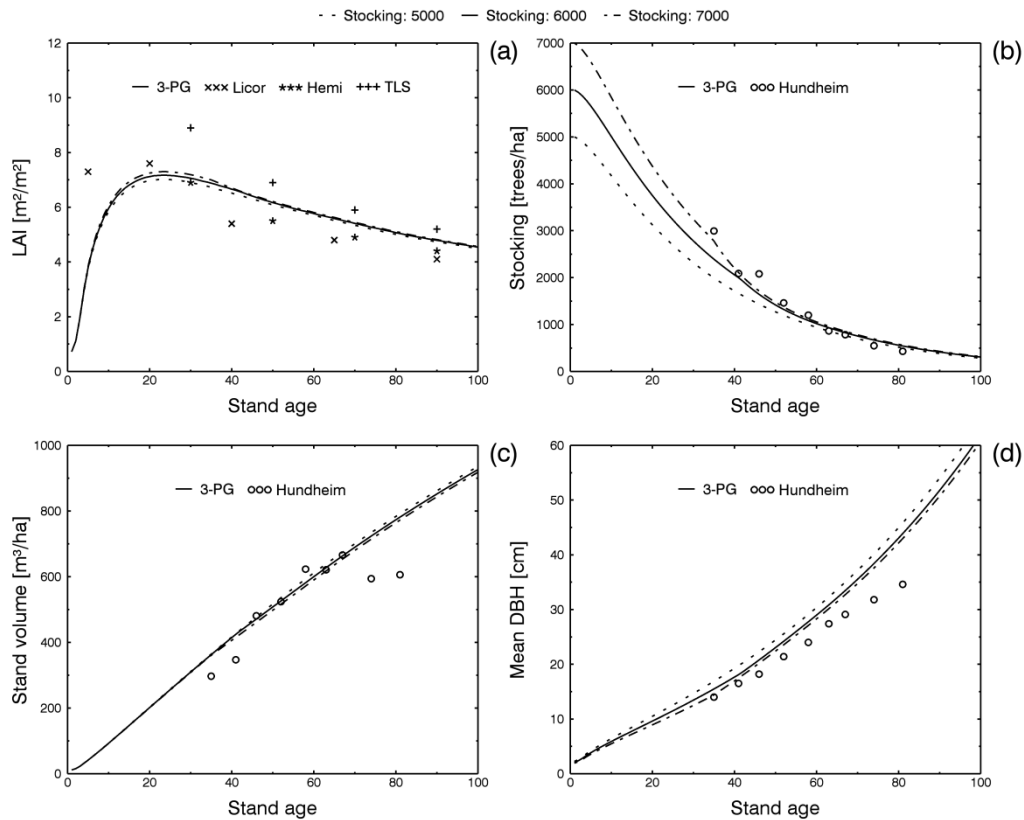
Figure 18. Basic model calibration parameter sensitivity for Hundheim. Parameter: Initial stocking.

3.5 Mean model calibration using artificial time series of forest structural parameters

In this study, the potential use of artificial time series of forest structural parameters derived from ground-based remote sensing and traditional manual inventory measurements in order to calibrate mean local 3-PG simulations was investigated. The results show that mean model simulations of LAI, stocking, stand volume, and mean DBH compared well with the manual inventory measurements (Fig. 19). However, the results also demonstrate the need to collect this data for forest stands covering a wide range of development phases. This is due to the observed high variability in forest structure resulting from forest management practices and locally varying environmental growing conditions (see Section 3.1). This prerequisite is even more evident for the time-series derived from ground-based RS-measurements (Fig. 20) since they showed an underestimation of stocking and an overestimation of mean DBH for young forest stands (see Section 3.1). As a consequence, calibrating a mean local model based on artificial time-series of only up to 60–70 years would result in a poor model calibration. Ground-based RS-measurements of young stands may even need to be excluded from such a mean model calibration.

Figure 19. Mean model simulations compared to artificial time series of forest structural parameters constructed from in situ reference measurements.

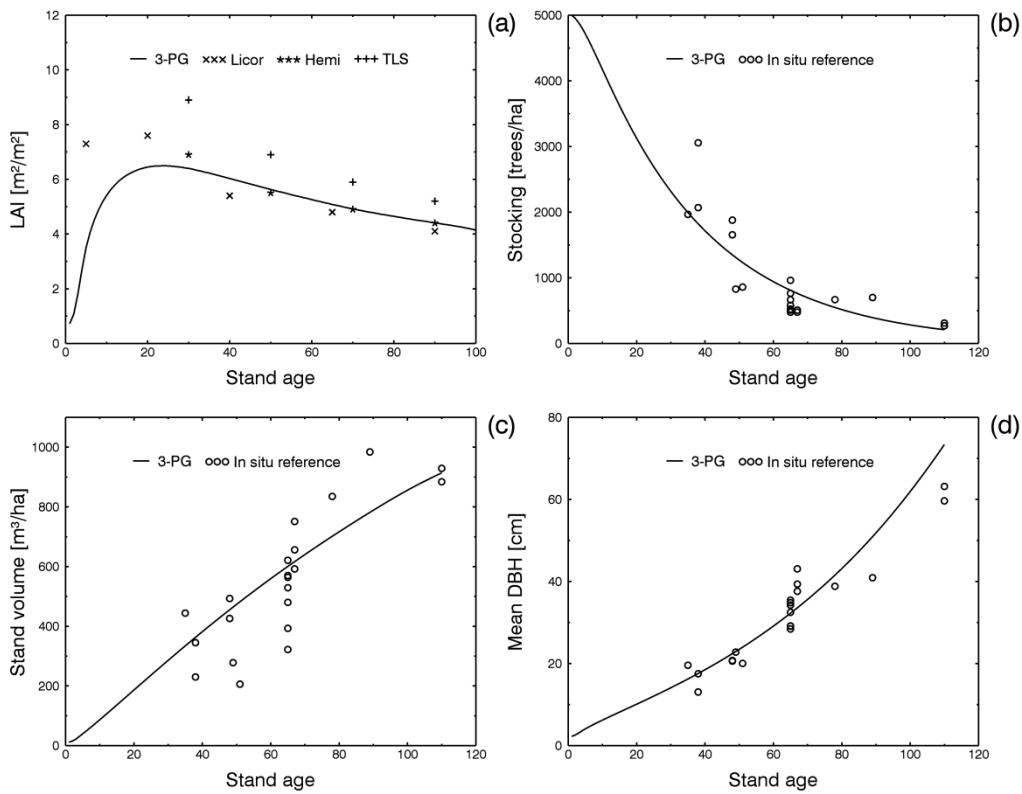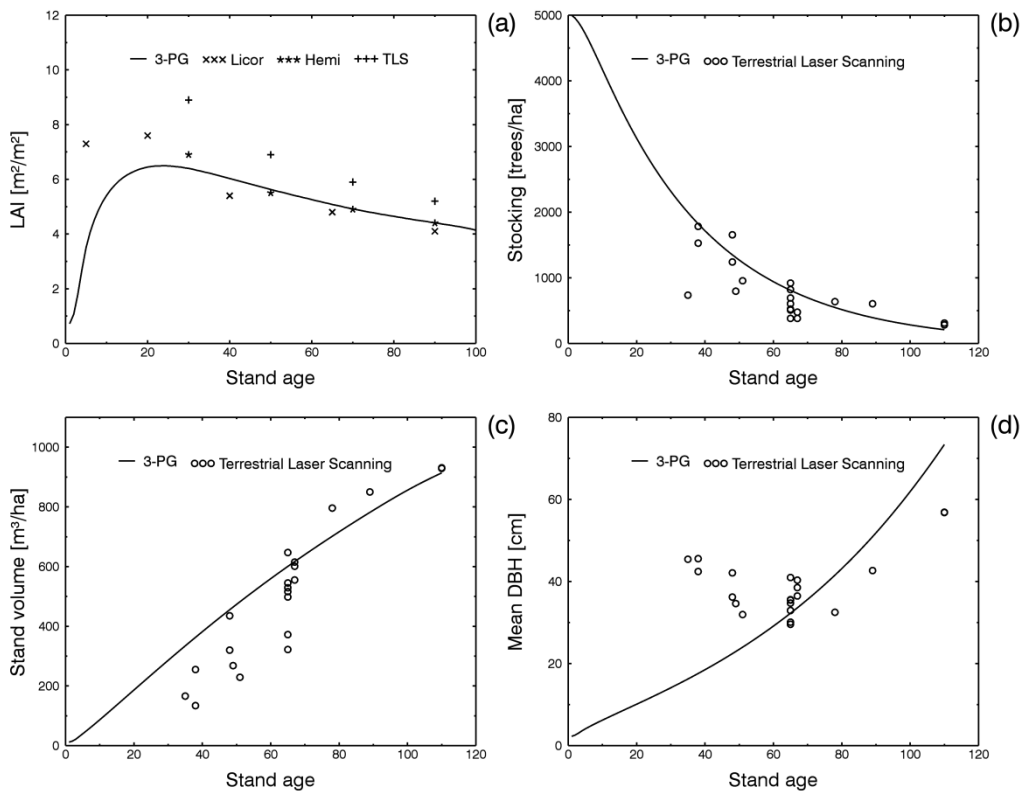**Figure 20. Mean model simulations compared to artificial time series of forest structural parameters constructed from ground-based remote sensing measurements. LAI, stocking, and DBH are based on in situ measurements. Stand volume was derived using an allometric equation.**

27

4   Discussion

4.1   Basic and extended model calibration

The present study could show that calibrating 3-PG with growth data from three monitoring sites yielded simulations that were in agreement with the potential growth at these sites (see Section 3.2). This is not surprising, though, as model simulations were compared to growth data that also served as input into the model calibration. An independent assessment of the model calibration (i.e. model validation) was not carried out in this study due to the limited number of long-term growth monitoring sites. To compensate to some degree for this lack of a proper model validation, a model parameter sensitivity study was carried out, which at least provided constraints on some of the main model parameters.

In addition, the simulation results of the basic model calibration also provided helpful insights into the behaviour of the 3-PG model and its potential limitations. One of the main issues found in this regard was 3-PG's static simulation of potential growth and yield, deviating considerably from the observed stand growth after 60–80 years, in particular for stand volume and mean DBH (see Section 3.2). This was the result of (a) the basic model calibration which did not account for the removal of trees other than by self-thinning, and (b) the fact that forest stands in the *Hoch- und Idarwald* are actively managed, i.e. forest management practices such as selective thinning are applied. As these can be explicitly accounted for in 3-PG, extended model simulations were carried out yielding more realistic stockings and stand volumes (see Section 3.3).

However, the results also showed that 3-PG is not able to react dynamically to forced changes in its biomass pools, i.e. 3-PG reduces these pools by specified fractions and continues to statically simulate the potential growth thereafter. Effects of tree removal on the development of the remaining trees, such as a change in the biomass allocation due to the increased light availability, cannot be accounted for in 3-PG. This is a major limitation for its application to managed forests. Another limitation lays in the model implementation of forest management practices itself since this requires the knowledge of stand management history. As this kind of information is not readily available over large areas, this seems to be the main bottleneck of the general application of 3-PG to simulate the growth and yield of managed forest stands.

The lack of information on large-scale forest stand development might be compensated for by inferring this information from repeated observations of airborne or satellite remote sensing, in particular active optical sensors such as LiDAR (Light Detection and Ranging) capable of providing direct measures of forest structure (e.g. Kangas and Maltamo, 2009). However, this would necessitate the development of a remote sensing based proxy (e.g. laser return density or a spectral index) that could be directly linked to the structural parameters required by the model.

4.2   Model parameter sensitivity

The model parameter sensitivity study showed that the applied variations of initial stocking and maximum available soil water did not strongly impact on the basic model simulations of LAI, stocking, stand volume, and DBH (see Section 3.4). This does not mean, though, that the accurate determination of these site parameters is not critical; rather they just had no effect on the basic model settings of this study. Due to the interactions between model parameters it can be expected that varying initial stocking and ASW will have an effect on simulations based on different model settings. For example, sites with sandy and clay soil types should be affected more strongly by variations in the ASW as these soil types are characterized by soil physical properties with unfavourable plant available water holding capacities. As a consequence of the spatial heterogeneity of soil physical properties and related soil water processes, the availability of spatially detailed soil data is limited and therefore difficult to be determined for forest stands at larger scales. The same applies to the site properties site fertility and initial stocking.

The parameter sensitivity study revealed that the site fertility has a significant effect on model simulations (see Section 3.4). The fact that model simulations varied strongly although site fertility was only varied by ± 0.1 demonstrates that determining site fertility is crucial for successfully applying 3-PG to sites that were not included in the model calibration. Indeed, determining site fertility accurately is a major challenge as this parameter cannot be directly linked to any easily measurable soil chemical property, in particular over large areas. Besides, the isolated effects of soil chemical properties such as soil water pH or the C/N ratio on tree growth and related physiological processes is difficult to quantify (Landsberg & Sands, 2011). This is due to the complex interactions between physiological processes and their driving factors as well as to the ability of trees to adapt to some degree to varying environmental

conditions. The difficulty to quantify site fertility is also the reason why it is implemented in 3-PG simply as a linear scaling of the canopy quantum efficiency (see Section 1). In general, site quality (i.e. the productive capacity of a site) is difficult to define and describe as it results from the combined effects of various site factors including soil water and topography (Mäkelä et al., 2000).

Despite these issues, a possibility to determine site fertility on a large scale could be to use forest stand growth rates. To infer site fertility or more generally site quality from tree growth itself is a traditional and established practice in forestry. It is linked to the height age curves obtained from yield tables (Pretzsch, 2009). Usually the top height at some reference age, also referred to as the site index (von Gadow, 2003), is used for this purpose because top height showed to be relatively insensitive to thinning (Van Laar and Akça, 2007). In order to account for the fact that height age curves for sites of different productivity are not necessarily of anamorphic shape, i.e. of constant proportion to each other, a relatively high age needs to be used as reference age.

This is demonstrated by the development of top height at the two monitoring sites *Hundheim* and *Allenbach* (Fig. 2): While top height at *Allenbach* exceeds top height at *Hundheim* up to a stand age of 60 years, it distinctly drops below the *Hundheim* height development thereafter. This means that the site index cannot be applied to forest stands of ages well below the reference age. In addition, the indicative strength of top height for site productivity is reduced for highly structured mixed stands and in case of thinning from above (Pretzsch, 2009).

Instead of using the static site index (i.e. static insofar as it is based on the present state of a variable), top height increment derived from repeated observations of airborne remote sensing could hold the potential for an improved estimation of site fertility and therefore forest growth. LiDAR that as an active optical sensor is capable of measuring height directly would especially qualify for this purpose. However, such an approach would require the knowledge of (a) stand age to normalize the growth rates and (b) thinning measures to account for their effect on growth (see von Gadow, 2003).

While information on stand age is available for public forests on a large scale through state forest management databases, information on the kind, severity, and intensity of thinning of stands is not readily available for large areas. As repeated remote sensing observations are able to capture changes in forest canopy structure, these might help deduce information about

thinning measures provided that these affect the forest canopy. Repeated observations from below the canopy made with ground-based remote sensing sensors (terrestrial laser scanning, hemispherical photography) should, however, be able to detect structural changes not visible from above. Alternatively, remotely sensed surrogates linked to above-ground productivity such as maximum LAI could be used to infer information on site fertility (Coops et al., 2012).

4.3 Mean model calibration using artificial time series of forest structural parameters

The results from the comparison of artificial time series of forest structural parameters with mean model simulations proved that it is possible to calibrate such a mean local model with inventory measurements (see Section 3.5). However, it could also be shown that constructing artificial time series suffers from the fact that stand development can vary locally as a result of forest management and varying site growing conditions. This showed in the high structural variability of the stands sampled this study, in particular for stands of the dimensioning phase.

Possible solutions to minimize the effect of this variability on model calibration would be to either sample only sites with similar site growing conditions or sample a sufficiently large number of forest stands covering the full range of stand development phases and site qualities. Covering the full range of development phases is especially important if the artificial time series are to be constructed from ground-based remote sensing measurements. This is due to the underestimation of stocking and the overestimation of DBH for young forest stands by TLS and its impact on model calibration (see Sections 3.1 and 3.5).

While TLS was shown to be able to successfully estimate stocking and mean DBH for stands of the development phases dimensioning and maturing, the estimation of these parameters for young stands of the qualification phase proved to be inaccurate. This, however, was mainly the result of scanning in single scan mode (i.e. from a single location), known to being prone to the occlusion effect (see Section 3.1). This effect can be reduced by scanning from multiple locations, therefore increasing the accuracy of the stocking and mean DBH estimates. Another observation made from the results was that the LAI derived from TLS is distinctly higher than the LAI derived from the passive optical instruments (see Section 3.1). This is in agreement with a number of studies on the LAI retrieval from TLS and is attributed to the scanner's laser beam divergence (e.g. Danson et al., 2008; Béland et al., 2014).

31

With regard to the use of artificially constructed time series of LAI for the model calibration, it has to be noted that all indirect LAI methods suffer from some degree of uncertainty (e.g. related to the data processing and/or LAI models). In addition, the conversion from effective plant area index (i.e. what the indirect methods actually measure) to LAI by accounting for clumping and the contribution of woody elements suffers from the fact that these correction factors can only be measured indirectly.

It is therefore crucial to compare the indirect LAI methods to measurements of litter fall and establish a sound empirical relationship between these in order to use the artificial LAI time series for the model calibration with confidence. Nevertheless, combining the artificial LAI time series from different indirect methods yields plausible ranges and allows calibrating a mean local model. The good results of the basic and extended model simulations also support the general use of these LAI time series for the model calibration (see Sections 3.2 and 3.3).

5   Conclusion

This study investigated the potential of ground-based remote sensing to assess forest growth models. This was done by comparing model simulations calibrated with (a) long-term growth data, (b) artificial time series constructed from traditional forest inventory, and (c) artificial time series constructed from ground-based remote sensing measurements. The study could demonstrate that it is possible to calibrate a mean local model based on manual inventory and ground-based remote sensing measurements of forest structural parameters.

However, it was also shown that the sampling design applied for the terrestrial laser scanning (i.e. scanning from a single location at the plot centre) impacts the accuracy of the parameter retrieval and therefore the model calibration. The estimation accuracies achieved in single scan mode for stocking and mean DBH of qualification stands were insufficient, and further research is required to optimize the TLS sampling design for model calibration including this development phase. In addition, this study revealed that the forest growth model 3-PG suffers from a number of drawbacks limiting its practical applicability in forest management. Besides the necessity to account for forest management practices such as thinning, the required model input of stand initialization and site data, in particular initial stocking and site fertility, were identified as the main limitations.

As information on both is spatially limited, airborne and/or satellite remote sensing could be potentially used to derive this information at larger scales. However, more research is needed to infer stand and site variables, e.g. soil properties (Coops et al., 2012), from remotely sensed surrogates to model forest development. A combination of active and passive optical sensors and of ground-based and airborne or satellite sensors will most likely provide the ideal basis for calibrating and validating forest growth models since these different sensors complement each other ideally with regard to how they capture forest structural and biophysical properties.

Appendix

Table A-1. Parameter values used for *Picea Abies* in the 3-PG model simulations.

Parameters	Abb./symbol	Unit	Value	Reference
Allometric relationships & partitioning				
Foliage:stem partitioning ratio @ D=2 cm	pFS2	-	0.6	Estimated
Foliage:stem partitioning ratio @ D=20 cm	pFS20	-	0.3	Estimated
Constant in the stem mass v. diam. relationship	aS	-	0.208	Schwarzmeier (2000)
Power in the stem mass v. diam. relationship	nS	-	2.15	
Maximum fraction of NPP to roots	pRx	-	0.8	Default
Minimum fraction of NPP to roots	pRn	-	0.25	Default
Litterfall & root turnover				
Maximum litterfall rate	gammaFx	1/month	0.019	White et al. (2000)
Litterfall rate at t = 0	gammaF0	1/month	0.001	Default
Age at which litterfall rate has median value	tgammaF	months	24	Default
Average monthly root turnover rate	gammaR	1/month	0.015	Default
Temperature modifier (fT)				
Minimum temperature for growth	Tmin	deg. C	-2	Landsberg et al. (2003)
Optimum temperature for growth	Topt	deg. C	15	
Maximum temperature for growth	Tmax	deg. C	22	
Frost modifier (fFRost)				
Days production lost per frost day	kF	days	1	Default
Soil water modifier (fSW)				
Moisture ratio deficit for $f_q = 0.5$	SWconst	-	0.5	Based on soil class estimate
Power of moisture ratio deficit	SWpower	-	5	
Atmospheric CO2 modifier (fCO2)				
Assimialtion enhancement factor at 700 ppm	fCalpha700	-	1.4	Default
Canopy conductance enhancement factor at 700 ppm	fCg700	-	0.7	Default
Fertitlity effects				
Value of 'm' when FR = 0	m0	-	0.015	Estimated
Value of 'fNutr' when FR = 0	fN0	-	0.5	Estimated
Power of (1-FR) in 'fNutr'	fNn	-	1	Default
Age modifier (fAge)				
Maximum stand age used in age modifier	MaxAge	years	200	Estimated
Power of relative age in function for fAge	nAge	-	4	Default
Relative age to give fAge = 0.5	rAge	-	0.95	Default
Stem mortality & self-thinning				
Mortality rate for large t	gammaNx	%/year	0	Default
Seedling mortality rate (t = 0)	gammaN0	%/year	0	Default
Age at which mortality rate has median value	tgammaN	years	3	Estimated
Shape of mortality response	ngammaN	-	3	Estimated
Max. stem mass per tree @ 1000 trees/hectare	wSx1000	kg/tree	300	Default
Power in self-thinning rule	thinPower	-	1.5	Default
Fraction mean single-tree foliage biomass lost per dead tree	mF	-	0.2	Default

Fraction mean single-tree root biomass lost per dead tree	mR	-	0.2	Default
Fraction mean single-tree stem biomass lost per dead tree	mS	-	0.2	Default
Specific leaf area				
Specific leaf area at age 0	SLA0	m^2/kg	6	Default
Specific leaf area for mature leaves	SLA1	m^2/kg	7.8	White et al. (2000)
Age at which specific leaf area = (SLA0+SLA1)/2	tSLA	years	15	Estimated
Light interception				
Extinction coefficient for absorption of PAR by canopy	k	-	0.5	Default
Age at canopy cover	fullCanAge	years	3	Default
Maximum proportion of rainfall evaporated from canopy	MaxIntcptn	-	0.15	Default
LAI for maximum rainfall interception	LAImaxIntcptn	-	5	Default
Production and respiration				
Canopy quantum efficiency	alpha	molC/molPAR	0.055	Default
Ratio NPP/GPP	Y	-	0.47	Default
Conductance				
Minimum canopy conductance	MinCond	m/s	0	Default
Maximum canopy conductance	MaxCond	m/s	0.02	Default
LAI for maximum canopy conductance	LAIgcx	-	3.33	Default
Defines stomatal response to VPD	CoeffCond	1/mBar	0.05	Default
Canopy boundary layer conductance	BLcond	m/s	0.2	Default
Wood and stand properties				
Branch and bark fraction at age 0	fracBB0	-	0.15	Default
Branch and bark fraction for mature stands	fracBB1	-	0.1	Pretzsch (2010)
Age at which fracBB = (fracBB0+fracBB1)/2	tBB	years	20	Estimated
Minimum basic density - for young trees	rhoMin	t/m3	0.440	Default
Maximum basic density - for older trees	rhoMax	t/m3	0.440	Default
Age at which rho = (rhoMin+rhoMax)/2	tRho	years	4	Default
Conversion factors				
Intercept of net v. solar radiation relationship	Qa	W/m2	-90	Default
Slope of net v. solar radiation relationship	Qb	-	0.8	Default
Molecular weight of dry matter	gDM_mol	gDM/mol	24	Default
Conversion of solar radiation to PAR	molPAR_MJ	mol/MJ	2.3	Default

Acknowledgements

References

The references to the publications cited in this chapter are included in the general reference list of the dissertation.

Chapter VII: Synthesis

1 Summary

The general objectives of this dissertation were (1) to contribute to a systematic assessment of factors influencing the retrieval of core forest structural parameters from ground-based remote sensing by investigating factors which have not or only scarcely been the focus of previous research so far, and (2) to investigate whether estimates of these core structural parameters can, in practice, be used to calibrate an eco-physiological forest growth model. Four specific objectives were formulated to pursue these general aims. In the following a summary of the main results in relation to the general objectives is given.

Objective 1: Assessing the influence of camera external and internal factors on the retrieval of gap fraction, LAI, and clumping index from hemispherical photos and standardizing their processing.

Hemispherical photography has become a widely used tool for the estimation of forest canopy structural parameters for a number of reasons (see Sections 3.1 and 4.1). However, it suffers from the major drawback of a lack of standardization. This is due to the numerous interrelated factors affecting the parameter retrieval from hemispherical photos, above all photo exposure and thresholding, which have not yet been studied regarding the interrelations with file format, radiometric image resolution, and image band selection. Therefore, the study in Chapter II dealt with these issues based on the comparison of four different threshold algorithms. The results showed that the radiometric image resolutions applied (16-bit vs. 8-bit) had no significant effect on the parameter retrieval, regardless of the remaining parameter combinations.

By contrast, the file format proved to impact the structural parameters, i.e. JPEG-based gap fractions were significantly lower than TIFF- and RAW-based gap fractions. This resulted in a bias in the log-averaged effective Plant Area Index (PAI_e) derived from the JPEGs, which affected the clumping correction. This effect was associated with the quantization process of the JPEG-compression and may vary widely for different cameras since they apply different quantization factors. The JPEG format, consequently, does not yield consistent measurements which are crucial for standardizing the hemispherical photo acquisition and analysis. Thus, the authors suggested abandoning the use of JPEG for canopy structural analysis.

The image band selection (red/blue channel) for the thresholding process was also found to affect the parameter retrieval as a result of a stronger blooming effect in the blue band. In addition, the study demonstrated that these effects are interrelated with the exposure setting and threshold algorithm. This is an important finding because previous studies on optimum exposure were based on specific image settings. As a consequence, an original approach was successfully developed in Chapter II to minimize the influence of interrelations between image exposure and band. This approach yielded PAI_e that were consistent with the PAI_e derived from the LiCOR LAI-2000, providing compatibility between these two passive optical methods. This is crucial for the standardization of methods when it comes to applying them for model calibration purposes.

Objective 2: Assessing the influence of main TLS scanner properties, firmware based noise compression and data filtering on the retrieval of gap fraction and LAI, and comparing TLS-derived estimates with LAI derived from litter fall measurements.

Section 4.1 highlighted not only the advantages of hemispherical photography over other passive optical sensors but also the main drawbacks of this method, including the sensitivity to variable sky illumination conditions and the lack of a true 3-D canopy representation, thus limiting the retrieval of clumping from hemispherical photos. Active optical sensors such as terrestrial laser scanning provide the means to overcome these limitations, hence yielding potentially more consistent estimates of the core structural parameters. However, a number of factors that may influence the retrieval of these parameters have not yet been investigated in detail for phase-shift terrestrial laser scanning.

The study in Chapter III dealt with some of the main factors including scan speed, scan resolution, scanner-specific noise compression, and firmware based data filtering. It could be demonstrated that the use of the FARO scanner-specific noise compression yielded LAI that strongly overestimated mean long-term LAI derived from litter fall measurements. As data filtering such as noise compression is routinely applied to reduce the TLS point cloud size and remove erroneous range measurements (e.g. Simonse et al., 2003; Bienert et al., 2006), this finding is highly significant to forest canopy structural analysis based on TLS. Scan speed and scan resolution were also shown to impact the retrieval of gap fraction and LAI but to a much lesser degree than noise compression. The resulting variability was lower than the variability induced by different LAI models, too (e.g. Miller, 1967; Jupp et al., 2008). Nevertheless, high

scan speeds exhibited higher noise levels, which led to the conclusion that these settings should be avoided when scanning forest canopies. More importantly though, concerning the potential use of phase-shift terrestrial laser scanning, it was found that LAI estimates not based on noise compression were quite consistent despite the various scan settings applied. They also showed good agreement with the LAI derived from litter fall measurements, giving confidence in the general applicability of TLS for LAI retrieval. Even so, the results indicated that the proposed approach of filtering scan data to derive gap fraction needs to be improved and compared to alternative approaches, in particular to 3-D voxel-based methods.

Objective 3: Assessing the influence of main TLS scanner and scan properties, firmware based noise compression and data filtering on the retrieval of stocking, DBH, and stem volume.

Similar to the use of TLS to retrieve canopy structural parameters, the retrieval of the standard forest inventory parameters stocking, DBH, and stem volume has not yet been investigated with respect to the interrelation of factors influencing the parameter retrieval. The studies presented in the Chapters IV and V intended to bridge this gap. Chapter IV mainly dealt with the effects of scan mode (i.e. single or multiple scans) and mathematical circle fitting on the estimation accuracy of stem diameter measurements. As part of these studies, an original approach to the automated detection of trees and calculation of stem diameter height profiles from TLS point clouds was developed.

The tree detection rates achieved within circular plots of 30 m radii were very good (85% and 84% for Beech and Douglas fir respectively), proving that stocking can be estimated with sufficient accuracy for stands within the observed stocking range (500-1000 trees/ha). The applied circle fit algorithms yielded DBH of similar accuracies, which suggests that the use of mathematical circle fitting to retrieve stem diameters from TLS point clouds is an appropriate and effective method. In addition, the results showed that the DBH errors are normally distributed with a slight mean bias and are also independent of range (i.e. within 30 m range), both regardless of tree species. This is of particular relevance to the estimation of an unbiased mean plot DBH, which is a core input parameter in forest growth models. DBH estimation errors were also shown to depend on scan mode: DBH derived from merged scans (i.e. scans from multiple locations) had significantly higher accuracies than DBH derived from single scans. This is of relevance to the modelling of short growth periods as could be shown in this study by comparing the estimation errors to the mean increment of different DBH size classes

over a 4-year period. For DBH less than 20 cm (Douglas fir) respectively 25 cm (Beech), single scan estimation errors exceeded the mean increment, which indicates that depending on increment and stem diameter, short-term growth of trees may not be reliably measured with TLS.

With regard to the direct measurement of stem volume based on TLS, six sample trees were selected and their stem diameter profiles measured up to a stem height of 10 m. From these, stem volume was calculated. The single scan volumes exhibited a large error range of -34% to +44%, which is clearly insufficient for scaling up to tree or even stand volumes. By comparison, the merged scans yielded volume errors of -2% to +6%, which demonstrates the potential of TLS to measure stem volume and hence stem biomass. As these results were based on a relatively small sample set, though, the feasibility of such retrieval in standard forest inventory has yet to be corroborated.

The study in Chapter V complemented Chapter IV by confirming its main findings (i.e. the range-independence and normal distribution of estimation errors) for different scan speeds and resolutions as well as for larger ranges (up to 50 m). However, it could be shown that the range within which DBH can be extracted from TLS point clouds decreases with a decrease in scan resolution. The latter also resulted in a decrease in tree detection rates. Moreover, the tree detection demonstrated the effect of occlusion on the retrieval of stocking, the magnitude of which was found to increase strongly with range. This is of relevance to the integration of TLS into forest inventory, especially regarding the sampling design. The practical application of TLS for forestry applications such as growth modelling was therefore a key aspect of objective N° 4.

Objective 4: Exploring the potential of estimates of stocking, DBH, LAI, and stem volume derived from ground-based remote sensing to calibrate an eco-physiological forest growth model and its comparison with model calibrations based on long-term growth and standard forest inventory data.

The potential of TLS to derive stocking, DBH, and stem volume was investigated thoroughly in Chapters IV and V. However, these studies were based on data collected in two stands representing only a limited range of stand densities. Therefore, the aim of this final study was to collect scans within forest stands covering a large range of stand densities and the main development phases. The purpose was to obtain estimates of the core structural parameters

that could then be used for the calibration of a forest growth model. The study demonstrated that it is possible to calibrate a mean local model using so-called artificial time series derived from standard inventory.

The use of ground-based remote sensing for this purpose was shown to suffer from biased estimates of the structural parameters for stands of the qualification phase. This was due to the effect of occlusion (see Section 4.2) and the sampling design used, i.e. a single scan was collected at each plot centre to simulate the radial sampling design traditionally applied in German forest inventory (see Section 3.2). As occlusion can be minimized by increasing the number of scans, it should be possible to remove the observed estimation bias. In any case, for stands of the development phases dimensioning and maturing, TLS-derived structural parameters agreed well with reference measurements.

The study also identified potential limitations of the applied growth model 3-PG, specifically its inability to predict the growth of managed forest stands. The main limitations were found to be the model input of initial stocking, site fertility, and the necessity to account for forest management practices such as thinning. Nevertheless, the basic model calibration based on long-term growth data resulted in good estimates of stand development (stocking, standing volume, mean DBH) up to the point in time at which strong thinning commenced.

2   Conclusions and outlook

The specific research objectives were successfully achieved with regard to the general aims of this dissertation. The findings from Chapters II-V contributed significantly to a systematic assessment of the factors influencing the retrieval of core forest structural parameters from ground-based remote sensing, corroborating the immense potential of these methods for forest structure and growth analysis. Notably, the capability of terrestrial laser scanning to capture stands in their three-dimensionality is the major advantage over traditional measurements (compare the introductory sections 3 and 4) and key to improving the analysis and modelling of forest structure and growth.

Nevertheless, the findings of this thesis also confirmed that the effect of occlusion remains the main limitation of TLS, in particular regarding the routine integrating of TLS into forest inventory and its use for model calibration. Occlusion may be minimized by increasing the number of scans and optimizing the sampling design. This approach in turn decreases its sampling efficiency, though, thus minimizing a crucial intrinsic advantage over the standard inventory measurements. In addition, increasing the number of scans increases the size of the scan data, which presents a challenge to an automated and efficient information extraction.

Despite using an optimized multiple scan-based sampling design, occlusion may still pose a problem depending on stand density (Antonarakis, 2011), degree of branching (Kankare et al., 2013), and the parameter of interest. As TLS scans from below the canopy, this particularly affects the upper canopy and within crown space, e.g. measurement of tree height (see Section 4.2). Statistical techniques to estimate the distribution of vegetative elements within occluded canopy areas and/or the virtual 3-D reconstruction of tree and canopy structure are promising approaches to deal with the problem of occlusion (e.g. Côté et al., 2009; Van der Zande et al., 2010).

Alternatively, the combination of airborne laser scanning (ALS) and TLS was suggested to minimize occlusion (e.g. Litkey et al., 2008; Tansey et al., 2009). ALS and TLS are also mutually beneficial when it comes to canopy structural measures such as LAI (e.g. Hilker et al., 2010; Hopkinson et al., 2013). Even though a number of studies including Chapter III of this thesis could show that consistent estimates of gap fraction and LAI can be achieved with TLS, these basically represent another indirect measure of leaf area and biomass. That is why

further research is required to compare the LAI derived from TLS with direct methods such as litter fall measurements, which has only rarely been done until now (e.g. Clawges et al., 2007; Fleck et al., 2011; Pueschel et al., 2014). In addition, the comparison of different LAI models (2-D vs. 3-D approaches) and the retrieval of a spatially explicit reference of gap fraction need further research attention (e.g. Côté et al., 2009; Henning and Radtke, 2006).

Despite these issues, TLS bears great potential for an improved retrieval of structural and bio-physical parameters due to its rapid technical advance (multi-spectral scanners, etc.). For example, dual wavelength scanners have already been successfully applied to separate foliage from woody components (e.g. Li et al., 2013) and to retrieve leaf water content (Gaulton et al., 2013). Forestry applications that integrate laser scanning will benefit significantly from these developments. This includes the eco-physiological modelling of forest growth with the model 3-PG which was shown in this study to be limited in its practical application to predict the development of managed forest stands (see Chapter VI).

The limitations were mainly related to the mandatory model inputs of initial stocking and site fertility as well as to the necessity to explicitly account for thinning measures. Both inputs are required in a spatially explicit form if the growth of managed stands is to be realistically simulated for larger areas. However, as stand-level information on site fertility and stand management is only available for small areas, it needs to be inferred from other sources for larger areas. Airborne and satellite remote sensing sensors are the most appropriate source for this purpose, even though remotely sensed metrics are far from yielding quantitative descriptions of site fertility and stand development. This is partly due to the fact that these properties are influenced by a multitude of factors (e.g. soil chemical and physical properties, tree competition), most of which cannot be derived from remote sensing.

Consequently, remote sensing can only provide surrogates from which site fertility and stand development can be inferred (see Chapter VI). Ideally, this is achieved by multi-temporal observations capturing actual stand dynamics. These repeated observations may also be used to dynamically parameterize model simulations (see Chapter I, Section 2). Laser scanning, which is able to provide direct measures of stand structure, particularly qualifies for this purpose. Other sensor types including imaging spectroscopy might be useful as well; see e.g. Waring et al. (2010) for a detailed review of the potential integration of remote sensing data into forest growth models. The synergistic use of different sensors and at different scales (e.g.

active/passive, ground-based/airborne) will most likely lead to an improved calibration and evaluation of forest growth models since these sensors complement one another ideally with respect to the information they provide on forest structural and biophysical properties.

In the context of a sustainable forest development ensuring the preservation of the forests' ecosystem services, this synergistic approach will provide a comprehensive framework for the remote sensing based support of sustainable forest management and policy. As mentioned above, such an approach will comprise different sensors on different platforms and at multiple scales to facilitate the different information requirements of the various forestry branches and their activities. For example, while satellite-based sensors such as ESA's upcoming Sentinel[5] missions, due to its large spatial and high temporal coverage, will provide ideal support for national and state forest inventories, airborne imaging spectroscopy and laser scanning will facilitate regional and local hotspot monitoring of effects such as drought stress or insect calamities. These observations will be complemented by ground-based remote sensing such as terrestrial laser scanning and unmanned aerial vehicle-based (i.e. drones) sensors that allow the retrieval of structural and bio-physical parameters at the stand level or even for individual trees. This linkage of remote sensing observations at multiple scales backed up by ground-based traditional inventory will contribute greatly to the multi-purpose approach of modern forestry and its future development.

---

[5] http://www.esa.int/Our_Activities/Observing_the_Earth/Copernicus/Overview3

References

Achard, F., & Hansen, M.C. (Eds.) (2013). *Global Forest Monitoring from Earth Observation*. Boca Raton: CRC Press

Antonarakis, A.S. (2011). Evaluating forest biometrics obtained from ground lidar in complex riparian forests. *Remote Sensing Letters, 2*, 61-70

Béland, M., Baldocchi, D.D., Widlowski, J.-L., Fournier, R.A., & Verstraete, M.M. (2014). On seeing the wood from the leaves and the role of voxel size in determining leaf area distribution of forests with terrestrial LiDAR. *Agricultural and Forest Meteorology, 184*, 82-97

Berger, A., Gschwantner, T., Gabler, K., & Schadauer, K. (2012). Analysis of tree measurement errors in the Austrian National Forest Inventory. *Austrian Journal of Forest Science, 129*, 153-181

Bienert, A., Scheller, S., Keane, E., Mullooly, G., & Mohan, F. (2006). Application of terrestrial laser scanners for the determination of forest inventory parameters. *International Archives of Photogrammetry, Remote Sensing and Spatial Information Sciences, XXXVI part 5*

Bittner, S., Gayler, S., Biernath, C., Winkler, J.B., Seifert, S., Pretzsch, H., & Priesack, E. (2012). Evaluation of a ray-tracing canopy light model based on terrestrial laser scans. *Canadian Journal of Remote Sensing, 38*, 619-628

Brolly, G., & Király, G. (2009). Algorithms for stem mapping by means of terrestrial laser scanning. *Acta Silvatica & Lignaria Hungarica, 5*, 119-130

Burkhart, H.E., & Tomé, M. (2012). *Modeling Forest Trees and Stands*. Dordrecht, Heidelberg, New York, London: Springer

Cannell, M.G.R., Cruz, R.V.O., Galinski, W., & Cramer, W.P. (1995). Climate Change Impacts on Forests. In T.R. Watson, M.C. Zinoywera & R.H. Moss (Eds.), *Contribution of Working Group II to the Second Assessment Report of the Intergovernmental Panel on Climate Change*

Chen, J.M., & Black, T.A. (1992). Defining leaf area index for non-flat leaves. *Plant, Cell & Environment, 15*, 421-429

Clawges, R., Vierling, L., Calhoon, M., & Toomey, M. (2007). Use of a ground-based scanning lidar for estimation of biophysical properties of western larch (Larix occidentalis). *International Journal of Remote Sensing, 28*, 4331-4344

Coops, N.C., Ferster, C.J., Waring, R.H., & Nightingale, J. (2009). Comparison of three models for predicting gross primary production across and within forested ecoregions in the contiguous United States. *Remote Sensing of Environment, 113*, 680-690

Coops, N.C., & Waring, R.H. (2001). The use of multiscale remote sensing imagery to derive regional estimates of forest growth capacity using 3-PGS. *Remote Sensing of Environment, 75*, 324-334

Coops, N.C., Waring, R.H., & Hilker, T. (2012). Prediction of soil properties using a process-based forest growth model to match satellite-derived estimates of leaf area index. *Remote Sensing of Environment, 126*, 160-173

Coops, N.C., Waring, R.H., & Landsberg, J.J. (1998). Assessing forest productivity in Australia and New Zealand using a physiologically-based model driven with averaged monthly weather data and satellite-derived estimates of canopy photosynthetic capacity. *Forest Ecology and Management, 104*, 113-127

Côté, J.-F., Widlowski, J.-L., Fournier, R.A., & Verstraete, M.M. (2009). The structural and radiative consistency of three-dimensional tree reconstructions from terrestrial lidar. *Remote Sensing of Environment, 113*, 1067-1081

Cracknell, A., & Hayes, L. (1991). *Introduction to Remote Sensing.* London, New York, Philadelphia: Taylor & Francis

Danson, F., Armitage, R., Bandugula, V., Ramirez, F., Tate, N.J., Tansey, K., & Tegzes, T. (2008). Terrestrial Laser Scanners to Measure Forest Canopy Gap Fraction. In *Proceedings of the 8th SilviLaser*, Edinburgh, Scotland, 17-19 September 2008

Dassot, M., Constant, T., & Fournier, M. (2011). The use of terrestrial LiDAR technology in forest science: application fields, benefits and challenges. *Annals of Forest Science, 68*, 959-974

Fleck, S., Mölder, I., & Eichhorn, J. (2011). Final report D1 (A D1 10) - Part 2: Report on methods to assess Leaf Area Index (LAI) including LIDAR. In *Further Development and Implementation of an EU-Level Forest Monitoring System - Futmon* Göttingen: Northwest German Forest Research Station

Frazer, G.W., Fournier, R.A., Trofymow, J.A., & Hall, R.J. (2001). A comparison of digital and film fisheye photography for analysis of forest canopy structure and gap light transmission. *Agricultural and Forest Meteorology, 109*, 249-263

Gaulton, R., Danson, F.M., Ramirez, F.A., & Gunawan, O. (2013). The potential of dual-wavelength laser scanning for estimating vegetation moisture content. *Remote Sensing of Environment, 132*, 32-39

Gonsamo, A. (2009). Remote sensing of leaf area index: enhanced retrieval from close-range and remotely sensed optical observations. PhD Thesis, Department of Geography, University of Helsinki, Finland. Available from: http://urn.fi/URN:ISBN:978-952-10-5873-8 [Last accessed on: 08 April 2014]

Greve, M. (2010). Vergleich von Methoden zur Erhebung des Blattflächenindex in Wäldern. Diploma Thesis, Department of Regional and Environmental Studies, University of Trier, Germany

Henning, J.G., & Radtke, P.J. (2006). Ground-based laser imaging for assessing three-dimensional forest canopy structure. *Photogrammetric Engineering and Remote Sensing, 72*, 1349-1358

Hill, J. (2010). State-of-the-art and review of algorithms with relevance for retrieving biophysical and structural information on forests and natural vegetation with hyperspectral remote sensing systems. In H. Kaufmann et al. (eds.): *Hyperspectral algorithms: report in the frame of EnMAP preparation activities.* Scientific Technical Report STR10/08. Potsdam. DO: 10.2312/GFZ.b103-10089.

Hilker, T., Leeuwen, M., Coops, N., Wulder, M., Newnham, G., Jupp, D.B., & Culvenor, D. (2010). Comparing canopy metrics derived from terrestrial and airborne laser scanning in a Douglas-fir dominated forest stand. *Trees, 24*, 819-832

Holopainen, M., Vastaranta, M., Kankare, V., Räty, M., Vaaja, M., Liang, X., X., Y., Hyyppä, J., Hyyppä, H., Viitala, R., & Kaasalainen, S. (2011). Biomass estimation of individual trees using stem and crown diameter TLS measurements. In *Proceedings of the ISPRS Workshop Laser Scanning* Calgary, Canada, 29-31 August 2011

Hopkinson, C., Lovell, J., Chasmer, L., Jupp, D., Kljun, N., & van Gorsel, E. (2013). Integrating terrestrial and airborne lidar to calibrate a 3D canopy model of effective leaf area index. *Remote Sensing of Environment, 136*, 301-314

Inoue, A., Yamamoto, K., Mizoue, N., & Kawahara, Y. (2004). Effects of image quality, size and camera type on forest light environment estimates using digital hemispherical photography. *Agricultural and Forest Meteorology, 126*, 89-97

Jonckheere, I., Fleck, S., Nackaerts, K., Muys, B., Coppin, P., Weiss, M., & Baret, F. (2004). Review of methods for in situ leaf area index determination: Part I. Theories, sensors and hemispherical photography. *Agricultural and Forest Meteorology, 121*, 19-35

Jonckheere, I., Nackaerts, K., Muys, B., & Coppin, P. (2005). Assessment of automatic gap fraction estimation of forests from digital hemispherical photography. *Agricultural and Forest Meteorology, 132*, 96-114

Jupp, D.L.B., Culvenor, D.S., Lovell, J.L., Newnham, G.J., Strahler, A.H., & Woodcock, C.E. (2008). Estimating forest LAI profiles and structural parameters using a ground-based laser called Echidna®. *Tree Physiology, 29*, 171-181

Kangas, A., & Maltamo, M. (Eds.) (2009). *Forest Inventory - Methodology and Applications*. Dordrecht, The Netherlands: Springer

Kankare, V., Holopainen, M., Vastaranta, M., Puttonen, E., Yu, X., Hyyppä, J., Vaaja, M., Hyyppä, H., & Alho, P. (2013). Individual tree biomass estimation using terrestrial laser scanning. *ISPRS Journal of Photogrammetry and Remote Sensing, 75*, 64-75

Kirschbaum, M.U.F. (2000). CenW: a generic forest growth model. *New Zealand Journal of Forestry, 45*, 15-19

Köhl, M., Magnussen, S., & Marchetti, M. (2006). *Sampling Methods, Remote Sensing and GIS Multiresource Forest Inventory*. Berlin: Springer

Kokaly, R.F., Asner, G.P., Ollinger, S.V., Martin, M.E., & Wessman, C.A. (2009). Characterizing canopy biochemistry from imaging spectroscopy and its application to ecosystem studies. *Remote Sensing of Environment, 113,* 78-91

Kucharik, C.J., Norman, J.M., Murdock, L.M., & Gower, S.T. (1997). Characterizing canopy nonrandomness with a multiband vegetation imager (MVI). *J. Geophys. Res., 102*, 29455-29473

Landini, G. (2011). Auto Treshold (ImageJ). Available from: http://fiji.sc/wiki/index.php/Auto_Threshold#Minimum [Last accessed on: 08 April 2014]

Landsberg, J., & Sands, P. (2011). *Physiological Ecology of Forest Production - Principles, Processes and Models*. London, Amsterdam, Burlington, San Diego: Academic Press

Landsberg, J.J., & Waring, R.H. (1997). A generalised model of forest productivity using simplified concepts of radiation-use efficiency, carbon balance and partitioning. *Forest Ecology and Management, 95*, 209-228

Landsberg, J.J., Waring, R.H., & Coops, N.C. (2003). Performance of the forest productivity model 3-PG applied to a wide range of forest types. *Forest Ecology and Management, 172*, 199-214

Lang, A.R.G., & Yueqin, X. (1986). Estimation of leaf area index from transmission of direct sunlight in discontinuous canopies. *Agricultural and Forest Meteorology, 37*, 229-243

Le Maire, G., Davi, H., Soudani, K., Francois, C., Le Dantec, V.r., & Dufréne, E. (2005). Modeling annual production and carbon fluxes of a large managed temperate forest using forest inventories, satellite data and field measurements. *Tree Physiology, 25*, 859-872

Le Maire, G., Francois, C., Soudani, K., Berveiller, D., Pontailler, J.-Y., Bréda, N., Genet, H., Davi, H., & Dufrêne, E. (2008). Calibration and validation of hyperspectral indices for the estimation of broadleaved forest leaf chlorophyll content, leaf mass per area, leaf area index and leaf canopy biomass. *Remote Sensing of Environment, 112*, 3846-3864

Leblanc, S.G., Chen, J.M., Fernandes, R., Deering, D.W., & Conley, A. (2005). Methodology comparison for canopy structure parameters extraction from digital hemispherical photography in boreal forests. *Agricultural and Forest Meteorology, 129*, 187-207

Li, Z., Douglas, E., Strahler, A., Schaaf, C., Yang, X., Wang, Z., Yao, T., Zhao, F., Saenz, E.J., Paynter, I., Woodcock, C.E., Chakrabarti, S., Cook, T., Martel, J., Howe, G., Jupp, D.L.B., Culvenor, D.S., Newnham, G.J., & Lovell, J.L. (2013). Separating Leaves from Trunks and Branches with Dual-Wavelength Terrestrial LiDAR Scanning In *Proceedings of the IEEE International Geoscience and Remote Sensing Symposium*. Melbourne, Australia, 21-26 July 2013

LI-COR (1992). LAI-2000 Plant Canopy Analyser. Instruction Manual. LICOR, Lincoln, NE, USA.

Lillesand, T.M., & Kiefer, R.W. (2000). *Remote Sensing and Image Interpretation*. New York, Chichester, Weinheim, Brisbane, Singapore, Toronto: John Wiley & Sons, Inc.

Litkey, P., Liang, X., Kaartinen, H., Hyyppä, J., Kukko, A., & Holopainen, M. (2008). Single-scan TLS methods for forest parameter retrieval. In *Proceedings of the 8th SilviLaser*, Edinburgh, Scotland, 17-19 September 2008

Lovell, J.L., Jupp, D.L.B., Newnham, G.J., & Culvenor, D.S. (2011). Measuring tree stem diameters using intensity profiles from ground-based scanning lidar from a fixed viewpoint. *ISPRS Journal of Photogrammetry and Remote Sensing, 66*, 46-55

Maas, H. G., Bienert, A., Scheller, S., & Keane, E. (2008). Automatic forest inventory parameter determination from terrestrial laser scanner data. *International Journal of Remote Sensing, 29*, 1579-1593

Macfarlane, C., Coote, M., White, D.A., & Adams, M.A. (2000). Photographic exposure affects indirect estimation of leaf area in plantations of Eucalyptus globulus Labill. *Agricultural and Forest Meteorology, 100*, 155-168

Mäkelä, A., Landsberg, J., Ek, A.R., Burk, T.E., Ter-Mikaelian, M., Agren, G.I., Oliver, C.D., & Puttonen, P. (2000). Process-based models for forest ecosystem management: current state of the art and challenges for practical implementation. *Tree Physiology, 20*, 289-298

Miller, J.B. (1967). A formula for average foliage density. *Australian Journal of Botany, 15*, 141-144

Monsi, M., & Saeki, T. (1953). Über den Lichtfaktor in den Pflanzengesellschaften und seine Bedeutung für die Stoffproduktion. *Japanese Journal of Botany, 14*, 22-52

Moskal, L.M., & Zheng, G. (2012). Retrieving Forest Inventory Variables with Terrestrial Laser Scanning (TLS) in Urban Heterogeneous Forest. *Remote Sensing, 4*, 1-20

Newnham, G.J., Armston, J., Muir, J., Goodwin, N., Tindall, D., Culvenor, D.S., Püschel, P., Nyström, M., & Johansen, K. (2012). Evaluation of Terrestrial Laser Scanners for Measuring Vegetation Structure. CSIRO Sustainable Agriculture Flagship, Manuscript ID: EP124571

Nightingale, J.M., Coops, N.C., Waring, R.H., & Hargrove, W.W. (2007). Comparison of MODIS gross primary production estimates for forests across the U.S.A. with those generated by a simple process model, 3-PGS. *Remote Sensing of Environment, 109*, 500-509

Nobis, M., & Hunziker, U. (2005). Automatic thresholding for hemispherical canopy-photographs based on edge detection. *Agricultural and Forest Meteorology, 128*, 243-250

Parker, G.G. (1995). Structure and microclimate of forest canopies. In M.D. Lowman & N.M. Nadkarni (Eds.), *Forest Canopies*. San Diego, CA: Academic Press

Pretzsch, H. (2009). *Forest Dynamics, Growth and Yield*. Heidelberg, Dordrecht, London, New York: Springer

Pueschel, P., Newnham, G., Rock, G., Udelhoven, T., Werner, W., & Hill, J. (2013a). The influence of scan mode and circle fitting on tree stem detection, stem diameter and volume extraction from terrestrial laser scans. *ISPRS Journal of Photogrammetry and Remote Sensing, 77*, 44-56

Pueschel, P. (2013b). The influence of scanner parameters on the extraction of tree metrics from FARO Photon 120 terrestrial laser scans. *ISPRS Journal of Photogrammetry and Remote Sensing, 78*, 58-68

Pueschel, P., Buddenbaum, H., & Hill, J. (2012). An efficient approach to standardizing the processing of hemispherical images for the estimation of forest structural attributes. *Agricultural and Forest Meteorology, 160*, 1-13

Pueschel, P., Newnham, G., & Hill, J. (2014). Retrieval of Gap Fraction and Effective Plant Area Index from Phase-Shift Terrestrial Laser Scans. *Remote Sensing, 6*, 2601-2627

Ramirez, F., Armitage, R., & Danson, F. (2013). Testing the Application of Terrestrial Laser Scanning to Measure Forest Canopy Gap Fraction. *Remote Sensing, 5*, 3037-3056

Richards, J.A., Jia, X. (2006). *Remote Sensing Digital Image Analysis - An Introduction*. Berlin, Heidelberg, New York: Springer

Sands, P. (2001). Technical Report No. 29, Edition 2. Cooperative Research Centre for Sustainable Production Forestry and CSIRO Forestry and Forest Products, Hobart, Australia

Sands, P. (2004). Technical Report 141 - Adaption of 3-PG to novel species: guidelines for data collection and parameter assignment. Cooperative Research Centre for Sustainable Production Forestry, CSIRO Forestry and Forest Products, Hobart, Australia

Sands, P. (2010). 3PGPJS User Manual. Available from: http://booksite.elsevier.com/9780123744609/ [Last accessed on: 08 April 2014]

Schlerf, M., Atzberger, C., & Hill, J. (2005). Remote sensing of forest biophysical variables using HyMap imaging spectrometer data. *Remote Sensing of Environment, 95*, 177-194

Schlerf, M., Buddenbaum, H., Vohland, M., Werner, W., Dong, P.H., & Hill, J. (2004). Assessment of Forest Productivity using an Ecosystem Process Model, Remotely Sensed LAI Maps and Field Data. In C. Kleinn, J. Nieschulze & B. Sloboda (Eds.), *Proceedings of the 1st Goettingen GIS and Remote Sensing Days*, Göttingen, Germany

Schober, R. (1995). *Ertragstafeln wichtiger Baumarten bei verschiedener Durchforstung*. Frankfurt a. M.: J. D. Sauerländer's Verlag

Schwarzmeier, M. (2000). Erhebung der oberirdischen Biomassevorräte von Fichtenbeständen (Picea abies (L.) Karst.) im Bereich der Waldklimastationen Ebersberg und Flossenbürg. Diploma Thesis, Fachbereich Forstwirtschaft, Fachhochschule Weihenstephan, Germany

Simonse, M., Aschoff, T., Spiecker, H., & Thies, M. (2003). Automatic determination of forest inventory parameters using terrestrial laserscanning. In *Proceedings of the ScandLaser Scientific Workshop on Airborne Laser Scanning of Forests*. Umea, Sweden, 3-4 Septemebr 2003

Solberg, S. (2010). Mapping gap fraction, LAI and defoliation using various ALS penetration variables. *International Journal of Remote Sensing, 31*, 1227-1244

Arbeitskreis Standortkartierung (2003). *Forstliche Standortsaufnahme*: IHW-Verlag

Stoffels, J., Mader, S., Hill, J., Werner, W., & Ontrup, G. (2012). Satellite-based stand-wise forest cover type mapping using a spatially adaptive classification approach. *European Journal of Forest Research, 131*, 1071-1089

Strahler, A.H., Jupp, D.L.B., Woodcock, C.E., Schaaf, C.B., Yao, T., Zhao, F., Yang, X., Lovell, J., Culvenor, D., Newnham, G., Ni-Miester, W., & Boykin-Morris, W. (2008). Retrieval of forest structural parameters using a ground-based lidar instrument (Echidna®). *Canadian Journal of Remote Sensing, 34*, 426-440

Tansey, K., Selmes, N., Anstee, A., Tate, N.J., & Denniss, A. (2009). Estimating tree and stand variables in a Corsican Pine woodland from terrestrial laser scanner data. *International Journal of Remote Sensing, 30*, 5195-5209

Thies, M., & Spiecker, H. (2004). Evaluation and future prospects of terrestrial laserscanning for standardized forest inventories. *International Archives of Photogrammetry, Remote Sensing and Spatial Information Sciences, 36*, 192-197

Tickle, P.K., Coops, N.C., & Hafner, S.D. (2001). Assessing forest productivity at local scales across a native eucalypt forest using a process model, 3PG-SPATIAL. *Forest Ecology and Management, 152*, 275-291

Turner, D.P., Ritts, W.D., Cohen, W.B., Gower, S.T., Running, S.W., Zhao, M., Costa, M.H., Kirschbaum, A.A., Ham, J.M., Saleska, S.R., & Ahl, D.E. (2006). Evaluation of MODIS NPP and GPP products across multiple biomes. *Remote Sensing of Environment, 102*, 282-292

Van der Zande, D., Stuckens, J., Verstraeten, W.W., Muys, B., & Coppin, P. (2010). Assessment of Light Environment Variability in Broadleaved Forest Canopies Using Terrestrial Laser Scanning. *Remote Sensing, 2*, 1564-1574

Van Genechten, B., Lerma, J.L., Heine, E., & Santana Quintero, M. (Eds.) (2008). *3D RiskMapping. Theory and practice on terrestrial laser scanning. Training material based on practical applications*. Valencia: Universidad Politécnica de Valencia

Van Laar, A., & Akça, A. (2007). *Forest Mensuration*. Dordrecht, The Netherlands: Springer

von Gadow, K. (2003). *Waldstruktur und Wachstum (Forest Structure and Growth)*. Göttingen: Universitätsdrucke Göttingen

Walter, J.-M.N. (2009). Hemispherical Photography of Forest Canopies - Practice. In *CIMES-FISHEYE 2009,* Université de Strasbourg, France

Waring, R.H., Coops, N.C., & Landsberg, J.J. (2010). Improving predictions of forest growth using the 3-PGS model with observations made by remote sensing. *Forest Ecology and Management, 259*, 1722-1729

Waring, R.H., Milner, K.S., Jolly, W.M., Phillips, L., & McWethy, D. (2006). Assessment of site index and forest growth capacity across the Pacific and Inland Northwest U.S.A. with a MODIS satellite-derived vegetation index. *Forest Ecology and Management, 228*, 285-291

Warren Wilson, J. (1960). Inclined point quadrats. *New Phytologist, 59*, 1-8

Watt, P.J., & Donoghue, D.N.M. (2005). Measuring forest structure with terrestrial laser scanning. *International Journal of Remote Sensing, 26*, 1437-1446

Weiss, M., Baret, F., Smith, G.J., Jonckheere, I., & Coppin, P. (2004). Review of methods for in situ leaf area index (LAI) determination: Part II. Estimation of LAI, errors and sampling. *Agricultural and Forest Meteorology, 121*, 37-53

West, P.W. (2009). *Tree and Forest Measurement*. Dordrecht, Heidelberg, London, New York Springer

White, M.A., Thornton, P.E., Running, S.W., & Nemani, R.R. (2000). Parameterization and Sensitivity Analysis of the BIOME-BGC Terrestrial Ecosystem Model: Net Primary Production Controls. *Earth Interactions, 4*, 1-85

Wolter, P.T., Mladeoff, D.J., Host, G.E., & R., C.T. (1995). Improved forest classification in northern lake states using multi-temporal Landsat imagery. *Photogrammetric Engineering and Remote Sensing, 61*, 1129-1143

Wulder, M.A., & Franklin, S.E. (Eds.) (2003). *Remote Sensing of Forest Environments - Concepts and Case Studies*. Dordrecht, The Netherlands: Kluwer Academic Publishers

Yang, X., Strahler, A.H., Schaaf, C.B., Jupp, D.L.B., Yao, T., Zhao, F., Wang, Z., Culvenor, D.S., Newnham, G.J., Lovell, J.L., Dubayah, R.O., Woodcock, C.E., & Ni-Meister, W. (2013). Three-dimensional forest reconstruction and structural parameter retrievals using a terrestrial full-waveform lidar instrument (Echidna®). *Remote Sensing of Environment, 135*, 36-51

Yao, T., Yang, X., Zhao, F., Wang, Z., Zhang, Q., Jupp, D., Lovell, J., Culvenor, D., Newnham, G., Ni-Meister, W., Schaaf, C., Woodcock, C., Wang, J., Li, X., & Strahler, A. (2011). Measuring forest structure and biomass in New England forest stands using Echidna ground-based lidar. *Remote Sensing of Environment, 115*, 2965-2974

Zhao, F., Yang, X., Schull, M.A., Román-Colán, M.O., Yao, T., Wang, Z., Zhang, Q., Jupp, D.L.B., Lovell, J.L., Culvenor, D.S., Newnham, G.J., Richardson, A.D., Ni-Meister, W., Schaaf, C.L., Woodcock, C.E., & Strahler, A.H. (2011). Measuring effective leaf area index, foliage profile, and stand height in New England forest stands using a full-waveform ground-based lidar. *Remote Sensing of Environment, 115*, 2954-2964

Zhao, K., & Popescu, S. (2009). Lidar-based mapping of leaf area index and its use for validating GLOBCARBON satellite LAI product in a temperate forest of the southern USA. *Remote Sensing of Environment, 113*, 1628-1645

Zheng, G., & Moskal, L.M. (2009). Retrieving Leaf Area Index (LAI) Using Remote Sensing: Theories, Methods and Sensors. *Sensors, 9*, 2719-2745

Zheng, G., & Moskal, L.M. (2012). Spatial variability of terrestrial laser scanning based leaf area index. *International Journal of Applied Earth Observation and Geoinformation, 19*, 226-237

Zheng, G., Moskal, L.M., & Soo-Hyung, K. (2013). Retrieval of Effective Leaf Area Index in Heterogeneous Forests With Terrestrial Laser Scanning. *Geoscience and Remote Sensing, IEEE Transactions on, 51*, 777-786

Zianis, D., Muukkonen, P., Mäkipää, R., & Mencuccini, M. (2005). Biomass and stem volume equations for tree species in Europe. *Silva Fennica Monographs, 4*

Curriculum Vitae

Pyare Hans Püschel
Am Deimelberg 36
D-54295 Trier, Germany

Date of Birth: 17.12.1981
Place of Birth: Starnberg

	School Education
09/1988 – 07/1993	Primary school in Heufeld, Germany
09/1993 – 06/2002	Secondary school in Bad Aibling, Germany
	Higher Education
10/2003 – 10/2004	Studies of Applied Physical Geography at the University of Trier, Germany
10/2004 – 01/2010	Studies of Applied Environmental Sciences at the University of Trier, Germany. Graduated with the degree „Diplom-Umweltwissenschaftler"
09/2006 – 06/2007	Study visit at the University of Glasgow, Scotland
03/2010 – Present	Doctoral studies at the Faculty of Regional and Environmental Sciences, University of Trier
	Work Experience
03/2010 – Present	Research assistant at the Department of Environmental Remote Sensing and Geoinformatics, University of Trier Project: EnMAP Core Science Team
10/2011– 01/2012	Research visit at the Remote Sensing Centre of the Queensland Department of Environment and Resource Management, Brisbane, Australia